# THE SCIENCE AND APPLICATION OF AQUEOUS TWO-PHASE SYSTEMS AND LIQUID-LIQUID PHASE SEPARATION IN BIOTECHNOLOGY AND BIOENGINEERING

EDITED BY: John Paul Frampton, Brendan M. Leung and Anderson Ho Cheung Shum

PUBLISHED IN: Frontiers in Chemistry

frontiers Research Topics

frontiers



ISSN 1664-8714
ISBN 978-2-88963-356-2
DOI 10.3389/978-2-88963-356-2

## About Frontiers

Frontiers is more than just an open-access publisher of scholarly articles: it is a pioneering approach to the world of academia, radically improving the way scholarly research is managed. The grand vision of Frontiers is a world where all people have an equal opportunity to seek, share and generate knowledge. Frontiers provides immediate and permanent online open access to all its publications, but this alone is not enough to realize our grand goals.

## Frontiers Journal Series

The Frontiers Journal Series is a multi-tier and interdisciplinary set of open-access, online journals, promising a paradigm shift from the current review, selection and dissemination processes in academic publishing. All Frontiers journals are driven by researchers for researchers; therefore, they constitute a service to the scholarly community. At the same time, the Frontiers Journal Series operates on a revolutionary invention, the tiered publishing system, initially addressing specific communities of scholars, and gradually climbing up to broader public understanding, thus serving the interests of the lay society, too.

## Dedication to Quality

Each Frontiers article is a landmark of the highest quality, thanks to genuinely collaborative interactions between authors and review editors, who include some of the world's best academicians. Research must be certified by peers before entering a stream of knowledge that may eventually reach the public - and shape society; therefore, Frontiers only applies the most rigorous and unbiased reviews.
Frontiers revolutionizes research publishing by freely delivering the most outstanding research, evaluated with no bias from both the academic and social point of view. By applying the most advanced information technologies, Frontiers is catapulting scholarly publishing into a new generation.

## What are Frontiers Research Topics?

Frontiers Research Topics are very popular trademarks of the Frontiers Journals Series: they are collections of at least ten articles, all centered on a particular subject. With their unique mix of varied contributions from Original Research to Review Articles, Frontiers Research Topics unify the most influential researchers, the latest key findings and historical advances in a hot research area! Find out more on how to host your own Frontiers Research Topic or contribute to one as an author by contacting the Frontiers Editorial Office: researchtopics@frontiersin.org

# THE SCIENCE AND APPLICATION OF AQUEOUS TWO-PHASE SYSTEMS AND LIQUID-LIQUID PHASE SEPARATION IN BIOTECHNOLOGY AND BIOENGINEERING

Topic Editors:
**John Paul Frampton,** Dalhousie University, Canada
**Brendan M. Leung,** Dalhousie University, Canada
**Anderson Ho Cheung Shum,** The University of Hong Kong, Hong Kong

The phase separation of incompatible liquids has been a topic of significant importance in chemical and industrial engineering for many years. Well-understood examples of this phenomenon include the phase separation of oil with water and the phase separation of non-polar organic solvents with water. Similar behavior is observed when aqueous solutions of two or more incompatible polymers or polymers and salts are mixed. In these mixtures (referred to as aqueous two-phase systems), the separated phases are composed mostly of water. Aqueous two-phase systems have been used extensively for the extraction of high-value biological products from mixtures of biological materials.

In recent years, aqueous two-phase systems have also found increased use as materials for streamlining and improving the capabilities of cell and molecular assays, and for the design of advanced cell culture systems. Similar behavior of biological materials in living systems has also been observed, with emerging roles in cell physiology.

**Citation:** Frampton, J. P., Leung, B. M., Shum, A. H. C., eds. (2020). The Science and Application of Aqueous Two-Phase Systems and Liquid-Liquid Phase Separation in Biotechnology and Bioengineering. Lausanne: Frontiers Media SA. doi: 10.3389/978-2-88963-356-2

# Table of Contents

frontiers in Chemistry

ORIGINAL RESEARCH
published: 04 September 2018
doi: 10.3389/fchem.2018.00379

# Collagen Partition in Polymeric Aqueous Two-Phase Systems for Tissue Engineering

*Sunil Singh and Hossein Tavana**

*Department of Biomedical Engineering, The University of Akron, Akron, OH, United States*

Aqueous two-phase systems (ATPS) of polyethylene glycol (PEG) and dextran (DEX) are commonly used to partition proteins. Protein partition in ATPS is a complex phenomenon and depends on factors including molecular weight of polymers, and electrochemical and ionic properties of the phases. We studied the effect of polymer molecular weight on the partition of a natural protein, collagen, in several ATPS formulations made with non-ionic polymers polyethylene glycol (PEG) and dextran (DEX). We found that partitioning of collagen to an aqueous phase significantly increases when the molecular weight of the corresponding phase polymer decreases. Additionally, a large difference between the molecular weight of the phase-forming polymers was necessary to cause a significant uneven collagen distribution between the aqueous phases. We then employed one of the systems to create a three-dimensional breast cancer microtissue by entrapping a spheroid of breast cancer cells within the partitioned collagen. This convenient technique to generate 3D microtissues offers a convenient and promising approach for tissue engineering applications.

**Keywords: collagen, partition, ATPS, spheroid, 3D culture**

OPEN ACCESS

***Edited by:***
*John Paul Frampton, Dalhousie University, Canada*

***Reviewed by:***
*Jangwook P. Jung, Louisiana State University, United States*
*Christopher Moraes, McGill University, Canada*

****Correspondence:***
*Hossein Tavana*
*tavana@uakron.edu*

***Specialty section:***
*This article was submitted to Chemical Engineering, a section of the journal Frontiers in Chemistry*

***Received:*** *31 May 2018*
***Accepted:*** *03 August 2018*
***Published:*** *04 September 2018*

***Citation:***
*Singh S and Tavana H (2018) Collagen Partition in Polymeric Aqueous Two-Phase Systems for Tissue Engineering. Front. Chem. 6:379. doi: 10.3389/fchem.2018.00379*

## INTRODUCTION

Aqueous two-phase systems (ATPS) may be formed by mixing aqueous solutions of two chemically incompatible polymers (Albertsson, 1961). Polyethylene glycol (PEG) and dextran (DEX) are the most commonly used polymers to form ATPS. Each ATPS has a characteristic phase diagram with a binodal curve that prescribes pairs of concentrations of polymers to result in two immiscible phases. Only polymer concentrations above the curve give a two-phase system. Separation of two distinct aqueous layers by an interface is visible and becomes more distinct by increase in the interfacial tension between these two phases (Atefi et al., 2014, 2015). ATPS are used for separation of biomolecules such as cells (SooHoo and Walker, 2009), proteins (Johansson, 1970), and nucleic acids and organelles (Walter and Larsson, 1994). High water content and low interfacial tensions of ATPS are key properties to provide a mild environment for sensitive biomolecules.

Partitioning of proteins to either phase of an ATPS is a complex process (Schmidt et al., 1994). Proteins may favor one of the phases of an ATPS or partition toward the interface. Distribution of protein molecules may be manipulated by altering the molecular weight of the polymers, concentration of polymers, ionic strength of the aqueous solutions, pH, and hydrophobicity of the polymers. For example, amylase partitioning to the top phase improved by adding salt to the aqueous solutions (Li et al., 2002). Using charged PEG increased partitioning of penicillin acylase from E. coli to the top phase in an ATPS (Gavasane and Gaikar, 2003). It was recently shown that

collagen partitions to the interface of aqueous PEG and DEX phases and this was used to generate cell-containing collagen microdrops to mimic matrix contraction (Moraes et al., 2013).

Our goal was to localize collagen to one phase, rather than to the interface, to conveniently form collagen microgels in ATPS. To demonstrate the feasibility of partitioning of collagen to the bottom DEX phase, we conducted experiments with two-phase systems of different molecular weights of PEG and DEX. Then, we selected a system that favors partition of collagen to the DEX phase and entrapped a spheroid of breast cancer cells in the partitioned collagen in the DEX phase. The resulting microtissue morphologically resembles solid breast tumors where a mass of cancer cells resides in a protein matrix (Ham et al., 2016b). This novel approach will enable future studies in tumor biology and antitumor drug discovery.

# MATERIALS AND METHODS

## Preparation of Aqueous Two-Phase Systems

Several ATPS were prepared with polyethylene glycol (PEG) (Sigma) and dextran (DEX) (Pharmacosmos). Two different molecular weights of PEG (8kDa & 35kDa) and DEX (40kDa & 500kDa) were used to prepare four ATPS: PEG8k-DEX40k (system A), PEG8k-DEX500k (system B), PEG35k-DEX40k (system C), and PEG35k-DEX500k (system D). From each system, different stock concentrations of PEG and DEX solutions were used to form three sets of two-phase systems: 15% PEG-21% DEX, 18% PEG-24% DEX, and 24% PEG-32% DEX. All concentrations of aqueous PEG and DEX solutions were calculated in %(w/v). Polymers were dissolved in a complete growth medium. To facilitate complete dissolution of polymers, the solutions were kept in a 37°C water bath for four hours and mixed using a vortex for two min every 30 min. All PEG and DEX solutions were filtered through syringe filters of 0.2 μm pore size to remove small particles and impurities. Resulting polymer solutions were stored at 4°C.

## Construction of Binodal Curves

Binodal curves for systems A, B, C, and D were constructed using a titration method (Albertsson and Tjerneld, 1994). Various ATPS were prepared in a complete growth medium in 1.5 mL microcentrifuge tubes from stock PEG and DEX solutions. Medium was added to each ATPS in 5 μL increments until the interface between the top and bottom phases disappeared. Concentrations of the polymers prior to formation of one phase were determined and used to construct a binodal curve.

## Cell Culture

BT474 breast cancer cells were obtained from ATCC and cultured in RPMI 1640 medium (Sigma) supplemented with 10% fetal bovine serum (FBS) (Sigma), 1% antibiotic (Thermo Fisher Scientific), 0.1 μM sodium pyruvate (Thermo Fisher Scientific), 1 μM nonessential amino acids (Thermo Fisher Scientific), and 0.1 mM Hepes buffer (Thermo Fisher Scientific). Cells were cultured in a humidified incubator at 37°C and 5% $CO_2$ in a T75 flask (Thermo Fisher Scientific). BT474 cells grew in multilayer patches. Cells were rinsed with phosphate buffered saline (PBS) (Sigma) and detached using 0.25% trypsin (Thermo Fisher Scientific) for cell seeding and passaging. Cells were sub-cultured at a ratio of 1:3.

## Preparation of Collagen Solution

A stock solution of type I rat tail collagen (Corning) with a concentration of 8.56 mg/ml dissolved in 0.02N acetic acid was diluted to desired concentrations using the manufacturer's protocol. For example, 1 mL of 4 mg/ml collagen solution was prepared by mixing 100 μL 10X DMEM medium, 422 μL sterile distill water, 467 μL collagen stock solution, and 11 μL 1N NaOH solution. All the reagents were kept on ice during collagen preparation to maintain the temperature at 4°C and prevent premature gelation of collagen. The pH of the solution was measured by a pH meter (Mettler Toledo) and maintained at 7.5. Prepared collagen solutions were stored at 4°C for a maximum of 1 h before use.

## Partition of Collagen in ATPS

Collagen partition experiments were performed with systems A-D in serum-free RPMI. From each system, three combinations were used: 15% PEG-21% DEX, 18% PEG-24% DEX, and 24% PEG-32% DEX. Equal volumes (200 μL) of a PEG solution, a DEX solution, and a 2 mg/ml type I collagen solution were mixed in a 1.5 mL microcentrifuge tube. The mixture was equilibrated at 4°C for 60 min to allow collagen to partition between the two phases and a clear interface form. Because collagen partition experiments were conducted with equal volumes of PEG, DEX, and collagen solutions, the resulting concentrations of PEG and DEX in each system in the partition assay reduced to 5% PEG-7% DEX, 6% PEG-8% DEX, and 8% PEG-10.6% DEX. Four replicates were used for each system. From each tube, the top phase solution was pipetted out first followed by the bottom phase solution. Samples were stored in separate microcentrifuge tubes.

## Hydroxyproline Assay

Collagen concentration in the bottom phase of each system was quantified using a hydroxyproline assay (Sigma). Briefly, equal volumes of the sample and concentrated hydrochloric acid (∼12 M HCl) were mixed in a Teflon-capped glass vial (Taylor Scientific). Next, the solution was hydrolyzed at 110°C in a hot air oven (Binder) for 16 h. Then, the vial was cooled down to room temperature and the hydrolyzed solution was transferred into a 1.5 mL centrifuge tube. The tube was centrifuged at 180 rcf for 10 min. Next, 10 μL of the supernatant was transferred into a flat-bottom 96-well plate. The plate was incubated in a 60°C oven with the lid on for 2 h for complete drying of the sample. Each sample was spiked with 0.4 μg of hydroxyproline standard to remove absorbance interference from endogenous compounds. Hydroxyproline standards were also run simultaneously to obtain a standard curve. To each well, 6 μL of chloramine T concentrate and 94 μL of an oxidation buffer was added. The plate was incubated at room temperature for 5 min. Then, 50 μL of 4-(dimethylamino)benzaldehyde concentrate and 50 μL of perchloric acid were added. The plate was incubated at 60°C for 90 min and absorbance was measured at 560 nm using a plate

reader (Synergy H1M) (Biotek Instruments). The hydroxyproline standard curve was used to determine the hydroxyproline amino acid content in the sample. The collagen content was approximated by multiplying the resulting value by a factor of 7.69 (Neuman and Logan, 1950).

## Cancer Cell Spheroid Formation

BT474 cancer cell spheroids were formed using ATPS technology (Atefi et al., 2014). PEG35k and DEX500k were used to form the spheroids. Aqueous PEG phase solution of 6.6% (w/v) and DEX phase solution of 3.2% (w/v) were prepared separately in a complete growth medium (Atefi et al., 2014). BT474 cells were mixed thoroughly with the DEX phase solution to form a cell suspension with a density of $50 \times 10^3$ cells/μL. Next, 30 μL of the PEG solution was loaded into a round-bottom, ultralow attachment 384-well plate (Corning). A 0.3 μL drop of the DEX phase containing $15 \times 10^3$ cells was dispensed into each well using a robotic liquid handler (SRT Bravo) (Agilent Technologies). The plate was incubated at 37°C for 24 h to allow formation of a spheroid in each DEX phase drop within each microwell. Phase contrast images of spheroids were captured using an inverted fluorescence microscope (Axio Observer A1) (Zeiss).

## Embedding Cancer Cell Spheroids in Partitioned Collagen

Aqueous DEX500k phase solution of 14% (w/v) was prepared in a complete growth medium and mixed with an equal volume of 4 mg/ml collagen solution to obtain a solution of 7% (w/v) DEX and 2 mg/ml collagen. After BT474 spheroids formed, 10 μL of the collagen-DEX solution was dispensed into each well containing the spheroids submerged in the PEG solution. These concentrations of PEG, DEX, and collagen were selected to replicate partition of 2 mg/ml collagen in a PEG-DEX system of 5% (w/v) PEG-7% (w/v) DEX system. The 384-well plate containing spheroids was maintained at 4°C for 30 min before dispensing the collagen-DEX solution. Again, the robotic liquid handler was used for uniform dispensing of the solution. The 384-well plate was kept on an ice tray for 60 min to allow collagen partitioning take place and another 30 min in room temperature. Then, the plate was incubated at 37°C to allow the collagen to gel. The 384-well plate was not transferred directly from 4°C to 37°C incubator to prevent potential thermal shock to cells.

## Statistical Analysis

Data from the experiments were expressed as mean ± standard error. Two-way ANOVA with Bonferroni *post hoc* tests (MINITAB) were used to compare means among experimental groups. Each group had at least $n = 4$ replicates. Statistical significance was defined at $p < 0.05$.

# RESULTS AND DISCUSSION

## Characterization of ATPS

We constructed binodal curves for four systems A-D made with different molecular weights of PEG and DEX using a titration method (**Figure 1**) (Atefi et al., 2016). Each curve represents critical concentrations of phase-forming polymers above which two distinct aqueous phases formed. Construction of binodal curves was necessary to determine working concentrations of the polymers to give two-phase systems. We selected the stock concentrations of PEG and DEX (15% PEG-21% DEX, 18% PEG-24% DEX, and 24% PEG-32% DEX) because two-phase solutions made at these concentrations contained equal volumes of PEG-rich top phase and DEX-rich bottom phase, making it convenient to measure volume of each phase during partition experiments. This also allowed visual comparison of partition of collagen in the bottom phase of two-phase systems made with the three sets of concentration pairs in each system A-D. As expected, the binodal curve was more asymmetric when the difference in molecular weights of PEG and DEX polymers increased (Atefi et al., 2016). System C had the most symmetric binodal curve, whereas system B had the most asymmetric binodal curve (**Figure 1**).

## Measurements of Collagen Concentration Using Hydroxyproline Assay

We quantified collagen content in samples using a commercially available hydroxyproline assay kit. To assess the accuracy of the assay, we prepared known concentrations (1, 2, 3, 4, 6, and 8 mg/mL) of collagen standards in serum-free RPMI medium to avoid interference of serum proteins with the hydroxyproline amino acids present in the collagen standards. We acid hydrolyzed collagen standards for 16 h and determined the protein concentration. The result in **Figure 2B** shows a strong correlation between the actual collagen concentrations used in the experiment and the measured collagen concentrations, indicating that this assay can precisely predict collagen concentration in sample solutions. Importantly, we generated hydroxyproline standard curves using distilled water, and PEG and DEX solutions and showed that polymers do not cause interference in the absorbance signal from the samples when quantifying collagen concentration in an aqueous polymeric solution (**Figure S1**).

## Collagen Partition in ATPS

We performed collagen partition experiments with systems A-D. We mixed equal volumes of PEG solution, DEX solution, and collagen solution in a microcentrifuge tube, equilibrated the mixture at 4°C, and transferred top and bottom phase into separate vials (**Figure 2A**). From each system, we selected three pairs of concentrations of aqueous phases: 15% PEG-21% DEX, 18% PEG-24% DEX, and 24% PEG-32% DEX. The resulting polymer concentrations in the collagen partition assay were 5% PEG-7% DEX, 6% PEG-8% DEX, and 8% PEG-10.2% DEX, respectively (**Figure 1**). These pairs located above the binodal curve and resulted in two-phase systems which we visually confirmed by observing a clear interface. We defined a partition coefficient ($K_c$) as the ratio of collagen concentration in bottom phase and the total collagen concentration used in each assay, i.e.,

$$K_c = \frac{\textit{Collagen concentration in bottom phase}}{\textit{Total collagen concentration}} \times 100\%$$

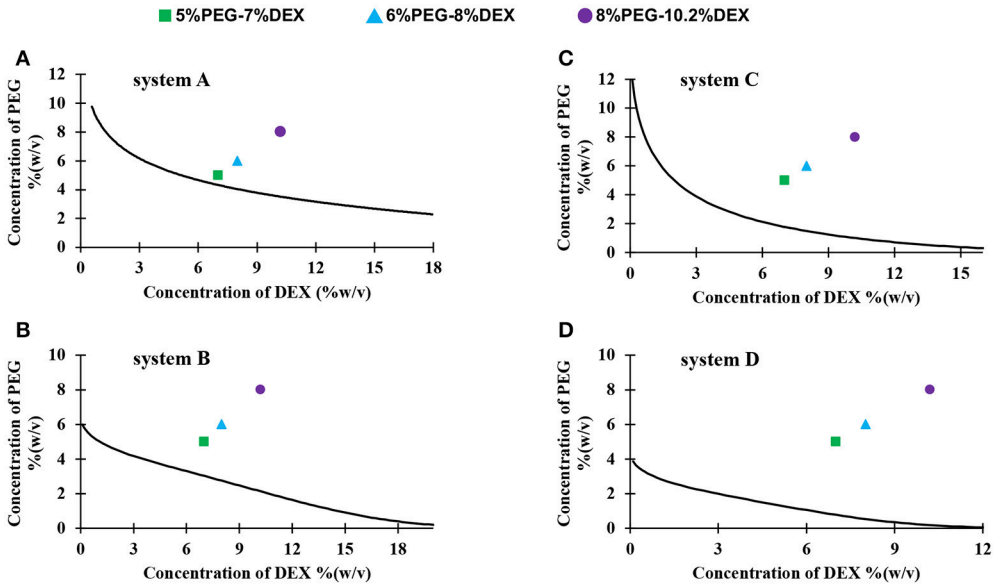


**FIGURE 1 |** Binodal curves of four systems made with different molecular weights PEG and DEX: **(A)** PEG8k-DEX40k, **(B)** PEG8k-DEX500k, **(C)** PEG35k-DEX40k, and **(D)** PEG35k-DEX500k. Colored symbols show the resulting concentrations of PEG and DEX in the partition assay; square: 5%PEG-7%DEX, triangle: 6%PEG-8%DEX, and circle: 8%PEG-10.2%DEX.

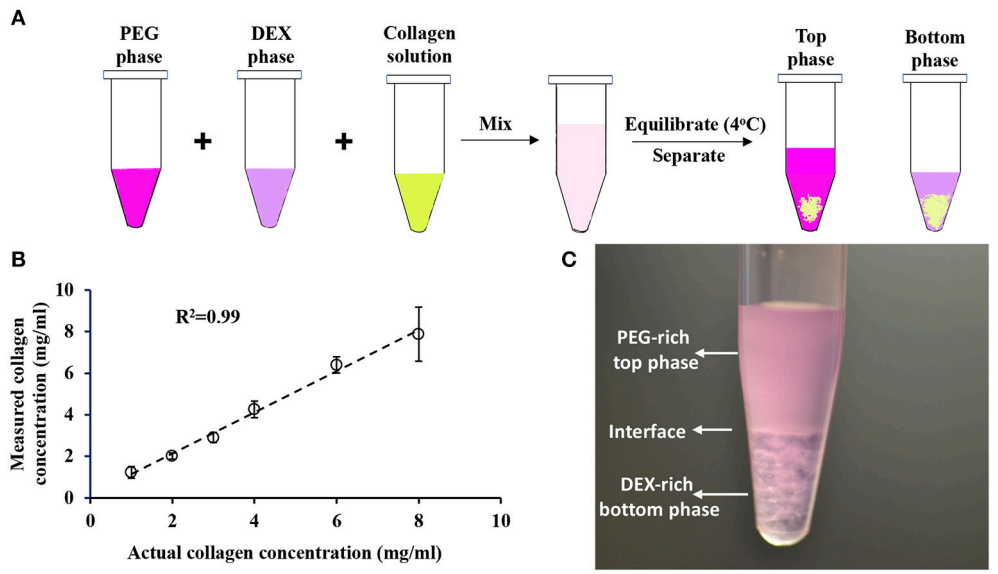


**FIGURE 2 | (A)** Schematic of collagen partition experiment in ATPS. **(B)** Quantification of collagen concentration using hydroxyproline assay. Error bars represent standard deviations. **(C)** Collagen partition assay containing equal volumes of 15% PEG35k, 21% DEX500k, and 2 mg/ml collagen results in formation of 5% PEG-7% DEX ATPS.

**Figure 2C** shows an image from a collagen partition assay using the 5% PEG-7% DEX pair of system A. A distinct interface between the PEG-rich top phase and DEX-rich bottom phase is clear. This two-phase system gave a collagen partition coefficient of 61 ± 3%.

**Figure 3** shows partition coefficients of collagen in systems A-D, using three concentration pairs from each system: 5% PEG-7% DEX, 6% PEG-8% DEX, and 8% PEG-10.2% DEX. In the 5% PEG-7% DEX pair, collagen partition coefficient was the highest in system A (61 ± 3%). When the molecular weight of DEX increased to 500 kDa but the molecular weight of PEG was kept constant (system B), the partition coefficient significantly decreased to 33 ± 4%. Increasing the molecular weight of PEG from 8 kDa in system B to 35 kDa in system D but keeping

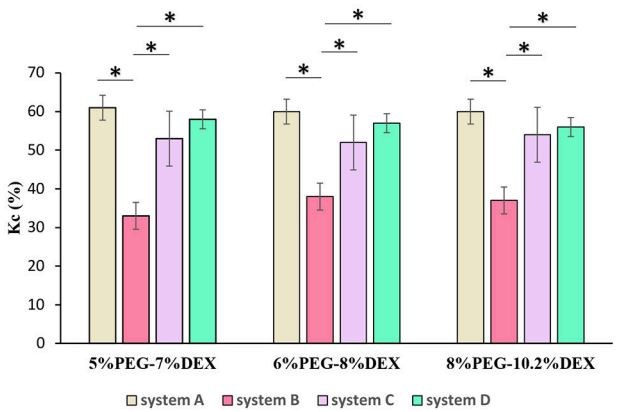


**FIGURE 3 |** Collagen partition coefficient ($K_C$) in four different systems using 5% PEG-7%DEX, 6% PEG-8% DEX, and 8% PEG-10.2% DEX concentration pairs. $n = 4$, $^*p < 0.05$ (ANOVA with Bonferroni *post-hoc* test).

the molecular weight of DEX constant at 500 kDa significantly increased the partition coefficient to 58 ± 2%. With systems A-D, we obtained similar results using 6% PEG-8% DEX and 8% PEG-10.2% DEX pairs of concentrations.

These results suggest that collagen partition in ATPS is highly sensitive to molecular weight of phase polymers. That is, reducing molecular weight of a polymer increases the propensity of collagen to partition to the aqueous phase of that polymer. This finding is consistent with a previous report that proteins in non-ionic ATPS attract to the aqueous phase with smaller polymer molecules if all other conditions such as polymer concentration, temperature, and salt concentrations are kept constant (Albertsson et al., 1987). Another interesting finding contrary to the above conclusion emerged from our results. That is, increasing PEG molecular weight from 8 kDa in system A to 35 kDa in system C but keeping DEX molecular weight fixed at 40 kDa decreased the partition coefficient by 8%. However, when PEG molecular weight increased from 8 kDa in system B to 35 kDa in system D but DEX molecular weight was fixed at 500 kDa, the partition coefficient significantly increased again. These results suggest that the above rule about the effect of molecular weight of phase polymers on significant uneven partition of collagen between the two aqueous phases is valid only when there is a large difference between molecular weights of the polymers. Finally, comparing results among the three pairs of PEG and DEX in a specific system, i.e., 5% PEG-7% DEX, 6% PEG-8% DEX, and 8% PEG-10.2% DEX, showed no statistical difference in collagen partition coefficient (**Figure 3**).

## Collagen Partitioning in ATPS for Tumor Tissue Engineering

A previous study showed that collagen primarily partitions to the interface of ATPS (Moraes et al., 2013). This property was used to generate low-volume collagen microdrops (<10 μL) that mimicked matrix contraction in tissue environments. Here, we demonstrated the utility of collagen partitioning to the DEX phase of ATPS by creating a 3D microtissue. In our study, we quantitatively showed improved partition of collagen to DEX phase of several ATPS. We selected system D with 5% PEG-7% DEX because our preliminary experiments and previous work showed that the PEG35k-DEX500k ATPS (system D) gives consistently-sized and compact spheroids over wide range of polymer concentrations compared to other ATPS used (Ham et al., 2016a). From this ATPS, we used the 5% PEG-7% DEX pair because it gave a similar collagen partition coefficient to those from the 6% PEG-8% DEX and 8% PEG-10.2% DEX pairs (**Figure 3**) but at lower concentration of the polymers that is preferable for cellular applications with ATPS (Tavana et al., 2009; Atefi et al., 2014). After a spheroid formed in each well of a 384-well plate, we dispensed 10 μl of the DEX solution containing collagen to the wells containing spheroids on the well-bottom submerged in the PEG phase solution (**Figure 4a**). Because the DEX phase is denser than the PEG phase, it sank to the bottom of the wells. Due to the propensity of collagen toward the DEX phase, it remained in the DEX phase during incubation. We confirmed confinement of collagen to the DEX phase by dispensing equal amounts of the PEG and DEX phases and collagen in a PCR tube (**Figure 4b**). Incubating the plate at 37°C led to the gelation of collagen that surrounded the spheroid (**Figure 4c**). We visually confirmed that the spheroid was embedded in collagen by performing this assay in a PCR tube (**Figure 4d**). Additionally, we removed the gelled collagen from the wells and mounted them on a glass slide for imaging (not shown).

Collagen embedding of spheroids has been previously done using different approaches. For example, after forming spheroids using a rocking method, spheroids were transferred into a well plate and then overlaid with a collagen solution (Liang et al., 2011). Liver cell spheroids were formed using a hanging drop method and transferred into a well plate containing a collagen solution to produce 3D collagen gel cultures (Yip and Cho, 2013). These methods of forming spheroids have several limitations such as medium evaporation from the hanging drops and difficulty of handling the hanging drop culture plates, and inconsistently-sized spheroids made with the plate rocking technique (Lemmo et al., 2014). More importantly, spheroids have to manually be transferred to another plate and the medium has to be removed before the collagen solution is dispensed onto the spheroids. This approach is labor-intensive and risks losing the spheroid during aspiration of medium. Unlike these methods, our method eliminates the tedious steps of transferring spheroids to a new plate and medium aspiration. We used the same ATPS formulation both to prepare spheroids and to partition collagen to embed the spheroids. The entire process was done in two pipetting steps (**Figure 4a**): First, a DEX phase drop containing cancer cells was dispensed into the PEG phase to form a spheroid in the drop phase. Then, a collagen-containing DEX phase drop was dispensed to merge with the spheroid containing drop and form a hydrogel that entrapped the spheroid. This approach significantly simplified the preparation of microtissues. Additionally, because partitioning of proteins in ATPS is independent of polymer concentrations (Albertsson, 1970), this approach can conveniently produce collagen gels of desired concentrations to reproduce mechanical properties of tumors *in vivo* (Plodinec et al., 2012), matrix stiffness and

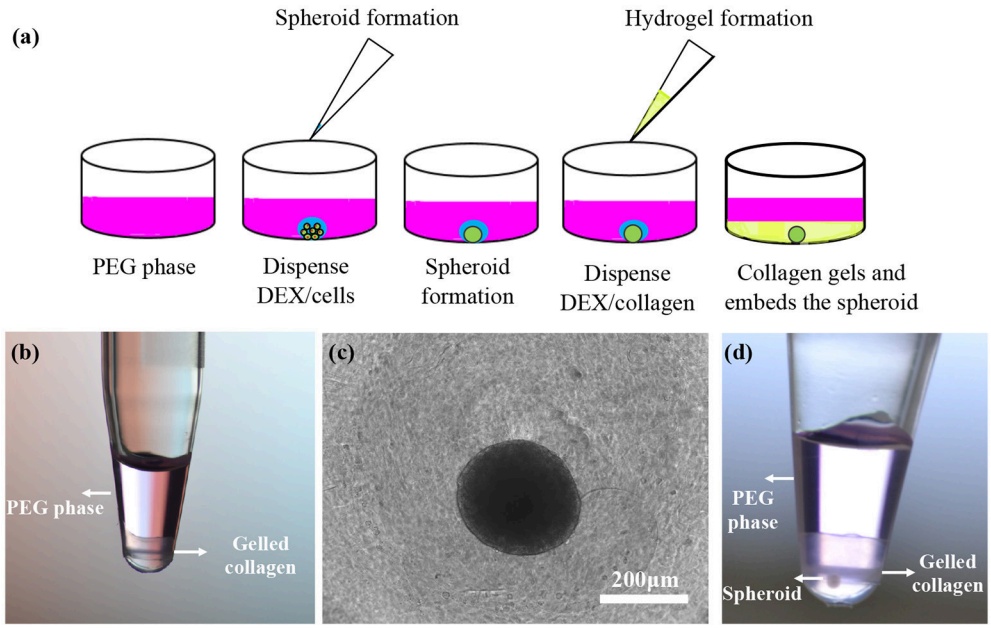


**FIGURE 4 | (a)** Schematic representation of spheroid formation and embedding in a collagen gel using ATPS in two pipetting steps. **(b)** A solution of 5 µL 14% DEX 500k and 5 µL 4 mg/ml collagen solution was dispensed into 30 µL of a 6.6% PEG 35k solution. Collagen gelled in the bottom phase during incubation. **(c,d)** Top and side views of a BT474 spheroid embedded in a collagen gel partitioned to the DEX phase.

porosity (Miron-Mendoza et al., 2010), and collagen permeability (Ramanujan et al., 2002). Our quantitative results of partition of collagen in ATPS (**Figure 3**) is key to facilitate this approach. This also allows us to produce hydrogels of different sizes and stiffness values simply by changing the volume of the DEX phase drops containing desired concentrations of collagen. This simplified approach is especially a major advantage for high throughput applications such as cancer drug screening (Shahi Thakuri et al., 2016). Encapsulating spheroids using collagen partitioning in ATPS is a novel technique to develop an *in vitro* 3D tumor model. More complex tumor models can also be conveniently developed by including other cellular components of tumor microenvironment such as fibroblasts and immune cells (Balkwill et al., 2012; Ham et al., 2016b, 2018).

## CONCLUSIONS

We used a quantitative approach to establish that collagen partitioning in polymeric ATPS is highly sensitive to polymer molecular weight. Using this property, we improved partitioning of collagen to the DEX phase of a PEG-DEX ATPS and employed this approach to conveniently develop physiologically-relevant *in vitro* 3D breast tumor models. This new technique will enable future studies to investigate the impact of components of tumor microenvironment on different functions of cancer cells.

## AUTHOR CONTRIBUTIONS

HT designed the project, helped write, and edited the manuscript. SS conducted experiments, analyzed data, and wrote the manuscript.

## ACKNOWLEDGMENTS

Financial support was provided by grant R15CA216413 from the 300 National Institutes of Health and grant 1801591 from National Science Foundation to HT. The authors are grateful to Dr. Ehsan Atefi for helping with constructing the binodal curves.

## SUPPLEMENTARY MATERIAL

The Supplementary Material for this article can be found online at: https://www.frontiersin.org/articles/10.3389/fchem.2018.00379/full#supplementary-material

## REFERENCES

Albertsson, P. Å., and Tjerneld, F. (1994). Phase diagrams. *Methods Enzymol.* 228, 3–13. doi: 10.1016/0076-6879(94)28003-7

Albertsson, P. A. (1961). Fractionation of particles and macromolecules in aqueous two-phase systems. *Biochem. Pharmacol.* 5, 351–358. doi: 10.1016/0006-2952(61)90028-4

Albertsson, P. A. (1970). Partition of cell particles and macromolecules in polymer two-phase systems. *Adv. Protein Chem.* 24, 309–341. doi: 10.1016/S0065-3233(08)60244-2

Albertsson, P. A., Cajarville, A., Brooks, D. E., and Tjerneld, F. (1987). Partition of proteins in aqueous polymer two-phase systems and the effect of molecular weight of the polymer. *Biochim. Biophys. Acta* 926, 87–93. doi: 10.1016/0304-4165(87)90185-1

Atefi, E., Fyffe, D., Kaylan, K. B., and Tavana, H. (2016). Characterization of Aqueous Two-phase systems from volume and density measurements. *J. Chem. Eng. Data* 61, 1531–1539. doi: 10.1021/acs.jced.5b00901

Atefi, E., Joshi, R., Mann, J. A., and Tavana, H. (2015). Interfacial tension effect on cell partition in aqueous two-phase systems. *ACS Appl. Mater. Interfaces* 7, 21305–21314. doi: 10.1021/acsami.5b05757

Atefi, E., Lemmo, S., Fyffe, D., Luker, G. D., and Tavana, H. (2014). High throughput, polymeric aqueous two-phase printing of tumor spheroids. *Adv. Funct. Mater.* 24, 6509–6515. doi: 10.1002/adfm.201401302

Balkwill, F. R., Capasso, M., and Hagemann, T., et al. (2012). The tumor microenvironment at a glance. *J. Cell Sci.* 125, 5591–5596. doi: 10.1242/jcs.116392

Gavasane, M. R., and Gaikar, V. G. (2003). Aqueous two-phase affinity partitioning of penicillin acylase from *E. Coli* in presence of PEG-derivatives. *Enzyme Microb. Technol.* 32, 665–675. doi: 10.1016/S0141-0229(03)00032-2

Ham, S. L., Joshi, R., Luker, G. D., and Tavana, H. (2016a). Engineered breast cancer cell spheroids reproduce biologic properties of solid tumors. *Adv. Healthc. Mater.* 5, 2788–2798. doi: 10.1002/adhm.201600644

Ham, S. L., Joshi, R., Thakuri, P. S., and Tavana, H. (2016b). Liquid-based three-dimensional tumor models for cancer research and drug discovery. *Exp. Biol. Med.* 241, 939–54. doi: 10.1177/1535370216643772

Ham, S. L., Thakuri, P. S., Plaster, M., Li, J., Luker, K. E., Luker, G. D., et al. (2018). Three-dimensional tumor model mimics stromal-breast cancer cells signaling. *Oncotarget* 9, 249–267. doi: 10.18632/oncotarget.22922

Johansson, G. (1970). Partition of salts and their effects on partition of proteins in a dextran-poly(ethylene glycol)-water two-phase system. *BBA Protein Struct.* 221, 387–390. doi: 10.1016/0005-2795(70)90283-7

Lemmo, S., Atefi, E., Luker, G. D., and Tavana, H. (2014). Optimization of aqueous biphasic tumor spheroid microtechnology for anti-cancer drug testing in 3D culture. *Cell. Mol. Bioeng.* 7, 344–354. doi: 10.1007/s12195-014-0349-4

Li, M., Kim, J. W., and Peeples, T. L. (2002). Amylase partitioning and extractive bioconversion of starch using thermoseparating aqueous two-phase systems. *J. Biotechnol.* 93, 15–26. doi: 10.1016/S0168-1656(01)00382-0

Liang, Y., Jeong, J., DeVolder, R. J., Cha, C., Wang, F., Tong, Y. W., et al. (2011). A cell-instructive hydrogel to regulate malignancy of 3D tumor spheroids with matrix rigidity. *Biomaterials* 32, 9308–9315. doi: 10.1016/j.biomaterials.2011.08.045

Miron-Mendoza, M., Seemann, J., and Grinnell, F. (2010). The differential regulation of cell motile activity through matrix stiffness and porosity in three dimensional collagen matrices. *Biomaterials* 31, 6425–6435. doi: 10.1016/j.biomaterials.2010.04.064

Moraes, C., Simon, A. B., Putnam, A. J., and Takayama, S. (2013). Aqueous two-phase printing of cell-containing contractile collagen microgels. *Biomaterials* 34, 9623–9631. doi: 10.1016/j.biomaterials.2013.08.046

Neuman, R. E., and Logan, M. A. (1950). The determination of hydroxyproline. *J. Biol. Chem.* 184, 299–306.

Plodinec, M., Loparic, M., Monnier, C. A., Obermann, E. C., Zanetti-Dallenbach, R., Oertle, P., et al. (2012). The nanomechanical signature of breast cancer. *Nat. Nanotechnol.* 7, 757–765. doi: 10.1038/nnano.2012.167

Ramanujan, S., Pluen, A., McKee, T. D., Brown, E. B., Boucher, Y., and Jain, R. K. (2002). Diffusion and convection in collagen gels: Implications for transport in the tumor interstitium. *Biophys. J.* 83, 1650–1660. doi: 10.1016/S0006-3495(02)73933-7

Schmidt, A. S., Ventom, A. M., and Asenjo, J. A. (1994). Partitioning and purification of α-amylase in aqueous two-phase systems. *Enzyme Microb. Technol.* 16, 131–142. doi: 10.1016/0141-0229(94)90076-0

Shahi Thakuri, P., Ham, S. L., Luker, G. D., and Tavana, H. (2016). Multiparametric analysis of oncology drug screening with aqueous two-phase tumor spheroids. *Mol. Pharm.* 13, 3724–3735. doi: 10.1021/acs.molpharmaceut.6b00527

SooHoo, J. R., and Walker, G. M. (2009). Microfluidic aqueous two phase system for leukocyte concentration from whole blood. *Biomed. Microdev.* 11, 323–329. doi: 10.1007/s10544-008-9238-8

Tavana, H., Jovic, A., Mosadegh, B., Lee, Q. Y., Liu, X., Luker, K. E., et al. (2009). Nanolitre liquid patterning in aqueous environments for spatially defined reagent delivery to mammalian cells. *Nat. Mater.* 8, 736–741. doi: 10.1038/nmat2515

Walter, H., and Larsson, C. (1994). Partitioning procedures and techniques: cells, organelles, and membranes. *Methods Enzymol.* 228, 42–63. doi: 10.1016/0076-6879(94)28006-1

Yip, D., and Cho, C. H. (2013). A multicellular 3D heterospheroid model of liver tumor and stromal cells in collagen gel for anti-cancer drug testing. *Biochem. Biophys. Res. Commun.* 433, 327–332. doi: 10.1016/j.bbrc.2013.03.008

**Conflict of Interest Statement:** The authors declare that the research was conducted in the absence of any commercial or financial relationships that could be construed as a potential conflict of interest.

frontiers in Chemistry

ORIGINAL RESEARCH
published: 02 October 2018
doi: 10.3389/fchem.2018.00454

# Factorial and Economic Evaluation of an Aqueous Two-Phase Partitioning Pilot Plant for Invertase Recovery From Spent Brewery Yeast

*Patricia Vázquez-Villegas*[1†], *Edith Espitia-Saloma*[1†], *Mario A. Torres-Acosta*[1], *Federico Ruiz-Ruiz*[1], *Marco Rito-Palomares*[2] *and Oscar Aguilar*[1*]

[1] Escuela de Ingenieria y Ciencias, Tecnologico de Monterrey, Monterrey, Mexico, [2] Escuela de Medicina y Ciencias de la Salud, Tecnologico de Monterrey, Monterrey, Mexico

Aqueous two-phase systems (ATPS) have been reported as an attractive biocompatible extraction system for recovery and purification of biological products. In this work, the implementation, characterization, and optimization (operational and economic) of invertase extraction from spent brewery yeast in a semi-automatized pilot plant using ATPS is reported. Gentian violet was used as tracer for the selection of phase composition through phase entrainment minimization. Yeast suspension was chosen as a complex cell matrix model for the recovery of the industrial relevant enzyme invertase. Flow rates of phases did not have an effect, given that a bottom continuous phase is given, while load of sample and number of agitators improved the recovery of the enzyme. The best combination of factors reached a recovery of 129.35 ± 2.76% and a purification factor of 4.98 ± 1.10 in the bottom phase of a PEG-Phosphate system, also resulting in the removal of inhibitor molecules increasing invertase activity as reported by several other authors. Then, an economic analysis was performed to study the production cost of invertase analyzing only the significant parameters for production. Results indicate that the parameters being analyzed only affect the production cost per enzymatic unit, while variations in the cost per batch are not significant. Moreover, only the sample load is significant, which, combined with operational optimization results, gives the same optimal result for operation, maximizing recovery yield (15% of sample load and 1 static mixer). Overall res ults of these case studies show continuous pilot-scale ATPS as a viable and reproducible extraction/purification system for high added-value biological compounds.

**Keywords: aqueous two-phase system, biosolve, invertase, operational parameters, pilot plant, spent yeast**

OPEN ACCESS

***Edited by:***
*Brendan M. Leung,*
*Dalhousie University, Canada*

***Reviewed by:***
*Maria Graca Rasteiro,*
*University of Coimbra, Portugal*
*Gaurav Chaudhary,*
*Bundelkhand University, India*

***Correspondence:**
*Oscar Aguilar*
*alex.aguilar@itesm.mx*

[†]*These authors have contributed equally to this work*

***Specialty section:***
*This article was submitted to Chemical Engineering, a section of the journal Frontiers in Chemistry*

***Received:*** *29 May 2018*
***Accepted:*** *13 September 2018*
***Published:*** *02 October 2018*

***Citation:***
*Vázquez-Villegas P, Espitia-Saloma E, Torres-Acosta MA, Ruiz-Ruiz F, Rito-Palomares M and Aguilar O (2018) Factorial and Economic Evaluation of an Aqueous Two-Phase Partitioning Pilot Plant for Invertase Recovery From Spent Brewery Yeast. Front. Chem. 6:454. doi: 10.3389/fchem.2018.00454*

## INTRODUCTION

With the improvement in recombinant technologies, great progress has been taking place in the upstream processes of bioproducts manufacturing. However, with the increasing of cell culture titers the downstream processing capacity arises as a bioprocessing bottleneck (Lowe, 2001; Rosa et al., 2010; Langer, 2011; Straathof, 2011; Dizon-Maspat et al., 2012; Sabalza et al., 2014). The currently available purification technology typically include unit operations with limited

operational windows or scaling up drawbacks, besides the use of high cost equipment (Xu et al., 2003; Aguilar et al., 2010; Rosa et al., 2011; Goja et al., 2013). This has promoted the development and implementation of alternative, easily scalable extraction procedures and purification systems that allow higher throughputs.

During the last decades, several research groups have consistently reported the advantages that aqueous two-phase systems (ATPS) possess as an extraction/purification technique: they show biological compatibility, high load capacity, scale-up easiness and continuous operation, among others (Raghavarao et al., 2003; Benavides and Rito-Palomares, 2008; Rosa et al., 2010; Asenjo and Andrews, 2012)]. There are some works on semi-continuous/pilot plant ATPS (Minuth et al., 1997; Huenupi et al., 1999; Kepka et al., 2003; Igarashi et al., 2004; Rosa et al., 2009; Sutherland et al., 2011), however, most of the practical attempts to apply ATPS have been carried out in batch mode or at bench scale. This makes continuous operation at pilot scale an open research area for the implementation of ATPS processes (Rosa et al., 2010; Benavides et al., 2011; Espitia-Saloma et al., 2014). Continous operation is acknowledged for its positive impact in processing time, costs and yields, having the potential to make bioproducts economically competitive at larger scales (Igarashi et al., 2004; Benavides et al., 2011). Conventional equipment used by the chemical industry for organic-aqueous extraction, such as column contactors, has been mostly employed for large-scale and continuous ATPS applications (Cuhna and Aires-Barros, 2002). However, the study of alternative equipment configurations such as mixer settlers and the development of novel separators for different ATPS variants, bioproducts and physicochemical characteristics could increase the interest toward the industrial implementation of continuous ATPS-based processes (Cuhna and Aires-Barros, 2002; Benavides and Rito-Palomares, 2008; Torres-Acosta et al., 2016). Recently, Vázquez-Villegas et al. (2011), proposed a novel mixer-settler device for continuous ATPS operation at bench scale. It is based on a tubular reactor approach with a large and adjustable length/diameter ratio to control settling time and separation of phases (Vázquez-Villegas et al., 2011).

Pilot plant studies, are of noteworthy value in the development of new processes, since they allow the study, in an efficient and relatively economic way, of different technical aspects (operation conditions, design parameters, construction materials, corrosion, and operational procedures) essential for any industrial process. The objective of this work is to present a continuous ATPS-based process at pilot plant level, and evaluate its operational and economic performance for the extraction of invertase from spent brewery yeast.

# MATERIALS AND METHODS

## Chemicals and Biological Material

Polyethylene glycol with molecular weight of 1,000 Da (PEG1000) was purchased from Avizor Química (Monterrey, Mexico). Gentian violet (GV) and bovine serum albumin (BSA) were obtained from Sigma Aldrich (St. Louis, MO, USA). Monobasic and dibasic potassium phosphate and other analytical grade reagents were purchased from Desarrollo de Especialidades Químicas (DEQ, Monterrey, Mexico). Spent brewery yeast was kindly donated by Cervecería Cuauhtémoc-Moctezuma, S.A. de C.V (Nuevo León, México).

### Spent Brewer's Yeast Preparation

Spent brewer's yeast, directly obtained from brewery, was centrifuged at 4,300 rpm at 4°C for 10 min (Thermo Scientific IEC CL40R, WaltHam, USA). The supernatant was discarded. The biomass was resuspended (40% w/v) in 50 mM phosphate buffer at pH 7. Cell disruption was accomplished in a bead mill with 0.5 mm glass beads (Dyno Mill-Multi Lab, Muttenz, Switzerland). The grinding chamber was initially filled with a 50% v/v bead load and the biomass was fed with a peristaltic pump (Watson–Marlow 323 S/D) at 5 mL/min and recirculated for 15 min. Temperature was kept constant at 4°C. The disrupted cell suspension was directly loaded into the ATPS.

## Preparation of ATPS

Two basic ATPS compositions were studied for their influence in performance of the pilot plant based on previous experiences, System 1: 17% w/w PEG 1000 and 15.2% w/w potassium phosphates and System 2: 14% w/w PEG 1000 and 18% w/w potassium phosphates. In all the cases the potassium phosphates mixture was composed of a 1.82:1 dibasic and monobasic potassium phosphates ratio to obtain a pH of 7. For the stock solutions, potassium phosphate and PEG 1000 were weighed separately and mixed with the appropriate amount of distilled water until complete dissolution.

## Batch ATPS

In order to compare the performance of the continuous system, ATPS batch systems were prepared with the same volume and composition as the total processed volume in the pilot plant continuous system (9 L of bottom phase and 3 L of top phase). The sample was pre-dissolved in the total initial bottom phase at the same concentration as the one employed in the continuous system. Afterwards, the top phase was added and the system was stirred for 10 min. At the end of the mixing stage samples from the top and bottom phases of the batch system were taken manually from the middle of each phase bulk every minute.

## Pilot Plant Configuration and Operating Procedure

The pilot plant prototype was manufactured in stainless steel by Patmon Automatización (Nuevo León, México). As shown in **Figures 1A,B** it consists of 5 main stages: ATPS formulation and storage of feeding stocks, a series of in-line static mixers (adaptable from 1 to 4 static mixers), an adaptable length polyurethane tubular coalescer (6.5 m long), a liquid-liquid gravity separator with three outlets for recollecting top, bottom phase and interface and three final phase storage tanks. Phases and sample are fed with three digital solenoid dosing metering pumps with maximum capacity of 1.5 L/min (Tekna Evo, Seko GmbH, Kastel, Germany). The static mixers are conformed of acrylic cylindrical columns with a stainless steel screw and nut packing. The gravity separator consists of a rectangular

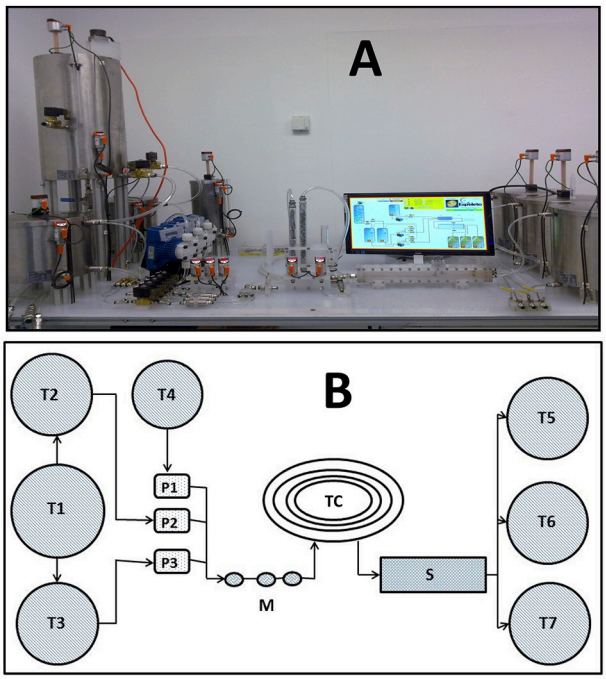


**FIGURE 1 |** Front view of the pilot plant configuration **(A).** Top view diagram **(B)** showing the main elements: Feeding tanks (**T1**, **T2**, **T3**, **T4**), Pumps (**P1**, **P2**, **P3**), Static mixers (**M**), Tubular Coalescer (**TC**), Gravity Separator (**S**), Recollecting tanks (**T5**, **T6**, **T7**).

**TABLE 1 |** Dimensions of the scaled-up prototype components.

| Pilot plant component | Dimension |
|---|---|
| Feeding tanks | TP tank (T2) volume: 16 L<br>BP tank (T3) volume: 16 L<br>Sample tank (T4) volume: 5.5 L |
| Static mixers | Length: 23.5 cm<br>Internal diameter: 2 cm<br>Void volume: 43.8 $cm^3$ |
| Phase coalescer | Internal diameter: 1 cm<br>Length: adaptable (3-6 m) |
| Separator | Inlet diameter: 1.27 cm<br>Outlets diameter: 0.64 cm<br>Length: 43 cm<br>Width: 7.7 cm<br>Height: 7.7 cm<br>Internal volume: 800 mL |
| Final recollecting tank | TP tank (T5) volume: 23 L<br>IP tank (T6) volume: 23 L<br>BP tank (T7) volume: 23 L |

**TABLE 2 |** Variables and levels of the central composite design (CCD) carried out for enzyme recovery from spent brewer's yeast using the pilot plant prototype.

| | Studied variables | Levels | |
|---|---|---|---|
| | | -1 | 1 |
| $x_1$ | Top phase feed flow (mL/min) | 100 | 300 |
| $x_2$ | Bottom phase feed flow (mL/min) | 200 | 400 |
| $x_3$ | Sample load percentage | 5 | 15 |
| $x_4$ | Number of static mixers | 1 | 3 |

container (round shaped inner corners) with one inlet and three vertical aligned outlets. Additional information about the pilot plant dimensions can be found in **Table 1**. Pilot plant operation was semi-automatized using a programmable logic controller (PLC) (IFM Efector, Nuevo León, México) allowing independent control of the flows.

Pilot plant runs were carried out at room temperature (25°C). The corresponding ATPS were mixed and equilibrated in tank T1. Afterwards top and bottom phases were separated through solenoid valves into T2 and T3 respectively. Starting in T4, the disrupted cell suspension was fed independently. Knowing its density as well of that of both phases, the feeding flow was setted up. Samples were taken every minute from the outlets to the final recollecting tanks during 30 min runs.

## Evaluation of Operational Performance

Phase entrainment profile (defined as the amount of carry-over of one phase into the other) was first studied with the two different system compositions, using a dye (gentian violet) as tracer (Giraldo-Zuniga et al., 2006). Entrainment behavior was compared with a batch system to choose the appropriate system composition. Dye concentration in top phase was also measured (580 nm, Bio-Tek Instruments, VT, U.S.A.). After the selection of the system that generated lower entrainment in the bottom phase, a duplicate full $2^4$ factorial design augmented with 6 center points was carried out (**Table 2**). This experimental design was implemented in order to study the effect of phases flow rates, number of static mixers and load of sample over invertase purification factor ($PF_{BP}$) and activity recovery ($R_{BP}$) in bottom phase as well as entrainment in that phase ($E_{BP}$), calculated as:

$$PF_{BP} = \frac{\left(\frac{EA}{Total\ protein}\right)_{BP}}{\left(\frac{EA}{Total\ protein}\right)_{0}} \quad (1)$$

$$R_{BP} = \frac{EA_{BP}}{EA_0} \quad (2)$$

$$E_{BP} = \frac{V_{TP}}{V_{TP} + V_{BP}} \quad (3)$$

Where $EA_0$ represents the enzymatic activity on the disrupted yeast supernatant, while $V_{BP}$ represents the bottom phase volume and $V_{TP}$ represents the top phase volume measured in the final recollecting tanks of the pilot plant. All experiments and replicates were modeled and analyzed with JMP 14.1.0 data software (SAS Institute, Cary, NC, USA) and response surface using Minitab 18 software (Minitab Inc.).

## Evaluation of Economic Performance

To perform an economic analysis, the commercial software platform Biosolve Process (Biopharm Services, Chesham, Buckinghamshire, UK) was used. For this, the methodology

presented before was followed (Torres-Acosta et al., 2016). Briefly, a model was created with which a determinisitic analysis was done to obtain the production cost per batch (CoG/batch) and cost per enzymatic unit (CoG/EU). Then production parameters were varied only in the selected ATPS from the previous section to analyze from an economic perspective the significant results from the factorial design experiments.

To create a model for the production of invertase, the process was simplified into a single unit operation which processed the total amount of sample and materiales required for the operation, then it was calculated the production cost per batch (CoG/batch) and per enzymatic unit (CoG/EU). To set up the model, the data presented in **Table 3** was used. Briefly, to fully construct a model, four main datasets should be completed: (1) capital, (2) materials, (3) consumables, and (4) labor.

Capital was calculated only taking into account equipment cost, as this process is performed in an already equipped space and only the acquisition of the main device and its static mixers for the performance of continuous ATPS were required. To obtain the capital charge per batch or per enzymatic unit, the cost of the equipment required was treated as a loan with 12% interest rate with a 10 years duration. Then it was divided by the year duration and by batches calculated per year (2.5 h per ATPS run−30 min runs plus setup and cleaning time).

Materials for this model only include those involved in the construction of the systems employed here (Polyethylene glycol 1,000 Da and monobasic and dibasic potassium phosphate). This particular process has the advantage of not requiring consumables, contrasted to other unit operations, like chromatography or different filtration types. Lastly, labor was calculated using the salary of a PhD student, as production was done like this in the pilot plant. Additionally, Biosolve is able to integrate a fifth area called "Others," in which maintance, waste disposal and utilities costs are automatically calculated. For this model it was calculated to be approximately 4.5% of the CoG/EU.

## Analytical Techniques

Invertase enzymatic activity was determined by the 3,5-dinitrosalycilic acid method (DNS, 98%, Sigma Aldrich) (Miller, 1959). Absorbance was read at 570 nm in a microplate spectrophotometer (Biotek, Vermont, USA). One unit of enzymatic activity (U) was defined as the amount of enzyme necessary to produce 1 μmol of glucose per minute in the assay reaction conditions. Total protein was calculated using the Bradford method and a calibration curve using BSA as protein standard (Bradford, 1976).

# RESULTS AND DISCUSSION

The knowledge of the system hydrodynamics is essential in extraction processes. Usually, the performance of liquid-liquid extraction systems can be affected for unwanted side effects related to hydrodynamic parameters (Asadollahzadeh et al., 2017). As an example, while low phase entrainment results in higher yields, some works, have demonstrated that mass transfer is improved in simplified equipments where the operating range is increased (Glyck et al., 2015). In recent years, the hydrodynamic parameters of different kinds of extraction columns have been investigated by several researchers but not for ATPS systems in pilot plant scale. In the present work, the design of a pilot plant ATPS continuous process has been simplified and optimized in terms of separation efficiency, load capacity, and economic suitability for downstream processing of spent brewery yeast as a model system.

Considering two ATPS compositions previously explored for the recovery of enzymes (Vázquez-Villegas et al., 2011, 2015), phase entrainments were compared. Top phase fed (TP) at 100 mL/min and bottom phase fed (BP) at 300 mL/min were employed. The stabilization time was defined as the time in which entrainment ($E_{BP}$) of bottom phase (or top phase) in the opposite phase does not change significantly for a period of 5 min. Entrainment was defined constant when the change is no more than 10% of the previous value. For System 1 the stabilization time was ca. 20 min, while for System 2 the time for complete separation of phases was almost immediate (**Figures 2A,B**). In this case, a larger difference between the composition of the two phases (typically expressed as the tie-line length value, TLL) benefits the equilibrium and separation of the ATPS yielding shorter processing times. This increment in the demixing rate as consequence of a higher TLL agrees with previous observations (Salamanca et al., 1998; Aguilar and Rito-Palomares, 2008; Narayan et al., 2011). Just for comparison, the concentration of GV in top phase was monitored. While the dye concentration was the same at the end of the sampling, a faster equilibrium was observed also in the System 2 (**Figure 2C**). So, this system was selected for the next experiments. The influence of physicochemical parameters on the separation efficiency when using mixer settler devices has been previously studied (Salamanca et al., 1998; Vázquez-Villegas et al., 2011). In these cases, as in this pilot plant, the operating volume ratio of the phases (defined as the ratio of top phase between bottom phase feeding flows) defines which of the phases acts as the continues or the dispersed phase, where the viscosities play a determinant factor for phase separation. A continuous salt phase, being much less viscous than the polymer phase, favors shorter separation times by lowering the friction between drops and the phase (Asenjo and Andrews, 2012).

Spent brewer's yeast was used as model of complex cellular matrix to challenge the recovery of invertase with the continuous pilot-scale device. Anticipating an altered hydrodynamic behavior of the effluents, due to the complex matrix addition, a full $2^4$ factorial experimental design with six central points was performed (**Table 2**). The experimental design allowed the analysis of the partitioning behavior patterns due to changes in the operation parameters. The ideal scenario for any enzyme will be having the optimal conditions for maximizing purity and recovery. In the case of invertase, when the results of different factor combinations were analyzed, an average of 110.98 ± 28.44 % for recovery and 4.47 ± 2.46 for purification fold in the bottom phase were obtained as a total average from the full factorial runs. The high variability observed is explained by the difference in response obtained at different factor levels. Enzyme activity recoveries above 100% have been extensively

**TABLE 3 |** Dataset used for model construction in Biosolve Process.

| | Cost component | Cost (US $) | Supplier |
|---|---|---|---|
| Capital *(Equipment)* | Main equipment | $ 35,240.90 | Patmon Automatizacion |
| | Static mixer | $ 836.27 | USA Blue Book |
| Consumables | None Required | $ – | None |
| Labor | Annual Salary (PhD Student in Mexico) | $ 8,520.00 | Conacyt (Mexican Science Council) |
| Materials *(Prices used were obtained for large-laboratory scale to overestimate worldwide distribution)* | Polyethylene Glycol 1,000 (1 kg) | $ 56.20 | Sigma-Aldrich |
| | Potassium phosphate monobasic (20 kg) | $ 607.70 | Sigma-Aldrich |
| | Potassium phosphate dibasic (10 kg) | $ 1,020.00 | Sigma-Aldrich |

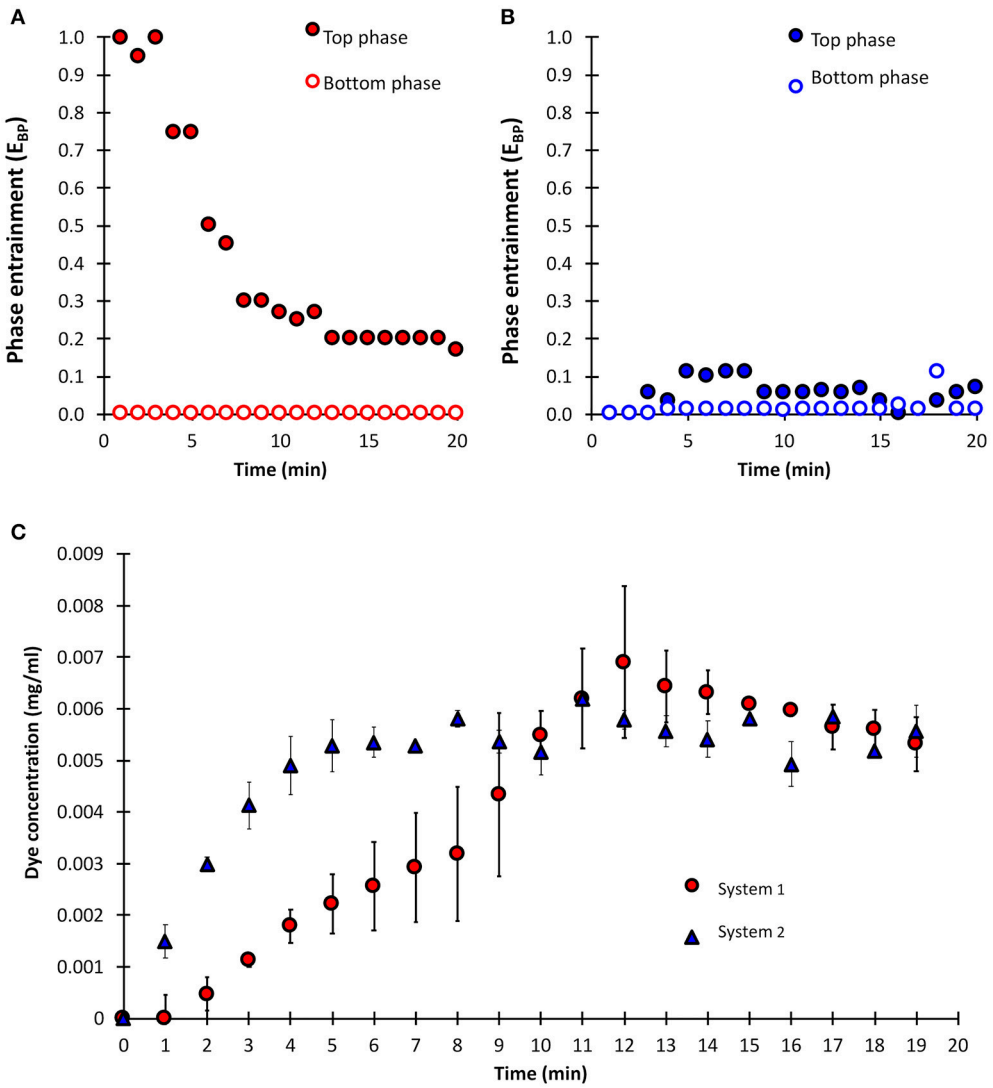


**FIGURE 2 |** Phase entrainment ($E_{BP}$) comparison between System 1 **(A)** and System 2 **(B).** Concentration of gentian violet used as tracer in top phase of Systems 1 and 2 **(C)**.

documented for invertase and other enzymes when recovered using ATPS (Cavalcanti et al., 2006; Babu et al., 2008; Porto et al., 2008; Madhusudhan and Raghavarao, 2011; Nandini and Rastogi, 2011; Rawdkuen et al., 2011; Karkas and Onal, 2012; Priyanka et al., 2012; Duque-Jaramillo et al., 2013; Ketnawa et al., 2014, 2017) and this phenomenon is attributed to the depletion

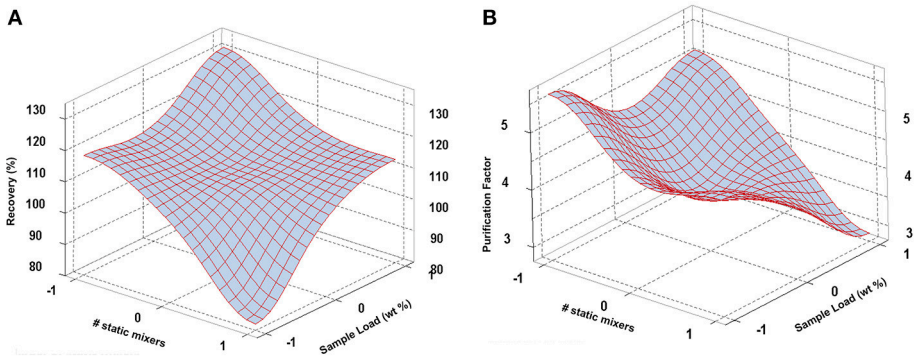


**FIGURE 3 |** Response surface plots for recovery yield **(A)** and purification factor **(B)** of invertase from spent brewer's yeast considering the effect of sample load (X3) and number of static mixers (X4).

**TABLE 4 |** Results for the economic analysis. Breakdown and totals for cost of Goods per Enzymatic Unit.

| CoG/EU (US$ x 10^-3) | | | | | | | | |
|---|---|---|---|---|---|---|---|---|
| **Sample load** | **Static mixers** | **Recovery yield** | **Capital** | **Materials** | **Consumables** | **Labor** | **Other** | **Total** |
| 5% | 1 | 115% | $0.34 | $15.86 | $ – | $4.91 | $1.01 | $22.12 |
| 5% | 3 | 80% | $0.51 | $22.79 | $ – | $7.06 | $1.46 | $31.82 |
| 15% | 1 | 142% | $0.09 | $4.28 | $ – | $1.33 | $0.27 | $5.97 |
| 15% | 3 | 108% | $0.13 | $5.63 | $ – | $1.74 | $0.36 | $7.86 |

of inhibiting proteins and common enzyme inhibitors by differential partitioning. Common identified inhibitors include Cu, Co and Ni salts which become insoluble in the presence of the high phosphate concentrations in ATPS. Enzyme activation has also been observed in ATPS due to an increase in the enzyme flexibility and the structural modification of the active sites in the presence of polymer chains of PEG (Babu et al., 2008; Porto et al., 2008; Madhusudhan and Raghavarao, 2011; Nandini and Rastogi, 2011; Karkas and Onal, 2012). Cavalcanti et al. (2006) in extraction studies of phospholipase C, used a similar PEG/phosphate ATPS and reported yields up to 230% attributed to removal of inhibiting phenoic compounds (Duque-Jaramillo et al., 2013).

The best combination of factors (1 mixer and 15% sample load) attained a recovery of 129.35 ± 2.76% and a purification factor of 4.98 ± 1.10 in the bottom phase of a PEG-phosphate system; however, only the sample load and the number of static mixers were significant, thus a surface response analysis was performed. As observed in **Figure 3**, higher sample load yielded major recoveries and slightly minor purity, as it would naturally occur, while for the number of mixers, the use of one static mixer yielded higher values for both recovery and purification factor. This would mean that the higher the mixing rate, for this particular system, the lower the efficiency of the pilot plant in terms of recovery and purification. This could be better explained when considering the amount of other contaminants also partitioning or dispersing into the bottom phase, promoted by higher mixing rates. Also, higher mixing promotes lower coalescence rates that could affect separation efficiency resulting in the lower purification observed in **Figure 3B** (Asenjo and Andrews, 2012). The high statistical variability of purification factor could also be the result of poor separation efficiency. For invertase, other studies have shown a tendency to partition toward the bottom phase in PEG/salt systems (Madhusudhan and Raghavarao, 2011; Karkas and Onal, 2012; Vázquez-Villegas et al., 2015), as it was observed in the present work. Taking this into account, the economic analysis was carried out.

The economic analysis performed obtained interesting results that further help to elucidate which parameters are relevant for the continuous operation of an ATPS pilot plant. With the results presented here (**Table 4**), linear regressions were calculated to summarize the effect of each variable and to determine which are economically significant. Results show that the only significant parameter is the sample load, while number of static mixers is not (**Table 5**). This can be explained by the fact that increasing the load of sample directly affects the amount of invertase being recovered, moreover, an increase in sample load gave as a result an increased recovery yield. On the other hand, modifying the amount of static mixers increased the capital charge in the cost but given the elevated cost of the main equipment, variations in the cost due to modifying the number of mixers are diluted.

From an economic perspective, it is relevant to maximize the sample load in an ATPS. It has been discussed before (Aguilar and Rito-Palomares, 2008; Torres-Acosta et al., 2015, 2016) that due to low sample input into an ATPS, costs cannot be further decreased. Sample load increases cannot be used lightly in bioprocess modeling as the physics underlying

**TABLE 5 |** Linear regression results.

| Parameters* | Coefficient | *p*-value | Significant?[a] |
|---|---|---|---|
| *Intercept* ($\beta_0$) | 29.71 | 0.0292 | Yes |
| *Sample Load* ($\beta_1$) | −1.71 | 0.0339 | Yes |
| *Static Mixers* ($\beta_2$) | 1.39 | 0.2001 | No |

**Equations of linear regression have the form: CoG/EU [US$ x10-3] = β0 + β1 x Sample Load [%] + β2 x Static Mixers [Amount of mixers].*
*[a] Using a significance level α = 0.05.*

protein separation are too complex to model and it is not certain the effect that modifying the amount of sample can have on the recovery yield and purification factor. However, having a proper analysis of sample input in this work, its impact in the economic analysis can be determined and quantified.

Further analysis is required to contrast continuous and batch operation modes. Still, results for recovery and economics together are promising, moreover if operational parameters can be further optimized production costs will drop. Having a continues ATPS, together with a phase forming chemical removal operation synchronized can significantly reduce production times and costs.

Novel strategies for the high throughput design of ATPS-based processes (microfluidic modeling) as well as different modes of operations (countercurrent modes) could also be considered in the process to optimize performance of continuous processes (Espitia-Saloma et al., 2016; Vázquez-Villegas et al., 2016). This work highlights the importance of the influence of the system properties on the hydrodynamics of the bioseparation process. In some case studies, TLL has little or no influence on the partition behavior of the desired product (Aguilar and Rito-Palomares, 2008), allowing the selection of the best system in terms of the hydrodynamic behavior in the equipment. It should be emphasized that even in a batch process the phase separation stage would imply a phase entrapment, meaning a carry-over of one phase into the other, and time (or a centrifuge) needed for the physical separation. In this continuous mode, the physical separation of the phases is already accounted as part of the stabilization time, the time in which the evaluated parameter ($E_i$) begins to be constant.

## CONCLUSIONS

The recovery of products of interest from fermentation broths and biological feedstock is one of the major bottlenecks in the bioprocessing industries. This article introduces a first approach for continuous pilot plant ATPS operation and process establishment. A robust, large-scale, automated process able to be managed by simple development strategies such as factorial and central composite designs was established in this work.

A semi-automatized mixer settler pilot plant with a maximum capacity of 1.5 L/min was characterized. The use of single molecule samples allowed to demonstrate some of the recognized advantages of continuous operation over batch mode. Short stabilization times inside the coalescer avoid the use of centrifugation steps, as typically suggested in batch processes, also contributing to process integration, as evidenced by processing a complex sample such as non-clarified spent brewer's yeast. Different combination of hydrodynamic operation parameters allowed the high yield recovery and the highest purification fold of invertase from a complex cell lysate. Adjustments in phases flows did not altered the extraction efficiency of the pilot plant. This works serves to boost the application of ATPS in different operation modes by combining a techno-economic approach to evaluate and optimize production parameters that can facilitate ATPS generic and commercial adoption.

## AUTHOR CONTRIBUTIONS

PV-V, EE-S, and FR-R performed experiments with pilot plant equipment, analytical assays, and wrote the paper. MT-A and FR-R performed economical analysis of the results. MR-P and OA designed the research, analyzed data and revised economical analysis performed. All authors read and approved the final manuscript.

## FUNDING

The authors wish to acknowledge the financial support of the Bioprocess and Synthetic Biology Research Group (GEE002EICIP01), Nutrigenomic Research Chair of Tecnológico de Monterrey and CONACYT for the doctoral scholarship of EE-S No. 246739.

## REFERENCES

Aguilar, O., and Rito-Palomares, M. (2008). Processing of soybean (*Glycine max*) extracts in aqueous two-phase systems as a first step for the potential recovery of recombinant proteins. *J. Chem. Technol. Biotechnol.* 83, 286–293. doi: 10.1002/jctb.1805

Aguilar, O., Rito-Palomares, M., and Glatz, C. E. (2010). Coupled application of aqueous two-phase partitioning and 2D-electrophoresis for characterization of soybean proteins. *Sep. Sci. Technol.* 45, 2210–2225. doi: 10.1080/01496395.2010.507648

Asadollahzadeh, M., Torkaman, R., and Torab-Mostaedi, M. (2017). New correlations for slip velocity and characteristic velocity in rotary liquid-liquid extraction column. *Chem. Eng. Res. Des.* 127, 146–153. doi: 10.1016/j.cherd.2017.07.032

Asenjo, J. A., and Andrews, B. A. (2012). Aqueous two-phase systems for protein separation: phase separation and applications. *J. Chromatogr. A* 18, 1–10. doi: 10.1016/j.chroma.2012.03.049

Babu, R. B., Rastogi, N. K., and Raghvarao, K. S. M. S. (2008). Liquid-liquid extraction of bromelain and polyphenol oxidase using aqueous two-phase system. *Chem. Eng. Process.* 47, 83–89. doi: 10.1016/j.cep.2007.08.006

Benavides, J., and Rito-Palomares, M. (2008). Practical experiences from the development of aqueous two phase processes for the recovery of high value biological products. *J. Chem. Technol. Biotechnol.* 83, 133–142. doi: 10.1002/jctb.1844

Benavides, J., Rito-Palomares, M., and Asenjo, J. A. (2011). Aqueous two-phase systems. *Compr. Biotechnol.* 2, 697–713. doi: 10.1016/B978-0-08-088504-9.00124-0

Bradford, M. (1976). A rapid and sensitive method for the quantitation of microgram quantities of protein utilizing the principle of protein–dye binding. *Anal. Biochem.* 72, 248–254.

Cavalcanti, M. T., Porto, T. S., de Barros Neto, B., Lima-Filho, J. L., Porto, A. L., and Pessoa A Jr., (2006). Aqueous two-phase systems extraction of alpha-toxin from *Clostridium perfringens* type A. *J. Chromatog. B.* 833, 135–140. doi: 10.1016/j.jchromb.2006.01.023

Cuhna, T., and Aires-Barros, R. (2002). Large scale extraction of proteins. *Mol. Biotechnol.* 20, 29–40. doi: 10.1385/MB:20:1:029

Dizon-Maspat, J., Bourret, J., D'Agostini, A., and Li, F. (2012). Single pass tangential flow filtration to debottleneck downstream processing for therapeutic antibody production. *Biotechnol. Bioeng.* 109, 962–970. doi: 10.1002/bit.24377

Duque-Jaramillo, P. M., Rocha-Gomes, H. A., de Siqueira, F. G., Homem-de-Mello, M., Ximenes-Ferreira-Filho, E., and Magalhães, P. O. (2013). Liquid–liquid extraction of pectinase produced by Aspergillus oryzae using aqueous two-phase micellar system. *Sep. Pur.echnol.* 120, 452–457. doi: 10.1016/j.seppur.2013.09.020

Espitia-Saloma, E., Vázquez-Villegas, P., Aguilar, O., and Rito-Palomares, M. (2014). Continuous aqueous two-phase systems devices for the recovery of biological products. *Food. Bioprod. Process.* 92, 101–112. doi: 10.1016/j.fbp.2013.05.006

Espitia-Saloma, E., Vázquez-Villegas, P., Rito-Palomares, M., and Aguilar, O. (2016). An integrated practical implementation of continuous aqueous two-phase systems for the recovery of human IgG: from the microfluidic device to a multistage bench-scale mixer-settler device. *Biotechnol. J.* 11, 708–716. doi: 10.1002/biot.201400565

Giraldo-Zuniga, A. D., Coimbra, J. S. R., Minim, L. A., and Garcia, R. E. E. (2006). Dispersed phase hold-up in a Graesser raining bucket contactor using aqueous two phase systems. *J. Food Eng.* 72, 302–309. doi: 10.1016/j.jfoodeng.2004.11.037

Glyck, A., Scheper, T., and Beutel, S. (2015). PEG–salt aqueous two-phase systems: an attractive and versatile liquid–liquid extraction technology for the downstream processing of proteins and enzymes. *App. Microbiol. Biotechnol.* 99, 6599–6616. doi: 10.1007/s00253-015-6779-7

Goja, A. M., Yang, H., Cui, M., and Li, C. (2013). Aqueous two-phase extraction advances for bioseparation. *J. Bioproces. Biotechniq.* 4, 1–8. doi: 10.4172/2155-9821.100014

Huenupi, E., Gomez, A., Andrews, B. A., and Asenjo, J. A. (1999). Optimization and design considerations of two-phase continuous protein separation. *J. Chem. Technol. Biotechnol.* 74, 256–263. doi: 10.1002/(SICI)1097-4660(199903)74:3<256::AID-JCTB27>3.0.CO;2-8

Igarashi, L., Kieckbusch, T. G., and Franco, T. T. (2004). Xylanase mass transfer studies in aqueous two-phase systems using spray and sieve plate columns. *Bioproc. Biosyst. Eng.* 26, 151–157. doi: 10.1007/s00449-003-0329-x

Karkas, T., and Onal, S. (2012). Characteristics of invertase partitioned in poly(ethylene glycol)/magnesium sulfate aqueous two-phase system. *Biochem. Eng. J.* 60, 142–150. doi: 10.1016/j.bej.2011.11.005

Kepka, C., Collet, E., Persson, J., Stahl, A., Lagerstedt, T., Tjerneld, F., et al. (2003). Pilot-scale extraction of an intracellular recombinant cutinase from *E. coli* cell homogenate using a thermoseparating aqueous two-phase system. *J. Bioctechnol.*103, 165–181. doi: 10.1016/S0168-1656(03)00104-4

Ketnawa, S., Benjakul, S., Ling, T. C., Matinez-Alvarez, O., and Rawdkuen, S. (2014). Enhanced recovery of alkaline protease from fish viscera by phase partitioning and its application. *Chem. Cent. J.* 7, 79–86. doi: 10.1186/1752-153X-7-79

Ketnawa, S., Rungraeng, N., and Rawdkuen, S. (2017). Phase partitioning for enzyme separation: An overview and recent applications. *Int. Food Res. J.* 24, 1–24.

Langer, E. (2011). Alleviating downstream process bottlenecks. *GEN.* 31, 1–49. doi: 10.1089/gen.31.13.18

Lowe, C. R. (2001). Combinatorial approaches to affinity chromatography. *Curr. Opin. Chem. Biol.* 5, 248–256. doi: 10.1016/S1367-5931(00)00199-X

Madhusudhan, M., and Raghavarao, K. S. M. S. (2011). Aqueous two phase extraction of invertase from baker's yeast: effect of process parameters on partitioning. *Process Biochem.* 46, 2014–2020. doi: 10.1016/j.procbio.2011.07.014

Miller, G. L. (1959). Use of dintrosalicylic acid reagent for determination of reducing sugar. *Anal. Chem.* 31, 426–428. doi: 10.1021/ac6014 7a030

Minuth, T., Gieren, H., Pape, U., Raths, H. C., Thömmes, J., and Kula, M. R. (1997). Pilot scale processing of detergent based aqueous two-phase systems. *Biotechnol. Bioeng.* 55, 339–347. doi: 10.1002/(SICI)1097-0290(19970720)55:2<339::AID-BIT11>3.0.CO;2-C

Nandini, K. E., and Rastogi, N. K. (2011). Integrated downstream processing of lactoperoxidase from milk whey involving aqueous two-phase extraction and ultrasound-assisted ultrafiltration. *Appl. Biochem. Biotechnol.* 163, 173–185. doi: 10.1007/s12010-010-9 026-9

Narayan, A. V., Madhusudhan, M. C., and Raghavarao, K. S. M. S. (2011). Demixing kinetics of phase systems employed for liquid-liquid extraction and correlation with system properties. *Food. Bioprod. Process* 89, 251–256. doi: 10.1016/j.fbp.2010.11.014

Porto, T. S., Medeiros e Silva, G. M., Porto, C. S., Cavalcanti, M. T. H., Neto, B. B., Lima-Filho, J. L., et al. (2008). Liquid-liquid extraction of proteases from fermented broth by PEG/citrate aqueous two-phase system. *Chem. Eng. Process.* 47, 716–721. doi: 10.1016/j.cep.2006.12.004

Priyanka, B. S., Rastogi, N. K., Raghvarao, K. M. S. M., and Thakur, M. S. (2012). Downstream processing of luciferase from fireflies (*Photinus pyralis*) using aqueous two-phase extraction. *Process Biochem.* 47, 1358–1363. doi: 10.1016/j.procbio.2012.04.022

Raghavarao, K. S. M. S., Ranganathan, T. V., Srinivas, N. D., and Barhate, R. S. (2003). Aqueous two phase extraction: an environmentally bengin technique. *Clean. Technol. Environ. Policy.* 5, 136–141. doi: 10.1007/s10098-003-0193-z

Rawdkuen, S., Pintathong, P., Chaiwut, P., and Benjakul, S. (2011). The partitioning of protease from *Calotropis procera* latex by aqueous two-phase systems and its hydrolytic pattern on muscle proteins. *Food Bioprod. Process.* 89, 73–80. doi: 10.1016/j.fbp.2010.02.001

Rosa, P. A., Azevedo, A. M., Sommerfeld, S., Mutter, A., Aires-Barros, M. R., and Bäcker, W. (2009). Application of aqueous two-phase systems to antibody purification: a multi-stage approach. *J. Biotechnol.* 139, 306–313. doi: 10.1016/j.jbiotec.2009.01.001

Rosa, P. A., Ferreira, I. F., Azevedo, A. M., and Aires-Barros, M. R. (2010). Aqueous two-phase systems: a viable platform in the manufacturing of biopharmaceuticals. *J. Chromatogr. A* 1217, 2296–2305. doi: 10.1016/j.chroma.2009.11.034

Rosa, P. A. J., Azevedo, A. M., Sommerfeld, S., Bäcker, W., and Aires-Barros, M. R. (2011). Aqueous two-phase extraction as a platform in the biomanufacturing industry: economical and environmental sustainability. *Biotechnol. Adv.* 29, 559–567. doi: 10.1016/j.biotechadv.2011. 03.006

Sabalza, M., Christou, P., and Capell, T. (2014). Recombinant plant-derived pharmaceutical proteins: current technical and economic bottlenecks. *Biotechnol. Lett.* 36, 2367–2379. doi: 10.1007/s10529-014-1 621-3

Salamanca, M. H., Merchuk, J. C., Andrews, B. A., and Asenjo, J. A. (1998). On the kinetics of phase separation in aqueous two-phase systems. *J. Chromatogr. B.* 711, 319–329. doi: 10.1016/S0378-4347(98)00173-X

Straathof, A. J. J. (2011). The proportion of downstream costs in fermentative production processes. *Compr. Biotechnol.* 2, 811–814. doi: 10.1016/B978-0-08-088504-9.00492-X

Sutherland, I., Hewitson, P., Siebens, R., van den Heuvel, R., Arbenz, L., Kinkel, J., et al. (2011). Scale-up of protein purifications using aqueous two-phase systems: comparing multilayer toroidal coil chromatography with centrifugal partition chromatography. *J. Chromatogr. A* 1218, 5527–5530. doi: 10.1016/j.chroma.2011.04.013

Torres-Acosta, M. A., Aguilar-Ya-ez, J. M., Rito-Palomates, M., and Titchener-Hooker, N. J. (2015). Economic analysis of Royalactin production under uncertainty: evaluating the effect of parameter optimization. *Biotechnol. Prog.* 31, 744–749. doi: 10.1002/btpr.2073

Torres-Acosta, M. A., Ruiz-Ruiz, F., Aguilar-Ya-ez, J. M., Benavides, J., and Rito-Palomares, M. (2016). Economic analysis of pilot-scale production

of B-Phycoerythrin. *Biotechnol. Prog.* 32, 1472–1479. doi: 10.1002/btpr.2344

Vázquez-Villegas, P., Aguilar, O., and Rito-Palomares, M. (2011). Study of biomolecules partition coefficients on a novel continuous separator using polymer-salt aqueous two-phase systems. *Sep. Purif. Technol.* 78, 69–75. doi: 10.1016/j.seppur.2011.01.023

Vázquez-Villegas, P., Aguilar, O., and Rito-Palomares, M. (2015). Continuous enzyme aqueous two-phase extraction using a novel tubular mixer-settler in multi-step counter-current arrangement. *Sep. Pur. Technol.* 141, 263–268. doi: 10.1016/j.seppur.2014.12.005

Vázquez-Villegas, P., Ouellet, E., González, C., Ruiz-Ruiz, F., Rito-Palomares, M., Haynes, C. A., et al. (2016). A microdevice assisted approach for the preparation, characterization and selection of continuous aqueous two-phase systems: from micro to bench-scale. *Lab. Chip.* 16, 2662–2672. doi: 10.1039/C6LC00333H

Xu, Y., Souza, M. A., Pontes, M. Z. R., Vitolo, M., Pessoa, A. (2003). Liquid-liquid extraction of enzymes by affinity aqueous two-phase systems. *Braz. Arch. Biol. Technol.* 46(4):741–750. doi: 10.1590/S1516-89132003000400030

**Conflict of Interest Statement:** The authors declare that the research was conducted in the absence of any commercial or financial relationships that could be construed as a potential conflict of interest.

frontiers in Chemistry

ORIGINAL RESEARCH
published: 05 October 2018
doi: 10.3389/fchem.2018.00448

# Extractive Bioconversion of Gamma-Cyclodextrin and Recycling of Cyclodextrin Glycosyltransferase in Liquid Biphasic System Using Thermo-Separating Polymer

*Yu Kiat Lin[1], Pau Loke Show[2]*, Yee Jiun Yap[3], Arbakariya Ariff[4], Mohamad Suffian Bin Mohamad Annuar[1], Oi Ming Lai[5], Tau Chuan Ling[1] and Eng Poh Ng[6]*

[1] Faculty of Science, Institute of Biological Sciences, University of Malaya, Kuala Lumpur, Malaysia, [2] Department of Chemical and Environmental Engineering, Faculty of Engineering, University of Nottingham Malaysia Campus, Semenyih, Malaysia, [3] Department of Applied Mathematics, Faculty of Engineering, University of Nottingham Malaysia Campus, Semenyih, Malaysia, [4] Faculty of Biotechnology and Biomolecular Sciences, Universiti Putra Malaysia, Serdang, Malaysia, [5] Department of Bioprocess Technology, Faculty of Biotechnology and Bimolecular Sciences, University Putra Malaysia, Serdang, Malaysia, [6] School of Chemical Sciences, Universiti Sains Malaysia, Gelugor, Malaysia

OPEN ACCESS

**Edited by:**
*Brendan M. Leung, Dalhousie University, Canada*

**Reviewed by:**
*Hideki Yamaji, Kobe University, Japan*
*Pik Han Chong, Zhejiang Gongshang University, China*

***Correspondence:**
*Pau Loke Show*
*showpauloke@gmail.com;*
*pauloke.show@nottingham.edu.my*

**Specialty section:**
*This article was submitted to Chemical Engineering, a section of the journal Frontiers in Chemistry*

**Received:** *06 July 2018*
**Accepted:** *07 September 2018*
**Published:** *05 October 2018*

**Citation:**
*Lin YK, Show PL, Yap YJ, Ariff A, Annuar MSBM, Lai OM, Ling TC and Ng EP (2018) Extractive Bioconversion of Gamma-Cyclodextrin and Recycling of Cyclodextrin Glycosyltransferase in Liquid Biphasic System Using Thermo-Separating Polymer. Front. Chem. 6:448. doi: 10.3389/fchem.2018.00448*

An extractive bioconversion conducted on soluble starch with cyclodextrin glycosyltransferase (CGTase) enzyme in ethylene oxide-propylene oxide (EOPO)/potassium phosphates liquid biphasic system (LBS) to extract gamma-cyclodextrin (γ-CD) was examined. A range of EOPO (with potassium phosphates) molecular weights was screen to investigate the effect of the latter on the partioning efficency of CGTase and γ-CD. The results show that the optimal top phase γ-CD yield (74.4%) was reached in 35.0% (w/w) EOPO 970 and 10.0% (w/w) potassium phosphate with 2.0% (w/w) sodium chloride. A theoretical explanation for the effect of NaCl on γ-CD was also presented. After a 2 h bioconversion process, a total of 0.87 mg/mL concentration of γ-CD was produced in the EOPO/ phosphates LBS top phase. After the extraction of top phase from LBS, four continuous repetitive batches were successfully conducted with relative CGTase activity of 1.00, 0.86, 0.45, and 0.40 respectively.

**Keywords: liquid biphasic system, ethylene oxide-propylene oxide, extractive bioconversion, cyclodextrin, *Bacillus cereus***

## INTRODUCTION

In this study, liquid biphasic system (LBS) extractive bioconversion was carried out to split the target product and the biocatalyst into top phase and bottom phases, partitioning target biomolecules into one of the phases. These molecules are selectively partitioned based on the surface properties of the molecules and particles such as size, charge, and hydrophobicity (Walter and Johansson, 1994). The LBS extractive bioconversion combined production and recovery technique into a single step. In contrast to conventional processes (e.g., enzymatic bioconversion), the biocatalyst that is retained in one phase is reusable, encouraging a continuous extractive bioconversion process (Charoenlap et al., 2004).

To date, Polymer/polymer LBS is a type of LBS that has been extensively studied and utilized. Efficient and biocompatible polyethylene glycol (PEG)/dextran LBS is the common polymer/polymer LBS that has been widely utilized for the purification and separation of diversified biomolecules such as proteins, nucleic acids, and cell organelles (Lu et al., 1996; Charoenlap et al., 2004). Nevertheless, the application of PEG/dextran LBS in industrial scale has been hampered by the high ocst of the phase-forming chemicals (i.e., dextran) (Lu et al., 1996). Gamma-cyclodextrin's recovery (γ-CD) by LBS was then improved by building a recyclable LBS in which the polymer PEGs were substituted through the use of the copolymer ethylene oxide-propylene oxide (EOPO). The latter is a more economical and environmentally friendly LBS with the ability to maintain the organic activity of the enzyme. EOPO is a copolymer capable of thermos-separating into two phases when the temperature is higher than the lower critical solution temperature (LCST) (Johansson et al., 1997). After heating the system above a certain temperature, the EOPOs split up into two phases, allowing the recovery and reutilization of polymers in subsequent LBS. This novel investigation on the CGTase recovery will bring about a simplification of the CGTase purification steps as well as a reduction in the cost incurred on the environment (Johansson et al., 1999; Dembczynski et al., 2010).

The Cyclodextrins (CDs) are cyclic oligosaccharides that are constructed using cyclodextrin glycosyltransferase (CGTase) enzymes via the transglycosylation process (Rodrigues et al., 2015). CDs have a structural feature enabling them to make up inclusion complexes with an abundance of guest compounds, promoting broad applications of CDs in different industries like pharmaceuticals, food, and chemical products (Martin, 2004). There are three major forms of CDs, namely, α, β, and γ CDs which are formed by six, seven, and eight glucopyranose units respectively (Singh et al., 2002). Among these three types of CDs, the γ-CD has the largest interior cavity and the highest solubility. As shown in the later part of this paper, the size of this interior cavity will, in the presence of the salt, affect the efficiency of the CD extraction, and the large interior cavity size of the γ-CD increases the γ-CD extraction efficiency. However, γ-CD is a lot more expensive than α and β-CD due to its lower production efficiency compared to α and β-CDs (Wang et al., 2007; Moriwaki et al., 2008).

Therefore, an LBS extractive bioconversion is carried in this work to study methods of enhancing the separation and productivity of γ-CD from *Bacillus cereus* CGTase. In addition, approaches of optimizing the γ-CD recovery were studied via the investigation of the effects of selected LBS variables on the γ-CD extraction. These variables include the EOPO molecular weight, tie-line lengths (TLLs), volume ratio and introduction of sodium chloride (NaCl).

# MATERIALS AND METHODS

## Materials

The γ-CD standard, poly (ethylene glycol-ran-propylene glycol) (3,900, 12,000 g/mol) and poly (ethylene glycol-ran-propylene glycol) mono butyl ether (970 g/mol) were bought from Sigma-Aldrich Co. (St. Loius, MO, USA). The potassium phosphate salts ($K_2HPO_4$, $KH_2PO_4$) were bought from Merck (Darmstadt, Germany). Phenolphthalein was sourced from Merck (Darmstadt, Germany). Soluble starch was bought from Becton, Dickinson and company (USA). All other chemicals that were used in this study were of analytic grade.

## *Bacillus cereus* Production

The *B. cereus* was cultivated following the process as describe previously (Ng et al., 2011). Culture medium was prepared using 1% (w/v) sago starch, 0.5% (w/v) peptone, 0.5% (w/v) yeast extract, 0.009% (w/v) 0.1% $K_2HPO_4$, 1% $Na_2CO_3$, and $MgSO_4$ (autoclaved separately). The inoculum was grown at 37○C for 18 hours (h) with a 250 rpm continuous agitation. The inoculum was then shifted into the CGTase production media, which was thereupon incubated at 37○C for 30 h with a continuous agitation speed of 250 rpm. CGTase was harvested from the supernatant after a 30 min centrifugation at 4,000 rpm.

## Partitioning of CGTase and γ-CDs in LBS

Partition experimentations were executed at room temperature with predetermined amounts of dissolved EOPO, potassium phosphate and distilled water which were mixed in a 15 mL centrifugal tube. 10% (w/w) of crude CGTase and 10% (w/w) of standard γ-CD (50 mg/mL) were then added into the LBSs to attain a total weight of 10 g. The established LBSs were then shaken utilizing vortex mixer and thereupon subjected to a 4,000 rpm centrifugation for 10 min. After the phase separation, bottom and top phases were collected for γ-CD concentrations and CGTase activity analysis.

## CGTase Activity Analysis

CGTase cyclizing activity was quantified by utilizing the phenolphthalein method (Ng et al., 2011). A 50 μL enzyme sample was added to a 750 μL substrate solutions [1% (w/v) starch in 0.05 M Tris-HCl buffer pH 8.0] which was incubated at 55○C for 10 min. The enzymatic reaction of the CGTase was terminated by introducing 375 μL of 0.15M NaOH, followed by adding 100 μL 0.02% (w/v) phenolphthalein (in 5 mM $Na_2CO_3$) for the spectrophotometrical (550 nm) evaluation of CGTase activity.

## Extractive Bioconversion of γ-CD in LBS

Extractive bioconversion of γ-CD was executed at a 50 g reaction total weight in a 250 mL Erlenmeyer flask. The reaction temperature was 55○C. Predetermined dissolved EOPO, potassium phosphates, distilled water, 5% (w/w) soluble starch substrate and 20% (w/w) of the CGTase were added into the LBS to attain a final total weight of 50 g. A control (without LBS phase-forming components) was conducted for soluble starch's enzymatic conversion. Top phases' samples were collected one at a time at regular time intervals and heated in boiling water for 5 min to denature the CGTase. The quantification of the γ-CD concentration was carried out by making use of HPLC instrument.

## Calculation

Relative CGTase activity is defined as the ratio of the enzyme activity (U/mL) to γ-CD concentrations in mg/mL unit.

The volume ratio (VR) is defined as the ratio of top phase volume ($V_T$) to the bottom phase volume ($V_B$)

$$V_R = \frac{V_T}{V_B}. \quad (1)$$

Partition coefficient of CGTase ($K_{CGTase}$) is defined as the ratio of top phase CGTase bioactivity ($A_T$) to the bottom phase CGTase bioactivity ($A_B$), that is,

$$K_{CGTase} = \frac{A_T}{A_B}. \quad (2)$$

Partition coefficient of γ-CD ($K_{CD}$) is defined as the ratio of top phase γ-CD concentration ($C_T$) to bottom phase γ-CD concentration ($C_B$)

$$K_{CD} = \frac{C_T}{C_B}. \quad (3)$$

Yield of γ-CD in top phase ($Y_T$) is defined as

$$Y_T = \frac{1}{1 + \left(\frac{1}{V_R \times K_{CD}}\right)} \times 100\%. \quad (4)$$

# RESULTS AND DISCUSSION

## Effects of EOPO Molecular Weight and TLL on $Y_T$ of γ-CD and CGTase Partitioning

Phase diagrams of different EOPO molecular weight and phosphate salt LBSs were referred to for the evaluation of LBS performance in the $Y_T$ of γ-CD and partitioning behavior of CGTase (Show et al., 2000). TLLs were constructed for the CGTase partition experiments and γ-CD. EOPO 970, EOPO 3900, and EOPO 12000 were selected for this study due to their compatibility with biomaterials and capability in developing two phases with the salt components (Persson et al., 2000; Dembczynski et al., 2010).

The highest $Y_T$ of γ-CD at 63.1% and CGTase with $K_{CGTase}$ at 3.14 were achieved in EOPO 970/potassium phosphate LBS at TLL of 54.6% (w/w). As seen from the results of **Table 1**, the highest $Y_T$ value was achieved in LBSs comprising of EOPO 970. The EOPO 970 with lower PO content (50%) results in higher $Y_T$ of γ-CD in comparison with EOPO with higher PO content (EOPO 3900, EOPO 12000). The lower PO content of EOPOs (EOPO 970) allows maximum solubility of γ-CD in the polymer phase, thereby making the γ-CD precipitation in the interphase avoidable (Huang and Forciniti, 2002). The $K_{CGTase}$ values generally decreased as TLL increased. A possible casue to this would be an additional rise in the concentration of the polymer, resulting in a drop in the free volume of LBS top phase, thereby pulling more CGTase to the LBS's bottom phase (Forciniti et al., 1991). Hence, EOPO 970/potassium phosphate in TLL of 54.6% (w/w) was selected for the following experiments since it exhibited the optimal condition for highest $Y_T$ of γ-CD with low $K_{CGTase}$.

**TABLE 1 |** Effect of the EOPO molecular weight and TLL upon the $K_{CGTase}$ and $Y_T$ (%).

| EOPO molecular weight (g/mol) | TLL (%,w/w) | $K_{CGTase}$ | $Y_T$ (%) |
|---|---|---|---|
| 970 | 52.3 | 5.16 | 47.6 |
| | 54.6 | 3.14 | 63.1 |
| | 58.0 | 4.20 | 58.4 |
| | 61.8 | 4.06 | 53.0 |
| 3,900 | 36.4 | 8.44 | 46.5 |
| | 41.2 | 8.69 | 46.3 |
| | 44.6 | 6.06 | 56.4 |
| | 48.5 | 4.19 | 55.9 |
| 12,000 | 31.6 | 3.74 | 52.1 |
| | 34.4 | 3.65 | 54.7 |
| | 42.5 | 2.79 | 51.6 |
| | 50.2 | 2.04 | 47.5 |

*The data obtained was presented as the average of approximated triplicate readings with an accuracy of ±5%.*

## Effect of $V_R$ on the $Y_T$ of γ-CD and Partitioning of CGTase

The $K_{CGTase}$ and $Y_T$ at different $V_R$ ($V_R$ = 0.3 to 4.0) for EOPO 970/potassium phosphate TLL 54.6% (w/w) were illustrated in **Figure 1**. The highest $Y_T$ of γ-CD ($Y_T$ = 68.7%) was reached at $V_R$ 2.0. The $Y_T$ was generally increasing as the $V_R$ increased. This may be due to the fact that a higher $V_R$ (i.e., $V_R > 1$) resulted in more free volume in the top phase, thereby increasing the solubility limit of $Y_T$, which in-turn caused more γ-CD to be attracted to the top phase (Schmidt et al., 1994). In the system of $V_R$ 0.5, it is noticeable that $V_R$ 05 was given the highest $K_{CGTase}$ which was around 3.5. This is because less free volume in the top phase which give indirectly stress the $K_{CGTase}$ increase. Since in this stage, we are aimed to get the highest $Y_T$ of γ-CD instead of high $K_{CGTase}$. Therefore, the optimal condition ($V_R$ = 2.0) was selected for subsequent studies.

## Effect of NaCl on $Y_T$ of γ-CD

The EOPO 970/potassium phosphate in TLL 54.6% (w/w) with VR 2.0 was used to examine the effect of adding NaCl, ranging from 0% (w/w) to 4% (w/w), on the $Y_T$ of γ-CD. The partitioning behavior of γ-CD in LBS was due to the difference in hydrophobicity between the phases caused by the addition of NaCl. In addition, the electrostatic potential created by the NaCl contributed to the driving of the γ-CD to the top phase, thereby proliferating the top phase partitioning of γ-CD (Zaslavsky et al., 1991). The interaction between the hydrophobic chain of the EOPO and hydrophobic surface of the γ-CD was enhanced by the addition of the salts. This enhancement was precipitated by the effect of the salt on the hydrophobic interactions and the water solvent structure. The target biomolecules would be thus partitioned to the polymer rich top phase (Albertsson, 1986). Just like the case of PEG-salt system mentioned in Huddleston et al. (1991), when the NaCl concentration is lower, the electrostatic field due to the $Na^+$ and $Cl^-$ ions will play a greater role in the γ-CD extraction. However, a high NaCl concentration causes a lot

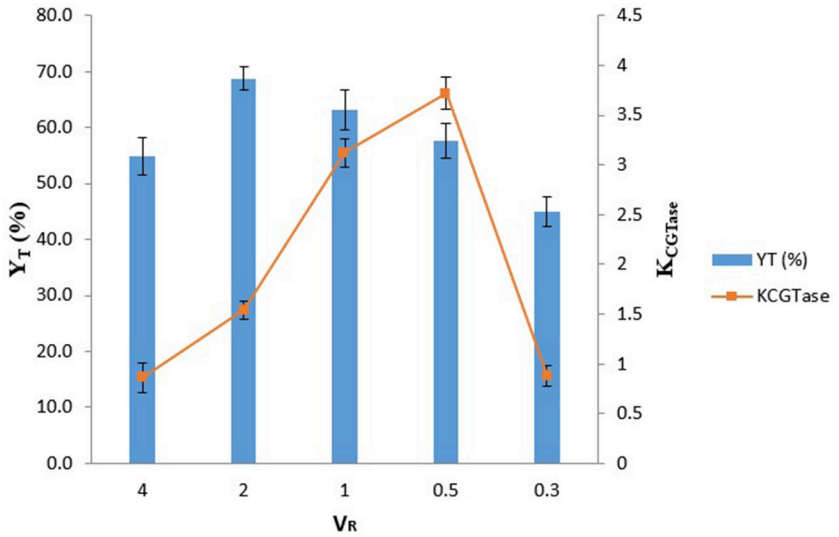


**FIGURE 1 |** Influence of $V_R$ on the partitioning of CGTase. The data obtained was presented as the average of triplicate readings.

of γ-CD to partition to the top phase. This large number of γ-CD molecules bind with the EOPO polymers through hydrophobic interactions, thereby forming larger hydrophobes and repelling the water molecules to the bottom phase. With a reduction in the water molecules in the top phase, there is less water for the γ-CD molecules to dissolve in, thereby causing a reduction in the yield of the γ-CD in the top phase. Thus, although the NaCl serves to help increase the yield of γ-CD, too high a salt level will have the reverse effect of reducing the yield. From **Table 2**, it can be seen that an optimal yield of γ-CD occurs at an NaCl concentration of roughly 2%(w/w).

The effect $V_E$ of the electric field (Lemeshko et al., 2013) on the molecules is given as

$$V_E = -\underline{E} \cdot \sum_n q_n \underline{r} n \tag{5}$$

where is the electric field, $q_n$ is the charge of electron $n$, $_n$ is the position vector of electron $n$. By approximating the perimeter of a γ-CD molecule to a circle with the origin of at the center of the circle and taking the charge of an electron to be a constant $k_e$ (i.e., the Coulomb constant), we can denote the radius of the γ-CD molecule as $R$, and Equation (5) can be rewritten as

$$\begin{aligned} V_E &= -\underline{E} \cdot \sum_n q_n r_n \hat{\underline{r}}_n = -\underline{E} \cdot \sum_n k_e R \hat{\underline{r}}_n = -k_e R \sum_n \underline{E} \cdot \hat{\underline{r}}_n \\ &= -k_e R \sum_0^{\frac{\pi}{2}} |\underline{E}| \cos\theta = -k_e R A \, |\underline{E}| \end{aligned} \tag{6}$$

where $\theta$ is the angle between and $_n$ and $A = \sum_0^{\frac{\pi}{2}} \cos\theta$=constant. Thus, from Equation (6), we can see that the higher the NaCl concentration, the larger the electric field, and hence the larger the effect on the molecule. Additionally, we will expect the γ-CD, which has a larger $R$ then $\alpha$-CD and $\beta$-CD, to be more affected by the presence of NaCl in terms of the electric field created.

**TABLE 2 |** Influence of the NaCl concentration on $Y_T$ (%).

| NaCl concentration %(w/w) | $Y_T$ (%) |
|---|---|
| 0 | 68.3 |
| 1 | 71.7 |
| 2 | 74.4 |
| 3 | 72.8 |
| 4 | 72.1 |

*The data obtained was presented as the average of approximated triplicate readings with an accuracy of ±5%.*

**Figure 2** illustrates γ-CD concentration in LBS top phase vs. the extractive bioconversion process time. A 50 mL of EOPO 970/potassium phosphate at TLL of 54.6% (w/w) with VR of 2.0 was employed in this study. 20% (w/w) crude CGTase and 5% (w/w) of soluble starch were added to the LBS. A 1.10 mg/mL concentration of γ-CD was collected in the LBS top phase sample after a 30 h extractive bioconversion process. Nevertheless, 2 h (0.87 mg/mL) is proposed as the harvest time since increase in the γ-CD concentration is minimal after 2 h. A comparison of the CD concentration ratios (for different CDs) between the control sample and the 2 h LBS top phase sample is shown in **Table 3**. The γ-CD concentration ratio of the top phase sample (17.5%) is much higher than that of the control sample (6.6%). This implies that a higher γ-CD ratio product is achievable by using the LBS extractive bioconversion process.

## Repetitive Batch for γ-CD Production and Comparative Study by Using PEG

LBS's repetitive batch investigation was conducted to study the recycling of the CGTase enzyme in the bottom phase. The repetitive batch of the γ-CD recovery was carried out through

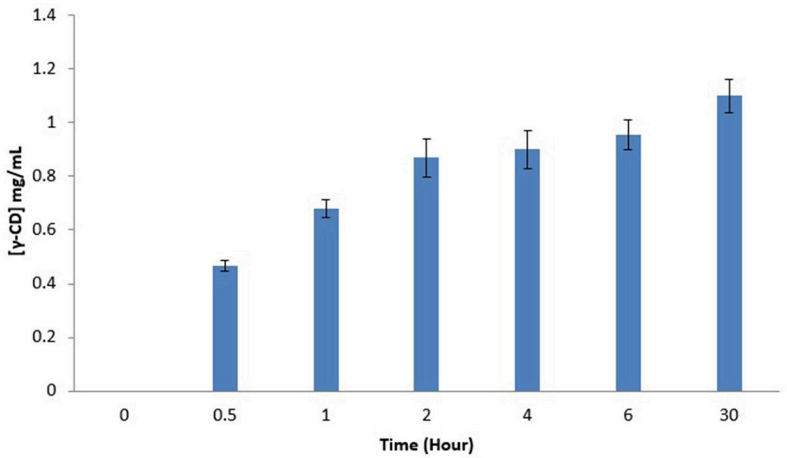


**FIGURE 2 |** Effects of LBS extractive bioconversion on γ-CD production over time. The data obtained was presented as the average of triplicate readings.

**TABLE 3 |** A comparison of CDs concentration ratio (%) between LBS top phase sample and control sample.

| CD type | Control (%) | 2 h LBS Top phase (%) (This work) | 1 h LBS Top phase (%) (Our previous work, Lin et al., 2015) |
|---|---|---|---|
| α | 67.1 | 59.0 | 55.4 |
| β | 26.3 | 23.5 | 25.6 |
| γ | 6.6 | 17.5 | 19.0 |
| Total | 100.0 | 100.0 | 100.00 |

*The data obtained was presented as the average of approximated triplicate readings with an accuracy of ±5%.*

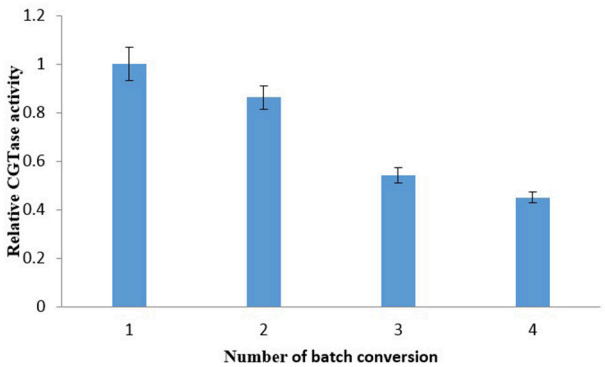


**FIGURE 3 |** Relative CGTase activity in each batch of soluble starch bioconversion by recycling of the phase components and CGTase. The data obtained was presented as the average of triplicate readings.

EOPO 970/potassium phosphate LBS at 54.6% (w/w) TLL, $V_R$ of 2.0, added with 20% (w/w) of crude CGTase, and 5% (w/w) of soluble starch. Top phase extractions were done at a regular interval of 2 h extractive bioconversion process. **Figure 3** shows CGTase activity of the bottom phase after extraction of the top phase, and it can be seen that the CGTase activity continues to drop with subsequent batches. The relative CGTase activity went down to 0.45 in the 4th batch of extractive bioconversion. This outcome revealed that the losing of CGTase occurred when the top phase, which contained a certain amount of CGTase (Tramice et al., 2008), was removed. Therefore, it can be seen that to ensure the effectiveness and performance of bioconversion, the CGTase enzyme in the bottom phase should not be recycled more than once. One of our earlier studies about extractive bioconversion of γ-CD from soluble starch with CGTase enzyme by using PEG instead of EOPO (Lin et al., 2015). **Table 3** shows the γ-CD concentration ratio within 2 h in the present study was lower than that within 1 h in our previous study (Lin et al., 2015). However, the LBS using EOPO is more economical and environmentally-friendly than that using PEG, as described in introduction. The comparative studies were shown in **Table 3**.

## CONCLUSIONS

In this study, EOPO polymer has been applied to the LBS extractive bioconversion of γ-CD. Generally, the partitioning of γ-CD in EOPO/potassium phosphate LBS was influenced by the PO content and concentration of the EOPO used. The optimal extractive bioconversion of γ-CD in top phase of the LBS was reached in EOPO 970/potassium phosphate LBS of 54.6% (w/w) TLL, $V_R$ of 2.0. A γ-CD concentration of 0.87 mg/mL with a 17.5% concentration ratio was retrieved after a 2 h extractive bioconversion process. The objective of this study, which is to produce and recover γ-CD by directly using LBS, has been achieved. In particular, it has been shown that the EOPO 970/potassium phosphate LBS extractive bioconversion is a better alternative technique for producing the γ-CD compared to the conventional method as this alternative technique merges γ-CD production and purification into a single-step process.

## AUTHOR CONTRIBUTIONS

YL performed the experiment and data analysis as well as wrote the manuscript. PS conceived and designed the experiment. YY provided theoretical explanation and analysis for the experimental data. AA, MA, OL, TL, and EN revised the manuscript.

## FUNDING

This research was financially supported by UMRG (RU018O-2016; RU018L-2016; ST003-2017; ST001-2017; RP025B-18SUS; TR001A-2015A; RP031B-15AET; ST002-2017) and Overseas Researcher under Fellowship of Japan Society for the Promotion of Science.

## REFERENCES

Albertsson, P. (1986). *Partition of Cell Particles and Macromolecules, 3rd Edn*. New York, NY: Wiley.

Charoenlap, N., Dharmsthiti, S., Sirisansaneeyakul, S., and Lertsiri, S. (2004). Optimization of cyclodextrin production from sago starch. *Bioresour. Technol. Bioresour*. 92, 49–54. doi: 10.1016/j.biortech.2003.07.007

Dembczynski, R., Bialas, W., and Jankowski, T. (2010). Recycling of phase components during lysozyme extraction from hen egg white in the EO50PO50/$K_2HPO_4$ aqueous two-phase system. *Biochem. Eng. J*. 51, 24–31. doi: 10.1016/j.bej.2010.04.011

Forciniti, D., Hall, C., and Kula, M. (1991). Influence of polymer molecular weight and temperature on phase composition in aqueous two-phase systems. *Fluid Phase Equilibr*. 61, 243–262. doi: 10.1016/0378-3812(91)80002-D

Huang, Y., and Forciniti, D. (2002). Ethylene oxide and propylene oxide random copolymer/ sodium chloride aqueous two-phase systems: wetting and adsorption on dodecyl–agarose and polystyrene. *Biotechnol. Bioeng*. 77, 786–795. doi: 10.1002/bit.10169

Huddleston, J., Veide, A., Köhler, K., Flanagan, J., Enfors, S. O., and Lyddiatt, A. (1991). The molecular basis of partitioning in aqueous two-phase systems. *Trends Biotechnol*. 9, 381–388. doi: 10.1016/0167-7799(91)90130-A

Johansson, H., Karlström, G., and Tjerneld, F. (1997). Temperature-induced phase partitioning of peptides in water solutions of ethylene oxide and propylene oxide random copolymers. *Biochim. Biophys. Acta* 1335, 315–325. doi: 10.1016/S0304-4165(96)00150-X

Johansson, H. O., Persson, J., and Tjerneld, F. (1999). Thermoseparating water/polymer system, a novel one-polymer aqueous two-phase system for protein purification. *Biotechnol. Bioeng*. 66, 247–257. doi: 10.1002/(SICI)1097-0290(1999)66:4<247::AID-BIT6>3.0.CO;2-5

Lemeshko, M., Krems, R. V., Doyle, J. M., and Kais, J. (2013). Manipulation of molecules with electromagnetic fields. *Mol. Phys*. 111, 1648–1682. doi: 10.1080/00268976.2013.813595

Lin, Y., Show, P., Yap, Y., Ariff, A., Mohammad Annuar, S., Lai, O., et al. (2015). Productionof g-cyclodextrin by *Bacillus cereus* cyclodextrin glycosyltransferase using extractive bioconversion in polymer-salt aqueous two-phase system. *J. Biosci. Bioeng*. 121, 692–696 doi: 10.1016/j.jbiosc.2015.11.001

Lu, M., Albertsson, P.-A., Johansson, G., and Tjerneld, F. (1996). Ucon-benzoyl dextran aqueous two-phase systems: protein purification with phase component recycling. *J. Chromatogr. B* 680, 65–70. doi: 10.1016/0378-4347(95)00484-X

Martin, E. (2004). Cyclodextrins and their uses: a review. *Process Biochem*. 39, 1033–1046. doi: 10.1016/S0032-9592(03)00258-9

Moriwaki, C., Costa, G., Ferracini, C., Zanin Pineda, G., and Matioli, E. (2008). Enhancement of solubility of albendazole by complexation with β-cyclodextrin. *Braz. J. Chem. Eng*. 25, 255–267. doi: 10.1590/S0104-66322008000200005

Ng, H., Tan, C., Chen, S., Mokhtar, M., Ariff, A., and Ling, T. (2011). Primary capture of cyclodextrin glycosyltransferase derived from *Bacillus cereus* by aqueous two phase system. *Purif. Technol*. 81, 318–324. doi: 10.1016/j.seppur.2011.07.039

Persson, J., Kaul, A., and Tjerneld, F. (2000). Polymer recycling in aqueous two-phase extractions using thermoseparating ethylene oxide-propylene oxide copolymers. *J. Chromatogr. B* 743, 115–126. doi: 101016/S0378-4347(00)00213-9

Rodrigues, J., Araújo, R., Prather, K., Kluskens, L., and Rodrigues, L. (2015). Production of curcuminoids from tyrosine by a metabolically engineered *Escherichia coli* using caffeic acid as an intermediate. *Biotechnol. J*. 10, 599–609. doi: 10.1002/biot.201400637

Schmidt, A., Ventom, A., and Asenjo, J. (1994). Partitioning and purification of α-amylase in aqueous two-phase systems. *Enzyme Microb. Tech*. 16, 131–142. doi: 10.1016/0141-0229(94)90076-0

Show, P., Tan, C., Anuar, M., Ariff, A., Yusoff, Y., Chen, S., et al. (2000). Primary recovery of lipase and recycling phase components in aqueous two phase system. *Biochem. Eng. J*. 60, 74–80. doi: 10.1016/j.bej.2011.10.005

Singh, M., Sharma, R., and Banerjee, U. (2002). Biotechnological applications of cyclodextrins. *Biotechnol. Adv*. 6, 341–359. doi: 10.1016/S0734-9750(02)00020-4

Tramice, A., Andreotti, G., and Trincone, A. (2008). Direct enzymatic glucosylation of naringin in grapefruit juice by α-D-glucosidase from the marine mollusc *Aplysia fasciata*. *Biotechnol. J*. 3, 545–554. doi: 10.1002/biot.200700161

Walter, H., and Johansson, G. (1994). *Aqueous Two-Phase Systems*. San Diego, CA: Academic Press.

Wang, Z., Wang, F., Gu, Z., Du, G., Wu, J., and Chen, J. (2007). γ-Cyclodextrin: A review on enzymatic production and applications. *Appl. Microbiol. Biot*. 77, 245–255. doi: 10.1007/s00253-007-1166-7

Zaslavsky, B., Borovskaya, A., Gulaeva, N., and Miheeva, L. (1991). Influence of ionic and polymer composition on the properties of the phases of aqueous twophase systems formed by non-ionic polymers. *J. Chem. Soc. Faraday T* 87, 141–145. doi: 10.1039/ft9918700141

**Conflict of Interest Statement:** The authors declare that the submitted work was not carried out in the presence of any personal, professional or financial relationships that could potentially be construed as a conflict of interest.

frontiers in Chemistry

ORIGINAL RESEARCH
published: 16 October 2018
doi: 10.3389/fchem.2018.00486

# Ionic Liquid Aqueous Two-Phase Systems for the Enhanced Paper-Based Detection of Transferrin and *Escherichia coli*

*Matthew F. Yee*[1], *Grace N. Emmel*[1], *Eric J. Yang*[1], *Eumene Lee*[1], *Justin H. Paek*[1], *Benjamin M. Wu*[2] *and Daniel T. Kamei*[1]*

[1] Kamei Laboratory, UCLA, Department of Bioengineering, Los Angeles, CA, United States, [2] Wu Laboratory, UCLA, Department of Bioengineering, Los Angeles, CA, United States

Aqueous two-phase systems (ATPSs) have been widely utilized for liquid-liquid extraction and purification of biomolecules, with some studies also demonstrating their capacity as a biomarker concentration technique for use in diagnostic settings. As the limited polarity range of conventional polymer-based ATPSs can restrict their use, ionic liquid (IL)-based ATPSs have been recently proposed as a promising alternative to polymer-based ATPSs, since ILs are regarded as tunable solvents with excellent solvation capabilities for a variety of natural compounds and proteins. This study demonstrates the first application of IL ATPSs to point-of-care diagnostics. ATPSs consisting of 1-butyl-3-methylimidazolium tetrafluoroborate ([Bmim][$BF_4$]) and sodium phosphate salt were utilized to quickly concentrate biomarkers prior to detection using the lateral-flow immunoassay (LFA). We found the phase separation speed of the IL ATPS to be very rapid and a significant improvement upon the separation speed of both polymer-salt and micellar ATPSs. This system was successfully applied to both sandwich and competitive LFA formats and enhanced the detection of both *Escherichia coli* bacteria and the transferrin protein up to 8- and 20-fold, respectively. This system's compatibility with a broad range of biomolecules, rapid phase separation speed, and tunability suggest wide applicability for a large range of different antigens and biomarkers.

**Keywords: ionic liquid, aqueous two-phase systems, lateral-flow immunoassay, transferrin, *Escherichia coli***

OPEN ACCESS

***Edited by:***
*John Paul Frampton, Dalhousie University, Canada*

***Reviewed by:***
*Ugur Tamer, Gazi University, Turkey*
*Grant Bruce Webber, University of Newcastle, Australia*

***Correspondence:**
*Daniel T. Kamei*
*kamei@seas.ucla.edu*

***Specialty section:***
*This article was submitted to Chemical Engineering, a section of the journal Frontiers in Chemistry*

***Received:*** *30 May 2018*
***Accepted:*** *24 September 2018*
***Published:*** *16 October 2018*

***Citation:***
*Yee MF, Emmel GN, Yang EJ, Lee E, Paek JH, Wu BM and Kamei DT (2018) Ionic Liquid Aqueous Two-Phase Systems for the Enhanced Paper-Based Detection of Transferrin and Escherichia coli. Front. Chem. 6:486. doi: 10.3389/fchem.2018.00486*

## INTRODUCTION

While global health has improved over the last few decades, health pandemics in resource-poor settings remain a large problem (Scarborough and Thwaites, 2008; Tang and Nour, 2010; Gunasekera and Pathiraja, 2016). These health issues include chronic health conditions, such as diabetes (Nugent, 2008) and infectious diseases, such as tuberculosis (Global Tuberculosis Report 2017, 2017). In countries like the U.S, many of these illnesses are readily treatable, especially when diagnosed early; however, in resource-poor settings, patients lack easy access to standard laboratory-based tests such as the enzyme-linked immunosorbent assay (ELISA), nucleic acid amplification tests, and serology tests (Elbireer et al., 2011). With issues such as poor infrastructure and limited funding already leading to underutilization of central laboratories in these resource-poor settings (Elbireer et al., 2011; Nkengasong et al., 2018), there is a growing interest in

developing point-of-care techniques to diagnose a variety of diseases. Devices, such as miniaturized bioelectronics and microfluidic tests like the lateral-flow immunoassay (LFA), have received much attention over recent years due to their ease-of-use, portability, and limited need for power (Li et al., 2015; Sharma et al., 2015; Gumustas et al., 2018; Wang et al., 2018). However, in comparison to the gold standard laboratory-based tests, these devices are still restricted by their limited sensitivity, indicating an increasing need for enhanced detection capabilities at the point-of-care.

One technique for enhancing point-of-care detection is the aqueous two-phase system (ATPS), a liquid-liquid extraction system that has previously been demonstrated to concentrate biological markers (Hatti-Kaul, 2001). ATPSs consist of two immiscible phases, similar to oil-water systems; however, both phases of an ATPS are aqueous-based. Molecules introduced into an ATPS can experience extreme partitioning between the two phases based on the excluded-volume, hydrophobic, and electrostatic interactions they experience with the components of each of the two phases. Furthermore, ATPSs are much more biocompatible than conventional oil-water systems, and have been widely utilized for the purification of proteins and nucleic acids (Hatti-Kaul, 2001). While the ATPS has been traditionally used in large-scale, industrial bioseparations, it also lends itself well for applications in point-of-care settings, as it is easy-to-use, can be rapid, and is scalable (to minimize sample volume) (Iqbal et al., 2016). In addition, ATPSs do not require laboratory equipment and are low in cost compared to more conventional laboratory tests such as the ELISA and nucleic acid amplification.

For these reasons, our research group has recently demonstrated the use of the ATPS as a pre-concentration tool to improve the sensitivity of portable paper-based diagnostic tools such as the LFA. Through the use of conventional polymer-salt and micellar systems, ATPSs combined with existing detection technologies have been shown to enhance sensitivity in detecting various biomarkers, including 10-fold improvements in LFA detection of parasitic biomarkers (Pereira et al., 2015) and viruses (Mashayekhi et al., 2010). In a similar manner, the ATPS was also shown to improve sensitivity and decrease time-to-detection of a paper-based spot immunoassay (Cheung et al., 2017). However, despite the efficacy of these systems, the limited polarity range of these ATPSs can restrict their use (Freire et al., 2012), particularly regarding the partitioning of small hydrophilic proteins. As micellar and polymer ATPSs predominantly rely on excluded-volume interactions to partition hydrophilic biomolecules to a particular phase, smaller hydrophilic biomarkers such as proteins can be difficult to partition extremely. One approach to improve upon this issue is to fine-tune the polarity of the ATPS components and introduce electrostatic effects as a more significant factor in partitioning.

One potential solution is through the use of ionic liquids (ILs), which are salts that are molten at low temperatures. ILs have been investigated as alternatives to traditional, volatile organic solvents as they exhibit non-flammability and negligible volatility (Freire et al., 2012) due to their ionic nature. In addition, they are particularly promising for use in an ATPS as they are highly tunable and have excellent solvation capabilities (Berthod et al., 2008) for a variety of natural compounds and proteins. This has led to their use in various extraction and separation processes (Liu et al., 2007; Berthod et al., 2008; Tang et al., 2012) including ATPSs. These systems were found to phase separate with the mixture of kosmotropic salts and imidazolium-based ILs (Gutowski et al., 2003). Since then, different classes of ILs have been discovered, developed, and utilized in the formation of ATPSs (Wilkes et al., 1982; Ventura et al., 2011); this variety in ILs, combined with an even greater variety in salts, could potentially allow researchers to precisely concentrate smaller biomolecules that would otherwise be difficult to partition extremely into one phase through excluded-volume interactions alone.

One of the most commonly investigated types of IL ATPSs are imidazolium-based. This class of ILs has shown promising potential as an extraction technique for a wide variety of compounds, including proteins, amino acids, and antibiotics (Freire et al., 2012). Additionally, these systems are optimal for point-of-care diagnostics since they are able to phase separate at room temperature and at physiological pH. In this study, IL ATPSs consisting of 1-butyl-3-methylimidazolium tetrafluoroborate ([Bmim][$BF_4$]) and sodium phosphate salt were utilized to demonstrate the compatibility of the IL ATPS with LFA and the ability of this technique to improve the sensitivity of LFA tests. This enhancement was applied to the model protein transferrin, using the competitive LFA format, and the model pathogen *Escherichia coli* O157:H7, using the sandwich LFA format. To our knowledge, this is the first application of an IL ATPS for the enhancement of point-of-care diagnostics. The IL ATPS demonstrated very fast phase separation and was found to be directly compatible with LFA, requiring no additional modification to existing LFA structure; by utilizing these benefits and also a significant enhancement effect, our system addresses limitations faced by existing paper-based portable diagnostics regarding the concentration of small biomarkers.

# MATERIALS AND METHODS

## Preparation of Bacterial Cell Cultures

*Escherichia coli* O157:H7 bacteria (*E. coli*) (ATCC® 700728™) were grown and cultured according to manufacturer protocol (ATCC, Manassas, VA) and plated onto Difco Nutrient Agar (Becton, Dickinson and Company, Sparks, MD) plates. Plated cells were subsequently incubated at 37°C aerobically overnight. The incubated plates were then sealed with Parafilm and stored at 4°C until use. To prepare bacterial suspensions for use in ATPS and LFA tests, single colonies were picked from the agar plate and cultured in 5 mL of Difco Nutrient Broth (Becton, Dickinson and Company, Sparks, MD). The cell suspension was then incubated in a shaker-incubator at 37°C and 200 rpm for 16 h. After use in LFA tests, the concentrations of bacteria in the suspensions were determined through plating of bacteria following serial dilutions. These bacteria were then incubated at 37°C aerobically overnight, after which the colonies were counted in order to quantify the bacterial concentrations used in the tests.

## Preparation and Visualization of IL ATPSs

Compositions of IL and salt necessary to achieve the desired equilibrium volume ratios, i.e., the volume of the top phase divided by the volume of the bottom phase, were determined by varying the initial concentrations of both [Bmim][$BF_4$] (Sigma-Aldritch, St. Louis, MO) and sodium phosphate (2:1 dibasic:monobasic) in solutions of Dulbecco's phosphate-buffered saline (PBS; Invitrogen, Grand Island, NY, pH 7.4). Conditions for 1:1 and 1:9 volume ratio ATPSs were found to be 35% w/w [Bmim][$BF_4$] and 3% w/w salt, and 65% w/w [Bmim][$BF_4$] and 0.5% w/w salt, respectively. Additionally, 0.01% w/w Triton X-100 surfactant (Sigma-Aldritch, St. Louis, MO) was added to the 1:9 IL ATPS to facilitate phase formation. These conditions were used for all of the following experiments.

For visualization of phase formation in the IL ATPSs, 44 or 8.8 μL of bovine serum albumin-coated dextran-coated gold nanoparticles were added to 1.5 g 1:1 volume ratio or 1:9 volume ratio ATPSs, respectively. These ATPSs were well-mixed to ensure a homogenous mixture. The ATPSs were then incubated at room temperature. Time-to-equilibrium was established when the visible domains arrived at their respective macroscopic phases, and the location of the interface remained stable.

## Viscosity and Interfacial Tension Measurements

Viscosity and interfacial tension measurements were performed using 30 g of IL-, polymer-, and micelle-based 1:1 volume ratio ATPSs. IL-based ATPSs were prepared as previously mentioned. Polymer-based ATPSs consisted of 12.5% w/w PEG 20k (Sigma-Aldritch, St. Louis, MO) and 7.5% w/w potassium phosphate (5:1 di:monobasic) in solutions of PBS. Micelle-based ATPSs consisted of 4% w/w Triton X-114 (Sigma-Aldritch, St. Louis, MO) in solutions of PBS.

Du Noüy ring interfacial tension measurements for each ATPS were obtained utilizing the Krüss K6 force tensiometer (Krüss USA, NC, USA). A standard platinum ring attached to the tensiometer was used in the measurements. Viscosity measurements were obtained using the Brookfield LVDV-I Prime digital viscometer (AMETEK Brookfield, MA, USA). All tests were performed at room temperature. Triplicate measurements of each condition were performed.

## Detection of Transferrin (Tf)

### Preparation of Dextran-Coated Gold Nanoprobes (DGNPs)

Purple colored dextran-coated gold nanoparticles (DGNs) were synthesized according to Min and coworkers with slight modifications (Jang et al., 2013; Chiu et al., 2014). Briefly, 0.75 g of dextran ($M_w$ 15000–25000) were dissolved in 9.9 mL of filtered UltraPure sterile water (Rockland Immunochemicals Inc., Gilbertsville PA). The solution was stirred and heated to a boil, after which 135 μL of 1% w/v gold (III) chloride hydrate were added. The color of the reaction mixture became dark purple, and the solution was stirred and boiled for 20 more minutes. The particles were stored at 4°C until use.

The dextran-coated gold nanoprobes (DGNPs) were prepared as follows. A 1 mL aliquot of dextran-coated gold nanoparticles was adjusted to pH 9.0 using 0.5 M NaOH. Subsequently, 4 μg of anti-transferrin (anti-Tf) antibodies were added to the solution. The mixture was placed on a shaker for 30 min to facilitate the formation of dative bonds between the antibodies and the dextran-coated gold nanoparticles. Free antibodies were removed by centrifugation. The pellet was resuspended in 100 μL of 0.1 M of sodium borate buffer at pH 9.0.

### Preparation of Competitive LFA Strips

LFA test strips utilizing the competitive assay format were assembled in a similar manner to our previous studies (Mashayekhi et al., 2012). Briefly, both Tf and rabbit anti-goat IgG secondary antibodies were dissolved in a 25% w/v sucrose solution for stabilization prior to being printed in lines on a CN140 nitrocellulose membrane. After drying overnight, the nitrocellulose was treated with 1% w/v BSA to prevent nonspecific binding. Subsequently, the 1% w/v BSA treated S17 fiberglass sample pad, the nitrocellulose membrane, and CF4 absorbent pad were assembled onto an adhesive backing into 5 mm wide LFA strips. In this format, immobilized Tf constitutes the test line and immobilized secondary antibodies specific to the primary anti-Tf antibody constitute the control line. If enough Tf is present to saturate the antibodies immobilized to the DGNPs in a sample, the Tf-DGNP complexes flowing through the LFA strip will not bind to the immobilized Tf on the test line. This results in the absence of a visible purple band at the test line region. If Tf is not present, unbound antibodies on the DGNPs will bind to the immobilized Tf, and a visual band will form at the test line. In either case, the antibodies on the DGNPs will bind the secondary antibodies immobilized at the control line and form a visible line, indicating successful sample flow through the strip. Therefore, a positive result is indicated by only one purple band at the control line, while a negative result is indicated by two purple bands at both the test line and control line (**Figure 1**).

### Detection of Tf With LFA Only

To verify the detection limit of Tf with LFA only tests, anti-Tf DGNPs were added to a sample solution in a test tube and allowed to bind to Tf present in the sample to form Tf-DGNP complexes. Tests consisted of 50 μL sample solution, which was composed of 3 μL of anti-transferrin DGNPs and 47 μL of a known amount of Tf dissolved in PBS, or only PBS for the negative control. The solution was incubated for 10 min at room temperature to allow the DGNPs to capture the Tf in solution. The LFA test strip was then inserted vertically into the sample solution, which wicked through the strip via capillary action toward the absorbent pad. Images of the test strips were taken immediately after 20 min with a Nikon D3400 camera in a controlled lighting environment. Triplicates of each test were obtained and analyzed with a custom MATLAB program.

### Detection of Tf With the IL ATPS/LFA Setup

For detection of Tf with the 1:1 volume ratio ATPS, 120 mg of a well-mixed 1:1 ATPS containing 3.6 μL of anti-Tf DGNPs and a known concentration of Tf were added into a test tube. The solution was incubated for 10 min at room temperature to allow the DGNPs to capture the Tf in solution and to allow

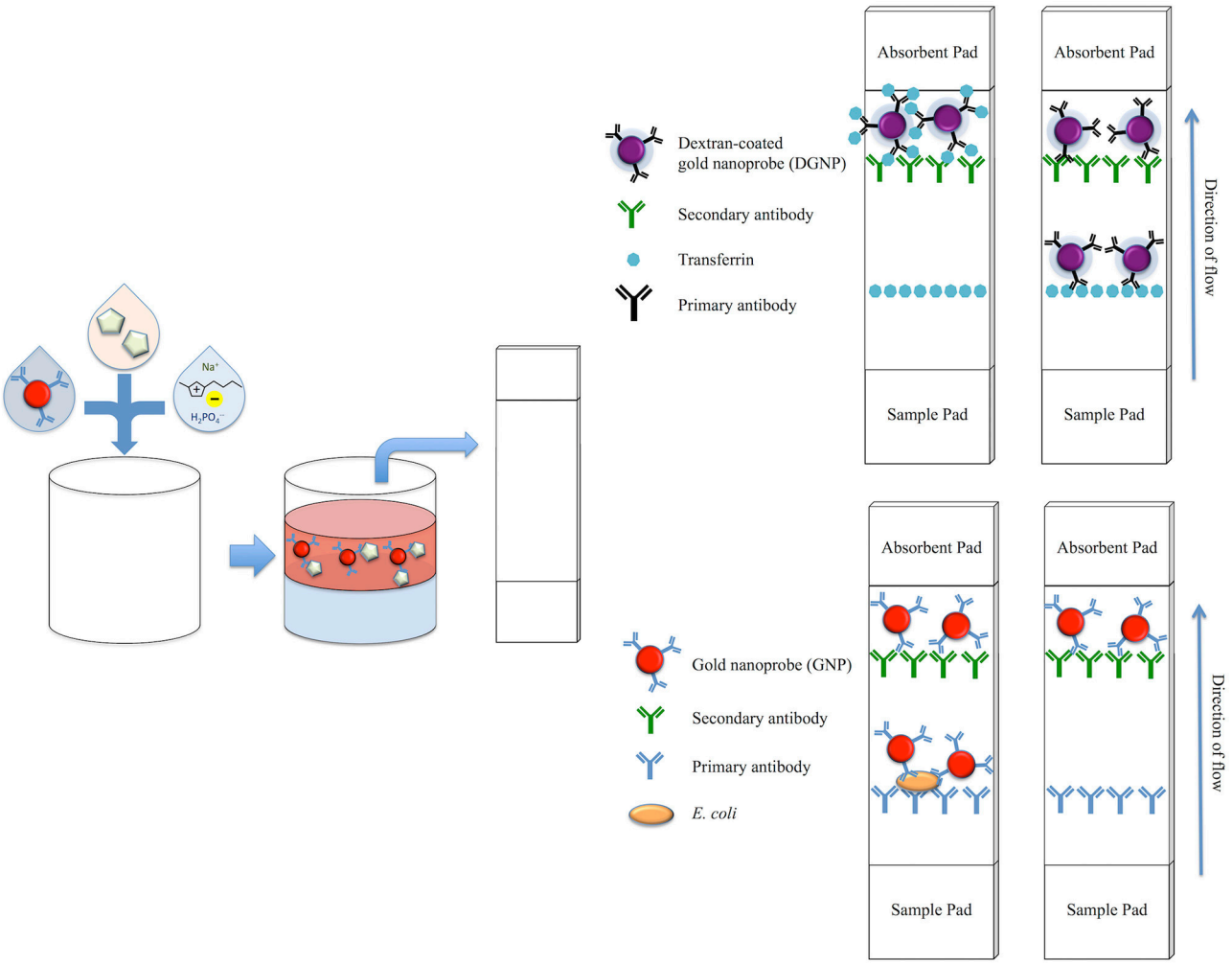


**FIGURE 1 |** Schematic of biomarker concentration with an IL ATPS and subsequent detection on the LFA. Gold nanoprobes and phase-forming components are first mixed with a known concentration of target analyte. Following phase separation, the top phase is extracted and applied to both the competitive format LFAs for detection of transferrin and sandwich format LFAs for the detection of *E. coli*. For the competitive format LFA, which utilizes purple-colored DGNPs, a positive test is indicated by a single purple band, while a negative test is indicated by two purple bands. For the sandwich format LFA, which utilizes red-colored GNPs, a positive test is indicated by two red bands, while a negative test is indicated by one red band.

the ATPS to phase separate. The top phase was extracted and placed in a new test tube, and the LFA test strip was inserted vertically into the sample solution as explained previously (**Figure 1**). For detection of Tf with the 1:9 ATPS, 600 mg of a well-mixed 1:9 volume ratio ATPS containing 4.8 μL of anti-Tf DGNPs and a known concentration of Tf were added into a test tube. These overall ATPS volumes were chosen to maintain the sample volume applied to the LFA at 50 μL. The remainder of the procedure follows the methods outlined for detection with the 1:1 ATPS. Images of the test strips were taken immediately after 20 min with a Nikon D3400 camera in a controlled lighting environment. Triplicates of each test were obtained and also analyzed with a custom MATLAB program.

## Detection of *E. coli*

### Preparation of Gold Nanoprobes (GNPs)

Cherry-colored gold nanoparticles of diameter 40 nm (Nanocomposix, San Diego, CA) were obtained and stored at 4°C until use. To prepare functional probes for use in the LFA tests, the pH of the gold nanoparticle solution was adjusted to pH 9.0 using 0.5 M NaOH. For every 1 mL of gold nanoparticle solution, 8 μg of anti-*E. coli* antibodies were added. The reaction mixture was placed on a shaker for 30 min to facilitate formation of dative bonds between the antibodies and gold nanoparticles. Free antibodies were removed through centrifugation. The pellet was resuspended in 100 μL of 0.1 M sodium borate buffer at pH 9.0 and subsequently stored at 4°C until use.

### Preparation of Sandwich LFA Strips

LFA test strips utilizing the sandwich style assay were prepared in a similar manner to our previous studies (Mashayekhi et al., 2010). Briefly, both primary anti-*E. coli* antibodies and rabbit anti-goat IgG secondary antibodies were dissolved in a 25% sucrose solution for stabilization prior to being printed in lines on the CN95 nitrocellulose membrane. After overnight drying, the membrane was treated with 1% BSA. Subsequently, the 1% BSA treated S17 fiberglass sample pad, the nitrocellulose membrane, and CF4 absorbent pad were assembled onto an adhesive backing into 5 mm wide LFA strips. For the sandwich style format, anti-*E. coli* antibodies specific for the target *E. coli* are immobilized at the test line, while secondary antibodies against the primary anti-*E. coli* antibody are immobilized at the control line. If enough *E. coli* is present in the sample, *E. coli* will bind to the antibodies on the GNPs, producing *E. coli*-GNP complexes. These will bind to primary antibodies on the test line, trapping the particles and forming a visual red band. Alternatively, if the target biomarker is not present, the colloidal gold will bypass the test line without binding. Regardless, antibodies immobilized on the GNPs will bind the secondary antibodies on the control line, forming a visual band and therefore indicating a valid test. Thus, the presence of one line at the control line indicates a negative test, while the presence of two lines at both the control line and test line indicates a positive test (**Figure 1**).

### Detection of *E. coli* With LFA Only

Tests with LFA only were performed as now described. Solutions containing *E. coli* suspensions in Nutrient Broth were first prepared, with *E. coli* concentrations serially diluted from an initially prepared culture in Nutrient Broth to achieve a range of concentrations for detection. Five microliters of diluted *E. coli* suspension, or 5 μL of pure Nutrient Broth for the negative control, were added to 40 μL of PBS and 5 μL of anti-*E.coli* GNPs for a constant sample volume of 50 μL. The resulting solutions were mixed and incubated for 10 min to allow for binding between *E. coli* and the GNPs. A test strip was dipped vertically into each solution, and the sample was allowed to wick up the LFA. After 20 min, the LFA strips were taken out of the solution, and an image of each strip was immediately taken with a Nikon D3400 camera in a controlled lighting environment. Triplicates of each test were obtained; images were analyzed visually and quantified using a custom MATLAB program.

### Detection of *E. coli* With the IL ATPS/LFA Setup

For tests combining the ATPS with LFA, 120 mg of a 1:1 ATPS containing 5 μL GNPs and 12 mg of an *E. coli* suspension were added to a test tube. The suspension was incubated for 10 min, after which the top phase was extracted and tested as described previously for the LFA only tests. For the 1:9 ATPS, 600 mg of an ATPS containing 5 μL GNPs and 60 mg of an *E. coli* suspension were added to a tube and tested in a similar manner to the 1:1 ATPS runs. These overall volumes were chosen to maintain the sample volume applied to the LFA at 50 μL. The tests were also run for 20 min and immediately imaged with a Nikon D3400 camera in a controlled lighting environment. Triplicates of each test were obtained, and the images were analyzed via a custom MATLAB program.

## LFA Quantification

A custom MATLAB script was written with an approach similar to Yager and coworkers (Fu et al., 2011) to quantitatively analyze the LFA tests. Images of the test strips were taken with a Nikon D3400 camera under controlled lighting, with each strip oriented the same way. The images were cropped and converted to an 8-bit grayscale matrix. The intensity was averaged along the axis perpendicular to the flow, and therefore parallel to both the control and test lines, generating a one-dimensional intensity map. The two maxima were identified as the control and test lines, with the distance between the two lines calibrated by using a reference LFA image with strong test and control lines. In the case of the transferrin competitive assay, this corresponded to the negative control, and in the case of the *E. coli* sandwich assay, this corresponded to the positive control.

To obtain test line intensity from our sample data, the location of the control line was determined from the reference LFA image, and its distance from the test line was calibrated as described above. The test line region was set as a 15 pixel-wide region centered at this location. The baseline for the measurement was determined by averaging the signal from two 25 pixel wide boxes beginning 25 pixels before and 25 pixels after the center of our determined test line region. The test line intensity was then calculated as the area under the curve for this test line region.

# RESULTS

## Visualization of IL ATPS Phase Separation

Several criteria were used to determine a suitable ATPS for use in this study. Our anticipated design involved taking advantage of rapid phase separation speeds of IL-based systems to avoid issues faced using polymer or micellar systems. To achieve ease-of-use and minimize extra user handling steps, we sought an ATPS where our probes would partition to the top phase. Additionally, maintaining physiological pH and low ionic content in the phase DGNs and GNs partition preferentially to (i.e., the salt-rich phase) were considered, to preserve antibody function for use in the LFAs. With these considerations, [Bmim][$BF_4$] and sodium phosphate salt (2:1 dibasic:monobasic) were chosen as the components of the ATPS. These components successfully phase separated, and allowed for relatively low salt concentrations as well as a pH of 7.0 in the top phase, which was optimal for our applications. A schematic of the IL ATPS, along with competitive and sandwich LFA formats, can be found in **Figure 1**.

1:1 and 1:9 volume ratio ATPSs were achieved, and phase separation was visualized through the addition of bovine serum albumin-coated DGNs. The DGNs partitioned preferentially into the top phase, indicated by the purple-colored top phase, while the bottom phase remained clear due to the absence of DGNs. The particles were found to be stable in the ATPS, exhibiting no signs of aggregation over several days. These visualization experiments were also performed utilizing bovine serum albumin-coated gold nanoparticles (GNs), which exhibited similar partitioning and stability behavior. In all cases,

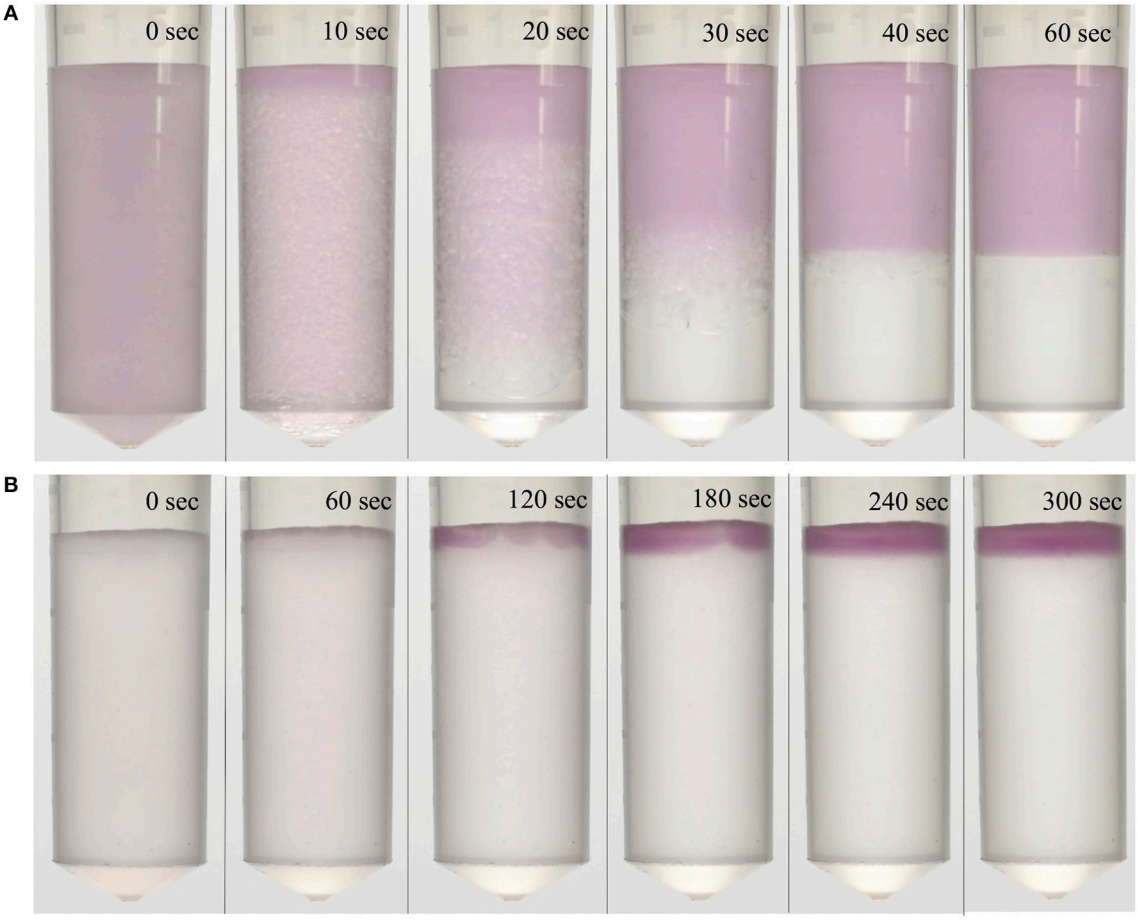


**FIGURE 2 |** Visualization of phase separation and speed of an IL ATPS. Purple-colored dextran-coated gold nanoparticles partitioned extremely to the top phase and were used to visualize separation. ATPSs separated within **(A)** 1 min for the 1:1 ATPS, and **(B)** 5 min for the 1:9 ATPS.

phase separation was found to be quite rapid, occurring in 1 min for the 1:1 ATPS (**Figure 2A**) and in 5 min for the 1:9 ATPS (**Figure 2B**). As 9:1 polymer-salt ATPSs can take an hour or so to phase separate, and 1:9 micellar systems even longer, this marked a great improvement in phase separation time compared to conventional ATPSs.

## Viscosity and Interfacial Measurements

The viscosities of the top and bottom phases of 1:1 volume ratio IL-, polymer-, and micelle-based ATPSs were measured, as shown in **Table 1**. While salt-rich and micelle-poor phase viscosities were comparable to one another for the three ATPSs, the IL-rich phase viscosity was significantly lower than those of the micelle-rich and polymer-rich phases.

Additionally, interfacial tension measurements were performed for the IL-, polymer-, and micellar-based ATPSs. The interfacial tension of the 1:1 volume ratio IL ATPS was found to be $1.8 \pm 0.3 \frac{mN}{m}$. The interfacial tensions for the polymer- and micelle-based ATPSs were below the equipment's lower limit of detection of $1 \frac{mN}{m}$. This is consistent with reports in the literature of interfacial tensions of polymer-based ATPSs being in the range of 0.1–1.9 $\frac{mN}{m}$ depending on their composition (Wu et al., 1996). Accordingly, the interfacial tension of the IL ATPS was significantly higher than the polymer- and micelle-based ATPSs that we have studied.

**TABLE 1 |** Viscosity measurements for the phases of 1:1 volume ratio IL-, polymer-, and micelle-based ATPSs.

| Type of ATPS | Type of phase | Viscosity (cP) |
|---|---|---|
| Polymer | Salt-rich | 1.83 ± 0.03 |
| | Polymer-rich | 23.9 ± 1.3 |
| Micellar | Micelle-poor | 1.55 ± 0.04 |
| | Micelle-rich | 120.7 ± 0.5 |
| Ionic Liquid | Salt-rich | 1.95 ± 0.02 |
| | Ionic liquid-rich | 4.1 ± 0.1 |

*The viscosity of the IL-rich phase was much lower than the viscosities of the polymer-rich and micelle-rich phases investigated.*

## Detection of Tf

Upon identifying compositions for 1:1 and 1:9 IL ATPSs, we investigated the degree of improvement in utilizing these ATPSs

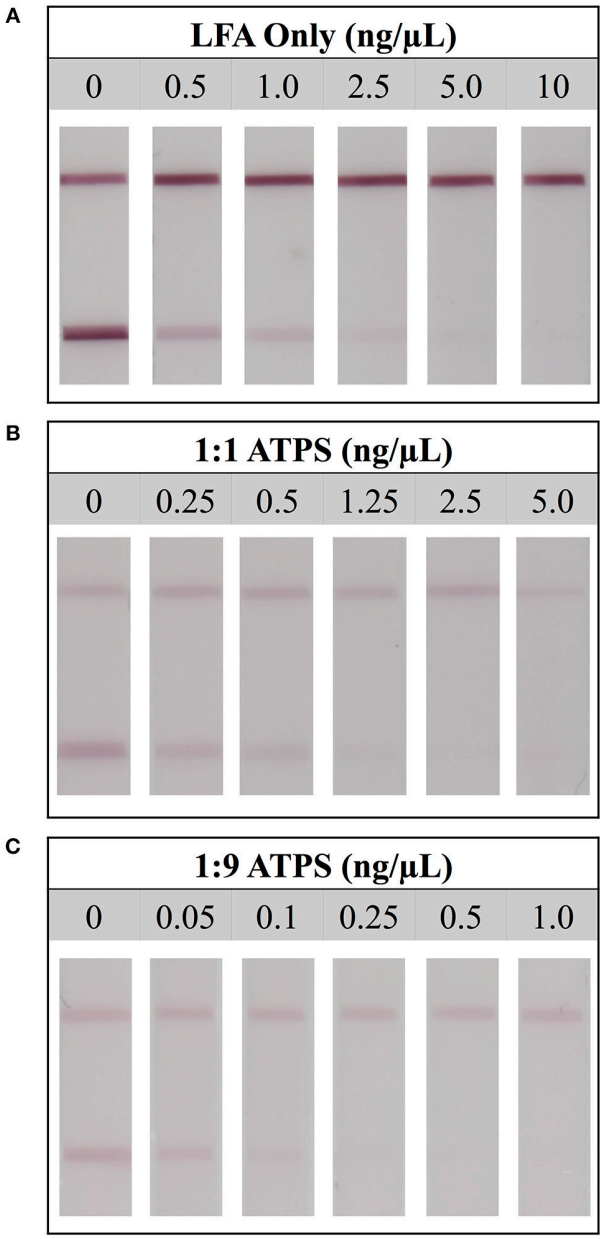


**FIGURE 3 |** Limit of detection for LFA tests detecting for protein transferrin. **(A)** Detection limit for the LFA-only test was found to be 5 ng/μL. **(B)** Detection limit for the LFA when combined with a 1:1 ATPS was 1.25 ng/μL, and **(C)** detection limit for the LFA when combined with a 1:9 ATPS was 0.25 ng/μL, indicating 4-fold and 20-fold improvements, respectively.

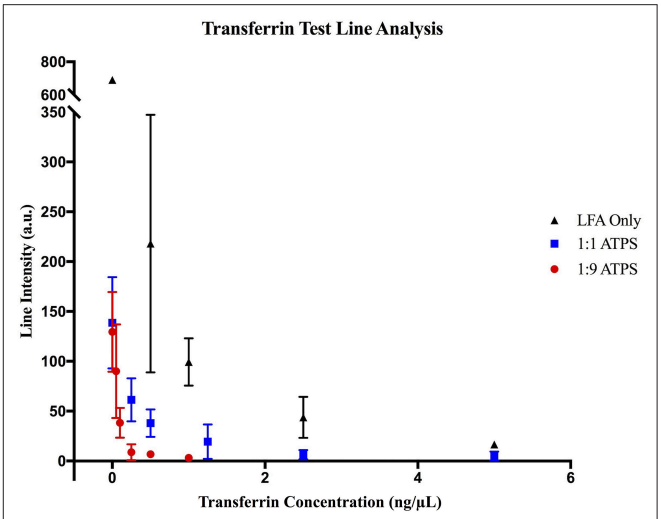


**FIGURE 4 |** MATLAB analysis of transferrin LFA tests. Data for (▲) LFA-only tests without ATPS enhancement, (■) enhancement with a 1:1 ATPS, and (●) enhancement with a 1:9 ATPS. At each concentration, test line intensities in arbitrary units (a.u.) were lower for the 1:1 ATPS/LFA test than the LFA-only test and lower for the 1:9 ATPS/LFA test than the 1:1 ATPS/LFA test, indicating improved detection with more extreme volume ratios.

for the detection of the model biomarker Tf. To do this, we sought to determine the limit of detection of Tf utilizing an LFA-only set-up, and then compare it directly with the limit of detection obtained utilizing the IL ATPS/LFA setup. As previously mentioned, these experiments were performed as competitive assays; two bands would indicate a negative test, as the antibodies on the DGNPs would be able to bind the immobilized Tf at the test line, and a single band at the control line would indicate a positive test, as DGNP antibody binding sites would be saturated and therefore unable to bind the Tf on the test line. With these mechanisms in mind, the limit of detection was defined as the lowest concentration of Tf at which the test line was not visible.

For the LFA-only tests, when a high concentration of Tf was used (10 ng/μL), test lines did not develop, indicating a true positive result. However, at a lower concentration (2.5 ng/μL), a test line was present, indicating a false negative result. This suggested that the limit of detection for LFA without ATPS enhancement was 5 ng/μL (**Figure 3A**). A similar analysis was performed for the 1:1 and 1:9 ATPS setups and the limits of detection were found to be 1.25 ng/μL (**Figure 3B**) and 0.25 ng/μL (**Figure 3C**), respectively, indicating 4- and 20-fold improvements in detection over LFA-only. The improvement was significant, but the test lines were fainter compared to the LFA only tests. The control line intensities were also fainter. These findings were confirmed via our MATLAB analysis; test lines were less developed across all concentrations, including our negative control at 0 ng/μL (**Figure 4**). We also observed a large standard deviation in the test line intensity of LFA only for 0.5 ng/μL, which is likely due to variability in the background signal. However, this variability did not have a significant effect on our conclusions from the MATLAB analysis, as the error bars for different tests did not overlap, and the entire range of intensities for this concentration corresponds to very visible lines. Since a less developed test line corresponds to an improvement in the limit of detection for the competitive assay, it was unclear if the improvement we observed was primarily a result of this diminished line intensity or of the ATPS concentration. To determine this, we also investigated the use of the IL ATPS with a sandwich format assay.

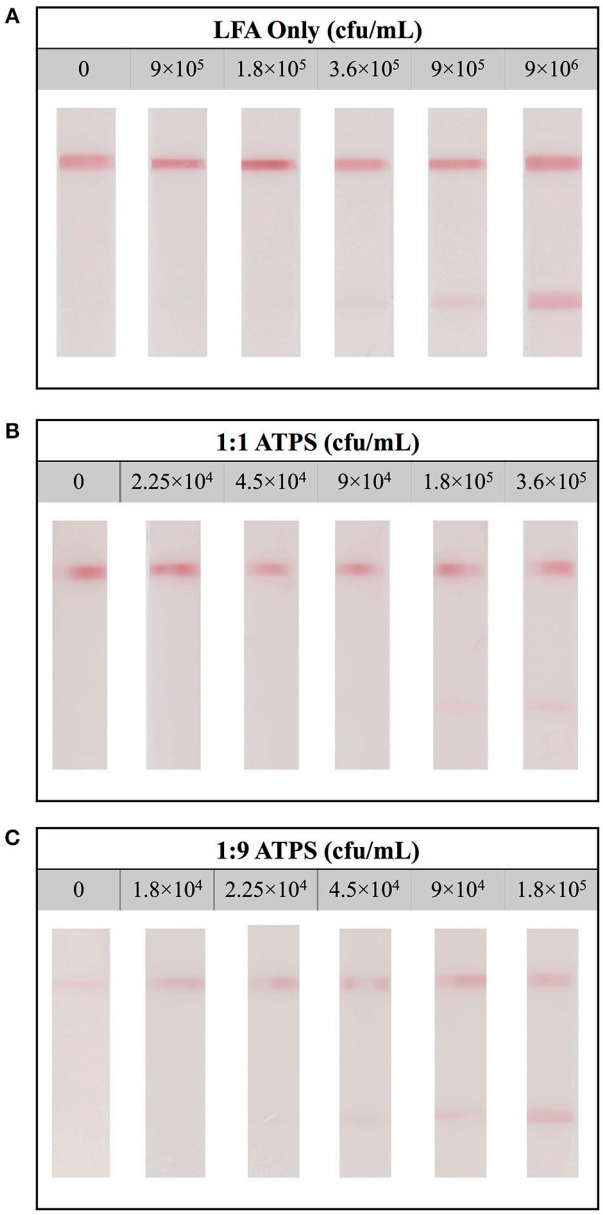


**FIGURE 5 |** Limit of detection for LFA tests detecting for *Escherichia coli*. **(A)** Detection limit for the LFA-only test was found to be 3.6 × $10^5$ cfu/mL. **(B)** Detection limit for the LFA when combined with a 1:1 ATPS was 1.8 × $10^5$ cfu/mL and **(C)** detection limit for the LFA when combined with a 1:9 ATPS was 4.5 × $10^4$ cfu/mL, indicating 2-fold and 8-fold improvements, respectively.

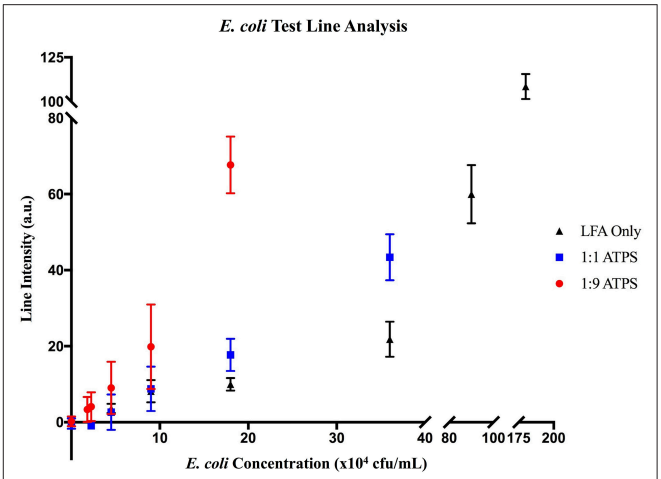


**FIGURE 6 |** MATLAB analysis of *E. coli* LFA tests. Data for (▲) LFA-only tests without ATPS enhancement, (■) enhancement with a 1:1 ATPS, and (●) enhancement with a 1:9 ATPS. At each concentration, test line intensities in arbitrary units (a.u.) were greater for the 1:1 ATPS/LFA test than the LFA-only test and greater for the 1:9 ATPS/LFA test than the 1:1 ATPS/LFA test, indicating improved detection with more extreme volume ratios.

## Detection of *E. coli*

Following the detection of Tf, we studied the detection of *E. coli* as a large biomarker to demonstrate improvement using an IL ATPS in a sandwich-format LFA, where diminishing of line intensities will have a negative impact on the detection limit. We performed experiments in a similar manner to the Tf tests. For this format, the top line still constituted the control line, indicating a valid test. However, the test line was comprised of primary antibodies specific to the target, rather than the target biomolecule itself. If the sample solution contains the target antigen, the antigen will bind antibodies on the GNPs, forming an antigen-antibody complex. This complex will then bind the immobilized antibodies on the test line, producing a visual red band. Conversely, if there is no target antigen, the antibody-antigen complex will not form and no test line will develop. Thus, for sandwich assays, two lines would indicate a positive test, while only one line would indicate a negative test. In this case, the limit of detection was defined as the lowest concentration of *E. coli* at which the test line was visible.

When testing with LFA only, at a high concentration of *E. coli* (1.8 × $10^6$ cfu/mL), two strong lines developed, indicating a true positive result. At a lower concentration (9 × $10^4$ cfu/mL), only one line formed, exhibiting a false negative result. These results suggest the limit of detection of *E. coli* using LFA only tests is 3.6 × $10^5$ cfu/mL (**Figure 5A**). Utilizing this analysis, the limits of detection for the 1:1 ATPS and 1:9 ATPS were determined to be 1.8 × $10^5$ cfu/mL (**Figure 5B**) and 4.5 × $10^4$ cfu/mL (**Figure 5C**), respectively, indicating 2-fold and 8-fold improvements in the limit of detection. While lighter line intensities than expected were still observed in these tests, the fact that improvement was still achieved in a sandwich LFA indicated that the concentration effect due to the IL ATPS was the dominant contributor to the improvement in detection limit. This analysis was confirmed via MATLAB analysis. As seen in **Figure 6**, test line intensity was improved with the application of more extreme volume ratio ATPSs, which corresponds with improvements in the detection limit of these tests.

## DISCUSSION

Our group had previously demonstrated enhanced detection through the combination of LFA with ATPSs, specifically using

polymer-salt and micellar systems; however, a primary handicap in the direct application of these ATPSs is their long phase separation time. As described previously, these systems can take hours to phase separate, which can limit their viability at the point-of-care. Our laboratory also demonstrated that the application of an ATPS to 3-D paper architecture drastically improves phase separation time (Pereira et al., 2015). However, this method requires modification to existing LFA devices to accommodate the enhancement technique. As the phase separation time of the IL ATPS for both 1:1 and 1:9 volume ratios were within 1 min and 5 min, this IL ATPS can be directly applied to existing LFA technologies, without necessitating modifications to the LFA. We hypothesize that this rapid phase separation speed can be due to several factors. This is further supported by the work of Gutowski et al., 2003; kosmotropic salts would increase the difference in dielectric constants between IL and water (Gutowski et al., 2003), promoting coalescing of similar domains in response to a high interfacial tension.

In addition to more rapid phase separation, the IL ATPS also displayed a greater degree of enhancement, specifically regarding the competitive LFA tests for Tf. While the degree of concentration for the 1:9 ATPS should be close to 10-fold, the improvement in the limit of detection was found to be 20-fold. We hypothesize this unexpected improvement is most likely due to the high ionic content of the system, which produces a screening effect that influences antibody-antigen binding. However, as use of the IL ATPS for the detection of *E. coli* still improved detection 8-fold, we determined that most of the enhancement seen for Tf is still a result of the ATPS concentration effect. The precise level of test line diminishment, and therefore the deviance from expected improvement, likely depends on the exact antibodies used in a particular assay. We do note that, in this study, both monoclonal and polyclonal antibodies for different antigens in different assay formats were successful, suggesting this system should still be widely applicable. Additionally, while the system does exhibit diminishing of line intensities, it should be noted that a primary motivation for use of this system would be to apply it to the partitioning of small biomarkers. These smaller biomarkers would generally require detection with the competitive LFA, as they typically do not contain many antigen binding sites required for use with the sandwich assay. Therefore, this screening effect only helps our system.

We envision the IL ATPS to be used for the detection of a wide range of proteins, with the ability to tailor the exact IL and salt system to accommodate the target of choice. To achieve this, we anticipate that a greater understanding of the phase separation mechanism of these IL-based ATPSs will be required. We also investigated the IL ATPS comprised of [Bmim][Cl] and potassium phosphate salt. Surprisingly, despite having similar components to our [Bmim][$BF_4$] ATPS, this system displayed different phase separation behavior, consisting of an IL-rich top phase and a salt-rich bottom phase. While the exact mechanism of IL ATPS phase separation is not precisely understood, it is commonly believed that separation occurs due to the salting out effect of kosmotropic salts on the IL component. The degree of this salting out is likely a large factor in determining partitioning behavior and relative hydrophobicity/hydrophilicity of each phase. We found that this [Bmim][Cl] system yielded different gold nanoprobe partitioning behavior from the [Bmim][$BF_4$] counterpart, with GNs partitioning extremely to the top IL-rich phase and DGNs partitioning extremely to the bottom salt-rich phase. While the ability to partition similar particles to different phases is promising, it is clear that a greater understanding of phase separation and partitioning behavior is needed to take full advantage of these capabilities.

## CONCLUSIONS

In summary, we successfully demonstrated the first use of an IL ATPS for the enhanced detection of biomarkers with the LFA. Specifically, a 20-fold improvement in the detection limit for transferrin was achieved utilizing a 1:9 volume ratio ATPS. This improvement can be seen as a combination of biomarker concentration, induced by the ATPS, as well as diminished test line intensity, likely due to screening effects from the ionic content of the ATPS. Despite the effects of the ATPS ionic content, an 8-fold improvement could still be achieved in the detection limit for *E. coli* using the sandwich-format LFA, where diminished test line intensities have a negative impact on the detection limit. Accordingly, most of the enhancement in the detection limit can be attributed to the preconcentration capability of the ATPS. Furthermore, this IL ATPS was found to phase separate very quickly, allowing for direct application to LFA without requiring modifications to existing LFA structure. While we demonstrated functionality using two biomarkers, we anticipate that further investigation into specific IL-salt pairings can enhance improvement for small biomarkers that would be difficult to concentrate otherwise. This combination of tunability and speed presents this system as a flexible, powerful enhancement tool for use with a wide variety of biomarkers and pathogens.

## AUTHOR CONTRIBUTIONS

MY, GE, and EY designed experiments, performed experiments, analyzed results, and drafted the manuscript. EL and JP performed experiments, analyzed results, and revised the manuscript. BW and DK designed experiments, analyzed results, and revised the manuscript.

## FUNDING

This work was funded by the National Institutes of Health (Grant No: 1R44AI127060-01A1).

## REFERENCES


Berthod, A., Ruiz-Ángel, M. J., and Carda-Broch, S. (2008). Ionic liquids in separation techniques. *J. Chromatogr. A* 1184, 6–18. doi: 10.1016/j.chroma.2007.11.109

Cheung, S. F., Yee, M. F., Le, N. K., Gomes, E. A., Afrasiabi, Z., and Kamei, D. T. (2017). A combined aqueous two-phase system and spot-test platform for the rapid detection of *Escherichia coli* O157:H7 in milk. *SLAS Technol.* 23, 57–63. doi: 10.1177/2472630317731892

Chiu, R. Y., Nguyen, P. T., Wang, J., Jue, E., Wu, B. M., and Kamei, D. T. (2014). Dextran-coated gold nanoprobes for the concentration and detection of protein biomarkers. *Ann. Biomed. Eng.* 42, 2322–2332. doi: 10.1007/s10439-014-1043-3

Elbireer, A. M., Opio, A. A., Brough, R. L., Jackson, J. B., and Manabe, Y. C. (2011). Strengthening public laboratory service in Sub-Saharan Africa: Uganda case study. *Lab. Med.* 42, 719–725. doi: 10.1309/LM2OBNYY9D0UXZJO

Freire, M. G., Cla, F. M., Coutinho, A. P., and Marrucho, I. M. (2012). Aqueous biphasic systems: a boost brought about by using ionic liquids. *Chem. Soc. Rev.* 41, 4966–4995. doi: 10.1039/c2cs35151j

Fu, E., Liang, T., Houghtaling, J., Ramachandran, S., Ramsey, S. A., Lutz, B., et al. (2011). Enhanced sensitivity of lateral flow tests using a two-dimensional paper network format. *Anal. Chem.* 83, 7941–7946. doi: 10.1021/ac201950g

Global Tuberculosis Report 2017 (2017). Geneva: World Health Organization.

Gumustas, A., Caglayan, M. G., Eryilmaz, M., Suludere, Z., Soykut, E. A., Uslu, B., et al. (2018). Paper based lateral flow immunoassay for the enumeration of *Escherichia coli* in urine. *Anal. Methods* 10, 1213–1218. doi: 10.1039/C7AY02974H

Gunasekera, D. P. S., and Pathiraja, R. P. (2016). Congenital zika infection: a challenge for resource poor settings. *Clin. Pediatr.* 1:e110. doi: 10.4172/2572-0775.1000e110

Gutowski, K. E., Broker, G. A., Willauer, H. D., Huddleston, J. G., Swatloski, R. P., Holbrey, J. D., et al. (2003). Controlling the aqueous miscibility of ionic liquids: aqueous biphasic systems of water-miscible ionic liquids and water-structuring salts for recycle, metathesis, and separations. *J. Am. Chem. Soc.* 125, 6632–6633. doi: 10.1021/ja0351802

Hatti-Kaul, R. (2001). Aqueous two-phase systems: a general overview. *Mol. Biotechnol.* 19, 269–277. doi: 10.1385/MB:19:3:269

Iqbal, M., Tao, Y., Xie, S., Zhu, Y., Chen, D., Wang, X., et al. (2016). Aqueous two-phase system (ATPS): an overview and advances in its applications. *Biol. Proced. Online* 18:18. doi: 10.1186/s12575-016-0048-8

Jang, H., Ryoo, S. R., Kostarelos, K., Han, S. W., and Min, D. H. (2013). The effective nuclear delivery of doxorubicin from dextran-coated gold nanoparticles larger than nuclear pores. *Biomaterials* 34, 3503–3510. doi: 10.1016/j.biomaterials.2013.01.076

Li, W., Liu, Y., Zhao, Y., Tao, R., Li, Y., and Shang, S. (2015). Rapid diagnosis of *Mycoplasma pneumoniae* in children with pneumonia by an immuno-chromatographic antigen assay. *Sci. Rep.* 5:15539. doi: 10.1038/srep15539

Liu, Q., Yu, J., Li, W., Hu, X., and Xia, H. (2007). Partitioning behavior of penicillin G in aqueous two phase system formed by ionic liquids and phosphate partitioning behavior of penicillin G. *Sep. Sci. Technol.* 41, 2849–2858. doi: 10.1080/01496390600786135

Mashayekhi, F., Chiu, R. Y., Le, A. M., Chao, F. C., Wu, B. M., and Kamei, D. T. (2010). Enhancing the lateral-flow immunoassay for viral detection using an aqueous two-phase micellar system. *Anal. Bioanal. Chem.* 398, 2955–2961. doi: 10.1007/s00216-010-4213-7

Mashayekhi, F., Le, A. M., Nafisi, P. M., Wu, B. M., and Kamei, D. T. (2012). Enhancing the lateral-flow immunoassay for detection of proteins using an aqueous two-phase micellar system. *Anal. Bioanal. Chem.* 404, 2057–2066. doi: 10.1007/s00216-012-6278-y

Nkengasong, J. N., Mesele, T., Orloff, S., Kebede, Y., Fonjungo, P. N., Timperi, R., et al. (2018). Critical role of developing national strategic plans as a guide to strengthen laboratory health systems in resource-poor settings. *Am. J. Clin. Pathol.* 852–7. doi: 10.1309/AJCPC51BLOBBPAKC

Nugent, R. (2008). Chronic diseases in developing countries: Health and economic burdens. *Ann. N. Y. Acad. Sci.* 1136, 70–79. doi: 10.1196/annals.1425.027

Pereira, D. Y., Chiu, R. Y. T., Zhang, S. C. L., Wu, B. M., and Kamei, D. T. (2015). Single-step, paper-based concentration and detection of a malaria biomarker. *Anal. Chim. Acta* 882, 83–89. doi: 10.1016/j.aca.2015.04.040

Scarborough, M., and Thwaites, G. E. (2008). The diagnosis and management of acute bacterial meningitis in resource-poor settings. *Lancet Neurol.* 7, 637–648. doi: 10.1016/S1474-4422(08)70139-X

Sharma, S., Zapatero-Rodríguez, J., Estrela, P., and O'Kennedy, R. (2015). Point-of-Care diagnostics in low resource settings: present status and future role of microfluidics. *Biosens.* 5, 577–601. doi: 10.3390/bios5030577

Tang, B., Bi, W., Tian, M., and Row, K. H. (2012). Application of ionic liquid for extraction and separation of bioactive compounds from plants. *J. Chromatogr. B* 904, 1–21. doi: 10.1016/j.jchromb.2012.07.020

Tang, J., and Nour, N. M. (2010). HIV and pregnancy in resource-poor settings. *Rev. Obstetr. Gynecol.* 3, 66–71.

Ventura, S. P. M., Sousa, S. G., Serafim, L. S., Lima, Á. S., Freire, M. G., and Coutinho, J. A. P. (2011). Ionic liquid based aqueous biphasic systems with controlled pH: the ionic liquid cation effect. *J. Chem. Eng. Data* 56, 4253–4260. doi: 10.1021/je200714h

Wang, R., Kim, K., Choi, N., Wang, X., Lee, J., Jeon, J. H., et al. (2018). Highly sensitive detection of high-risk bacterial pathogens using SERS-based lateral flow strips. *Sens. Actuators B* 270, 72–79. doi: 10.1016/j.snb.2018.04.162

Wilkes, J. S., Levisky, J. A., Wilson, R. A., and Hussey, C. L. (1982). Dialkylimidazolium chloroaluminate melts: a new class of room-temperature ionic liquids for electrochemistry, spectroscopy, and synthesis. *Inorg. Chem.* 21, 1263–1264. doi: 10.1021/ic00133a078

Wu, Y. T., Zhu, Z. Q., and Mei, L.,H. (1996). Interfacial tension of poly(ethlyene glycol) + salt + water systems. *J. Chem. Eng. Data* 41, 1032–1035. doi: 10.1021/je960044g


**Conflict of Interest Statement:** BW and DK are founders of the company Phase Diagnostics that intends on commercializing this core technology. They have financial interests in Phase Diagnostics, which has licensed this intellectual property from the UC Regents.

The remaining authors declare that the research was conducted in the absence of any commercial or financial relationships that could be construed as a potential conflict of interest.

frontiers in Chemistry

ORIGINAL RESEARCH
published: 31 October 2018
doi: 10.3389/fchem.2018.00529

# Purification of the Recombinant Green Fluorescent Protein Using Aqueous Two-Phase System Composed of Recyclable $CO_2$-Based Alkyl Carbamate Ionic Liquid

*Cher Pin Song*[1,2], *Poh En Liew*[1], *Zora Teh*[1], *Schian Pei Lim*[1], *Pau Loke Show*[3] *and Chien Wei Ooi*[1]*

[1] *Chemical Engineering Discipline, School of Engineering, Selangor, Malaysia,* [2] *Advanced Engineering Platform, School of Engineering, Monash University Malaysia, Selangor, Malaysia,* [3] *Bioseparation Research Group, Department of Chemical and Environmental Engineering, Faculty of Engineering, University of Nottingham Malaysia, Selangor, Malaysia*

The formation of aqueous two-phase system (ATPS) with the environmentally friendly and recyclable ionic liquid has been gaining popularity in the field of protein separation. In this study, the ATPSs comprising *N*,*N*-dimethylammonium *N*′,*N*′-dimethylcarbamate (DIMCARB) and thermo-responsive poly(propylene) glycol (PPG) were applied for the recovery of recombinant green fluorescent protein (GFP) derived from *Escherichia coli*. The partition behavior of GFP in the PPG + DIMCARB + water system was investigated systematically by varying the molecular weight of PPG and the total composition of ATPS. Overall, GFP was found to be preferentially partitioned to the hydrophilic DIMCARB-rich phase. An ATPS composed of 42% (w/w) PPG 1000 and 4.4% (w/w) DIMCARB gave the optimum performance in terms of GFP selectivity (1,237) and yield (98.8%). The optimal system was also successfully scaled up by 50 times without compromising the purification performance. The bottom phase containing GFP was subjected to rotary evaporation of DIMCARB. The stability of GFP was not affected by the distillation of DIMCARB, and the DIMCARB was successfully recycled in three successive rounds of GFP purification. The potential of PPG + DIMCARB + water system as a sustainable protein purification tool is promising.

**Keywords: purification, green fluorescent protein, aqueous two-phase system, dialkyl carbamate, poly(propylene glycol), recycling**

OPEN ACCESS

***Edited by:***
*John Paul Frampton,*
*Dalhousie University, Canada*

***Reviewed by:***
*Zhibao Huo,*
*Shanghai Jiao Tong University, China*
*Wee-Jun Ong,*
*Xiamen University Malaysia, Malaysia*

***Correspondence:**
*Chien Wei Ooi*
*ooi.chien.wei@monash.edu*

***Specialty section:***
*This article was submitted to Chemical Engineering, a section of the journal Frontiers in Chemistry*

***Received:*** *30 July 2018*
***Accepted:*** *11 October 2018*
***Published:*** *31 October 2018*

***Citation:***
*Song CP, Liew PE, Teh Z, Lim SP, Show PL and Ooi CW (2018) Purification of the Recombinant Green Fluorescent Protein Using Aqueous Two-Phase System Composed of Recyclable $CO_2$-Based Alkyl Carbamate Ionic Liquid. Front. Chem. 6:529. doi: 10.3389/fchem.2018.00529*

## INTRODUCTION

Green fluorescent protein (GFP) has been widely applied in the cellular and molecular biology research due to its unique properties such as the intense fluorescence visibility, high thermal stability, and the adjustable fluorescence intensity via a proper manipulation of the protein structure (Skosyrev et al., 2003; Li et al., 2009; Quental et al., 2015). Additionally, GFP can be easily quantified via spectrofluorimetric assay, making it a good candidate as a biosensor (Wouters et al., 2001) and biomarker (Gerisch et al., 1995) in the biotechnological application. The recombinant GFP has been successfully expressed by various organisms, including *Escherichia coli*

(*E. coli*) (Lo et al., 2018), zebrafish (Amsterdam et al., 1996), *Drosophila* (Wang and Hazelrigg, 1994), and yeast (Amsterdam et al., 1996). Nevertheless, the purification of GFP with the conventional chromatographic techniques generally involves complex and tedious operations, resulting in a higher purification cost (Deschamps et al., 1995; Cabanne et al., 2005; McRae et al., 2005; Zhuang et al., 2008).

Aqueous two-phase system (ATPS) has been widely viewed as a potential alternative method for the separation of biomolecules. The advantages of ATPS include the high extraction efficiency, the cost effectiveness, and the simplicity of operation. This type of liquid-liquid extraction is commonly exploited for the primary recovery and purification of valuable biological products such as proteins (Merchuk et al., 1998), enzymes (Kroner et al., 1982), nucleic acids (Gomes et al., 2009), and viruses (Liu et al., 1998). ATPS is conventionally made of two types of incompatible polymers, or a polymer coupled with a salting-out inducing salt; the concentrations of phase-forming components in an aqueous solution must exceed the threshold value. ATPS has been widely perceived as a biocompatible medium for preserving the biological properties of biomolecules, owing to the large proportion of water content in both phases (Yao et al., 2018). The extraction of GFP has been successful achieved using the traditional ATPSs consisting of phase-forming components such as polymer, surfactant, alcohol, and inorganic salts (Jain et al., 2004; Johansson et al., 2008; Li and Beitle Robert, 2008; Samarkina et al., 2009; Lopes et al., 2011; Lo et al., 2018). However, the limited polarity range of the coexisting phases and the poor recyclability of the conventional phase-forming components have constituted a major bottleneck that hampers the vast use of these conventional ATPSs (Hatti-Kaul, 2000).

Over the past decade, ionic liquid (IL) has been envisaged as an alternative phase-forming component of ATPS due to its highly tunable properties (Freire et al., 2012). IL is a type of molten organic salt with a melting point below 100°C. By properly selecting the cation and anion counterparts, the resultant ILs possess the desired polarity and affinity suitable for the separation of protein in ATPS. In comparison to the conventional polymer-based ATPS, the flexibility of IL-based ATPS allows a better design of the separation system for the target protein in a highly complex crude mixture. Nonetheless, the wide implementation of IL in liquid-liquid extraction is still restricted by the synthesis cost of IL, which is generally more expensive than the conventional phase-forming components (Plechkova and Seddon, 2008). Moreover, some of the conventionally used ILs (i.e., imidazolium- and pyridinium-based ILs) are reported to be highly toxic (Docherty and Kulpa, 2005). With the rising environmental consciousness in public, the application of environmentally benign ILs (e.g., cholinium- and amino acids-based ILs) in forming ATPS has been on the rise (Song et al., 2015, 2017, 2018a).

The $CO_2$-based alkyl carbamate IL, which is formed by the combination of $CO_2$ with dimethylamine (Bhatt et al., 2006; Chowdhury et al., 2010; Idris et al., 2014; Vijayaraghavan and MacFarlane, 2014), has recently emerged as a potential phase-forming component of IL-based ATPS. In general, the synthesis of the alkyl carbamate IL is considerably simpler and cheaper than the conventional ILs (Kreher et al., 2004). It has been reported that the alkyl carbamate IL possesses the characteristics of biodegradability and biocompatibility (Stark et al., 2009). More importantly, the $CO_2$-based alkyl carbamate IL can be distilled at a relatively low temperature under vacuum condition, thereby allowing a simple recovery of IL for the subsequent extraction process (Vijayaraghavan and MacFarlane, 2014). Recently, our group reported a novel type of IL + polymer ATPS comprising *N*,*N*-dimethylammonium *N*′,*N*′-dimethylcarbamate (DIMCARB, i.e., the simplest form of $CO_2$-based alkyl carbamate IL) and the thermo-responsive poly(propylene) glycol (PPG) (Song et al., 2018b). Both DIMCARB and PPG used in this ATPS can be recovered via rotary evaporation and thermo-separation, respectively, for a viable recycling of phase-forming component.

Here, the application of DIMCARB + PPG + water systems for separating the target biomolecule from a real crude protein mixture was reported for the first time. The purification of recombinant GFP from the clarified lysate of microbial feedstock was performed using ATPSs made of DIMCARB and PPG. The stability and partition behavior of GFP in the ATPSs were studied, and the composition of ATPS was optimized for the purification of GFP. To evaluate the sustainability of this ATPS for practical use, DIMCARB was also recycled for several rounds of GFP purification.

# MATERIALS AND METHODS

## Materials

DIMCARB, and PPG (molecular weight of 400, 700, and 1,000 g.mol$^{-1}$) were obtained from Sigma-Aldrich (St. Louis, U.S.A.). Tris base (ULTROL grade) was obtained from CalBiochem (San Diego, U.S.A.). Luria-Bertani (LB) broth, kanamycin sulfate, chloramphenicol, ethanol, isopropyl β-D-1-thiogalactopyranoside (IPTG), methanol, and acetic acid were purchased from Merck (Darmstadt, Germany). Coomassie Brilliant Blue R-250 (CBB-R250) staining solution were sourced from Bio-Rad Laboratories (Singapore). Protein marker (ExcelBand$^{TM}$ 3-color Broad Range) with the molecular weight ranging from 5–245 kDa was acquired from SMOBiO Technology (Taiwan). All chemicals were of analytical reagent grade.

## Methods

### Production of Recombinant GFP

The GFP was expressed by *E. coli* strain BL21(DE3)pLysS transformed with pET28a-GFP plasmid. The cells were cultured at 30°C in LB broth medium containing 50 μg/ml kanamycin and 50 μg/ml chloramphenicol. When the optical density ($OD_{600}$) of cell culture reached 0.7–0.9, 0.5 mM IPTG was added to the culture for the induction of GFP expression. The cell culture was incubated in an orbital shaker for another 12 h at 30°C and 200 rpm. Then, the culture broth was centrifuged at 4,000 rpm and 4°C for 20 min. The harvested cell pellets were resuspended in 50 mM Tris-HCl (pH 8) buffer, and the concentration of biomass was adjusted to 10% (w/v). The disruption of cells was performed using an ultrasonic homogenizer (Cole-Palmer, U.S.A.) equipped

with a horn-tip of 3 mm diameter (Model KH-04710-42, Cole-Parmer, U.S.A.) and operated at a frequency of 20 kHz, 40% amplitude for 40 min in pulse mode (Lo et al., 2016). Finally, the ultrasonicated solution was centrifuged for 10 min at 14,000 rpm and 4°C. The supernatant containing the soluble GFP was collected and used as the feedstock for ATPS.

## Protein Quantification

The concentration of GFP was determined spectrofluorometrically using a standard curve of pure GFP. The preparation of the pure GFP is described elsewhere (Lo et al., 2018). In brief, 100 µl of the sample was first loaded in a black microtiter plate. The relative fluorescence unit (RFU) of the sample were measured using a spectrofluorometer (Infinite® 200 PRO, Tecan) at the excitation wavelength of 448 nm and the emission wavelength of 512 nm. The concentration of protein in the sample solution was estimated from the polyacrylamide gel using densitometric method as described (Lee et al., 2015). In the gel, the protein bands in a sample lane were evaluated individually based on the intensity ratio of a single band to the total bands in a lane. The intensity of control band (i.e., pure GFP) was used in the calculation of the protein concentration.

## Sodium Dodecyl Sulfate Polyacrylamide Gel Electrophoresis (SDS-PAGE)

Prior to the SDS-PAGE analysis, the protein samples were subjected to ethanol precipitation for the removal of phase-forming components (e.g., ionic DIMCARB) that could interfere the electrophoresis. A mixture containing one part of sample solution and nine parts of chilled absolute ethanol was first prepared. The mixture was vortexed vigorously, before being stored at −20°C for 60 min. Next, the solution was centrifuged at 15,000 rpm for 10 min. After discarding the supernatant, the pellet was resuspended in the chilled ethanol and the solution was centrifuged again. The washing step was performed twice, and the pellet was then dried at room temperature for 10 min.

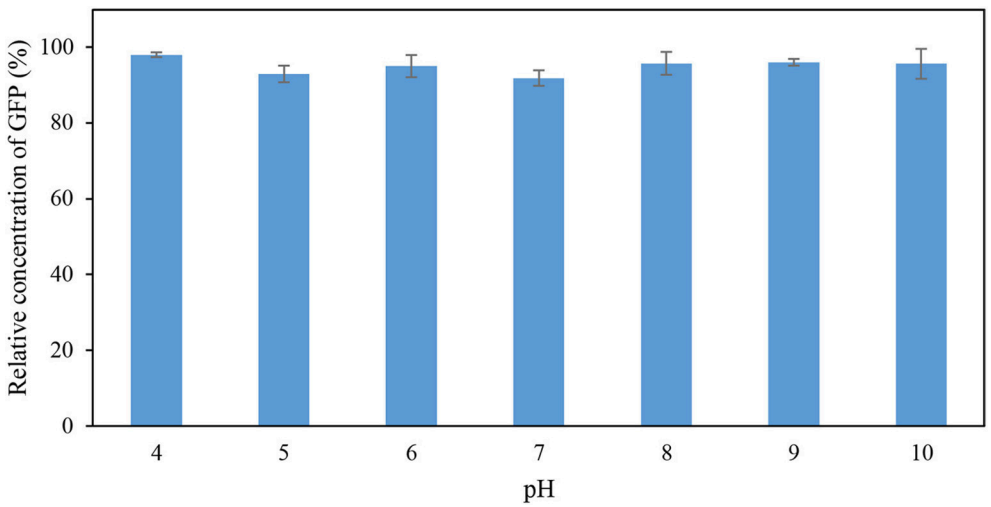


**FIGURE 1 |** Percentage relative concentration of GFP incubated in 50 mM Tris-HCl buffer at different pH for 60 min at 25°C.

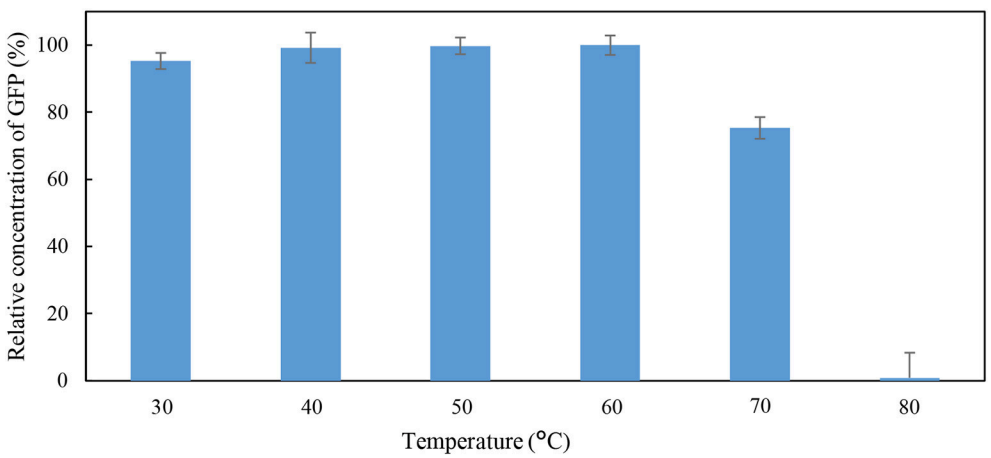


**FIGURE 2 |** Percentage relative concentration of GFP incubated in 50 mM Tris-HCl buffer at pH 8 for 60 min at different temperature.

**TABLE 1 |** Partition of GFP in PPG 400/700/1000 + DIMCARB + water systems at different phase compositions.

| System | Sampl number | TLL[a] | log $K$[b] | | $S$ | $Y$ (%) | |
|---|---|---|---|---|---|---|---|
| | | | GFP | Protein | | Top phase | Bottom phase |
| PPG 400 + DIMCARB + water | 1 | 46.4 | 2.81 | 0.360 | 279.0 | 0.16 | 96.2 |
| | 2 | 69.8 | 2.78 | 0.219 | 365.8 | 0.15 | 89.2 |
| | 3 | 78.7 | 2.85 | 0.380 | 293.5 | 0.13 | 91.5 |
| | 4 | 85.6 | 2.83 | 0.365 | 294.7 | 0.13 | 90.9 |
| | 5 | 93.1 | 2.76 | 1.130 | 42.28 | 0.17 | 96.2 |
| PPG 700 + DIMCARB + water | 6 | 90.0 | −2.88 | −1.249 | 0.023 | 74.2 | 0.10 |
| | 7 | 92.9 | −1.35 | −0.858 | 0.325 | 76.6 | 3.45 |
| | 8 | 94.3 | 3.09 | 1.008 | 119.9 | 0.08 | 98.2 |
| | 9 | 95.2 | 3.09 | 0.974 | 131.1 | 0.08 | 95.3 |
| | 10 | 95.8 | 3.12 | 0.934 | 154.8 | 0.07 | 95.3 |
| PPG 1000 + DIMCARB + water | 11 | 92.9 | −2.73 | −1.397 | 0.047 | 78.2 | 0.15 |
| | 12 | 94.8 | −2.96 | −0.429 | 0.003 | 79.4 | 0.09 |
| | 13 | 95.8 | 3.10 | 0.609 | 307.1 | 0.08 | 98.2 |
| | 14 | 96.7 | 3.05 | 0.493 | 358.9 | 0.09 | 96.6 |
| | 15 | 97.4 | 3.20 | 0.105 | 1237 | 0.14 | 98.8 |

[a] *Data taken from literature (Song et al., 2018b).*
[b] *K values are expressed as a mean of triplicate readings with the estimated error of <5%.*

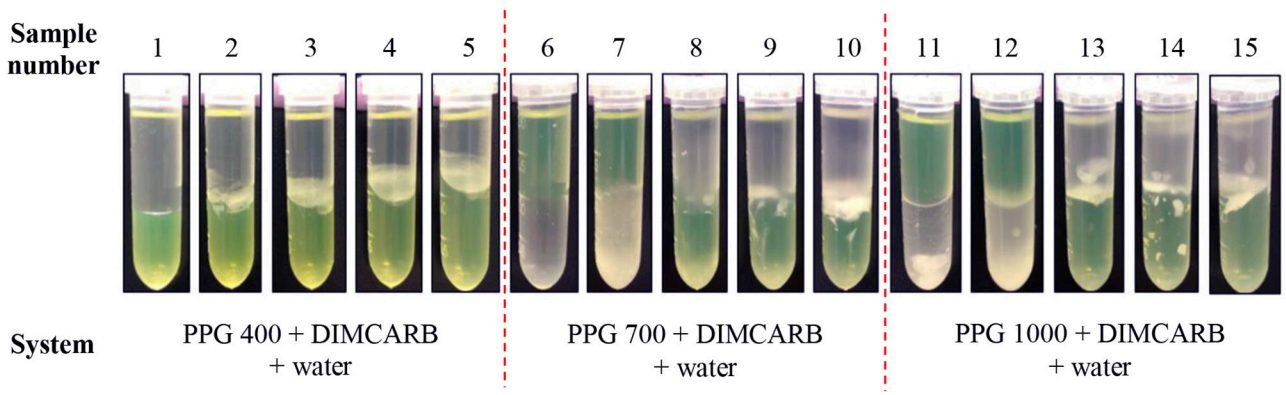


**FIGURE 3 |** Photos of PPG 400/700/1000 + DIMCARB + water systems showing the partitioning of GFP between phases.

Lastly, the pellet was re-solubilized in Tris-HCl buffer (pH 8; 50 mM).

The SDS-PAGE was conducted using a 12% (w/v) resolving gel in combination with a 5% (w/v) stacking gel (Laemmli, 1970). The thickness of the polyacrylamide gel was 1 mm. The electrophoresis was conducted at 180 V for 60 min using an electrophoresis unit (Mini Protean™ 3, Bio-Rad, U.S.A.). After the electrophoresis, the gel was stained with Coomassie Brilliant Blue R-250 for 45 min. Subsequently, the gel was destained with a destaining solution made of 10% (v/v) methanol and 10% (v/v) acetic acid until a clear background in the gel was formed. The protein bands on the gel were visualized and analyzed using a gel imaging system (Gel Doc™ XR +, Bio-Rad).

## Partitioning of GFP in ATPSs

ATPS was prepared in a 2-ml micro-centrifuge tube by adding the appropriate amounts of PPG, DIMCARB, buffer solution (50 mM Tris-HCl) and 10% (w/w) crude feedstock, with the pH of final mixture was adjusted to the optimum pH. Next, the system was mixed thoroughly using a vortex mixer prior to settling for 3 h to attain the phase equilibrium. The temperature of the system was maintained at 25°C during the incubation in a thermostatic bath. Subsequently, the system was centrifuged at 4,000 rpm for 10 min to achieve a complete phase separation. The partition coefficient of GFP ($K_{GFP}$) or total protein ($K_{protein}$) was determined using Equation (1):

$$K = \frac{C_B}{C_T} \quad (1)$$

where $C_B$ and $C_T$ are the concentrations of proteins in the bottom and top phases, respectively.

**TABLE 2 |** Compositions of the selected PPG 700/1000 (1) + DIMCARB (2) + water (3) systems at 25°C and 101.32 kPa.

| Sample number | Total compositions | | Without crude feedstock | | | | With crude feedstock[b] | | | |
|---|---|---|---|---|---|---|---|---|---|---|
| | | | Top phase[a] | | Bottom phase[a] | | Top phase[c] | | Bottom phase[c] | |
| | 100 $w_1$ | 100 $w_2$ | 100 $w_1$ | 100 $w_2$ | 100 $w_1$ | 100 $w_2$ | 100 $w_1$ | 100 $w_2$ | 100 $w_1$ | 100 $w_2$ |
| **PPG 700 + DIMCARB + water** | | | | | | | | | | |
| 6 | 46.0 | 3.0 | 94.2 | 0.58 | 1.40 | 5.35 | 1.08 | 5.87 | 87.8 | 0.68 |
| 7 | 44.0 | 2.5 | 92.7 | 0.59 | 2.70 | 4.14 | 2.32 | 4.48 | 84.0 | 0.74 |
| **PPG 1000 + DIMCARB + water** | | | | | | | | | | |
| 11 | 50.0 | 1.7 | 95.0 | 0.41 | 2.14 | 3.11 | 1.70 | 4.03 | 88.2 | 0.52 |
| 12 | 48.0 | 2.3 | 95.6 | 0.40 | 0.87 | 4.31 | 0.65 | 5.54 | 88.8 | 0.55 |

[a] *Data taken from literature (Song et al., 2018b).*

[b] *The concentrations of PPG, DIMCARB, and water in both top and bottom phases of the investigated ATPSs were analyzed using the methods described in previous study (Song et al., 2018b).*

[c] *Standard uncertainty of temperature = 1°C and pressure = 0.5 kPa. Expanded uncertainty: for PPG 700 + DIMCARB + water system, Uc are Uc(PPG 700) = Uc(DIMCARB) = 0.0021 (95% level of confidence); for PPG 1000 + DIMCARB + water system, Uc(PPG 1000) = Uc(DIMCARB) = 0.0023 (95% level of confidence).*

**TABLE 3 |** Compositions and purification efficiencies of 2- and 100-g ATPSs comprising 42% (w/w) PPG 1000, 4.4% (w/w) DIMCARB, and 10% (w/w) feedstock at pH 8.

| Total system weight (g) | Compositions | | | | *S* | *Y* (%) | |
|---|---|---|---|---|---|---|---|
| | Top phase | | Bottom phase | | | | |
| | 100 $w_1$ | 100 $w_2$ | 100 $w_1$ | 100 $w_2$ | | Top phase | Bottom phase |
| 2 | 97.6 | 0.37 | 0.40 | 7.82 | 1237 | 0.14 | 98.9 |
| 100 | 96.9 | 0.32 | 0.34 | 7.71 | 1229 | 0.13 | 98.3 |

Selectivity ($S$) was defined as the ratio of $K_{GFP}$ to $K_{protein}$, as shown in Equation (2):

$$S = \frac{K_{GFP}}{K_{protein}} \quad (2)$$

The yield of GFP partitioned to a specific phase of the system ($Y$) was calculated using Equation (3):

$$Y\ (\%) = \frac{C_{P(GFP)}}{C_{C(GFP)}} \times 100 \quad (3)$$

where $C_{P(GFP)}$ and $C_{C(GFP)}$ represent the concentration of GFP in the top phase or the bottom phase of ATPS and the crude feedstock, respectively.

# RESULTS AND DISCUSSION

## Stability Test for GFP

The effects of pH and temperature on the stability of GFP were evaluated by incubating the feedstock solution of GFP under different conditions of pH and temperature for 60 min. The GFP suspended in Tris-HCl buffer (pH 8; 50 mM) at 25°C for 60 min was used as the control. The stability of GFP was assessed using the indicator "percentage relative concentration of GFP," which is calculated as the RFU of sample as a percent of the RFU of the control. The results are shown in **Figures 1**, **2**. At pH ranging from 4 to 10, the percentage relative concentration of GFP was >91.8%, showing that the stability of the protein was well preserved. A previous study (Johansson et al., 2008) reported that GFP is stable in a broad range of pH (5.0–11.5). An extreme pH condition affects the structural stability and solubility of protein, leading to an irreversible denaturation of protein.

As shown in **Figure 2**, a low percentage relative concentration of GFP (i.e., 24.7%) was observed when the incubation temperature was raised to 70°C. Thus, it can be concluded that the GFP was stable when incubated at temperature below 70°C. The GFP was mostly denatured when the incubation temperature increased to 80°C, as indicated by the 0.89% of the relative concentration of GFP. Generally, the matured GFP is relatively stable and is able to fluoresce at temperature up 65°C (Tsien, 1998). An increase in incubation temperature promotes the unfolding of native secondary and tertiary structures of GFP (Penna et al., 2005). Bokman and Ward (1981) reported that the native secondary structure of GFP is essential to maintain the fluorescent form of the chromophore.

## GFP Partitioning in PPG + DIMCARB + Water System

The partitioning of proteins in ATPSs is typically governed by the interaction between phase-forming components and biomolecules (Tubio et al., 2004). In an ATPS, a protein will interact with the surrounding molecules through interactions such as hydrophobic interactions, hydrogen bonding, electrostatic interactions, steric effects, and van der Waals forces (Dreyer et al., 2009). To design the ATPS for an efficient separation of protein, it is important to understand the factors governing the partitioning of protein between phases in an ATPS.

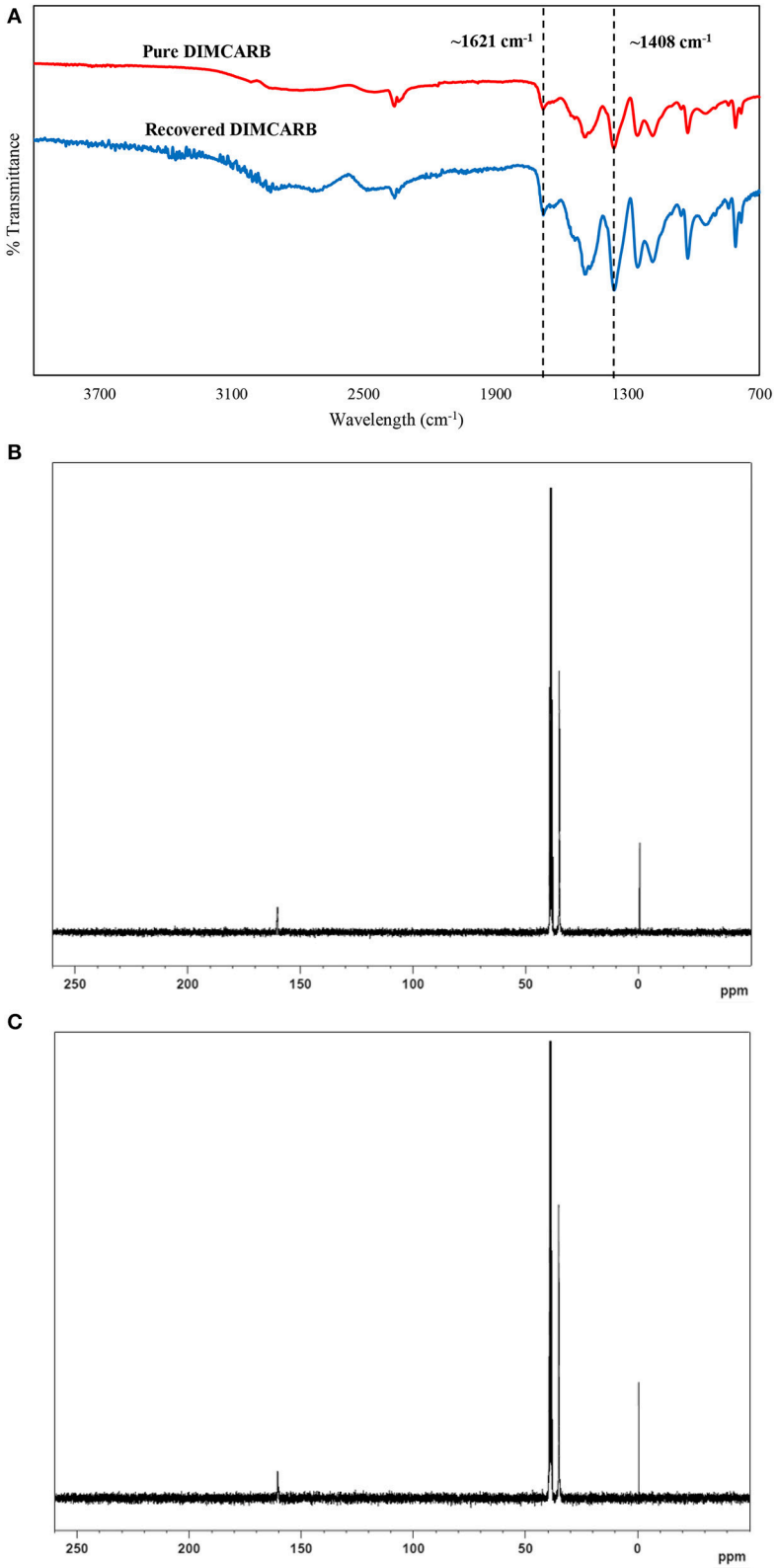


**FIGURE 4 |** Characterization of DIMCARB. **(A)** FT-IR spectra of the pure DIMCARB and the DIMCARB recovered from distillation; **(B)** $^{13}C$ NMR spectra of the pure DIMCARB; **(C)** $^{13}C$ NMR spectra of the DIMCARB recovered from distillation.

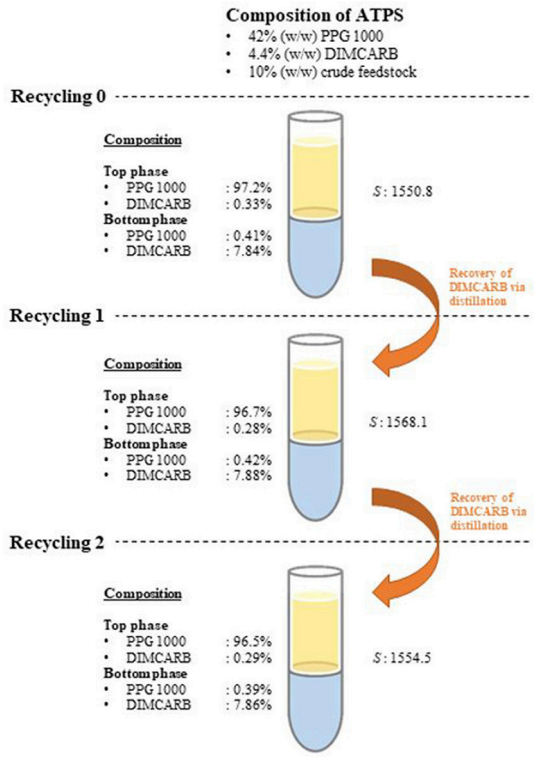


**FIGURE 5 |** Schematic diagram of the recycling ATPSs for three successive rounds of GFP purification.

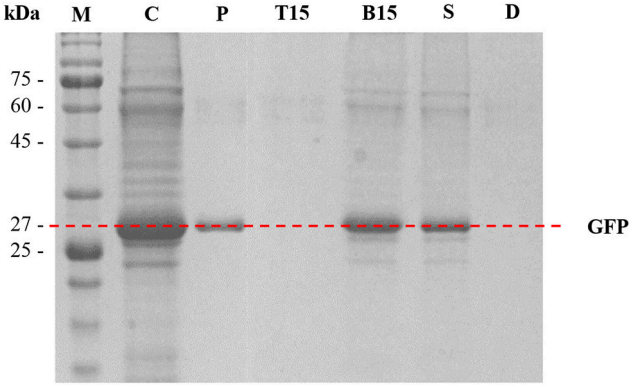


**FIGURE 6 |** SDS-PAGE analysis. Lane M, protein marker; Lane C, crude feedstock; Lane P, GFP standard; Lanes T15 and B15, the top phase and bottom phase of the optimized ATPS (sample number 15, as stated in **Table 1**), respectively; Lane S, distilled bottom phase of 100-g ATPS; Lane D, distillate obtained from the recovery of DIMCARB.

The partitioning of GFP in PPG + DIMCARB + water systems was investigated, and the results are presented in **Table 1** and **Figure 3**. The compositions of the phase-forming components were selected based on the corresponding phase diagrams reported from our previous work (Song et al., 2018b). The concentrations of phase-forming components were varied according to the tie-line length (TLL). To exclude the effect of volume ratio on the GFP partitioning, the volume ratio of top and bottom phases was fixed at 1:1. From **Table 1**, majority of the investigated systems showed a positive value of log $K_{GFP}$, indicating that the GFP was preferably partitioned to the DIMCARB-rich bottom phase. Among the investigated ATPSs, PPG 1000 + DIMCARB + water system at TLL = 97.4% (sample number 15) gave the highest $S$ value (1237) and $Y$% of GFP in bottom phase (98.8%).

However, an inverse trend of partition behavior of GFP was noted in some of the systems (sample number: 6 7, 11, and 12), which are reflected by the negative values of log $K_{GFP}$ (see **Table 1**). The compositions of systems undergone the phase inversion were analyzed, and the results are summarized in **Table 2**. From the liquid-liquid equilibrium data of these systems, the top phase mainly consisted of DIMCARB, whereas PPG was predominantly concentrated in the bottom phase. Prior to the addition of feedstock to these systems, the concentration of PPG 700/1000 was in the range of 44–50% (w/w) and the concentration of DIMCARB was ≤3% (w/w). The phase inversion occurred upon the addition of feedstock to these systems. As shown in **Table 2**, the addition of feedstock reduced the concentrations of PPG 700/1000 in both phases. The phase inversion may be associated to the temperature-responsiveness of PPG; the lower critical solution temperature (LCST) of PPG 700 and PPG 1000 may increase with a decreasing concentration of polymer. At room temperature and a lower concentration of PPG 700/1000, the hydrophobic moieties along the polymer chains were suspected to experience desolvation, resulting in the polymer aggregates, and a denser polymer-rich phase. Therefore, the inversion of phases occurred in the system and rendered the DIMCARB-rich fraction as the top phase.

**Figure 3** shows that the volumes of the top phases of PPG 400 + DIMCARB + water + feedstock systems decreased with an increasing TLL. This indicated that the equilibrium of these PPG400-based systems was affected by the addition of feedstock. In contrast, the volume ratio of PPG 700/1000 + DIMCARB + water + feedstock systems remained mostly constant. Furthermore, the amount of noticeable protein precipitate at the interphase of PPG 400 + DIMCARB + water + feedstock systems increased as the TLL of the system increased. This may be attributed to a higher degree of salting-out of host cell proteins in the systems. The presence of protein debris was also found at the interphase of ATPSs composed of PPG 700/1000. Nonetheless, the precipitation of the host cell protein in these systems also served as a means for the removal of protein contaminant, thereby assisting in the purification of GFP by ATPS.

## Recovery of Phase-Forming Components

Despite the promising potential of IL-based ATPS for the application in protein separation, these systems are yet to be widely adopted in the industrial operations due to the high cost of IL. In contrast to the conventional ILs, DIMCARB is relatively cheaper because of the use of $CO_2$ as the raw material.

Nevertheless, the cost of DIMCARB is still about 2 to 5 times higher than that of the conventional phase-forming components (e.g., inorganic salts, alcohol and carbohydrates). Therefore, the recycling of IL for the practical application of ATPS is highly desirable.

The recyclability of DIMCARB was evaluated using the optimized ATPS composed of 42% (w/w) PPG 1000 and 4.4% (w/w) DIMCARB. Firstly, the scale of ATPS was increased from 2 g to 100 g. The compositions and purification efficiencies of the scaled-up system are presented in **Table 3**. Regardless of the scale of ATPS, the composition of the system and the purification efficiencies remained nearly identical. The results affirmed that the performance of GFP purification was not compromised by the scalability of this IL-based ATPS. DIMCARB can be easily distilled and recovered via evaporation (Song et al., 2018b). In this study, the DIMCARB-rich bottom phase of the 100-g ATPS containing the partitioned GFP was subjected to rotary evaporation at 45°C and 85 mbar for 1 hr. During the process, DIMCARB dissociated into the gaseous dimethylamine and $CO_2$. As the gasses passed through a condenser unit, the re-association occurred and the DIMCARB was reformed in the liquid state.

The DIMCARB recovered from the distillation was characterized by Fourier Transform-Infrared (FT-IR) and carbon-13 nuclear magnetic resonance ($^{13}$C NMR) spectroscopies. The results of FT-IR and $^{13}$C NMR analyses are presented in **Figure 4**. In the FT-IR spectra, the symmetric carbamate (∼1408 $cm^{-1}$) and the carbamate C–O stretching (∼1621 $cm^{-1}$) peaks were noted in both pure and recycled DIMCARB samples (see **Figure 4A**). Similarly, the carbamate signal at ∼162 ppm was observed in the $^{13}$C NMR spectra of pure and recovered DIMCARB samples (see **Figures 4B,C**). These analyses confirmed the successful recovery DIMCARB from the bottom phase of the ATPS. Moreover, the percentage relative concentration of GFP before and after the distillation of DIMCARB was found to be 99.4% (data not shown), indicating that the stability of GFP was well preserved during the distillation of DIMCARB. The DIMCARB recovered from the distillation was used to prepare the new batch of ATPS for use in GFP purification. As illustrated in **Figure 5**, this recycling step was performed for three successive rounds of GFP purification, which is denoted as Recycling 0, Recycling 1, and Recycling 2, respectively. Overall, the phase compositions of the recycling ATPSs were almost similar to that of the primary ATPS. Moreover, the partition behavior of GFP in the recycling ATPSs did not deviate significantly (as indicated by the *S*-values shown in **Figure 5**).

### SDS-PAGE Analysis of Purified GFP Using PPG + DIMCARB + Water Systems

SDS-PAGE analysis was performed to assess the purity of protein and the performance of protein separation by the ATPSs. The results are shown in **Figure 6**. In Lane P, GFP standard was identified as a single thick band at approximately 27 kDa. In Lane C (crude feedstock sample), multiple protein bands were detected along with a thick band of GFP at 27 kDa, indicating the presence of protein impurities in the harvested culture broth prior to the purification process. For the optimized ATPS made of 42% (w/w) PPG 1000 and 4.4% (w/w) DIMCARB (sample number 15), the top phase of the system (Lane T15) did not exhibit any protein band. This hinted that the protein impurities had been mostly precipitated and concentrated at the interphase of the system (see **Figure 3**). On the other hand, the bottom phase of the system (Lane B15) showed a single dark band at ∼27 kDa (i.e., GFP) and some faint bands representing minor impurities. Similarly, the bottom phase from the scaled-up ATPS (Lane S) had the similar profile of protein bands as Lane B15. The Lane D representing distillate recovered from the rotary evaporation of DIMCARB-rich phase did not show any protein band.

## CONCLUSIONS

The PPG + DIMCARB + water systems were successfully applied for the purification of GFP from the clarified *E. coli* lysate. In general, GFP has a higher affinity toward the DIMCARB-rich phase. The optimal purification of GFP was attained with an ATPS composed of 42% (w/w) PPG 1000 and 4.4% (w/w) DIMCARB. The optimized ATPS was also successfully scaled up by 50 times. Moreover, DIMCARB was successfully recovered from the IL-rich phase and was reused for three successive rounds of GFP purification. Overall, PPG + DIMCARB + water system has demonstrated the satisfactory performance in the purification of protein from microbial lysate. The ease of recycling DIMCARB via distillation makes the ATPS even more sustainable and environmentally benign for application in protein purification.

## AUTHOR CONTRIBUTIONS

The experiments were designed by CS, PL, and CO. The experiments were carried out by ZT and SL. The manuscript was written by CS, PL, PS, and CO. All authors have read and approved the final manuscript.

## FUNDING

This work was funded by the Fundamental Research Grant Scheme (Ref. no. FRGS/1/2015/SG05/MUSM/02/4) awarded by the Ministry of Higher Education (MOHE) of Malaysia. This work was also supported by the e-Science fund (02-02-10-SF0290) from the Ministry of Science, Technology and Innovation (MOSTI) of Malaysia.

## ACKNOWLEDGMENTS

The authors were grateful to Jorge F. B. Pereira, João A. P. Coutinho, and Sónia P. M. Ventura for the provision of *E. coli* strain used in this work.

## REFERENCES


Amsterdam, A., Lin, S., Moss, L., G., and Hopkins, N. (1996). Requirements for green fluorescent protein detection in transgenic zebrafish embryos. *Gene* 173, 99–103. doi: 10.1016/0378-1119(95)00719-9

Bhatt, A. I., Bond, A. M., MacFarlane, D. R., Zhang, J., Scott, J. L., et al. (2006). A critical assessment of electrochemistry in a distillable room temperature ionic liquid, DIMCARB. *Green Chem.* 8, 161–171. doi: 10.1039/B512263E

Bokman, S. H., and Ward, W. W. (1981). Renaturation of *Aequorea* green-fluorescent protein. *Biochem. Biophys. Res. Commun.* 101, 1372–1380. doi: 10.1016/0006-291X(81)91599-0

Cabanne, C., Noubhani, A. M., Hocquellet, A., Dole, F., Dieryck, W., and Santarelli, X. (2005). Purification and on-column refolding of EGFP overexpressed as inclusion bodies in *Escherichia coli* with expanded bed anion exchange chromatography. *J. Chromatogr. B* 818, 23–27. doi: 10.1016/j.jchromb.2004.10.023

Chowdhury, S. A., Vijayaraghavan, R., and MacFarlane, D. (2010). Distillable ionic liquid extraction of tannins from plant materials. *Green Chem.* 12, 1023–1028. doi: 10.1039/b923248f

Deschamps, J. R., Miller, C. E., and Ward, K. B. (1995). Rapid purification of recombinant green fluorescent protein using the hydrophobic properties of an HPLC size-exclusion column. *Protein Expr. Purif.* 6, 555–558. doi: 10.1006/prep.1995.1073

Docherty, K. M., and Kulpa, C. F. Jr. (2005). Toxicity and antimicrobial activity of imidazolium and pyridinium ionic liquids. *Green Chem.* 7, 185–189. doi: 10.1039/b419172b

Dreyer, S., Salim, P., and Kragl, U. (2009). Driving forces of protein partitioning in an ionic liquid-based aqueous two-phase system. *Biochem. Eng. J.* 46, 176–185. doi: 10.1016/j.bej.2009.05.005

Freire, M. G., Cláudio, A. F., M., Araújo, J. M., Coutinho, J. A., Marrucho, I. M., et al. (2012). Aqueous biphasic systems: a boost brought about by using ionic liquids. *Chem. Soc. Rev.* 41, 4966–4995. doi: 10.1039/c2cs35151j

Gerisch, G., Albrecht, R., Heizer, C., Hodgkinson, S., and Maniak, M. (1995). Chemoattractant-controlled accumulation of coronin at the leading edge of *Dictyostelium* cells monitored using a green fluorescent protein–coronin fusion protein. *Curr. Biol.* 5, 1280–1285. doi: 10.1016/S0960-9822(95)00254-5

Gomes, G. A., Azevedo, A. M., Aires-Barros, M. R., and Prazeres, D. M. F. (2009). Purification of plasmid DNA with aqueous two phase systems of PEG 600 and sodium citrate/ammonium sulfate. *Separat. Purif. Technol.* 65, 22–30. doi: 10.1016/j.seppur.2008.01.026

Hatti-Kaul, R. (2000). *Aqueous Two-Phase Systems*. Totowa, NJ: Humana Press.

Idris, A., Vijayaraghavan, R., Patti, A., and MacFarlane, D. (2014). Distillable protic ionic liquids for keratin dissolution and recovery. *ACS Sustain. Chem. Eng.* 2, 1888–1894. doi: 10.1021/sc500229a

Jain, S., Teotia, S., and Gupta, M. N. (2004). Purification of green fluorescent protein overexpressed by a mutant recombinant *Escherichia coli*. *Protein Expr. Purif.* 36, 76–81. doi: 10.1016/j.pep.2004.04.008

Johansson, H.-O., Ishii, M., Minaguti, M., Feitosa, E., Penna, T., C. V., and Pessoa, A. Jr. (2008). Separation and partitioning of green fluorescent protein from *Escherichia coli* homogenate in poly (ethylene glycol)/sodium-poly (acrylate) aqueous two-phase systems. *Separat. Purif. Technol.* 62, 166–174. doi: 10.1016/j.seppur.2008.01.017

Kreher, U. P., Rosamilia, A. E., Raston, C. L., Scott, J. L., and Strauss, C. R. (2004). Self-associated,distillable ionic media. *Molecules* 9, 387–393. doi: 10.3390/90600387

Kroner, K. H., Hustedt, H., and Kula, M. R. (1982). Evaluation of crude dextran as phase-forming polymer for the extraction of enzymes in aqueous two-phase systems in large scale. *Biotechnol. Bioeng.* 24, 1015–1045. doi: 10.1002/bit.260240502

Laemmli, U. K. (1970). Cleavage of structural proteins during the assembly of the head of bacteriophage T4. *Nature* 227, 680–685. doi: 10.1038/227680a0

Lee, M. F., Chan, E. S., Tam, K. C., and Tey, B. T. (2015). Thermo-responsive adsorbent for size-selective protein adsorption. *J. Chromatogr. A* 1394, 71–80. doi: 10.1016/j.chroma.2015.03.034

Li, J.-J., Wang, A.-Q., Janson, J.-C., Ballagi, A., Chen, J., Liu, Y.-D., et al. (2009). Immobilized Triton X-100-assisted refolding of green fluorescent protein-tobacco etch virus protease fusion protein using β-cyclodextrin as the eluent. *Process Biochem.* 44, 277–282. doi: 10.1016/j.procbio.2008.10.021

Li, Y., and Beitle Robert, R. (2008). Protein purification via aqueous two-phase extraction (ATPE) and immobilized metal affinity chromatography. Effectiveness of salt addition to enhance selectivity and yield of GFPuv. *Biotechnol. Prog.* 18, 1054–1059. doi: 10.1021/bp025526x

Liu, C.-L., Kamei, D. T., King, J. A., Wang, D. I., and Blankschtein, D. (1998). Separation of proteins and viruses using two-phase aqueous micellar systems. *J. Chromatogr. B* 711, 127–138. doi: 10.1016/S0378-4347(98)00013-9

Lo, S. C., Ramanan, R. N., Tey, B. T., Tan, W. S., Show, P. L., et al. (2016). A versatile and economical method for the release of recombinant proteins from *Escherichia coli* by 1-propanol cell disruption. *RSC Adv.* 6, 62291–62297. doi: 10.1039/C6RA10550E

Lo, S. C., Ramanan, R. N., Tey, B. T., Tan, W. S., Show, P. L., et al. (2018). Purification of the recombinant enhanced green fluorescent protein from *Escherichia coli* using alcohol+salt aqueous two-phase systems. *Separat. Purif. Technol.* 192, 130–139. doi: 10.1016/j.seppur.2017.09.072

Lopes, A. M., Magalhães, P. O., Mazzola, P. G., Rangel-Yagui, C. O., de Carvalho, J. C. M., et al. (2011). Green fluorescent protein extraction and LPS removal from *Escherichia coli* fermentation medium using aqueous two-phase micellar system. *Separat. Purif. Technol.* 81, 339–346. doi: 10.1016/j.seppur.2011.07.043

McRae, S. R., Brown, C. L., and Bushell, G. R. (2005). Rapid purification of EGFP, EYFP, and ECFP with high yield and purity. *Protein Expr. Purif.* 41, 121–127. doi: 10.1016/j.pep.2004.12.030

Merchuk, J. C., Andrews, B. A., and Asenjo, J. A. (1998). Aqueous two-phase systems for protein separation: studies on phase inversion. *J. Chromatogr. B* 711, 285–293. doi: 10.1016/S0378-4347(97)00594-X

Penna, T. C. V., Ishii, M., Kunimura, J. S., and Cholewa, O. (2005). Stability of recombinant green fluorescent protein (GFPuv) in glucose solutions at different concentrations and pH values. *Appl. Biochem. Biotechnol.* 122, 501–527. doi: 10.1385/ABAB:122:1-3:0501

Plechkova, N. V., and Seddon, K. R. (2008). Applications of ionic liquids in the chemical industry. *Chem. Soc. Rev.* 37, 123–150. doi: 10.1039/B006677J

Quental, M. V., Caban, M., Pereira, M. M., Stepnowski, P., Coutinho, J. A., and Freire, M. G. (2015). Enhanced extraction of proteins using cholinium-based ionic liquids as phase-forming components of aqueous biphasic systems. *Biotechnol. J.* 10, 1457–1466. doi: 10.1002/biot.201500003

Samarkina, O. N., Popova, A. G., Gvozdik, E. Y., Chkalina, A. V., Zvyagin, I. V., et al. (2009). Universal and rapid method for purification of GFP-like proteins by the ethanol extraction. *Protein Expr. Purif.* 65, 108–113. doi: 10.1016/j.pep.2008.11.008

Skosyrev, V. S., Rudenko, N. V., Yakhnin, A. V., Zagranichny, V. E., Popova, L. I., et al. (2003). EGFP as a fusion partner for the expression and organic extraction of small polypeptides. *Protein Expr. Purif.* 27, 55–62. doi: 10.1016/S1046-5928(02)00595-8

Song, C. P., Ramanan, R. N., Vijayaraghavan, R., MacFarlane, D., R., Chan, E.-S., and Ooi, W. (2018a). Effect of salt-based adjuvant on partition behaviour of protein in aqueous two-phase systems composed of polypropylene glycol and cholinium glycinate. *Separat. Purif. Technol.* 196, 281–286. doi: 10.1016/j.seppur.2017.09.017

Song, C. P., Ramanan, R. N., Vijayaraghavan, R., MacFarlane, D. R., Chan, E.-S., and Ooi, C.-W. (2015). Green, aqueous two-phase systems based on cholinium aminoate ionic liquids with tunable hydrophobicity and charge density. *ACS Sustain. Chem. Eng.* 3, 3291–3298. doi: 10.1021/acssuschemeng.5b00881

Song, C. P., Ramanan, R. N., Vijayaraghavan, R., MacFarlane, D. R., Chan, E.-S., and Ooi, W. (2017). Primary and secondary aqueous two-phase systems composed of thermo switchable polymers and bio-derived ionic liquids. *J. Chem. Thermodynam.* 115, 191–201. doi: 10.1016/j.jct.2017.07.028

Song, C. P., Yap, Q., Y., aigness Chong, M. Y., Ramakrishnan Nagasundara, R., Ranganathan, V., Macfarlane, D. R., et al. (2018b). Environmentally benign and recyclable aqueous two-phase system composed of distillable $CO_2$-based alkyl carbamate ionic liquid. *ACS Sustain. Chem. Eng.* 6, 10344–10354. doi: 10.1021/acssuschemeng.8b01685

Stark, A., Huebschmann, S., Sellin, M., Kralisch, D., Trotzki, R., and Ondruschka, B. (2009). Microwave-assisted kolbe-schmitt synthesis using ionic liquids or dimcarb as reactive solvents. *Chem. Eng. Technol.* 32, 1730–1738. doi: 10.1002/ceat.200900331

Tsien, R. Y. (1998). The green fluorescent protein. *Ann. Rev.* 67, 509–544. doi: 10.1146/annurev.biochem.67.1.509

Tubio, G., Nerli, B., and Picó, G. (2004). Relationship between the protein surface hydrophobicity and its partitioning behaviour in aqueous two-phase systems of polyethyleneglycol–dextran. *J. Chromatogr. B* 799, 293–301. doi: 10.1016/j.jchromb.2003.10.060

Vijayaraghavan, R., and MacFarlane, D. (2014). $CO_2$-based alkyl carbamate ionic liquids as distillable extraction solvents. *ACS Sustain. Chem. Eng.* 2, 1724–1728. doi: 10.1021/sc5002066

Wang, S., and Hazelrigg, T. (1994). Implications for bcd mRNA localization from spatial distribution of exu protein in *Drosophila oogenesis*. *Nature* 369, 400–403. doi: 10.1038/369400a0

Wouters, F. S., Verveer, P. J., and Bastiaens, P. I. (2001). Imaging biochemistry inside cells. *Trends Cell Biol.* 11, 203–211. doi: 10.1016/S0962-8924(01)01982-1

Yao, T., Zang, H., Yao, S., Dai, X., and Song, H. (2018). Measurement and correlation of phase equilibria in aqueous two-phase systems containing functionalized magnetic ionic liquids and potassium phosphate at different temperatures. *J. Mol. Liquids* 263, 72–80. doi: 10.1016/j.molliq.2018.04.131

Zhuang, R., Zhang, Y., Zhang, R., Song, C., Yang, K., Yang, A., et al. (2008). Purification of GFP fusion proteins with high purity and yield by monoclonal antibody-coupled affinity column chromatography. *Protein Expr. Purif.* 59, 138–143. doi: 10.1016/j.pep.2008.01.020

**Conflict of Interest Statement:** The authors declare that the research was conducted in the absence of any commercial or financial relationships that could be construed as a potential conflict of interest.

frontiers in Chemistry

ORIGINAL RESEARCH
published: 01 February 2019
doi: 10.3389/fchem.2019.00044

# Aqueous/Aqueous Micro Phase Separation: Construction of an Artificial Model of Cellular Assembly

*Hiroki Sakuta*[1], *Tadashi Fujimoto*[1], *Yusuke Yamana*[1], *Yusuke Hoda*[1], *Kanta Tsumoto*[2]* *and Kenichi Yoshikawa*[1]

[1] Graduate School of Life and Medical Sciences, Doshisha University, Kyoto, Japan, [2] Division of Chemistry for Materials, Graduate School of Engineering, Mie University, Tsu, Japan

To artificially construct a three-dimensional cell assembly, we investigated the availability of long-duration microdroplets that emerged near a critical point in an aqueous two-phase system (ATPS) with the hydrophilic binary polymers, polyethylene glycol (PEG), and dextran (DEX), as host containers. We found that erythrocytes (horse red blood cells; RBCs) and NAMRU mouse mammary gland epithelial cells (NMuMG cells) were completely and spontaneously entrapped inside DEX-rich microdroplets. RBCs and NMuMG cells were located in the interior and at the periphery of the droplets at PEG/DEX = 5%:5%. In contrast, the cells exhibited opposite localizations at PEG/DEX = 10%:5%, where, interestingly, NMuMG cells apparently assembled to achieve cell adhesion. We simply interpreted such specific localizations by considering the alternative responses of these cells to the properties of the PEG/DEX interfaces with different gradients in polymer concentrations.

**Keywords: aqueous two-phase system, microdroplet, phase separation, cell assembly, red blood cell, epithelial cell, polyethylene glycol, dextran**

OPEN ACCESS

***Edited by:***
*John Paul Frampton,*
*Dalhousie University, Canada*

***Reviewed by:***
*Li Liu,*
*Osaka University, Japan*
*Xin Huang,*
*Harbin Institute of Technology, China*
*Ryugo Tero,*
*Toyohashi University of Technology, Japan*

***Correspondence:**
*Kanta Tsumoto*
*tsumoto@chem.mie-u.ac.jp*

***Specialty section:***
*This article was submitted to Chemical Engineering, a section of the journal Frontiers in Chemistry*

***Received:*** *10 August 2018*
***Accepted:*** *16 January 2019*
***Published:*** *01 February 2019*

***Citation:***
*Sakuta H, Fujimoto T, Yamana Y, Hoda Y, Tsumoto K and Yoshikawa K (2019) Aqueous/Aqueous Micro Phase Separation: Construction of an Artificial Model of Cellular Assembly. Front. Chem. 7:44. doi: 10.3389/fchem.2019.00044*

## INTRODUCTION

Living organisms exhibit the self-organization of cells and intracellular organelles in a self-consistent manner. For decades, biochemical studies have unveiled the mechanisms that underlie such regulatory systems at the molecular level. Many macromolecules including nucleic acids and proteins are considered to act in a well-orchestrated manner to express biological functions, by building sophisticated structures under the specific interaction of gene products. On the other hand, it is also considered that even a single-cell system cannot be completely controlled through specific key-lock interactions. In these situations, the self-organization, or self-assembly, of biomolecules is indispensable for the development of various ordered structures, like phospholipid bilayers for cell membranes. Recently, it has been reported that membraneless organelles may arise from the micro phase separation of cytosols, which generates submicron-scale liquid droplets containing proteins and RNAs (Brangwynne, 2013; Courchaine et al., 2016). Since intracellular environments are highly crowded by such macromolecules, the emergence of liquid/liquid phase separation (LLPS) on a microscopic scale is a ubiquitous phenomenon inside living cells (Walter and Brooks, 1995; Spitzer and Poolman, 2013; Rivas and Minton, 2016; Uversky, 2017).

Along these lines, many pioneering researchers have tried to model cellular and intracellular microcompartments by simply using an aqueous two-phase system (ATPS) consisting of solutions with hydrophilic polymers that exhibit LLPS on a micro-scale (Aumiller and Keating, 2017). There are both some similarities and differences in

the properties of micro phase separation between *in vitro* ATPS droplets and actual protein/nucleic acid-based droplets (Zaslavsky et al., 2018). Polyethylene glycol (PEG), a flexible polymer, and dextran (DEX), a semi-flexible polymer, are popularly selected for the preparation of a typical ATPS (Esquena, 2016). Upon the vigorous mixing of a PEG/DEX solution, aqueous/aqueous (water-in-water) microdroplets are transiently formed, and various biomolecules and even inorganic materials can be partitioned into, or excluded from, these droplets, due to the chemical and morphological characteristics of the substances partitioned (Akbulut et al., 2012; Jia et al., 2014; Vis et al., 2015). Generally, this behavior of LLPS droplets is sharp (Nott et al., 2016), and could be associated with the origin of life and prebiotic functions (Poudyal et al., 2018). Originally, ATPSs with various hydrophilic polymers, in addition to the above PEG/DEX, have been developed to extract molecules and supramolecules from biological materials (Albertsson, 1971). Their simplicity makes them suitable for harboring functional proteins and living cells. For example, these microdroplets have been used to promote interaction between entrapped proteins to achieve their alignment (Monterroso et al., 2016; Song et al., 2018). Previously, we have reported DNA entrapment (Tsumoto et al., 2015), the formation of microparticles by crosslinking proteins (Tsumoto and Yoshikawa, 2017), and the selective entrapment of filamentous actin (F-actin) and subdomain formation with dsDNAs and F-actin proteins, inside PEG/DEX microdroplets (Nakatani et al., 2018).

ATPS is known as a useful system to get selective partition on various biomacromolecules, DNAs, proteins, etc., under certain compositions of polymers. As has been indicated by Albertsson (1971), previous literatures reveal a large number of phase diagrams for the phase separation of binary or more-component polymer solutions. The ATPS with PEG/DEX is popular in biochemical and biophysical research, and we previously used this system to investigate the dynamics (time-course development) of phase segregation of micro-scale regions (Toyama et al., 2008), as well as the specific localization of DNAs and proteins, such as the cytoskeletal protein actin (Tsumoto et al., 2015; Nakatani et al., 2018). In these studies, we observed aqueous/aqueous (water-in-water) microdroplets with an average diameter of ∼10–100 μm. Importantly, the droplets are stably generated and remain after vigorous mixing using a vortex mixer, etc., near the critical point in a phase diagram, because there is only a very small difference in density between the phases containing the two polymers in addition to the weak surface tension, which are unique characteristics of a polymer solution.

Compared to bulk ATPS, the above mentioned aqueous/aqueous microdroplet is suitable for microscopic observation; therefore, we can frequently observe intriguing phenomena with biological macromolecules only when these molecules are encapsulated within such microcompartments. For example, interestingly, actin proteins apparently change their preferred location (distributed evenly, encapsulated within the interior, and adhered to the inner surface) in droplets in PEG/DEX ATPS as their higher-ordered structure changes from monomeric (G-actin) through polymeric (F-actin) to bundled actin (Nakatani et al., 2018). DNAs and F-actin entrapped simultaneously exclude each other to form subdomains inside the droplets. Thus, generally, biopolymers with semi-flexible and rigid chains are usually excluded from the PEG-rich exterior environment to the interior of DEX-rich microdroplets. In addition, further transformation of their structures as well as coexistence with other polymers possessing different properties could cause a change in their own positions.

Considering the unique characteristics to entrap certain biomolecules, it would also be expected that in even simple systems, living cells can find preferred locations in microdroplets and their localization can change with a change in the composition of the ATPS. Cells are much larger than the biomacromolecules, and cellular systems are more complicated. However, even though the model artificial system is quite simple, we would expect it to mimic the migration and arrangement of cells in an aqueous environment inside living bodies in a most basic manner, i.e., without any specific molecular interactions among genetic products.

Recently, Han et al. reported the formation and manipulation of cell spheroids (Han et al., 2015), clearly indicating that ATPS could be a powerful tool for controlling cell position without causing important damage. In the present study, we used two different kinds of cells, erythrocytes (horse red blood cells; RBCs) and NAMRU mouse mammary gland epithelial cells (NMuMG cells) as models, and investigated how these cells are localized when entrapped inside ATPS microdroplets. Interestingly, we found that RBCs and NMuMG cells alternatively preferred to localize either in the interior or at the periphery of microdroplets, and this preference could be switched by changing the PEG/DEX ratio. We considered that the PEG/DEX interface property could change with a change in the interface composition, and this could affect how the interface interacts with different types of cells to cause this switching.

# MATERIALS AND METHODS

## Reagents

We used polyethylene glycol (PEG) and dextran (DEX) to form an aqueous/aqueous two-phase system (ATPS): PEG 6,000 (molecular weight ($M_w$) 7,300–9,300 Da) and DEX 200,000 ($M_w$ 180,000–210,000 Da) were purchased from FUJIFILM Wako Pure Chemical Industries (Osaka, Japan). PEG and DEX were stocked as solutions of 20 wt% dissolved in isotonic sodium chloride solution (0.9 wt% solution of NaCl) to regulate the osmotic pressure similar to that of cell membranes. The isotonic sodium chloride solution was prepared with nuclease-free water (Milli-Q, 18.2 MΩ·cm). Other reagents used were of analytical grade.

## Microdroplets

A PEG/DEX solution shows the micro phase segregation at the conditions near to the bimodal line, i.e., the boundary of the homogeneous phase (mono-phase region) to the separated phase (two-phase region) of the solution. Due to the micro phase segregation of polymers, the microdroplets whose diameters range from ∼10 to 100 μm could be stable for around several

hours after mechanical agitation. In this study, we used the two types of conditions of PEG and DEX concentrations, PEG/DEX = 10%:5%, 5%:5%. Details of experimental solutions used here are described separately in the **Supplementary Material**.

## Cells

For observations of red blood cells (RBCs), we used the preserved blood of horse purchased from Nippon Bio-test Laboratories, Inc. (Saitama, Japan) and gently added a small aliquot of the blood to the PEG/DEX system without any washing. As model epithelial cells, we used NAMRU mouse mammary gland epithelial cells (NMuMG cells), which were cultivated from cultured cells at regular intervals as previously reported (Yoshida et al., 2017). For mixing in the PEG/DEX system, the epithelial cells were separated in advance from the culture medium by centrifuge.

## Microscopy

We observed ATPS microdroplets using bright field microscopy or confocal laser scanning microscopy (CLSM). Bright field microscopy images were obtained with an Axio Observer.A1 (Carl Zeiss, Germany) equipped with a 40× objective and a CCD digital camera (C11440, Hamamatsu Photonics). CLSM images were acquired with an FV-1000 laser scanning microscope (Olympus, Japan) and the images were analyzed using FV10-ASW software (Olympus). The images acquired with the bright field microscope were analyzed using ImageJ software (Rasband, W.S., ImageJ, US National Institutes of Health, Bethesda, Maryland, USA, http://imagej.nih.gov/ij/, 1997–2016). In the CLSM observation, we used fluorescein isothiocyanate (FITC)-dextran (average $M_w$ 250,000, Sigma-Aldrich; Ex. 488 nm) and the lipophilic dye Nile red (Thermo Fisher Scientific; Ex. 543 nm) to fluorescently visualize DEX-rich domains and RBCs, respectively. The details of experimental solutions subjected to the aforesaid observations are described in the **Supplementary Material**.

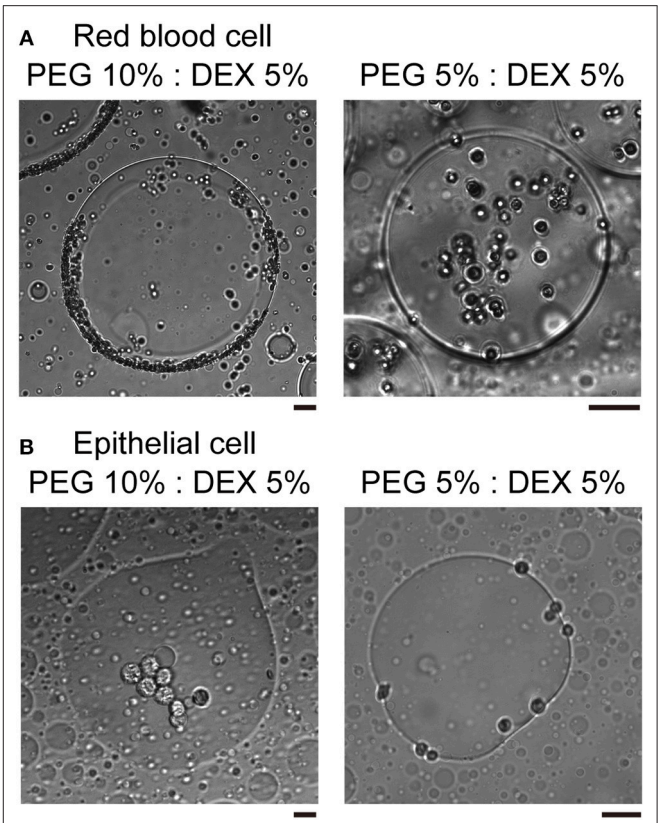


**FIGURE 1 |** Specific distribution depending on the cell type and the concentration of PEG/DEX. **(A)** Microscopic images of red blood cells (RBCs) in microdroplets for each concentration of PEG/DEX (10%:5%, 5%:5%). The scale bar corresponds to 50 μm. **(B)** Microscopic images of mouse mammary gland epithelial cells (NMuMG cells) in microdroplets for each concentration of PEG/DEX (10%:5%, 5%:5%). Note that the difference in color of cells could be due to a little variation in distance from the focus. Bar: 20 μm.

# RESULTS AND DISCUSSION

In the present study, we used two kinds of mammal cells: red blood cells (RBCs) and NMuMG cells, which are a type of epithelial cell. As shown in typical microscopic images in **Figure 1**, both RBCs and NMuMG cells were entrapped inside DEX-rich microdroplets when they were mixed in the ATPS with PEG/DEX = 10%:5% and 5%:5%. However, a close look at their distribution revealed that their location switched between the center and the periphery of the droplet with a change in the PEG/DEX ratio. In both cases, DEX-rich microdroplets were located on the bottom of the chamber due to their a little bit larger density as observed in the bulk experiment. Interestingly, these cells showed an opposite preferred distribution inside the droplets (**Figure 1**); at PEG/DEX 10%:5%, RBCs gathered near the interface, while NMuMG cells gathered inside the droplets rather than the interface. In contrast, at PEG/DEX 5%:5%, these preferences were reversed; i.e., RBCs were situated inner part of the droplets, and NMuMG cells were localized at their periphery. RBCs tended not to contact each other when they were trapped inside the droplets at either concentration of the coexisting polymers, whereas NMuMG cells positioned inside the droplets adhered more strongly to each other. Since NMuMG cells are adherent in their intrinsic property, encapsulation within DEX-rich droplets could enhance their attachment propensities (Yoshida et al., 2017).

**Figure 2** shows histograms of the cell population vs. the position of microdroplets. Along the radial distance ($r/L$) normalized to unity by the average radius $L$ of each droplet, entrapped cells were counted and the numbers were converted into a cell frequency. In both types of cells, the median location, which is indicated by arrow, of entrapped cells shifted from around the center (relative radial distance $r/L$ ∼0.5) to the periphery (relative radial distance $r/L$ 1.0). But the preference is opposite; i.e., RBCs and NMuMG cells (epithelial cells) were observed adsorbed to the interfaces at PEG/DEX = 10%:5% and 5%:5%, respectively. It should be noted that if cells were included inside a droplet without any attraction but with some repulsion to the interface, a peak of the population may appear around $r/L$ ∼0.5 because of the larger area compared to the region near the center.

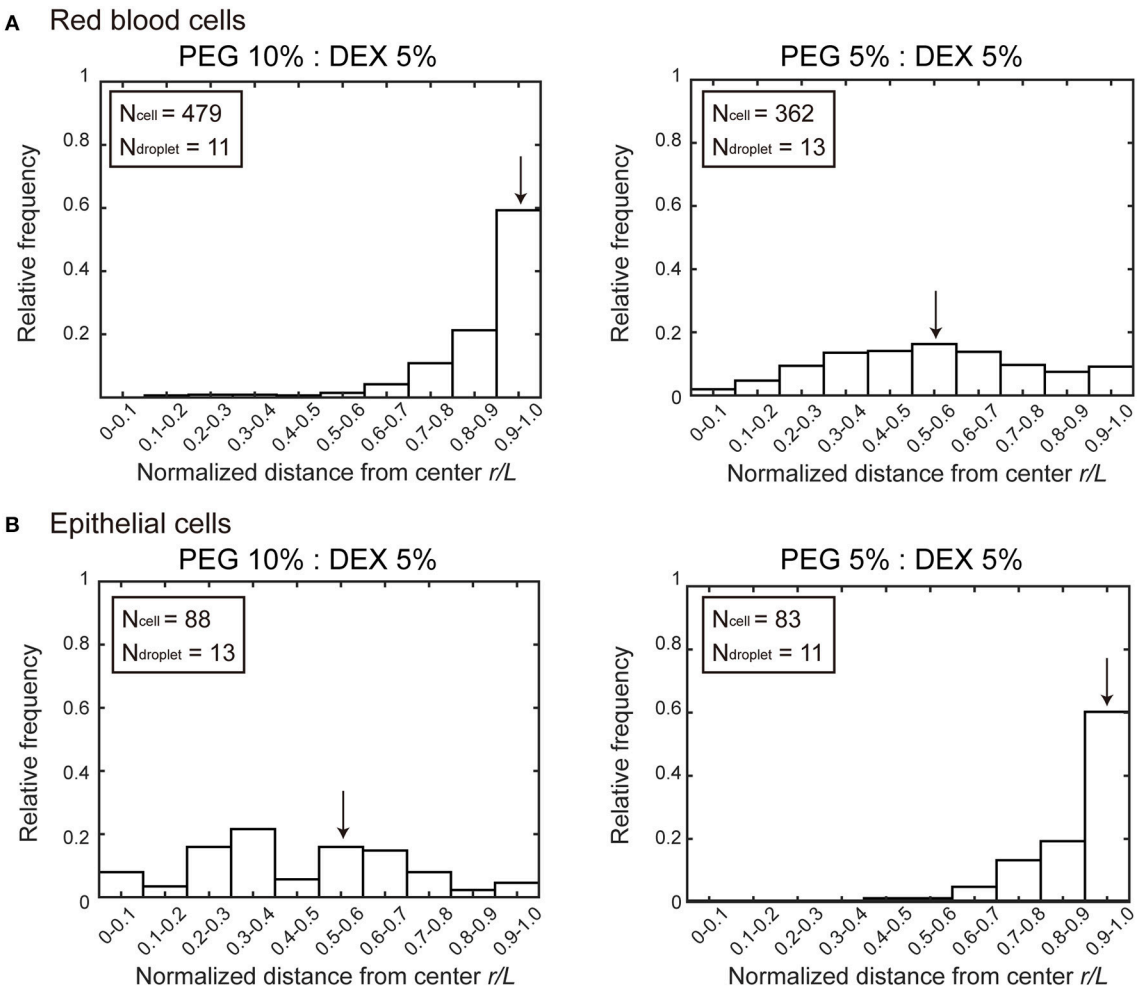


**FIGURE 2 |** Histograms of positions where **(A)** RBCs and **(B)** NMuMG cells were distributed inside microdroplets with PEG/DEX = 10%:5% and 5%:5%. Horizontal axes indicate normalized distances (*r/L*) from the center of the droplets to the positions of the entrapped cells. The relative radial distance normalized to unity by the average radius *L* of each droplet is 0 at the center and 1.0 at the periphery. The average radius is calculated from the area section of each microdroplet observed by microscopy, the distance *r* at which a cell was observed is divided by *L* of the droplet entrapping the cell to give the normalized radial distance. Some cells were observed at normalized distances greater than unity because some droplets assumed a somewhat aspherical shape, and then the number of these cells are included in the number at *r/L* of 0.9–1.0. Arrows indicate the medians to express the trends in cell localizations. The total numbers of counted cells ($N_{cell}$) and droplets ($N_{droplet}$) are indicated.

To further examine how cells switched their distribution inside the droplets, we conducted CLSM observation of the PEG/DEX ATPS containing RBCs labeled fluorescently by Nile red (**Figure 3**). FITC-DEX illuminated the microdroplets and RBCs emitting red fluorescence were fully entrapped, but their distribution was apparently different at PEG/DEX = 10%:5% and 5%:5%, as in **Figure 1**. Under the former condition, RBCs were visualized on the inner interface of the DEX-rich droplet emitting green fluorescence, and in the latter, RBCs were relatively dispersed into the DEX-rich droplets. Fewer cells were observed at the top than the middle of the droplet, indicating that entrapped cells could fall under the present conditions. A number of RBCs were here also found at the interface of the microdroplet at PEG/DEX = 5%/5% (**Figure 3B**), and this trend is consistent with the localization shown in **Figure 2A**.

We here observed the simple switching of cell localization inside DEX-rich droplets. Both cell types, RBCs and NMuMG cells, preferred the interior, but they exhibited opposite trends when settling in different compartments. The preference in cell localization may be caused by various factors related to difference in cell properties, including their sizes, morphologies, surface structures, adhesive (non-adhesive) behaviors, number density, etc., so it is too complicated to permit us to give a detailed precise explanation for the mechanism. Therefore, the present condition we investigated is considered to be moderately suitable for simple demonstration of switchable behavior of cell localization inside ATPS droplets. For speculation, instead, we try to simply discuss this different preference by imagining cells with different dimensions under a crowded environment with PEG/DEX schematically illustrated in **Figure 4** as follows.

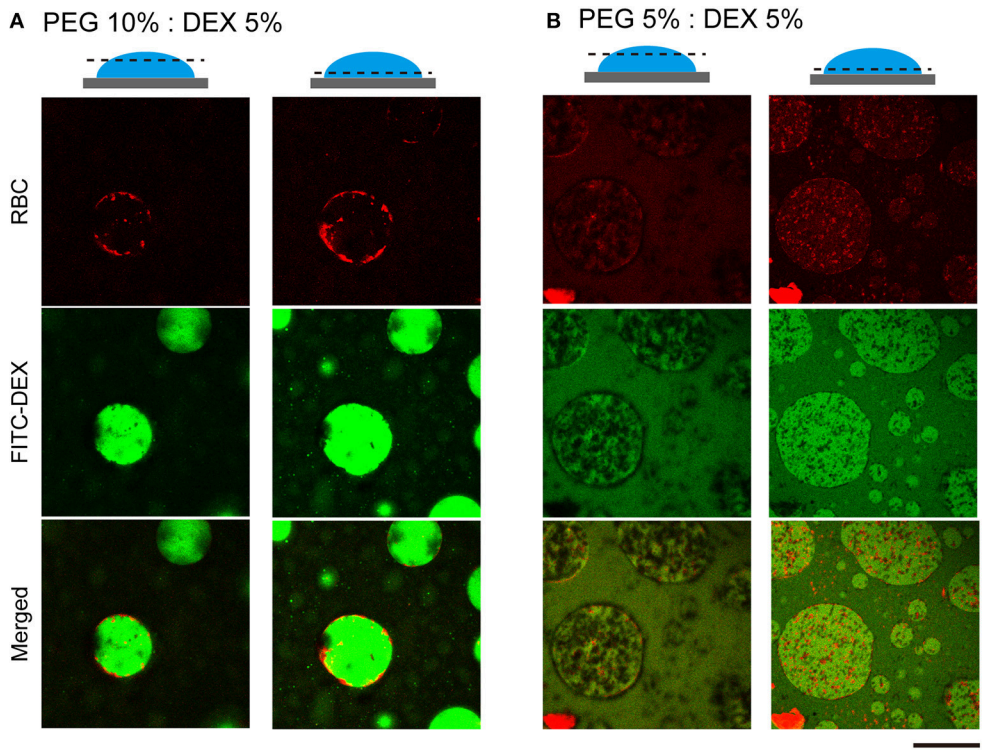


**FIGURE 3 |** Confocal laser scanning microscopy (CLSM) images of RBCs in microdroplets. Top: RBCs labeled with Nile red. Middle: FITC-DEX. Bottom: Merged. The focal planes of the left and right columns for each condition are around the top and below the middle, respectively, as schematically illustrated for PEG/DEX = **(A)** 10%: 5% and **(B)** 5%: 5%. Bar: 100 μm.

Generally, DEX molecules have branched structures with some room for harboring other biomacromolecules, and PEG molecules have linear flexible structures with a high excluded volume under concentrated conditions. Since these polymers provide different aqueous environments, not only large biomolecules but also cells prefer the DEX-rich phase, which is less crowded than the PEG-rich phase. In the present study, we used two PEG/DEX ATPSs with different conditions; one is near the critical point in the phase diagram (5%:5%); the other is somewhat far from that point, and accordingly, the binodal line (10%:5%).

The surface tension with such aqueous/aqueous interfaces is not so strong compared to oil/water interfaces (Atefi et al., 2014). Therefore, it can be finely modulated by changing the PEG/DEX ratio. In the present case, at PEG/DEX = 10%:5%, the interface has a higher tension (surface energy) with a steeper gradient of polymer concentrations, and thus RBCs, which are relatively smaller than NMuMG cells, could keep located on the surface, leading to reduction of the surface energy (**Figure 4A**). On the other hand, at PEG/DEX = 5%:5%, the surface free energy, or surface tension, is so low due to a small gradient of polymer concentrations that small RBCs with weaker effects on stabilization of the interface alternatively tend to leave and enter the interior of DEX-rich droplets, which can accommodate these cells (**Figure 4B**).

To interpret the opposite preference of NMuMG cells along the same scenario as the case of RBCs, their larger size can be taken into account in relation to depletion effects by PEG. NMuMG cells appear to move to the interior of DEX-rich droplets, avoiding the interface where PEG exists more densely at PEG/DEX = 10%:5%. In other words, PEG could effectively induce depletion effect on NMuMG cells due to their larger sizes (surface areas), so these cells can be located not near a PEG-rich surrounding but in a DEX-rich inner space, where they might be associated with each other by moderate depletion force with DEX polymers (Atefi et al., 2015). At PEG/DEX = 5%:5%, where most RBCs are located inside the droplets, NMuMG cells can stand adhering to the interface, leading to the efficient stabilization due to their greater dimension. Note that the surface free energy of the interface through the phase segregation of polymer solutions is generally much smaller than those for interfaces with small molecules, because of the small contribution of the mixing entropy for polymer systems (Nakatani et al., 2018).

It has been shown that interface properties are in general strongly correlated to the positioning and qualities of cells with various origins (Atefi et al., 2015; Han et al., 2015) with some changes in genetic activities (Yu et al., 2018). To achieve assembly of highly organized compartments including cells in microfluidics, interfacial environments where cells and biopolymers are accumulated should be well-regulated (Yamada et al., 2016). We here simply chose physiological saline for suspending cells, but it is not suitable for cell proliferation, but, along this line, when some conditions that facilitate micro phase separation and cell growth are available, our results would be expected to aid development of such techniques for constituting assembled cell systems.

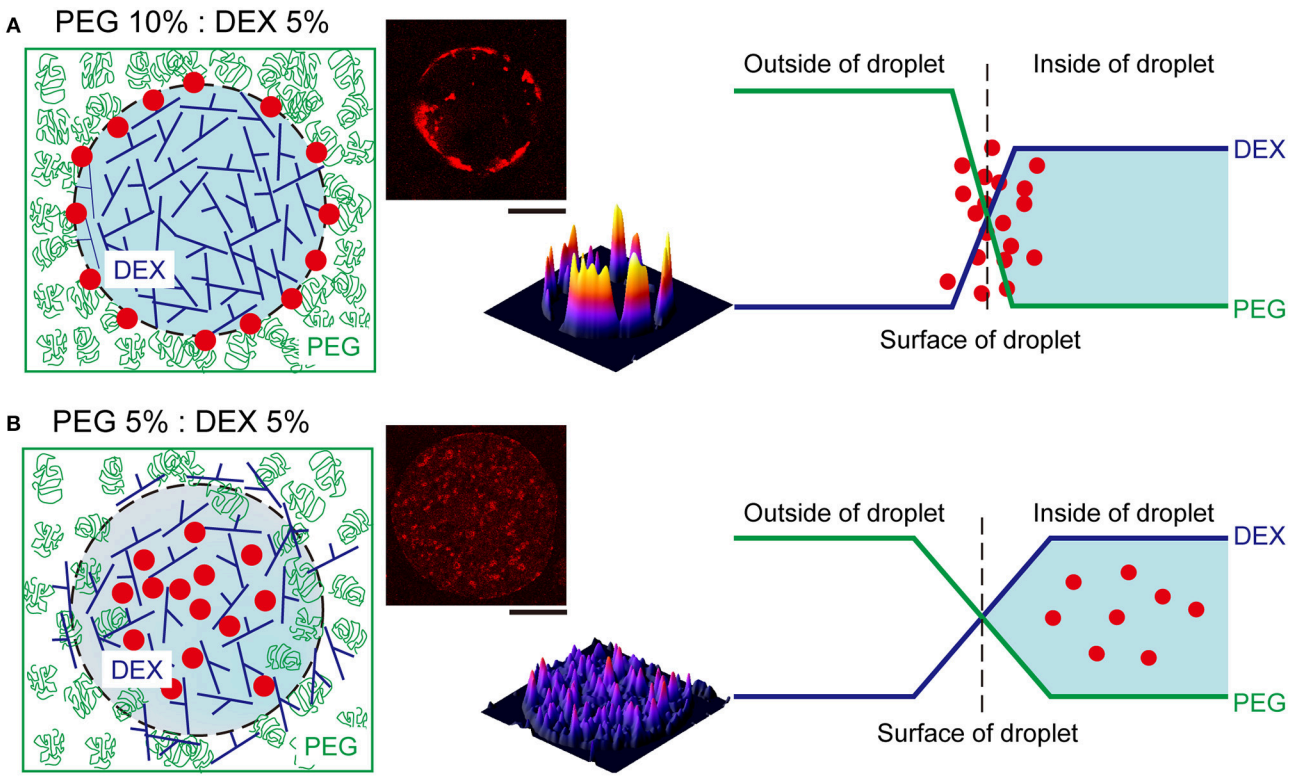


**FIGURE 4 |** Schematic representation of the proposed mechanism of RBC distribution inside microdroplets generated by PEG and DEX. The leftmost illustrations show localization of RBCs (red closed circles) in droplets of DEX (blue branching line) surrounded with PEG (green random coil). The rightmost graphs depict the profiles of concentrations of DEX and PEG at the interfaces of droplets. **(A)** At PEG/DEX = 10%: 5%, the high surface energy due to the steep gradient of polymer concentrations may cause the accumulation of RBCs at the interface to lower the tension. **(B)** In contrast, at PEG/DEX = 5%: 5%, the surface tension can be moderately reduced to permit mutual invasion to some extent, and thus RBCs cannot be pushed to the interface so strongly. The pseudo three-dimensional images in the middle show the fluorescence intensities of Nile red from RBCs entrapped inside the DEX-rich microdroplets shown in the upper-left side, also in each upper-right panel of **Figure 3**. Bar: 100 μm.

In conclusion, it was found that living cells exhibit specific localization in an aqueous solution with water/water microdroplets generated through phase separation in the presence of hydrophilic binary polymers. It was revealed that two type of cells are situated either in the interior or at the periphery of the droplets. By changing the relative ratio of the polymer content, switching of the cell localization was observed. The mechanism of such observations were interpreted in terms of polymer depletion effect on the micro phase separation. It is highly expected that the simple mixing procedure with micro water/water droplets provides novel methodology to construct 3D cellular assembly composed with difference cell species.

## AUTHOR CONTRIBUTIONS

HS and TF conducted the experiments with the help of KT under direction by KY. HS, TF, and KT wrote the manuscript with the help of YY and YH under supervision by KY.

## FUNDING

This work was supported, in part, by JSPS KAKENHI Grant Numbers JP15H02121, JP16K07293, JP18J12947, and JP16K13655 and by MEXT KAKENHI Grant Number JP18H04976.

## ACKNOWLEDGMENTS

We thank Dr. Hiroaki Taniguchi (The Institute of Genetics and Animal Breeding, Polish Academy of Sciences) for help on the experiments with NMuMG cells.

## SUPPLEMENTARY MATERIAL

The Supplementary Material for this article can be found online at: https://www.frontiersin.org/articles/10.3389/fchem.2019.00044/full#supplementary-material

## REFERENCES


Akbulut, O., Mace, C. R., Martinez, R. V., Kumar, A. A., Nie, Z., Patton, M. R., et al. (2012). Separation of nanoparticles in aqueous multiphase systems through centrifugation. *Nano Lett.* 12, 4060–4064. doi: 10.1021/nl301452x

Albertsson, P.-Å. (1971). *Partition of Cell Particles and Macromolecules, 2nd Ed.* New York, NY: Wiley.

Atefi, E., Joshi, R., Mann, J. A. Jr., and Tavana, H. (2015). Interfacial tension effect on cell partition in aqueous two-phase systems. *ACS Appl. Mater. Interfaces* 7, 21305–21314. doi: 10.1021/acsami.5b05757

Atefi, E., Mann, J. A Jr., and Tavana, H. (2014). Ultralow interfacial tensions of aqueous two-phase systems measured using drop shape. *Langmuir* 30, 9691–9699. doi: 10.1021/la500930x

Aumiller, W. M Jr., and Keating, C. D. (2017). Experimental models for dynamic compartmentalization of biomolecules in liquid organelles: reversible formation and partitioning in aqueous biphasic systems. *Adv. Colloid. Interface Sci.* 239, 75–87. doi: 10.1016/j.cis.2016.06.011

Brangwynne, C. P. (2013). Phase transitions and size scaling of membrane-less organelles. *J. Cell Biol.* 203, 875–881. doi: 10.1083/jcb.201308087

Courchaine, E. M., Lu, A., and Neugebauer, K. M. (2016). Droplet organelles? *EMBO J.* 35, 1603–1612. doi: 10.15252/embj.201593517

Esquena, J. (2016). Water-in-water (W/W) emulsions. *Curr. Opin. Colloid Interface Sci.* 25, 109–119. doi: 10.1016/j.cocis.2016.09.010

Han, C., Takayama, S., and Park, J. (2015). Formation and manipulation of cell spheroids using a density adjusted PEG/DEX aqueous two phase system. *Sci. Rep.* 5:11891. doi: 10.1038/srep11891

Jia, T. Z., Hentrich, C., and Szostak, J. W. (2014). Rapid RNA exchange in aqueous two-phase system and coacervate droplets. *Orig. Life Evol. Biosph.* 44, 1–12. doi: 10.1007/s11084-014-9355-8

Monterroso, B., Zorrilla, S., Sobrinos-Sanguino, M., Keating, C. D., and Rivas, G. (2016). Microenvironments created by liquid-liquid phase transition control the dynamic distribution of bacterial division FtsZ protein. *Sci. Rep.* 6, 35140. doi: 10.1038/srep35140

Nakatani, N., Sakuta, H., Hayashi, M., Tanaka, S., Takiguchi, K., Tsumoto, K., et al. (2018). Specific spatial localization of actin and DNA in a water/water microdroplet: Self-emergence of a cell-like structure. *Chem. Bio. Chem.* 19, 1370–1374. doi: 10.1002/cbic.201800066

Nott, T. J., Craggs, T. D., and Baldwin, A. J. (2016). Membraneless organelles can melt nucleic acid duplexes and act as biomolecular filters. *Nat. Chem.* 8, 569–575. doi: 10.1038/nchem.2519

Poudyal, R. R., Pir Cakmak, F., Keating, C. D., and Bevilacqua, P. C. (2018). Physical principles and extant biology reveal roles for RNA-containing membraneless compartments in origins of life chemistry. *Biochemistry* 57, 2509–2519. doi: 10.1021/acs.biochem.8b00081

Rivas, G., and Minton, A. P. (2016). Macromolecular crowding *in vitro*, *in vivo*, and in between. *Trends Biochem. Sci.* 41, 970–981. doi: 10.1016/j.tibs.2016.08.013

Song, Y., Michaels, T. C. T., Ma, Q., Liu, Z., Yuan, H., Takayama, S., et al. (2018). Budding-like division of all-aqueous emulsion droplets modulated by networks of protein nanofibrils. *Nat. Commun.* 9:2110. doi: 10.1038/s41467-018-04510-3

Spitzer, J., and Poolman, B. (2013). How crowded is the prokaryotic cytoplasm? *FEBS Lett.* 587, 2094–2098. doi: 10.1016/j.febslet.2013.05.051

Toyama, H., Yoshikawa, K., and Kitahata, H. (2008). Homogenization of a phase-separated droplet in a polymer mixture caused by the dielectric effect of a laser. *Phys. Rev. E Stat. Nonlin. Soft Matter Phys.* 78:060801. doi: 10.1103/PhysRevE.78.060801

Tsumoto, K., Arai, M., Nakatani, N., Watanabe, S. N., and Yoshikawa, K. (2015). Does DNA exert an active role in generating cell-sized spheres in an aqueous solution with a crowding binary polymer? *Life* 5, 459–466. doi: 10.3390/life5010459

Tsumoto, K., and Yoshikawa, K. (2017). The aqueous two phase system (ATPS) deserves plausible real-world modeling for the structure and function of living cells. *MRS Adv.* 2, 2407–2413. doi: 10.1557/adv.2017.358

Uversky, V. N. (2017). Intrinsically disordered proteins in overcrowded milieu: Membrane-less organelles, phase separation, and intrinsic disorder. *Curr. Opin. Struct. Biol.* 44, 18–30. doi: 10.1016/j.sbi.2016.10.015

Vis, M., Opdam, J., van't Oor, I. S. J., Soligno, G., van Roij, R., Tromp, R. H., et al. (2015). Water-in-water emulsions stabilized by nanoplates. *ACS Macro Lett.* 4, 965–968. doi: 10.1021/acsmacrolett.5b00480

Walter, H., and Brooks, D. E. (1995). Phase separation in cytoplasm, due to macromolecular crowding, is the basis for microcompartmentation. *FEBS Lett.* 361, 135–139. doi: 10.1016/0014-5793(95)00159-7

Yamada, A., Renault, R., Chikina, A., Venzac, B., Pereiro, I., Coscoy, S., et al. (2016). Transient microfluidic compartmentalization using actionable microfilaments for biochemical assays, cell culture and organs-on-chip. *Lab Chip.* 16, 4691–4701. doi: 10.1039/C6LC01143H

Yoshida, A., Tsuji, S., Taniguchi, H., Kenmotsu, T., Sadakane, K., and Yoshikawa, K. (2017). Manipulating living cells to construct a 3D single-cell assembly without an artificial scaffold. *Polymers* 9:319. doi: 10.3390/polym9080319

Yu, L., Li, J., Hong, J., Takashima, Y., Fujimoto, N., Nakajima, M., et al. (2018). Low cell-matrix adhesion reveals two subtypes of human pluripotent stem cells. *Stem Cell Rep.* 11, 142–156. doi: 10.1016/j.stemcr.2018.06.003

Zaslavsky, B. Y., Ferreira, L. A., Darling, A. L., and Uversky, V. N. (2018). The solvent side of proteinaceous membrane-less organelles in light of aqueous two-phase systems. *Int. J. Biol. Macromol.* 117, 1224–1251. doi: 10.1016/j.ijbiomac.2018.06.030


**Conflict of Interest Statement:** The authors declare that the research was conducted in the absence of any commercial or financial relationships that could be construed as a potential conflict of interest.

frontiers in Chemistry

MINI REVIEW
published: 15 March 2019
doi: 10.3389/fchem.2019.00135

# Ionic Liquid Aqueous Two-Phase Systems From a Pharmaceutical Perspective

*Lisa McQueen*[1]* *and David Lai*[2,3]*

[1] Drug Product Design and Development, GlaxoSmithKline, Collegeville, PA, United States, [2] Product and Process Engineering, GlaxoSmithKline, Collegeville, PA, United States, [3] Advanced Manufacturing Technologies, GlaxoSmithKline, Collegeville, PA, United States

Aqueous Two-Phase Systems (ATPSs) have been extensively studied for their ability to simultaneously separate and purify active pharmaceutical ingredients (APIs) and key intermediates with high yields and high purity. Depending on the ATPS composition, it can be adapted for the separation and purification of cells, nucleic acids, proteins, antibodies, and small molecules. This method has been shown to be scalable, allowing it to be used in the milliliter scale for early drug development to thousands of liters in manufacture for commercial supply. The benefits of ATPS in pharmaceutical separations is increasingly being recognized and investigated by larger pharmaceutical companies. ATPSs use identical instrumentation and similar methodology, therefore a change from traditional methods has a theoretical low barrier of adoption. The cost of typical components used to form an ATPS at large scale, particularly that of polymer-polymer systems, is the primary challenge to widespread use across industry. However, there are a few polymer-salt examples where the increase in yield at commercial scale justifies the cost of using ATPSs for macromolecule purification. More recently, Ionic Liquids (ILs) have been used for ATPS separations that is more sustainable as a solvent, and more economical than polymers often used in ATPSs for small molecule applications. Such IL-ATPSs still retain much of the attractive characteristics such as customizable chemical and physical properties, stability, safety, and most importantly, can provide higher yield separations of organic compounds, and efficient solvent recycling to lower financial and environmental costs of large scale manufacturing.

**Keywords: aqueous two-phase systems, biphasic systems, ionic liquids, pharmaceutical extractions, pharmaceutical separations**

OPEN ACCESS

***Edited by:***
*John Paul Frampton,*
*Dalhousie University, Canada*

***Reviewed by:***
*Daniel Kamei,*
*University of California, Los Angeles, United States*
*Marcello Locatelli,*
*Università degli Studi G. d'Annunzio Chieti e Pescara, Italy*

***Correspondence:**
*Lisa McQueen*
*lisa.l.mcqueen@gsk.com*
*David Lai*
*david.x.lai@gsk.com*

***Specialty section:***
*This article was submitted to Chemical Engineering, a section of the journal Frontiers in Chemistry*

***Received:*** *24 August 2018*
***Accepted:*** *21 February 2019*
***Published:*** *15 March 2019*

***Citation:***
*McQueen L and Lai D (2019) Ionic Liquid Aqueous Two-Phase Systems From a Pharmaceutical Perspective. Front. Chem. 7:135. doi: 10.3389/fchem.2019.00135*

## INTRODUCTION

The adoption of methods from the scientific literature into industrial applications often follows a period of dormancy. While ATPSs have experienced a recent prolific rise in applications in microfluidics, cellular engineering, bioprinting, and biopatterning since the 2000s (Teixeira et al., 2017), the industrial applications of ATPSs are typically separations and purification, first described in the 1950s (Albertsson, 1956, 1958). Such ATPSs popularized by Albertsson are polymer-polymer or polymer-salt emulsions that have been well-studied for viral (Norrby and Albertsson, 1960; Liu et al., 1998; Effio et al., 2015), cellular (Walter et al., 1976; Sharp et al., 1986; Kumar et al., 2001), nucleic acid (Ribeiro et al., 2002; Gomes et al., 2009; Nazer et al., 2017),

protein (Schmidt et al., 1994; Balasubramaniam et al., 2003), and antibody (Desbuquois and Aurbach, 1971; Selber et al., 2004; Rosa et al., 2007b; Azevedo et al., 2009a) separations. Examples can be found for batch (Tavana et al., 2009; Frampton et al., 2011, 2014; Lai et al., 2011) or continuous (Yamada et al., 2004; Nam et al., 2005; SooHoo and Walker, 2009; Tsukamoto et al., 2009; Rosa et al., 2012) processes. While polymer ATPSs are limited to partitioning of macromolecules due to size of the polymers used, the isolation and separation of small molecules (<900 Daltons) in ATPSs, especially those developed in the pharmaceutical industry, commonly employ ionic liquids (ILs).

## Polymer-Based ATPS Separations and Considerations

The mechanism for purification of a material using ATPSs is driven by physical and chemical affinity toward a select phase and the contaminant's affinity toward the other liquid phase. Accurate prediction of partitioning is complicated by several factors. Physical and chemical properties of each phase, such as viscosity, relative volume, density, charge, pH, and volatility are known to impact performance, and thus the choice of polymer or salt is used to tune the systems for effectiveness (Albertsson, 1960). In general, the process of ATPS separations and purification occurs in three major steps: molecular partitioning, physical separation, and isolation of phase of interest (**Figure 1**). The use of ATPSs was shown to be a high-yield and environmentally sustainable alternative to some current pharmaceutical purification and extraction processes (Chen et al., 2005). Although its adoption in the pharmaceutical industry is relatively early for manufacturing, it currently has its niche applications in pharmaceutical development as well as other industries (Diuzheva et al., 2018; Mocan et al., 2018). Clear documentation of advantages in cost savings, yield and sustainability combined with ease of adoption is needed to ease its widespread use in biopharmaceutical or vaccine manufacturing process (Chen et al., 2005).

Selective partitioning is the first step of separation design. It is advantageous to increase the liquid-liquid interface to accelerate molecular partitioning by producing a fine emulsion of the dispersed aqueous phase inside the continuous aqueous phase. The ability to selectively partition is dependent on the affinity differences for the material of interest for each phase. Polyethylene glycol (PEG) is a widely used component of ATPSs due to its high biocompatibility, biodegradability, water solubility, and low cost. Aside from changes in molecular weight, the properties of PEG with respect to partitioning are limited. To overcome this challenge, multiple groups have functionalized PEG in PEG/salt and PEG/dextran ATPSs with glutaric acid to improve extraction yields of immunoglobins from 28 to 93% (Rosa et al., 2007a), and 23 to 97% (Azevedo et al., 2009b) as well as increasing extraction efficiencies of penicillin up to 96% using imidazole-terminal PEG (Jiang et al., 2009). The addition of a small percentage of a biospecific ligand to ATPSs was shown to increase purification efficiency and yield by several fold (Kula et al., 1991) in a concentration-dependent manner that can be optimized for manufacturing scale of monoclonal antibodies. The use of ATPSs present an opportunity to simplify the manufacturing process of plasmid DNA by allowing for the lysis, recovery, purification and extraction in a single high yield step (Frerix et al., 2005). Polymer ATPSs have been shown to extract plasmid DNA and RNA up to 90 and 70% respectively (Frerix et al., 2006).

The second step is physical coalescence of the emulsion into two continuous, phase-separated, liquids. While numerous physical and chemical properties drive selective partitioning, coalescence of ATPS is simply driven by interfacial tension, density and viscosity. ATPSs will spontaneously coalesce into two continuous phases over time by sedimentation according to Stoke's Laws, and physical characteristics such as viscosity slow the process (Asenjo and Andrews, 2012). Centrifugation is often used to accelerate the natural coalescence and sedimentation.

Lastly, the liquid phase containing the purified material is isolated. The interface between the two liquid phases is avoided to prevent contamination, thus resulting in a yield loss. Multi-stage ATPS separations can improve recovery (Benavides et al., 2006) and may be justifiable depending on the relative ATPS cost and compound value. Vessels with a high aspect ratio are recommended to minimize the liquid-liquid interface where compound loss occurs, however homogenization in a high aspect ratio vessel generally has longer mixing times or suffers from undesirable fluid compartmentalization (Magelli et al., 2013). Furthermore, tall vessels result in long centrifugal distances and longer sedimentation times to achieve complete separation.

## Polymer-Based ATPS Pharmaceutical Industry Applications

After fermentation, separation of API from cells and cell debris is often achieved *via* centrifugation, however centrifugation becomes increasingly complex on scale up from bench (50 mL) to industrial scale (1,000 L) (Majekodunmi, 2015). Thus, there exists a need to explore advanced scalable separation processes that maintain yield for a single-step extraction. Polymer-based ATPSs are showing promise for a wide range of commercially valuable molecules, however their versatility also complicates its adoption. The principles governing high-value molecule partitioning has been investigated (Willauer et al., 2002) and the consultation of such toolboxes (Huddleston et al., 1999) to assist in ATPS design and development is highly encouraged.

One other factor that prohibits the attractiveness of polymer-polymer ATPSs is the cost of high molecular weight polymers at industrial scale (Torres-Acosta et al., 2018). As a result, cheaper phosphate or sulfate salts as replacements for polymer-polymer ATPSs to become polymer-salt ATPSs are more attractive. Such polymer-salt ATPSs were demonstrated to have high yield and scalability from bench to industrial scale (Hart et al., 1994). The substitution of a high molecular weight polymer with a salt, introduces an osmotic pressure concern which limits ATPS application in some cellular and biomolecular recoveries (Kühn, 1980; Zijlstra et al., 1996; Li et al., 2000). Despite this, in certain products with challenging

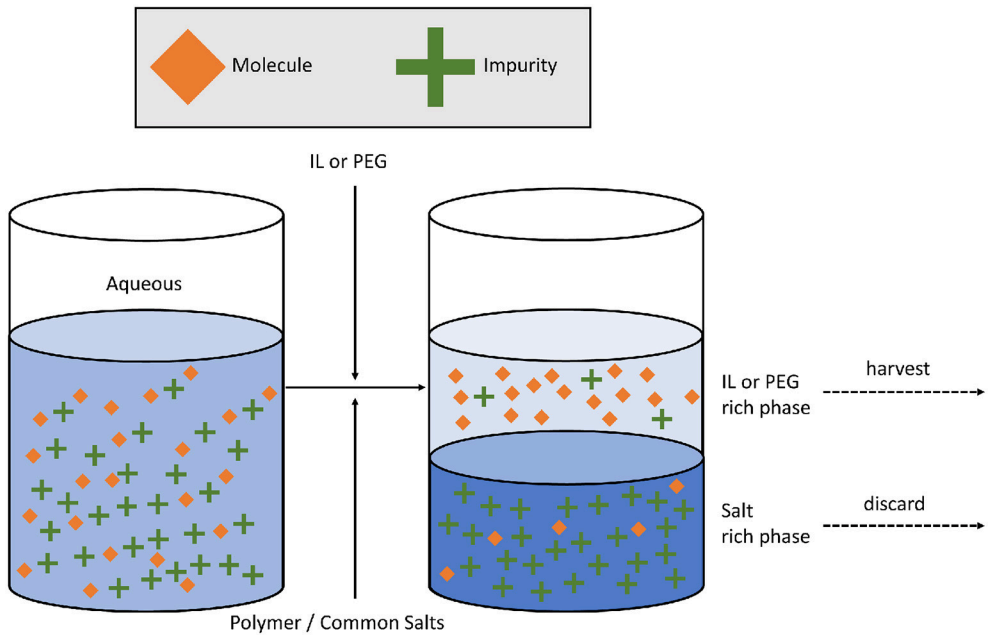


**FIGURE 1 |** The use of polymer-based or IL-based ATPSs for separations critically depends on selective partitioning of the molecule over impurities. Impeller agitation is often employed to speed up equilibrium partitioning. Depending on viscosity and density differences and interfacial tension values, physical separation can be as simple as sedimentation or as complex as industrial centrifugation to isolate the liquid phase containing the molecule of interest.

yields, ATPSs have financial justification at the industrial scale especially with the reduced costs of polymer-salt ATPSs and IL-ATPSs (Torres-Acosta et al., 2018).

## IONIC LIQUID ATPS

Ionic liquids have similar tunable properties such as hydrophobicity, polarity, solvation, and phase separation (Greaves et al., 2006; Moreno et al., 2015; Anderson and Clark, 2018). The stark similarities of polymer-based and IL-based ATPSs have facilitated the adoption of IL-based ATPSs. IL-ATPSs provide improvements in separation performance, selectivity, and broader design opportunities for a diverse range of molecules, including small molecules and biomolecules. IL-ATPSs also possess lower molecular weight and viscosity which enables faster separations making them industrially attractive. We note that the separation of cells, which is frequently performed in drug discovery experiments, and an obvious area for improvement through use of IL-ATPSs is not possible or demonstrated with IL-ATPSs, to the best of our awareness, likely due to osmotic pressure effects.

While this review provides a pharmaceutical focus, the reader is encouraged to reference other IL-ATPS reviews that informatively summarize properties for partitioning (Li et al., 2010; Oppermann et al., 2011; Ma et al., 2018), phase behavior and IL recovery (Freire et al., 2012), enzyme separations (Nadar et al., 2017), deep eutectic solvents (DES) (Shishov et al., 2017; Zainal-Abidin et al., 2017), and capillary electrophoresis applications (El-Hady et al., 2016). A review of various roles of ILs in pharmaceutical applications is also recommended (Huddleston et al., 1998).

Except where noted, all processes, physical properties and performance information described were generated at 25°C.

## TYPES AND PROPERTIES OF IL-ATPS

Phase separation can be controlled by the differing nature of the IL and second phase hydrogen bonding properties (Bridges et al., 2007). The IL-rich environment, often the upper phase, is relatively more hydrophobic thus attracting hydrophobic molecules. Phase separation is thus understood to be solvophobic and driven by electrostatic attractions and hydrophobic interactions. Several different systems have been discovered, characterized, and investigated for their potential applications in the pharmaceutical industry. IL-ATPSs can be tuned to improve solubility and thus extraction efficiency and partitioning properties which in turn improves speed and completion of phase separation. Generally, the lower the salt concentration required, the stronger the phase separation ability of the ILs from aqueous solutions of salts.

### IL Cation

$C_n$-methyl-imidazolium based ILs, where $n = 2$, 4, 6, and 8, are the most frequent systems studied in the literature, along with other functionalized imidazolium cores (Gutowski et al., 2003; Wu et al., 2015). Other systems such as cholinium based carboxylate ILs (oxalate, malonate, succinate, L-malate, fumarate,

glutarate, and citrate), and pyridinium based -ILs are described with PEG 400 and 600 as the second phase former (Passos et al., 2012; Mourão et al., 2014). Varying $CH_2$ length resulted in the coexistence of distinct types of self-assembly in the IL-ATP system. The behavior was inconsistent on changing the IL anion. For example, increasing the imidazolium alkyl chain length increased phase separation for a series of $BF_4^-$ ILs and decreased for the same series as $Br^-$ ILs (Wei et al., 2013). IL-ATPS and their applications were also demonstrated for dodecyl trimethylammonium-based (Flieger et al., 2013), functionalized amino acid and nucleotide ILs, for example glycine and guanidine (Wu et al., 2013; Zeng et al., 2013; Ding et al., 2014; Yao et al., 2016). Phosphonium-based ILs have the advantage of being less dense than water and less viscous than imidazolium based ILs, thus prospectively facilitating the separation of the aqueous waste stream of biomolecule separations in production scale equipment (Louros et al., 2010).

## IL Anion

Several different IL counterions have been described in the IL-ATPS literature, although simple anions such as bromide and chloride are most typical. Amino acid anions, L -serine, L-glycine L-alanine, and L-leucine with [bmim] cations formed IL-ATPS with $K_3PO_4$ (Wu C. et al., 2011). The ability to form IL-ATPS was related to hydrophobicity of the amino acid anion such that phase formation occurs with increasing hydrophobicity of the anion. Formate, acetate, propionate, lactate, chloride, and bromide salts of functionalized guanidinium ILs were shown to be effective at protein partitioning (Ding et al., 2014). Antioxidant anions (butanoate, propanoate, acetate, lactate, glycolate, bitartrate, dihydrogen phosphate, chloride, dihydrogen citrate, gallate, syringate, vanillate, and caffeate) of cholinium ILs were effective in separating immunoglobulin G (Ramalho et al., 2018).

## ATPS-Forming Salts

IL-ATPSs can be formed with conventional kosmotropic salts (potassium sulfate, citrate, ammonium sulfate), common salts (citric, fumaric, succinic, and tartaric acid sodium salts), amino acids, PEG and surfactants (3-p-nonylphenoxy-2-hydroxypropy trimethyl ammonium bromide, NPTAB and sodium dodecyl sulfonate, SDS), and combinations (Wu C. et al., 2011; Passos et al., 2012; Wei et al., 2013; Abdolrahimi et al., 2015; Dai et al., 2015; Pereira et al., 2015). The size of the biphasic region can be controlled by functionalizing the PEG terminal groups with –OH, –OMe, or $–NH_2$ to change the hydrogen bonding donor or acceptor. Improvements in the extraction performance for a hydrophobic molecule, tryptophan was demonstrated in citrate-based IL-ATPSs for use in continuous extraction of amino acids. The incorporation of surfactants decreased the viscosities of both phases and flipped the IL-rich phase to the bottom phase as a result of density changes (Wei et al., 2013; Dai et al., 2015).

The molecular mechanisms that govern the ability of salt ions to induce IL-ATPS formation was studied using a wide range of salts with diverse combinations of cations and anions, with [bmim][$CF_3SO_3$] a hydrophilic ionic liquid (Shahriari et al., 2012). The ions' trend to salt-out the IL into an ATPS follows the Hofmeister series and demonstrates the molar entropy of salt ion hydration as the driving force.

## Additives

Addition of a third component to create an IL-ATPS is another tactic used to enhance separation, presumably by increasing the solvophobic nature of the systems. For example, addition of SDS to [bmim]Br/NaCl IL-ATPS enhanced antibiotic extractions into the surfactant-rich upper phase (Yang et al., 2014). Addition of $CO_2$ into aqueous solutions of ILs and amines was shown to be effective in recovering ILs from aqueous mixtures (Xiong et al., 2012). Simply by bubbling $CO_2$ at atmospheric pressure into aqueous IL forms an IL-ATPS and allowed up to 99% recovery of the IL. Interestingly, these systems also modified densities such that the IL-rich phase is at the bottom. They also found phase separation of ammonium salts and the recovery efficiency for ILs are predominantly driven by the pKa of the amine, following the order: 1,2-propylenediamine > monoethanolamine > diethanolamine > N-methylmonoethanolamine > N-ethyldiethanolamine > triethanolamine, except for > N-methyldiethanolamine.

Application of an electrokinetically stable three-phase IL-ATPS, [bmim]Cl/ $K_2HPO_4$, [bmim]$BF_4$/ $NaH_2PO_4$, and [bmim]$BF_4$/ $Na_3$(citrate) enabled electrokinetic de-mixing (Li et al., 2017). Increased salt concentration and decreased IL concentration were observed to phase separate faster and have a higher efficiency of electrokinetic demixing due to a salting-out effect, whereas electric field had no impact on protein distribution.

In addition, pH-dependent reversible partitioning of IL-ATPS systems at ambient conditions offers dual functionality as a catalytic medium and separation extraction (Ferreira et al., 2017). Adjustment of pH was achieved through changes in salt speciation or bubbling in $CO_2$ or $NH_3$.

# IL EXTRACTIONS

## Small Molecule Separations

Several types of small molecules such as antioxidants, flavonoids, alkaloids, sulfonamides, functionalized amino acids, antibiotics such as tetracycline, oxytetracycline, cephalexin, and chloramphenicol effectively partition and extract in IL-ATPSs (Li et al., 2005; Freire et al., 2010; Louros et al., 2010; Han et al., 2011; Berton et al., 2012; Lin et al., 2012; Wu et al., 2013; Mourão et al., 2014; Yang et al., 2014; Abdolrahimi et al., 2015; Yao and Yao, 2017). In general, small molecules partition into the IL-rich upper phase. These systems are advantageous as a sample pre-treatment technique offering reduction of steps, materials and volatiles, and a sample concentration method (Basheer et al., 2008). IL-ATPSs have broad application in selective separation and extraction of small molecules and biomolecules through simple modifications of the IL structure and composition along with parameters that affect the extraction efficiency, such as the salt concentration, pH and extraction temperature, to appropriately modulate the IL-rich phase.

Pei et al. determined the partition coefficients for a series of amino acids in [$C_n$mim]Br ($n$ = 4, 6, 8)/ $K_2HPO_4$ IL-ATPS

and showed that they increased with increasing hydrophobicity of the amino acids and ionic liquids, solution pH value, tie-line length of the ATPSs and temperature (Pei et al., 2012). Pre-treatment of aqueous solutions for trace analysis of chloramphenicol with a 147-fold concentration enrichment and high recovery was achieved by applying an electric field across the IL-ATPS (Yao and Yao, 2017). A simple and sensitive method for selective extraction of quinine from human plasma was developed with [bmim]Cl/potassium phosphate buffer (Flieger and Czajkowska-Zelazko, 2015).

Extraction of pharmaceutical molecules (active ingredients or intermediates) is often from plant materials. The isolation of high purity secoisolariciresinol diglucoside, a multi-functional pharmaceutical, from flaxseed, was simplified and improved with an ultrasonic-assisted extraction followed by IL-ATPS formation by the addition of $Na_2SO_4$ (Tan et al., 2015). A similar example where fractionation and recovery of bioactive hydroxycinnamic derivatives from stressed carrot mass using IL-ATPS formed from [emim]acetate/potassium buffers gave a different phenolic ratio than conventional ATPS (Sánchez-Rangel et al., 2016).

Enantiomeric separation of 7 racemic amino acid mixtures was achieved by designing task-specific hydrophilic hexafluorophophate IL-ATPSs (Wu et al., 2015). Enantioselectivity was dependent on IL structure with energetically-favored intermolecular interactions between the IL cation, water and the D-enantiomer, allowing separation of the D-enantiomer to the bottom IL-rich phase. The IL-ATPS extraction efficiency was further improved for D,L-phenylalanine using chiral tropine-based ILs, [$C_n$Tropine]proline ($n$ = 2, 3, 4, 5, 6, 7, 8) with Cu(acetate)$_2$ and potassium phosphate buffers (Wu et al., 2015).

## Macromolecule Extractions/Analytical Biochemistry

The introduction of IL-ATPSs is a significant advancement in analytical biochemistry in terms of time, materials, complexity and efficiency for purification and separation of macromolecules in aqueous fluids. Due to the high water content in both phases, they are biocompatible media for the extraction and purification of a wide range of biomolecules by offering protection from denaturation. Separation is attributed to electrostatic potential differences between the coexisting phases, hydrophobic, and hydrogen bonding interactions of the biomolecules with the IL components in the upper IL-rich phase, and the salting-out effect.

Proteins, such as hemoglobin, ovalbumin, bovine serum albumin (BSA), bovine hemoglobin proteins, lysozyme, cytochrome c, and trypsin appear to require task-specific ILs per entity for successful separation and efficiencies as high as 99.6% (Lin et al., 2013; Wu et al., 2013; Zeng et al., 2013; Ding et al., 2014; Wang et al., 2015; Xu et al., 2015; ČíŽová et al., 2017). Extraction efficiencies are influenced by the amount of IL, the concentration of salt solution, temperature, and protein concentration. Separations were driven by hydrophobic interactions between IL cations and the proteins with minor contributions from electrostatic interactions and the salting-out effect.

In addition to separation, IL-ATPS were also used to improve binding constant estimation by stabilizing the protein of interest (El-Hady et al., 2015; Abd El-Hady and Albishri, 2018). For example, binding constants of (+)-propranolol, methotrexate and vinblastine to human alpha (a1)-acid glycoprotein, the plasma protein were determined by combining affinity capillary electrophoresis with reversible temperature-dependent

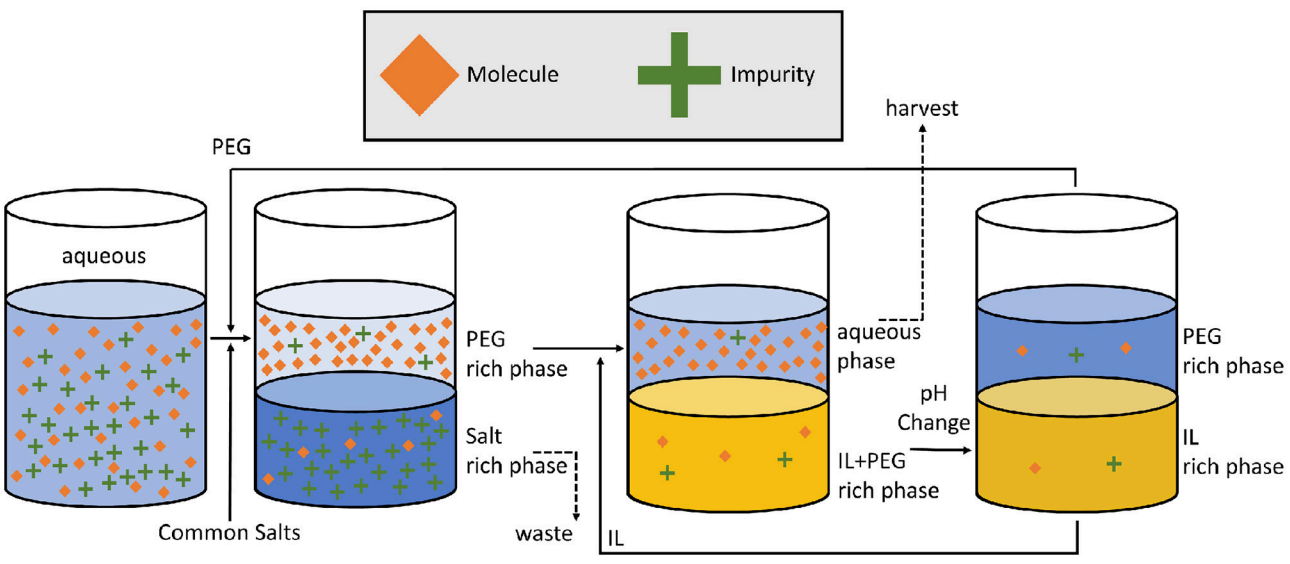


**FIGURE 2 |** IL assisted polymer recovery for ATPS extraction proposed by Jiang et al. (2009). The recent merge between IL and conventional ATPSs creates new opportunities to further decrease the carbon footprint of ATPS extractions which also result in cost savings. Such financial and environment drivers are key to industrial adoption.

phase separation using [bmim]Cl/ phosphate IL-ATPS with improved precision.

The antibody, immunoglobulin G (IgG) was extracted from serum samples using cholinium based IL-ATPSs (Ramalho et al., 2018). Although some systems had superior IgG recovery values to conventional techniques, improvement in IgG purity levels was insignificant. IL-ATPS represents a far simpler separation method when compared to current multistep methods for antibody isolation from serum samples. Such technology is worth further development and optimization.

## CATALYTIC ENHANCEMENT

IL-ATPS also found utility as catalyst performance enhancers that offer a dual advantage in synthetic processes when selective separation is considered (Dyson et al., 2001; Wu D. X.et al., 2011; Mai and Koo, 2014). The bioconversion of the steroid 16a,17-epoxyprogesterone to 11a-hydroxy-16a, 17-epoxyprogesterone catalyzed by free *R. nigricans* cells was improved when performed in an IL-ATPS without the addition of salt, and demonstrated in semi-continuous production for 60 h at ∼5 mL (total) scale (Wu D. X.et al., 2011). A temperature-dependent reversible IL-ATPS was demonstrated as a medium for transition metal catalyzed hydrogenation of a water-soluble substrate, offering potential re-use of the high-value catalyst and avoidance of product metal contamination (Dyson et al., 2001). Similarly, temperature-controlled reversible phase separation offers the advantage of product recovery and maintaining catalytic activity of an *in-situ* penicillin G hydrolysis (Mai and Koo, 2014). In keeping with the well-known trends of enzymatic activity in ILs, catalytic activity was found to increase in IL hydrophobicity.

## CONVENTIONAL AND IL-ATPS CROSSOVER

There are a few examples of note where polymer-based ATPS were combined with ILs. Extraction efficiency of three antioxidants, gallic, vanillic, and syringic acids, was further improved by tuning the polarity of the PEG-rich bottom phase with the addition of an IL (Almeida et al., 2014). The relationship between hydrogen bonding of the IL with the phenolic acids and extraction was found to be more important than the total amount of IL and increasing the polymer molecular weight increased the likelihood of phase separation. Tropine-salt IL-ATPSs were used to remove or recover hydrophilic ILs that cannot form IL-ATPSs with kosmotropic salts, polymers or carbohydrates, in an attempt to provide a means to reduce environmental contamination (Wu et al., 2016). The ILs preferentially partitioned to the tropine-rich upper phase, which is then further processed to complete the recovery. IL-ATPSs have also been employed for polymer recovery and recycling (Jiang et al., 2009) which offers the benefits of cost and carbon footprint reduction and may be key to wider industrial adoption (**Figure 2**).

## FORWARD STATEMENT

ATPSs have already found industrial use in niche areas of pharmaceutical development and possibly manufacturing. Meanwhile, ILs are simultaneously emerging as sustainable alternatives for small molecule pharmaceutical extractions. The recent development of IL-based ATPSs provides new opportunities for decreasing the carbon footprint and costs of pharmaceutical extractions which are important drivers for wider industrial adoption. The body of literature is clear that IL-based and polymer-based ATPSs are suitable sustainable alternatives to organic solvents and produce higher or equivalent yields. We believe the barriers to industrial adoption have been cracked due, in part, to the scientific works highlighted in this review, and that there is a bright pharmaceutical future for polymer and IL-based ATPSs.

## AUTHOR CONTRIBUTIONS

LM provided review on ILs and DL provided review on polymer-based ATPS processes.

## ACKNOWLEDGMENTS

The authors would like to acknowledge their colleagues of GlaxoSmithKline for their support in writing this article, specifically Kenneth Wells, Philip Dell'Orco and Alex Povey for their review and insights.

## REFERENCES

Abd El-Hady, D., and Albishri, H. M. (2018). Temperature controlled ionic liquid aqueous two phase system combined with affinity capillary electrophoresis for rapid and precise pharmaceutical-protein binding measurements. *Methods.* 146, 120–125. doi: 10.1016/j.ymeth.2018.02.007

Abdolrahimi, S., Nasernejad, B., and Pazuki, G. (2015). Influence of process variables on extraction of Cefalexin in a novel biocompatible ionic liquid based-aqueous two phase system. *Phys. Chem. Chem. Phys.* 17, 655–669. doi: 10.1039/C4CP02923B

Albertsson, P. A. (1958). Partition of proteins in liquid polymer–polymer two-phase systems. *Nature.* 182. 709–711. doi: 10.1038/182709a0

Albertsson, P. E. R. Å (1956). Chromatography and partition of cells and cell fragments. *Nature.* 177, 771–774. doi: 10.1038/177771a0

Albertsson, P. E. R. Å. (1960). *Partition of Cell Particles and Macromolecules.* New York, NY: Wiley.

Almeida, M. R., Passos, H., Pereira, M. M., Lima, Á. S., Coutinho, J. A. P., and Freire, M. G. (2014). Ionic liquids as additives to enhance the extraction of antioxidants in aqueous two-phase systems. *Sep. Purif. Technol.* 128, 1–10. doi: 10.1016/j.seppur.2014.03.004

Anderson, J. L., and Clark, K. D. (2018). Ionic liquids as tunable materials in (bio)analytical chemistry. *Anal. Bioanal. Chem.* 410, 4565–4566. doi: 10.1007/s00216-018-1125-4

Asenjo, J. A., and Andrews, B. A. (2012). Aqueous two-phase systems for protein separation: phase separation and applications. *J. Chromatogr. A.* 1238, 1–10. doi: 10.1016/j.chroma.2012.03.049

Azevedo, A. M., Gomes, A. G., Rosa, P. A., Ferreira, I. F., Pisco, A. M., and Aires-Barros, M. R. (2009a). Partitioning of human

antibodies in polyethylene glycol–sodium citrate aqueous two-phase systems. *Sep. Purif. Technol.* 65, 14–21. doi: 10.1016/j.seppur.2007.12.010

Azevedo, A. M., Rosa, P. A. J., Ferreira, I. F., Pisco, A. M. M. O., de Vries, J., Korporaal, R., et al. (2009b). Affinity-enhanced purification of human antibodies by aqueous two-phase extraction. *Sep. Purif. Technol.* 65, 31–39. doi: 10.1016/j.seppur.2008.03.006

Balasubramaniam, D., Wilkinson, C., Van Cott, K., and Zhang, C. (2003). Tobacco protein separation by aqueous two-phase extraction. *J. Chromatogr. A*. 989, 119–129. doi: 10.1016/S0021-9673(02)01900-3

Basheer, C., Alnedhary, A. A., Madhava Rao, B. S., Balasubramanian, R., and Lee, H. K. (2008). Ionic liquid supported three-phase liquid-liquid-liquid microextraction as a sample preparation technique for aliphatic and aromatic hydrocarbons prior to gas chromatography-mass spectrometry. *J. Chromatogr. A*. 1210, 19–24. doi: 10.1016/j.chroma.2008.09.040

Benavides, J., Mena, J. A., Cisneros-Ruiz, M., Ramírez, O. T., Palomares, L. A., and Rito-Palomares, M. (2006). Rotavirus-like particles primary recovery from insect cells in aqueous two-phase systems. *J. Chromatogr. B.* 842, 48–57. doi: 10.1016/j.jchromb.2006.05.006

Berton, P., Monasterio, R. P., and Wuilloud, R. G. (2012). Selective extraction and determination of vitamin B12 in urine by ionic liquid-based aqueous two-phase system prior to high-performance liquid chromatography. *Talanta* 97, 521–526. doi: 10.1016/j.talanta.2012.05.008

Bridges, N. J., Gutowski, K. E., and Rogers, R. D. (2007). Investigation of aqueous biphasic systems formed from solutions of chaotropic salts with kosmotropic salts (salt–salt ABS). *Green Chem.* 9, 177–183. doi: 10.1039/B611628K

Chen, J., Spear, S. K., Huddleston, J. G., and Rogers, R. D. (2005). Polyethylene glycol and solutions of polyethylene glycol as green reaction media. *Green Chem.* 7, 64-82. doi: 10.1039/b413546f

ČíŽová, A., Korcová, J., Farkaš, P., and Bystrický, S. (2017). Efficient separation of mannan–protein mixtures by ionic liquid aqueous two-phase system, comparison with lectin affinity purification. *Int. J. Biol. Macromol.* 98, 314–318. doi: 10.1016/j.ijbiomac.2017.02.001

Dai, C., Liu, Y., Wang, S., Du, M., Peng, D., Wang, K., et al. (2015). Investigation on the phase behaviors of aqueous surfactant two-phase systems in a mixture of N-dodecyl-N-methylpiperidinium bromide (C12MDB) and sodium dodecyl sulfate (SDS). *Colloi. Surf. A* 468, 322–326. doi: 10.1016/j.colsurfa.2014.12.061

Desbuquois, B., and Aurbach, G. (1971). Use of polyethylene glycol to separate free and antibody-bound peptide hormones in radioimmunoassays. *J. Clin. Endocrinol. Metab.* 33, 732–738. doi: 10.1210/jcem-33-5-732

Ding, X., Wang, Y., Zeng, Q., Chen, J., Huang, Y., and Xu, K. (2014). Design of functional guanidinium ionic liquid aqueous two-phase systems for the efficient purification of protein. *Anal. Chim. Acta.* 815, 22–32. doi: 10.1016/j.aca.2014.01.030

Diuzheva, A., Carradori, S., Andruch, V., Locatelli, M., De Luca, E., Tiecco, M., et al. (2018). Use of innovative (Micro)extraction techniques to characterise harpagophytum procumbens root and its commercial food supplements. *Phytochem. Anal.* 29, 233–241. doi: 10.1002/pca.2737

Dyson, P. J., Ellis, D. J., and Welton, T. (2001). A temperature-controlled reversible ionic liquid - Water two phase - Single phase protocol for hydrogenation catalysis. *Can. J. Chem.* 79, 705–708. doi: 10.1139/v01-084

El-Hady, D. A., Albishri, H. M., Rengarajan, R., Deeb, S. E., and Wätzig, H. (2015). Stabilizing proteins for affinity capillary electrophoresis using ionic liquid aqueous two phase systems: pharmaceuticals and human serum albumin. *Electrophoresis.* 36, 3080–3087. doi: 10.1002/elps.201500199

El-Hady, D. A., Albishri, H. M., and Wätzig, H. (2016). Ionic liquids in enhancing the sensitivity of capillary electrophoresis: off-line and on-line sample preconcentration techniques. *Electrophoresis.* 37, 1609–1623. doi: 10.1002/elps.201600069

Ferreira, A. M., Cláudio, A. F. M., Válega, M., Domingues, F. M. J., Silvestre, A. J. D., Rogers, R. D., et al. (2017). Switchable (pH-driven) aqueous biphasic systems formed by ionic liquids as integrated production–separation platforms. *Green Chem.* 19, 2768–2773. doi: 10.1039/C7GC00157F

Flieger, J., and Czajkowska-Zelazko, A. (2015). Aqueous two phase system based on ionic liquid for isolation of quinine from human plasma sample. *Food Chem.* 166, 150–157. doi: 10.1016/j.foodchem.2014.06.037

Flieger, J., Siwek, A., Pizon, M., and Czajkowska-Zelazko, A. (2013). Ionic liquids as surfactants in micellar liquid chromatography. *J. Sep. Sci.* 36, 1530–1536. doi: 10.1002/jssc.201201059

Frampton, J. P., Lai, D., Sriram, H., and Takayama, S. (2011). Precisely targeted delivery of cells and biomolecules within microchannels using aqueous two-phase systems. *Biomed. Microdevices.* 13, 1043–1051. doi: 10.1007/s10544-011-9574-y

Frampton, J. P., White, J. B., Simon, A. B., Tsuei, M., Paczesny, S., and Takayama, S. (2014). Aqueous two-phase system patterning of detection antibody solutions for cross-reaction-free multiplex ELISA. *Sci. Rep.* 4:4878. doi: 10.1038/srep04878

Freire, M. G., Cláudio, A. F. M., Araújo, J. M. M., Coutinho, J. A. P., Marrucho, I. M., Lopes, J. N. C., et al. (2012). Aqueous biphasic systems: a boost brought about by using ionic liquids. *Chem. Soc. Rev.* 41, 4966–4995. doi: 10.1039/c2cs35151j

Freire, M. G., Neves, C.M.S.S., Marrucho, I. M., Canongia Lopes, J. N., Rebelo, L. P. N., and Coutinho, J. A. P. (2010). High-performance extraction of alkaloids using aqueous two-phase systems with ionic liquids. *Green Chem.* 12, 1715–1718. doi: 10.1039/c0gc00179a

Frerix, A., Müller, M., Kula, M.-R., and Hubbuch, J. (2005). Scalable recovery of plasmid DNA based on aqueous two-phase separation. *Biotechnol. Appl. Biochem.* 42, 57–66. doi: 10.1042/BA20040107

Frerix, A., Schönewald, M., Geilenkirchen, P., Müller, M., Kula, M.-R., and Hubbuch, J. (2006). Exploitation of the coil-globule plasmid DNA transition induced by small changes in temperature, pH salt, and poly(ethylene glycol) compositions for directed partitioning in aqueous two-phase systems. *Langmuir.* 22, 4282–4290. doi: 10.1021/la052745u

Gomes, G. A., Azevedo, A. M., Aires-Barros, M. R., and Prazeres, D. M. F. (2009). Purification of plasmid DNA with aqueous two phase systems of PEG 600 and sodium citrate/ammonium sulfate. *Sep. Purif. Technol.* 65, 22–30. doi: 10.1016/j.seppur.2008.01.026

Greaves, T. L., Weerawardena, A., Fong, C., Krodkiewska, I., and Drummond, C. J. (2006). Protic ionic liquids: solvents with tunable phase behavior and physicochemical properties. *J. Phys. Chem. B* 110, 22479–22487. doi: 10.1021/jp0634048

Gutowski, K. E., Broker, G. A., Willauer, H. D., Huddleston, J. G., Swatloski, R. P., Holbrey, J. D., et al. (2003). Controlling the aqueous miscibility of ionic liquids: aqueous biphasic systems of water-miscible ionic liquids and water-structuring salts for recycle, metathesis, and separations. *J. Am. Chem. Soc.* 125, 6632–6633. doi: 10.1021/ja0351802

Han, J., Wang, Y., Yu, C. L., Yan, Y. S., and Xie, X. Q. (2011). Extraction and determination of chloramphenicol in feed water, milk, and honey samples using an ionic liquid/sodium citrate aqueous two-phase system coupled with high-performance liquid chromatography. *Anal. Bioanal. Chem.* 399, 1295–1304. doi: 10.1007/s00216-010-4376-2

Hart, R. A., Lester, P. M., Reifsnyder, D. H., Ogez, J. R., and Builder, S. E. (1994). Large Scale, *In situ* Isolation of Periplasmic IGF–I from *E. coli. Biotechnology.* 12, 1113–1117. doi: 10.1038/nbt1194-1113

Huddleston, J. G., Willauer, H. D., Griffin, S. T., and Rogers, R. D. (1999). Aqueous polymeric solutions as environmentally benign liquid/liquid extraction media. *Ind. Eng. Chem. Res.* 38, 2523–2539. doi: 10.1021/ie980505m

Huddleston, J. G., Willauer, H. D., Swatloski, R. P., Visser, A. E., and Rogers, R. D. (1998). Room temperature ionic liquids as novel media for 'clean' liquid–liquid extraction. *Chem. Commun.* 1765–1766.

Jiang, Y., Xia, H., Yu, J., Guo, C., and Liu, H. (2009). Hydrophobic ionic liquids-assisted polymer recovery during penicillin extraction in aqueous two-phase system. *Chem. Eng. J.* 147, 22–26. doi: 10.1016/j.cej.2008.11.012

Kühn, I. (1980). Alcoholic fermentation in an aqueous two-phase system. *Biotechnol. Bioeng.* 22, 2393–2398. doi: 10.1002/bit.260221114

Kula, M.-R., Elling, L., and Walsdorf, A. (1991). Investigations of liquid-liquid partition chromatography of proteins. *J. Chromatogr. A* 548, 3–12. doi: 10.1016/S0021-9673(01)88589-7

Kumar, A., Kamihira, M., Galaev, I. Y., Mattiasson, B., and Iijima, S. (2001). Type-specific separation of animal cells in aqueous two-phase systems using antibody conjugates with temperature-sensitive polymers. *Biotechnol. Bioeng.* 75, 570–580. doi: 10.1002/bit.10080

Ladd Effio C, Wenger L, Ötes O., Oelmeier S.A., Kneusel R., Hubbuch J. (2015). Downstream processing of virus-like particles: single-stage and multi-stage aqueous two-phase extraction. *J. Chromatogr. A* 1383, 35–46. doi: 10.1016/j.chroma.2015.01.007

Lai, D., Frampton, J. P., Sriram, H., and Takayama, S. (2011). Rounded multi-level microchannels with orifices made in one exposure enable aqueous two-phase system droplet microfluidics. *Lab Chip.* 11, 3551–3554. doi: 10.1039/c1lc20560a

Li, C., Ouyang, F., and Bai, J. (2000). Extractive cultivation of *Lactococcus lactis.* using a polyethylene glycol/MgSO4· 7H2O aqueous two-phase system to produce nisin. *Biotechnol. Lett.* 22, 843–847. doi: 10.1023/A:1005634626801

Li, S., He, C., Liu, H., Li, K., and Liu, F. (2005). Ionic liquid-based aqueous two-phase system, a sample pretreatment procedure prior to high-performance liquid chromatography of opium alkaloids. *J. Chromatogr. B Anal. Technol. Biomed. Life Sci.* 826, 58–62. doi: 10.1016/j.jchromb.2005.08.005

Li, X., Liu, Y., and Li, F. (2017). Effects of DC electric field on phase equilibrium and partitioning of ionic liquid-based aqueous two-phase systems. *Biochem. Eng. J.* 126, 146–154. doi: 10.1016/j.bej.2016.09.008

Li, Z., Pei, Y., Wang, H., Fan, J., and Wang, J. (2010). Ionic liquid-based aqueous two-phase systems and their applications in green separation processes. *TrAC Trends Anal. Chem.* 29, 1336–1346. doi: 10.1016/j.trac.2010.07.014

Lin, X., Wang, Y., Liu, X., Huang, S., and Zeng, Q. (2012). ILs-based microwave-assisted extraction coupled with aqueous two-phase for the extraction of useful compounds from Chinese medicine. *Analyst.* 137, 4076–4085. doi: 10.1039/c2an35476d

Lin, X., Wang, Y., Zeng, Q., Ding, X., and Chen, J. (2013). Extraction and separation of proteins by ionic liquid aqueous two-phase system. *Analyst* 138, 6445–6453. doi: 10.1039/c3an01301d

Liu, C.-L., Kamei, D. T., King, J. A., Wang, D. I. C., and Blankschtein, D. (1998). Separation of proteins and viruses using two-phase aqueous micellar systems. *J. Chromatogr. B Biomed. Sci. Appl.* 711, 127–138. doi: 10.1016/S0378-4347(98)00013-9

Louros, C. L. S., Cláudio, A. F. M., Neves, C. M. S. S., Freire, M. G., Marrucho, I. M., Pauly, J., et al. (2010). Extraction of biomolecules using phosphonium-based ionic liquids + K3PO4 aqueous biphasic systems. *Int. J. Mol. Sci.* 11, 1777–1791. doi: 10.3390/ijms11041777

Ma, C., Laaksonen, A., Liu, C., Lu, X., and Ji, X. (2018). The peculiar effect of water on ionic liquids and deep eutectic solvents. *Chem. Soc. Rev.* 47, 8685–8720. doi: 10.1039/C8CS00325D

Magelli, F., Montante, G., Pinelli, D., and Paglianti, A. (2013). Mixing time in high aspect ratio vessels stirred with multiple impellers. *Chem. Eng. Sci.* 101, 712–720. doi: 10.1016/j.ces.2013.07.022

Mai, N. L., and Koo, Y. M. (2014). Enzymatic hydrolysis of penicillin and *in situ* product separation in thermally induced reversible phase-separation of ionic liquids/water mixture. *Enzyme Microb. Technol.* 63, 34–38. doi: 10.1016/j.enzmictec.2014.05.002

Majekodunmi, S. O. (2015). A review on centrifugation in the pharmaceutical industry. *Am. J. Biomed. Eng.* 5, 67–78. doi: 10.5923/j.ajbe.20150502.03

Mocan, A., Diuzheva, A., Carradori, S., Andruch, V., Massafra, C., Moldovan, C., et al. (2018). Development of novel techniques to extract phenolic compounds from Romanian cultivars of *Prunus domestica* L. and their biological properties. *Food Chem. Toxicol.* 119, 189–198. doi: 10.1016/j.fct.2018.04.045

Moreno, J. S., Jeremias, S., Moretti, A., Panero, S., Passerini, S., Scrosati, B., et al. (2015). Ionic liquid mixtures with tunable physicochemical properties. *Electrochim. Acta.* 151, 599–608. doi: 10.1016/j.electacta.2014.11.056

Mourão, T., Tomé, L. C., Florindo, C., Rebelo, L. P. N., and Marrucho, I. M. (2014). Understanding the role of cholinium carboxylate ionic liquids in PEG-based aqueous biphasic systems. *ACS Sustain. Chem. Eng.* 2, 2426–2434. doi: 10.1021/sc500444w

Nadar, S. S., Pawar, R. G., and Rathod, V. K. (2017). Recent advances in enzyme extraction strategies: a comprehensive review. *Int. J. Biol. Macromol.* 101, 931–957. doi: 10.1016/j.ijbiomac.2017.03.055

Nam, K.-H., Chang, W.-J., Hong, H., Lim, S.-M., Kim, D.-I., and Koo, Y.-M. (2005). Continuous-flow fractionation of animal cells in microfluidic device using aqueous two-phase extraction. *Biomed. Microdevices.* 7, 189–195. doi: 10.1007/s10544-005-3025-6

Nazer, B., Dehghani, M. R., and Goliaei, B. (2017). Plasmid DNA affinity partitioning using polyethylene glycol–sodium sulfate aqueous two-phase systems. *J. Chromatogr. B.* 1044, 112–119. doi: 10.1016/j.jchromb.2017.01.002

Norrby, E. C. J., and Albertsson, P. Å. (1960). Concentration of poliovirus by an aqueous polymer two-phase system. *Nature* 188:1047. doi: 10.1038/1881047a0

Oppermann, S., Stein, F., and Kragl, U. (2011). Ionic liquids for two-phase systems and their application for purification, extraction and biocatalysis. *Appl. Microbiol. Biotechnol.* 89, 493–499. doi: 10.1007/s00253-010-2933-4

Passos, H., Ferreira, A. R., Cláudio, A. F. M., Coutinho, J. A. P., and Freire, M. G. (2012). Characterization of aqueous biphasic systems composed of ionic liquids and a citrate-based biodegradable salt. *Biochem. Eng. J.* 67, 68–76. doi: 10.1016/j.bej.2012.05.004

Pei, Y., Li, Z., Liu, L., and Wang, J. (2012). Partitioning behavior of amino acids in aqueous two-phase systems formed by imidazolium ionic liquid and dipotassium hydrogen phosphate. *J. Chromatogr. A.* 1231, 2–7. doi: 10.1016/j.chroma.2012.01.087

Pereira, J. F. B., Kurnia, K. A., Freire, M. G., Coutinho, J. A. P., and Rogers, R. D. (2015). Controlling the formation of ionic-liquid-based aqueous biphasic systems by changing the hydrogen bonding ability of polyethylene glycol end groups. *Chemphyschem.* 16, 2219–2225. doi: 10.1002/cphc.201500146

Ramalho, C. C., Neves, C. M., Quental, M. V., Coutinho, J. A., and Freire, M. G. (2018). Separation of immunoglobulin G using aqueous biphasic systems composed of cholinium-based ionic liquids and poly(propylene glycol). *J. Chem. Technol. Biotechnol.* 93, 1931–1939. doi: 10.1002/jctb.5594

Ribeiro, S., Monteiro, G., Cabral, J., and Prazeres, D. (2002). Isolation of plasmid DNA from cell lysates by aqueous two-phase systems. *Biotechnol. Bioeng.* 78, 376–384. doi: 10.1002/bit.10227

Rosa, P., Azevedo, A., Sommerfeld, S., Bäcker, W., and Aires-Barros, M. (2012). Continuous aqueous two-phase extraction of human antibodies using a packed column. *J. Chromatogr. B* 880, 148–156. doi: 10.1016/j.jchromb.2011.11.034

Rosa, P. A., Azevedo, A., Ferreira, I., De Vries, J., Korporaal, R., Verhoef, H., et al. (2007a). Affinity partitioning of human antibodies in aqueous two-phase systems. *J. Chromatogr. A* 1162, 103–113. doi: 10.1016/j.chroma.2007.03.067

Rosa, P. A., Azevedo, A. M., and Aires-Barros, M. R. (2007b). Application of central composite design to the optimisation of aqueous two-phase extraction of human antibodies. *J. Chromatogr. A* 1141, 50–60. doi: 10.1016/j.chroma.2006.11.075

Sánchez-Rangel, J. C., Jacobo-Velázquez, D. A., Cisneros-Zevallos, L., and Benavides, J. (2016). Primary recovery of bioactive compounds from stressed carrot tissue using aqueous two-phase systems strategies. *J. Chem. Technol. Biotechnol.* 91, 144–154. doi: 10.1002/jctb.4553

Schmidt, A., Ventom, A., and Asenjo, J. (1994). Partitioning and purification of α-amylase in aqueous two-phase systems. *Enzyme Microb. Technol.* 16, 131–142. doi: 10.1016/0141-0229(94)90076-0

Selber, K., Tjerneld, F., Collén, A., Hyytiä, T., Nakari-Setälä, T., Bailey, M., et al. (2004). Large-scale separation and production of engineered proteins, designed for facilitated recovery in detergent-based aqueous two-phase extraction systems. *Proc. Biochem.* 39, 889–896. doi: 10.1016/S0032-9592(03)00198-5

Shahriari, S., Neves, C. M. S. S., Freire, M. G., and Coutinho, J. A. P. (2012). Role of the Hofmeister series in the formation of ionic-liquid-based aqueous biphasic systems. *J. Phys. Chem. B* 116, 7252–7258. doi: 10.1021/jp300874u

Sharp, K. A., Yalpani, M., Howard, S. J., and Brooks, D. E. (1986). Synthesis and application of a poly (ethylene glycol)-antibody affinity ligand for cell separations in aqueous polymer two-phase systems. *Anal. Biochem.* 154, 110–117. doi: 10.1016/0003-2697(86)90503-8

Shishov, A., Bulatov, A., Locatelli, M., Carradori, S., and Andruch, V. (2017). Application of deep eutectic solvents in analytical chemistry. A review. *Microchem. J.* 135, 33–38. doi: 10.1016/j.microc.2017.07.015

SooHoo, J. R., and Walker, G. M. (2009). Microfluidic aqueous two phase system for leukocyte concentration from whole blood. *Biomed. Microdevices* 11, 323–329. doi: 10.1007/s10544-008-9238-8

Tan, Z. J., Wang, C. Y., Yang, Z. Z., Yi, Y. J., Wang, H. Y., Zhou, W. L., et al. (2015). Ionic liquid-based ultrasonic-assisted extraction of secoisolariciresinol diglucoside from flaxseed (*Linum usitatissimum.* L.) with further purification by an aqueous two-phase system. *Molecules.* 20, 17929–17943. doi: 10.3390/molecules201017929

Tavana, H., Jovic, A., Mosadegh, B., Lee, Q., Liu, X., Luker, K., et al. (2009). Nanolitre liquid patterning in aqueous environments for spatially

defined reagent delivery to mammalian cells. *Nat. Mater.* 8, 736–741. doi: 10.1038/nmat2515

Teixeira, A. G., Agarwal, R., Ko, K. R., Grant-Burt, J., Leung, B. M., and Frampton, J. P. (2017). emerging biotechnology applications of aqueous two-phase systems. *Adv. Healthc. Mater*. 7:e1701036. doi: 10.1002/adhm.201701036

Torres-Acosta, M. A., Pereira, J. F. B., Freire, M. G., Aguilar-Yáñez, J. M., Coutinho, J. A. P., Titchener-Hooker, N. J., et al. (2018). Economic evaluation of the primary recovery of tetracycline with traditional and novel aqueous two-phase systems. *Sep. Purif. Technol.* 203, 178–184. doi: 10.1016/j.seppur.2018.04.041

Tsukamoto, M., Taira, S., Yamamura, S., Morita, Y., Nagatani, N., Takamura, Y., et al. (2009). Cell separation by an aqueous two-phase system in a microfluidic device. *Analyst.* 134, 1994–1998. doi: 10.1039/b909597g

Walter, H., Krob, E. J., and Brooks, D. E. (1976). Membrane surface properties other than charge involved in cell separation by partition in polymer, aqueous two-phase systems. *Biochemistry.* 15, 2959–2964. doi: 10.1021/bi00659a004

Wang, Z., Pei, Y., Zhao, J., Li, Z., Chen, Y., and Zhuo, K. (2015). Formation of ether-functionalized ionic-liquid-based aqueous two-phase systems and their application in separation of protein and saccharides. *J. Phys. Chem. B* 119, 4471–4478. doi: 10.1021/jp510984d

Wei, X. L., Wang, X. H., Ping, A. L., Du, P. P., Sun, D. Z., Zhang, Q. F., et al. (2013). Formation and characteristics of aqueous two-phase systems formed by a cationic surfactant and a series of ionic liquids. *J. Chromatogr. B Anal. Technol. Biomed. Life Sci.* 939, 1–9. doi: 10.1016/j.jchromb.2013.09.006

Willauer, H. D., Huddleston, J. G., and Rogers, R. D. (2002). Solute partitioning in aqueous biphasic systems composed of polyethylene glycol and salt: the partitioning of small neutral organic species. *Ind. Eng. Chem. Res.* 41, 1892–1904. doi: 10.1021/ie010598z

Wu, C., Wang, J., Li, Z., Jing, J., and Wang, H. (2013). Relative hydrophobicity between the phases and partition of cytochrome-c in glycine ionic liquids aqueous two-phase systems. *J. Chromatogr. A* 1305, 1–6. doi: 10.1016/j.chroma.2013.06.066

Wu, C., Wang, J., Wang, H., Pei, Y., and Li, Z. (2011). Effect of anionic structure on the phase formation and hydrophobicity of amino acid ionic liquids aqueous two-phase systems. *J. Chromatogr. A* 1218, 8587–8593. doi: 10.1016/j.chroma.2011.10.003

Wu, D. X., Guan, Y. X., Wang, H. Q., and Yao, S. J. (2011). 11α-Hydroxylation of 16α,17-epoxyprogesterone by Rhizopus nigricans in a biphasic ionic liquid aqueous system. *Bioresour. Technol.* 102, 9368–9373. doi: 10.1016/j.biortech.2011.07.060

Wu, H., Yao, S., Qian, G., and Song, H. (2016). Development of tropine-salt aqueous two-phase systems and removal of hydrophilic ionic liquids from aqueous solution. *J. Chromatogr. A* 1461, 1–9. doi: 10.1016/j.chroma.2016.06.081

Wu, H., Yao, S., Qian, G., Yao, T., and Song, H. (2015). A resolution approach of racemic phenylalanine with aqueous two-phase systems of chiral tropine ionic liquids. *J. Chromatogr. A* 1418, 150–157. doi: 10.1016/j.chroma.2015.09.058

Xiong, D., Wang, H., Li, Z., and Wang, J. (2012). Recovery of ionic liquids with aqueous two-phase systems induced by carbon dioxide. *ChemSusChem.* 5, 2255–2261. doi: 10.1002/cssc.201200307

Xu, K., Wang, Y., Huang, Y., Li, N., and Wen, Q. (2015). A green deep eutectic solvent-based aqueous two-phase system for protein extracting. *Anal. Chim. Acta.* 864, 9–10. doi: 10.1016/j.aca.2015.01.026

Yamada, M., Kasim, V., Nakashima, M., Edahiro, J.I., and Seki, M. (2004). Continuous cell partitioning using an aqueous two-phase flow system in microfluidic devices. *Biotechnol. Bioeng.* 88, 489–494. doi: 10.1002/bit.20276

Yang, X., Zhang, S., Yu, W., Liu, Z., Lei, L., Li, N., et al. (2014). Ionic liquid-anionic surfactant based aqueous two-phase extraction for determination of antibiotics in honey by high-performance liquid chromatography. *Talanta.* 124, 1–6. doi: 10.1016/j.talanta.2014.02.039

Yao, T., and Yao, S. (2017). Magnetic ionic liquid aqueous two-phase system coupled with high performance liquid chromatography: a rapid approach for determination of chloramphenicol in water environment. *J. Chromatogr. A* 1481, 12–22. doi: 10.1016/j.chroma.2016.12.039

Yao, T., Yao, S., Tang, D., Jing, L., Wang, D., and Song, H. (2016). Synthesis, magnetism, aqueous-two phase formation and physical properties of novel guanidinium-based magnetic ionic liquids. *RSC Adv.* 6, 52898–52904. doi: 10.1039/C6RA09879G

Zainal-Abidin, M. H., Hayyan, M., Hayyan, A., and Jayakumar, N. S. (2017). New horizons in the extraction of bioactive compounds using deep eutectic solvents: a review. *Anal. Chim. Acta* 979, 1–23. doi: 10.1016/j.aca.2017.05.012

Zeng, Q., Wang, Y., Li, N., Huang, X., Ding, X., Lin, X., et al. (2013). Extraction of proteins with ionic liquid aqueous two-phase system based on guanidine ionic liquid. *Talanta.* 116, 409–416. doi: 10.1016/j.talanta.2013.06.011

Zijlstra, G. M., de Gooijer, C. D., van der Pol, L. A., and Tramper, J. (1996). Design of aqueous two-phase systems supporting animal cell growth: a first step toward extractive bioconversions. *Enzyme Microb. Technol.* 19, 2–8. doi: 10.1016/0141-0229(95)00173-5

**Conflict of Interest Statement:** LM and DL are employed by GlaxoSmithKline.

frontiers in Chemistry

ORIGINAL RESEARCH
published: 03 April 2019
doi: 10.3389/fchem.2019.00201

# Liquid Biphasic Electric Partitioning System as a Novel Integration Process for Betacyanins Extraction From Red-Purple Pitaya and Antioxidant Properties Assessment

*Hui Yi Leong[1], Yu-Kaung Chang[2], Chien Wei Ooi[3], Chung Lim Law[4], Advina Lizah Julkifle[5] and Pau Loke Show[1]**

[1] Bioseparation Research Group, Department of Chemical and Environmental Engineering, Faculty of Science and Engineering, University of Nottingham Malaysia, Semenyih, Malaysia, [2] Department of Chemical Engineering, Graduate School of Biochemical Engineering, Ming Chi University of Technology, Taipei, Taiwan, [3] Chemical Engineering Discipline, School of Engineering, Monash University Malaysia, Bandar Sunway, Malaysia, [4] Department of Chemical and Environmental Engineering, Faculty of Science and Engineering, University of Nottingham Malaysia, Semenyih, Malaysia, [5] Crops For the Future, Semenyih, Malaysia

OPEN ACCESS

**Edited by:**
John Paul Frampton,
Dalhousie University, Canada

**Reviewed by:**
Papa Niokhor Diouf,
Service de Recherche et d'EXpertise en Transformation des Produits Forestiers, Canada
Nguyen Thi Dong Phuong,
Da Nang University of Technology, Vietnam

***Correspondence:**
Pau Loke Show
showpauloke@gmail.com;
pauloke.show@nottingham.edu.my

**Specialty section:**
This article was submitted to Chemical Engineering, a section of the journal Frontiers in Chemistry

**Received:** 30 May 2018
**Accepted:** 15 March 2019
**Published:** 03 April 2019

**Citation:**
Leong HY, Chang Y-K, Ooi CW, Law CL, Julkifle AL and Show PL (2019) Liquid Biphasic Electric Partitioning System as a Novel Integration Process for Betacyanins Extraction From Red-Purple Pitaya and Antioxidant Properties Assessment. Front. Chem. 7:201. doi: 10.3389/fchem.2019.00201

Nowadays, downstream bioprocessing industries inclines towards the development of a green and high efficient bioseparation technology. Betacyanins are presently gaining higher interest in the food science as driven by their high tinctorial strength and health promoting functional properties. In this study, a novel green integration process of liquid biphasic electric partitioning system (LBEPS) was proposed for betacyanins extraction from peel and flesh of red-purple pitaya. Initially, the betacyanins extraction using LBEPS with initial settings was compared with that of liquid biphasic partitioning system (LBPS), and the results revealed that both systems demonstrated a comparable betacyanins extraction. This was followed by further optimizing the LBEPS for better betacyanins extraction. Several operating parameters including operation time, voltage applied, and position of graphitic electrodes in the system were investigated. Moreover, comparison between optimized LBEPS and LBPS with optimized conditions of electric system (as post-treatment) as well as color characterization and antioxidant properties assessment were conducted. Overall, the betacyanins extraction employing the optimized LBEPS showed the significant highest values of betacyanins concentration in alcohol-rich top phase ($C_t$) and partition coefficient (K) of betacyanins from peel (99.256 ± 0.014% and 133.433 ± 2.566) and flesh (97.189 ± 0.172% and 34.665 ± 2.253) of red-purple pitaya. These results inferred that an optimal betacyanins extraction was successfully achieved by this approach. Also, the LBEPS with the peel and flesh showed phase volume ratio ($V_r$) values of 1.667 and 2.167, respectively, and this indicated that they have a clear biphasic separation. In addition, the peel and flesh extract obtained

from the optimized LBEPS demonstrated different variations of red color as well as their antioxidant properties were well-retained. This article introduces a new, reliable, and effective bioseparation approach for the extraction of biomolecules, which is definitely worth to explore further as a bioseparation tool in the downstream bioprocessing.

**Keywords: antioxidant, betacyanins, electric system, integration process, liquid biphasic partitioning system, red-purple pitaya**

## INTRODUCTION

Lately, betacyanins are of growing interest in the applications of food processing, such as foods, nutraceuticals, and pharmaceuticals, owing to their versatile properties including attractive visual attributes, pigments stability between pH 3 and 7, natural coloring feature (E-162), powerful antioxidant and health promoting functional properties (Ciriminna et al., 2018; Leong et al., 2018c). The most common and simplest structure of betacyanin found in plants is betanin, also known as betanidin-5-O-β-glucoside. Betacyanins are red-violet pigments which is an important constituent of betalains. Betalains are water-soluble nitrogen-containing natural pigments that have presently received attention as a source of natural colorant (Aberoumand, 2011; Carocho et al., 2015). The pigments contain a chromophore of betalamic acid, in which its conjugation with *cyclo*-3,4-dihydroxyphenylalanine can produce the red-violet betacyanins, whereas yellow-orange betaxanthins can be synthesized through the conjugation of betalamic acid with different amino acids or amines. As compared to betaxanthins, betacyanins are known to be more stable in terms of their structural aspects (Azeredo, 2009). One of the rich sources of betacyanins is red-purple pitaya (*Hylocereus polyrhizus*), in addition to red beetroot and other Caryophyllales. Red-purple pitaya is a type of *Hylocereus* species which belongs to the family of Cactaceae. It is a red-skinned fruit with red-purple flesh and black seeds. Additionally, red-purple pitaya is high in nutritional contents and is a promising source of betacyanins, and hence, it possesses positive effects on health (Stintzing and Carle, 2007; Moreno et al., 2008; Dembitsky et al., 2011; Esatbeyoglu et al., 2015; Khan and Giridhar, 2015; Ciriminna et al., 2018).

Extraction of betalains from various plant sources normally utilizes conventional solid-liquid extraction approaches, such as maceration and Soxhlet extraction (Castellar et al., 2003; Chong et al., 2014; Ramli et al., 2014; Celli and Brooks, 2017). These extraction procedures are reported to have limitations, for example, inefficiency, time-, energy-, and cost-consuming, lower yields production as well as not eco-friendly (Wang and Weller, 2006; Dai and Mumper, 2010; Azmir et al., 2013; Ciriminna et al., 2018). Development of a green, reliable, economically effective, and high efficient bioseparation technology is now a rapidly growing field in biotechnology industries including downstream bioprocessing industries (Tang and Zhao, 2009; Chemat et al., 2017; Sankaran et al., 2018). To address this need, non-conventional innovative extraction techniques for the betalains extraction have been recently developed. Indeed, several green extraction techniques, such as ultrasound (Ramli et al., 2014; Laqui-Vilca et al., 2018), microwave (Bastos and Gonçalves, 2017), pulsed electric field (Fincan et al., 2004), and high pressure $CO_2$ (Ciriminna et al., 2018) have been applied along with conventional extraction methods for the betalains extraction, and a better extraction efficiency of betalains at a reduced extraction time were reported (Celli and Brooks, 2017; Xu et al., 2017). Other than that, application of a liquid biphasic system, such as aqueous two-phase system (ATPS) (Chethana et al., 2007; Chandrasekhar et al., 2015; Santos et al., 2018) and liquid biphasic flotation (LBF) system (Leong et al., 2018a) for the separation, purification, and concentration of betalains from plants have been studied. The liquid biphasic system is well-known as an easy, scalable, time-, cost-, and energy-saving, effective as well as mild and green separation approach for many biotechnological products (Show et al., 2013; Yau et al., 2015) (Zimmermann et al., 2017).

Taking the above into account, in the present study, an integration process of liquid biphasic partitioning and electric system, namely liquid biphasic electric partitioning system (LBEPS) was proposed for betacyanins extraction from red-purple pitaya. In this study, both peel and flesh of red-purple pitaya were fully utilized for their betacyanins extractions. Liquid biphasic partitioning system (LBPS) is a new and green liquid biphasic system for separation of biomolecules as well as possesses the gifted advantages of the current liquid biphasic system. The LBPS was integrated with electricity treatment (electric system) in this study as to further enhance the LBPS for improving biomolecules separation. Electricity treatment is a non-thermal processing approach that ameliorates extraction efficiency of biomolecules. The betacyanins extraction using LBEPS was first compared with that of LBPS, and then followed by optimization study on the LBEPS for the betacyanins extraction. In addition, comparison between optimized LBEPS and LBPS with optimized conditions of electric system (as post-treatment) as well as color characterization and antioxidant properties assessment were carried out. To the best of our knowledge, this is the first article reporting the betacyanins extraction process by employing LBEPS. It is worth noting that the LBEPS is a novel green integration process, and it is also of significance that the separation of biomolecules was performed for the first time using LBEPS.

## MATERIALS AND METHODS

### Materials

Red-purple pitaya was purchased from a local fruit stall in Semenyih, Selangor Darul Ehsan, Malaysia. Ultrapure water produced from Milli-Q integral water purification system

(Merck, Darmstadt, Germany) was used throughout this experiment. Graphitic electrodes which were modified from 2B pencil leads (diameter: 2 mm) were acquired from My Family Art & Stationery (Semenyih, Selangor Darul Ehsan, Malaysia). Absolute ethanol, dipotassium hydrogen phosphate ($K_2HPO_4$), sodium chloride (NaCl), sodium bicarbonate ($NaHCO_3$), iron (III) chloride hexahydrate ($FeCl_3{\cdot}6H_2O$), and iron (II) sulfate heptahydrate ($FeSO_4{\cdot}7H_2O$) were purchased from R&M Chemicals (Selangor Darul Ehsan, Malaysia). Acetic acid ($CH_3COOH$) and sodium acetate trihydrate ($C_2H_3NaO_2{\cdot}3H_2O$) were obtained from Merck (Darmstadt, Germany). Hydrochloric acid (HCl) was purchased from Fisher Scientific (Selangor Darul Ehsan, Malaysia). 2,4,6-tripyridyl-s-triazine (TPTZ), 2,2′-azino-bis(3-ethylbenzothiazoline-6-sulfonic acid) diammonium salt (ABTS), potassium persulfate ($K_2O_8S_2$), 6-hydroxy-2,5,7,8-tetramethychroman-2-carboxylic acid (Trolox), Folin-Ciocalteu (F-C) reagent and gallic acid were acquired from Sigma-Aldrich (St. Louis, MO, USA). All the above mentioned chemicals were of analytical grade (purity > 95%).

## Apparatus

A regulated dual direct current (DC) power supply (ATTEN APS3003S-3D, 30 V/3 $A^{*2}$) (Mobicon-Remote Electronic, Petaling Jaya, Selangor Darul Ehsan, Malaysia) was used to supply electricity in this experiment (i.e., electric system), and was kindly provided by the Department of Electrical and Electronic Engineering, University of Nottingham Malaysia.

## Preparation of Crude Extract

The preparation of crude extract was conducted in dim light condition in order to minimize its pigment losses. The peel and flesh of red-purple pitaya were firstly cut into thin pieces after washed and dried with tissue towel, subsequently, they were stored at −80°C for 48 h. To prepare dried crude extract (DE), the sample was freeze dried at −30°C and 0.37 atm for 48 h using a freeze dryer (CHRIST Alpha 1-2 LDplus, Germany). After that, the freeze-dried crude extract was ground into powder using a grinder (Tefal Blendforce, Triple'Ax Technology 400 Watt, Malaysia). The DE of the peel and flesh of red-purple pitaya were stored at −20°C for further use.

## Betacyanins Extraction Using LBEPS

The LBEPS was created by equipping two graphitic electrodes into the LBPS. The electrodes (anode and cathode; former to apply voltage and latter to detect current flow) were connected to a regulated dual DC power supply in order to supply electricity continuously (**Figure 1**). A 10 g LBPS with optimized conditions (Leong et al., 2018b) was further incorporated with electric system (i.e., LBEPS). The operating parameters of the 10 g LBEPS including operation time, voltage apply, and position of graphitic electrodes were optimized using one-factor-at-a-time (OFAT) approach for the betacyanins extraction from peel and flesh of red-purple pitaya. The initial settings of the LBEPS were 15 min of operation time, 3 V of voltage applied and graphitic electrodes positioned at bottom phase (**Table 1**). The experiment was conducted at room temperature (25 ± 1°C).

### Comparison Between LBPS and LBEPS

A 10 g LBPS was prepared in a 15 mL graduated centrifugal tube by mixing phase-forming components and DE in accordance with their respective compositions (%, w/w), as shown in **Table 1**. After thorough mixing of all the components by gentle agitation, the mixture was centrifuged at 3,000 rpm for 20 min to induce a phase separation. On the other hand, in the 10 g LBEPS, a biphasic system was firstly formed; the phase-forming components were mixed well and centrifuged at 3,000 rpm for 5 min, subsequently, 1% of DE was added to the biphasic system and gently mixed. After that, the mixture was supplied with electricity, as mentioned in section Betacyanins Extraction using LBEPS (i.e., LBEPS with initial settings). The Volumes of the top and bottom phase in LBPS and LBEPS were then measured, followed by the collection of sample from both phases for analysis of total betacyanins content (TBC).

## Comparison Between Optimized LBEPS and LBPS With Optimized Conditions of Electric System as Post-treatment

A 10 g LBPS was firstly prepared, as mentioned in section Comparison Between LBPS and LBEPS, subsequently, the optimized conditions of the electric system (operation time, voltage applied, and position of graphitic electrodes in the LBEPS) were used in further treatment of the mixture (i.e., post-treatment). The results obtained were compared with optimized LBEPS.

## Analytical Procedures

### Color Characterization

Lightness ($L^*$), redness ($a^*$), and yellowness ($b^*$) of the peel and flesh extract of red-purple pitaya were analyzed using a colorimeter (Lovibond LC 100, model RM 200; The Tintometer Ltd., United Kingdom). Additionally, their hue angle (h°) and chroma ($C^*$) were calculated according to Equations (1, 2), respectively.

$$h^\circ = \tan^{-1}\frac{b^*}{a^*} \quad (1)$$

$$C^* = \sqrt{a^{*2} + b^{*2}} \quad (2)$$

### Analysis of Total Betacyanins Content (TBC)

The TBC in the crude extract was analyzed using a UV-vis spectrophotometer (UV-1,800; Shimadzu Corporation, Japan) at 538 nm. The TBC was expressed as mg of betanin equivalents (BEs) per 100 g of crude extract, and was calculated according to Equation (3) (Ramli et al., 2014; Leong et al., 2018a,b):

$$\text{TBC} = \frac{A_{538} \times \text{MW} \times \text{V} \times \text{DF}}{\varepsilon \times \text{L} \times \text{W}} \times 100 \quad (3)$$

Where $A_{538}$ = absorbance value at 538 nm, MW = molecular weight of betanin (550 g.mol$^{-1}$), V = volume of sample (mL), DF = dilution factor, ε = molar extinction coefficient of betanin (65,000 L.mol$^{-1}$.cm$^{-1}$), L = path length of cuvette (1 cm), W = weight of crude extract (g).

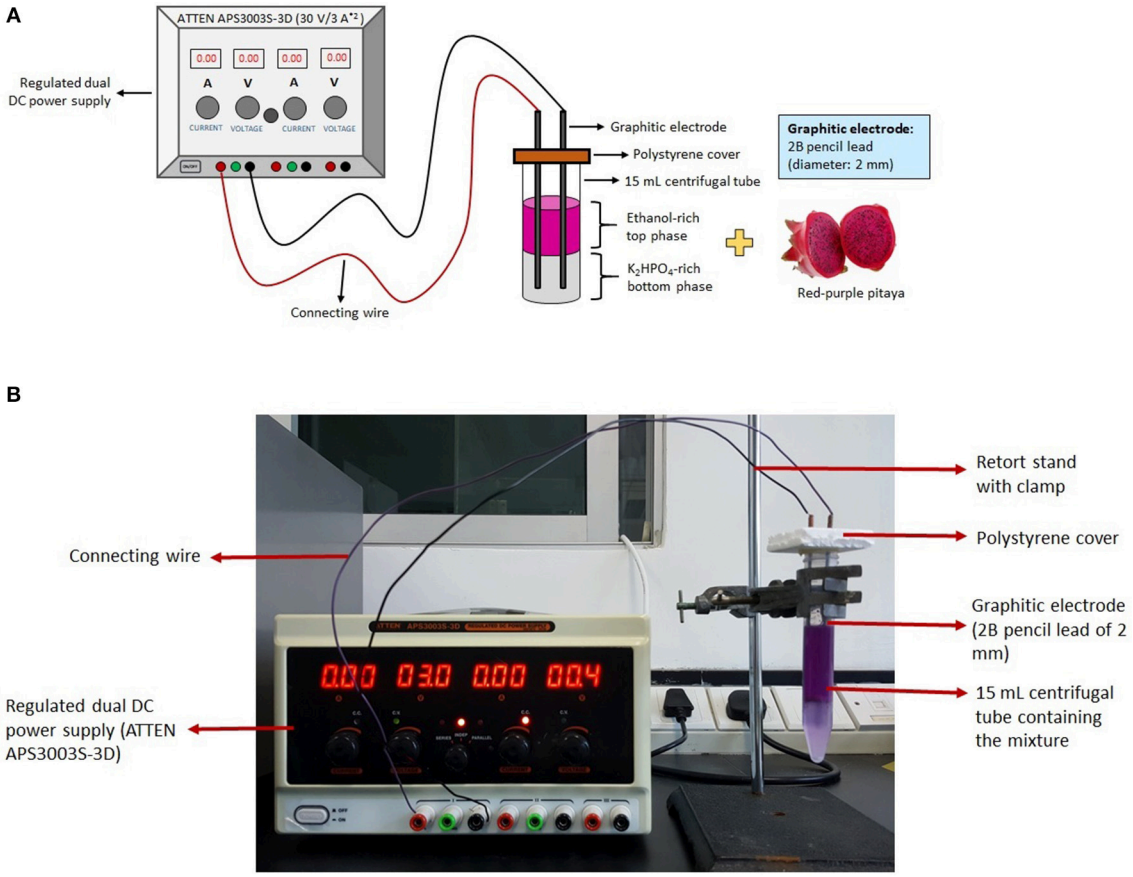


**FIGURE 1 | (A)** Schematic diagram of LBEPS for betacyanins extraction from peel and flesh of red-purple pitaya. **(B)** Experimental setup for the betacyanins extraction using LBEPS.

## Analysis of Total Phenolic Content (TPC)

The Folin-Ciocalteu (F-C) method as described in Singleton et al. (1999), Fu et al. (2011), and Hajimahmoodi et al. (2013) was employed to analyze the TPC in the crude extract. A diluted F-C reagent which consists of 10 mL of F-C reagent and 90 mL of purified water was freshly prepared. Next, 100 μL of sample or gallic acid solution (i.e., standard) was mixed with 500 μL of diluted F-C reagent. The mixture was then incubated for 5 min at room temperature under dark condition. Subsequently, 2 mL of 60 g/L of $NaHCO_3$ solution was added to the mixture. The mixture was mixed well and kept for 90 min at room temperature under dark condition. The absorbance value of the mixture was measured at 725 nm using a UV-vis spectrophotometer. The TPC was expressed as mg of gallic acid equivalents (GAEs) per 100 g of crude extract.

## Analysis of Ferric Reducing Antioxidant Power (FRAP)

The FRAP in the crude extract was analyzed using method as described in literature (Benzie and Strain, 1996; Fu et al., 2011; Leong et al., 2018a). The FRAP reagent was freshly prepared; 10 mL of 10 mmol/L TPTZ solution (0.0031 g of TPTZ in 1 mL of 40 mmol/L HCl) and 10 mL of 20 mmol/L $FeCl_3 \cdot 6H_2O$ solution (0.0054 g/mL) for every 100 mL of 300 mmol/L acetate buffer (pH 3.6; mixture of 3.1 g of $C_2H_3NaO_2 \cdot 3H_2O$ with 16 mL of $CH_3COOH$ per liter of purified water). The FRAP reagent was preheated to 37°C before use. The FRAP assessment was carried out by mixing 100 μL of sample or $FeSO_4 \cdot 7H_2O$ solution (i.e., standard), 300 μL of purified water and 3 mL of FRAP reagent. The mixture was subsequently incubated for 4 min at 37°C. The absorbance value of mixture was measured at 593 nm using a UV-vis spectrophotometer. The result was expressed as μmol of Fe(II) per g of crude extract.

## Analysis of Trolox Equivalent Antioxidant Capacity (TEAC)

The ABTS radical (ABTS·) method as described in Re et al. (1999), Fu et al. (2011) was employed to analyze the TEAC in the crude extract. The ABTS· stock solution (mixture of 7 mmol/L of ABTS solution and 2.45 mmol/L of $K_2O_8S_2$ solution at v:v ratio of 1:1) was first prepared, and was then incubated for 12–16 h at room temperature under dark condition. Next, the ABTS· stock solution was diluted with ethanol to reach an absorbance value of 0.70 ± 0.05 at 734 nm, and was incubated at 30°C. As to analyze the TEAC, 100 μL of sample or Trolox solution (i.e., standard) or ethanol (i.e., control) was mixed with 3.8 mL

**TABLE 1 |** Operating parameters of LBEPS for betacyanins extraction from peel and flesh of red-purple pitaya.

| No. | Condition | Initial setting | Variables | Unit |
|---|---|---|---|---|
| 1. | 10 g LBPS with optimized conditions (constant throughout the experiment) (%, w/w) (Leong et al., 2018b) | | | |
| | Peel | | Flesh | |
| | 1% of DE | | 1% of DE | |
| | 27% of undiluted ethanol | | 33% of undiluted ethanol | |
| | 20% of $K_2HPO_4$ solution | | 20% of $K_2HPO_4$ solution | |
| | 50% of purified water | | 44% of purified water | |
| | 2% of 0.4M NaCl | | 2% of 0.2M NaCl | |
| **ELECTRIC SYSTEM** | | | | |
| 2. | Operation time | 20 | 10, 15, 25, 30 | min |
| 3. | Voltage apply | 3 | 1, 2, 4, 5 | V |
| 4. | Position of graphitic electrodes | Bottom phase | Top and middle phase; middle position refers to the interphase between top and bottom phase | N/A |

of diluted ABTS• solution. The absorbance value of the mixture was measured at 734 nm using a UV-vis spectrophotometer after 6 min of incubation at 30°C. The result was expressed as μmol of Trolox equivalents (TEs) per g of crude extract. The percentage of scavenging on ABTS• was calculated using Equation (4) (Leong et al., 2018a):

$$\text{Percentage of scavenging (\%)} = \frac{\text{control} - \text{sample or standard}}{\text{control}} \times 100 \quad (4)$$

## Calculations

Partition coefficient (K) of betacyanins in the LBPS and LBEPS was calculated according to Equation (5) (Leong et al., 2018a,b):

$$\mathrm{K} = \frac{\mathrm{TBC_t}}{\mathrm{TBC_b}} \quad (5)$$

Where $TBC_t$ and $TBC_b$ are TBC in the alcohol-rich top phase and salt-rich bottom phase at equilibrium, respectively.

Betacyanins concentration (%) in alcohol-rich top phase ($C_t$) and salt-rich bottom phase ($C_b$) was calculated according to Equations (6, 7), respectively:

$$\mathrm{C_t(\%)} = \frac{\text{TBC in top phase}}{\text{TBC in crude extract}} \times 100 = \frac{\mathrm{TBC_t}}{\mathrm{TBC_t} + \mathrm{TBC_b}} \times 100 \quad (6)$$

$$\mathrm{C_b(\%)} = \frac{\text{TBC in bottom phase}}{\text{TBC in crude extract}} \times 100 = \frac{\mathrm{TBC_b}}{\mathrm{TBC_t} + \mathrm{TBC_b}} \times 100 \quad (7)$$

Phase volume ratio ($V_r$) is defined as ratio of the volume of alcohol-rich top phase to the volume of salt-rich bottom phase at equilibrium, and was calculated according to Equation (8).

$$\mathrm{V_r} = \frac{\mathrm{V_t}}{\mathrm{V_b}} \quad (8)$$

Where $V_t$ and $V_b$ are volume of the alcohol-rich top phase and salt-rich bottom phase at equilibrium, respectively.

## Statistical Analysis

The statistical analysis was performed using IBM SPSS statistics software (SPSS version 23.0 for window, IBM Corporation, Armonk, New York, United States). Triplicate readings were recorded and were used in the analysis, and the values were expressed as mean ± standard deviation (SD). The data were subjected to One-Way analysis of variance, and the mean differences were compared using Tukey HSD *post-hoc* multiple comparisons test. The data were considered for their statistically significant difference where $p < 0.05$. Moreover, the relationship among the antioxidant properties was analyzed using Pearson's correlation test.

# RESULTS AND DISCUSSION

## Comparison Study of Betacyanins Extraction Using LBPS and LBEPS

An initial study was conducted by comparing the betacyanins extraction from peel and flesh of red-purple pitaya using LBPS with optimized conditions (Leong et al., 2018b) and LBEPS (i.e., an integration process of LBPS and electricity treatment) with initial settings. Our findings showed that the betacyanins extraction from the peel using LBPS was slightly better than that of using LBEPS. The application of LBPS showed the significant highest values of $C_t$ (98.080 ± 0.051%) and K of betacyanins (51.097 ± 1.354) compared to that of the values obtained from LBEPS ($C_t$: 96.820 ± 0.046% and K of betacyanins: 30.450 ± 0.459). Both systems showed a similar value of $V_r$ (1.667) (**Figure 2A**). Likewise, a similar trend was observed for the betacyanins extraction from the flesh, as shown in **Figure 2B**. However, the betacyanins extraction from the flesh using LBPS showed the non-significant highest values of $C_t$ (96.256 ± 0.207%) and K of betacyanins (25.764 ± 1.525) as compared to that of the LBEPS ($C_t$: 96.010 ± 0.144% and K of betacyanins: 24.086 ± 0.911) ($p > 0.05$). Both systems also showed a similar value of $V_r$ (2.167). The similar value of $V_r$ revealed that the biphasic separation was not affected by the difference in these two extraction methods. In LBPS, centrifugation process alongside biphasic system was utilized in the betacyanins extraction, whereas electricity treatment alongside biphasic system was applied to the betacyanins extraction in LBEPS. Both approaches are different in terms of their working mechanisms. Although LBPS resulted in the slightly higher betacyanins extraction, we decided to further optimize our LBEPS for the betacyanins extraction in this study. The reasons are that both systems showed a comparable betacyanins extraction from red-purple pitaya and LBEPS seems to be promising for achieving a more efficient betacyanins extraction than LBPS due to the fact that its conditions used in this study could still be optimized.

## Effect of the Operation Time in LBEPS

The betacyanins extraction from the peel and flesh using LBEPS were further studied by optimizing the operation time (10–30 min) in the system. Other parameters of the LBEPS included 3 V of voltage applied and graphitic electrodes located at bottom phase in the system. As depicted in **Figure 3A**, an increase in the operation time from 10 to 15 min in the LBEPS greatly improved the betacyanins extraction from the peel, and further extending the operation time up to 30 min resulted in a slightly lower betacyanins extraction compared to that of with 15 min of operation time. Meanwhile, LBEPS with 15 min of operation time showed a better betacyanins extraction compared to LBPS with 20 min of operation time (control). The significant highest values of $C_t$ and K of betacyanins obtained from the LBEPS with 15 min of operation time were 99.256 ± 0.014% and 133.433 ± 2.566, respectively, among the others. The control and LBEPS with different operation times showed a similar $V_r$ value of 1.667, and this inferred that their biphasic separation was not affected by

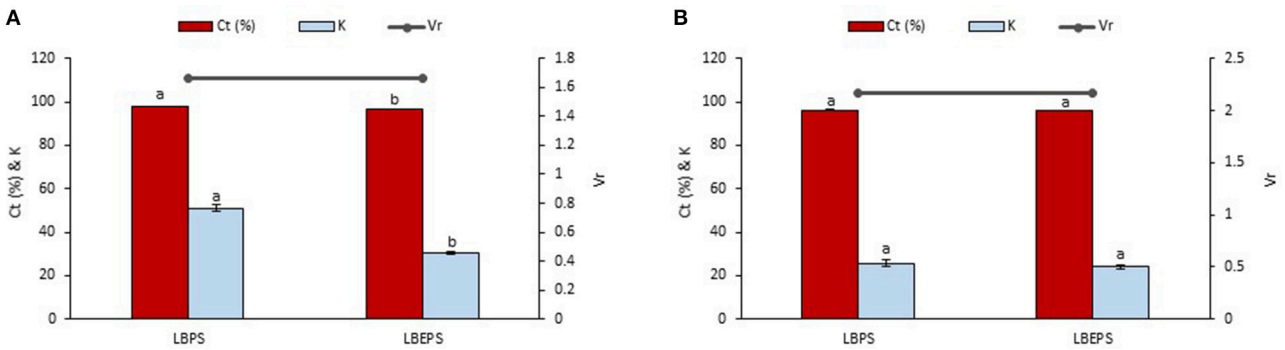


**FIGURE 2 |** Comparison study of betacyanins extraction from **(A)** peel and **(B)** flesh of red-purple pitaya using LBPS and LBEPS with initial settings. Values are mean ± SD of triplicate readings. Different letter(s) represent a significant difference ($p < 0.05$) using Tukey's test within $C_t$ and K.

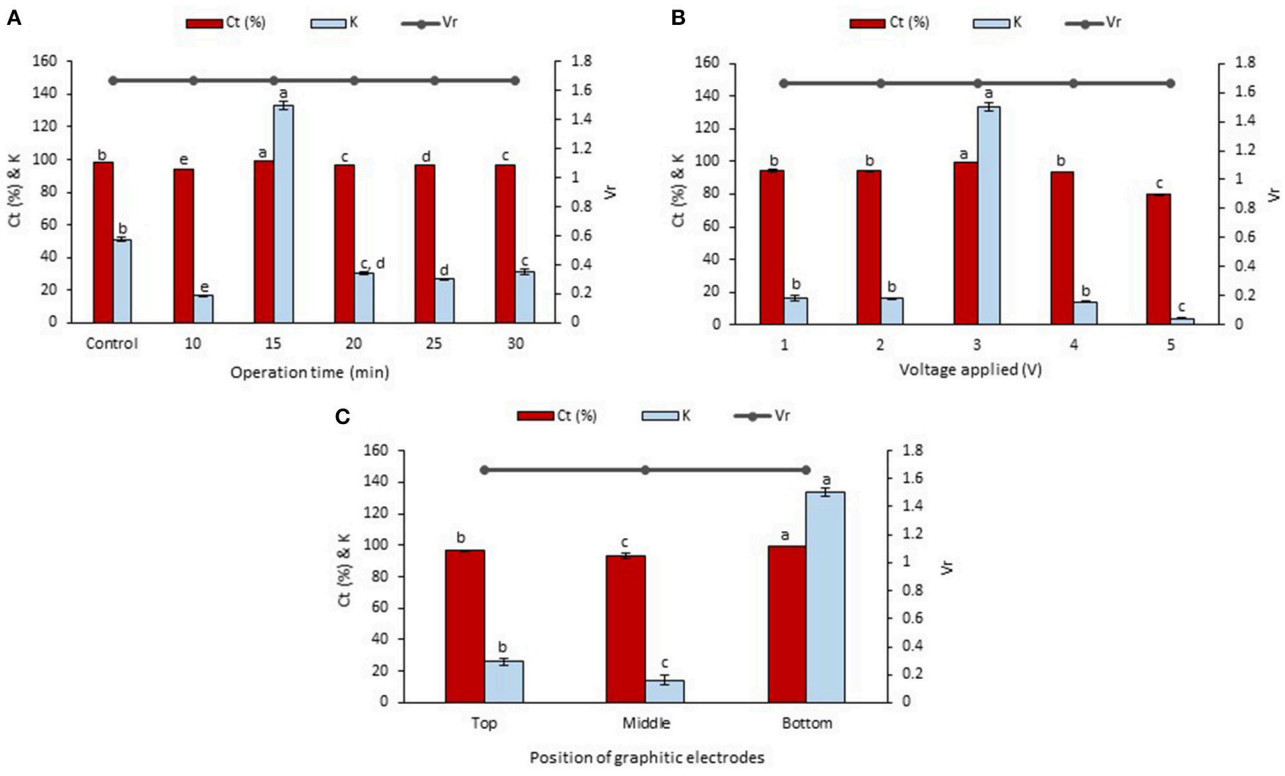


**FIGURE 3 |** Effects of various parameters in LBEPS for betacyanins extraction from peel of red-purple pitaya; OFAT approach was applied in the optimization study: **(A)** operation time (control: LBPS), **(B)** voltage applied and **(C)** position of graphitic electrodes. Values are mean ± SD of triplicate readings. Different letter(s) represent a significant difference ($p < 0.05$) using Tukey's test within $C_t$ and K.

the different extraction methods (as mentioned earlier in section Comparison Study of Betacyanins Extraction Using LBPS and LBEPS). Also, a similar trend was noted for the betacyanins extraction from the flesh, as shown in **Figure 4A**. The significant highest values of $C_t$ and K of betacyanins obtained from the LBEPS with 15 min of operation time were 97.189 ± 0.172% and 34.665 ± 2.253, respectively, among the others. The control and LBEPS with different operation times also showed a similar $V_r$ value (2.167).

Collectively, a higher betacyanins extraction from the peel and flesh was achieved through the use of LBEPS with 15 min of operation time compared to that of with LBPS with 20 min of operation time as well as to that of with LBEPS with other operation times. Application of LBEPS can shorten the extraction time from 20 to 15 min; compared to control (i.e., LBPS). The possible reason might be due to the different working extraction mechanisms between LBPS and LBEPS, as mentioned earlier in section Comparison Study of Betacyanins Extraction Using LBPS and LBEPS. The LBEPS uses electricity treatment alongside biphasic system for the betacyanins extraction, while LBPS employs centrifugation process alongside biphasic system for the betacyanins extraction. The electricity treatment occurred between the two graphitic electrodes is suggested to enhance the betacyanins extraction and cause a higher extraction efficiency compared to the centrifugation process. Other than that, as compared among the 10–30 min of operation time of LBEPS, 15 min of the operation time was noted to be the most effective extraction time. This could be explained by the mass transfer energy of the system reaching equilibrium and the maximum at 15 min. Moreover, a longer extraction time can cause oxidation of betacyanins due to their highly sensitive features (Esatbeyoglu et al., 2015; Khan, 2016; Celli and Brooks, 2017; Ciriminna et al., 2018; Leong et al., 2018a). Hence, 15 min of operation time was chosen for the betacyanins extraction using LBEPS.

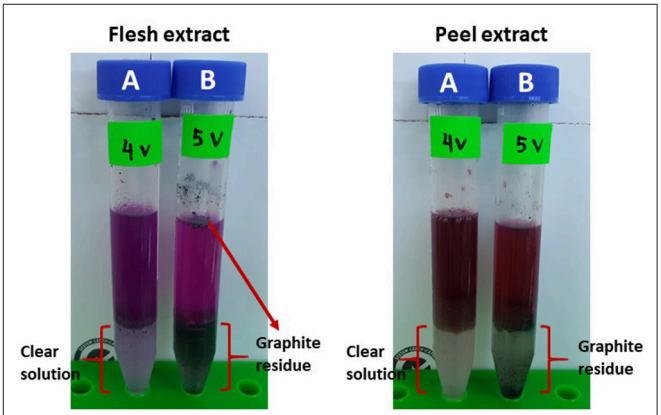


**FIGURE 5 |** Effect of different voltages applied in LBEPS; comparison between **(A)** 4 V and **(B)** 5 V of voltage applied for the peel and flesh extract.

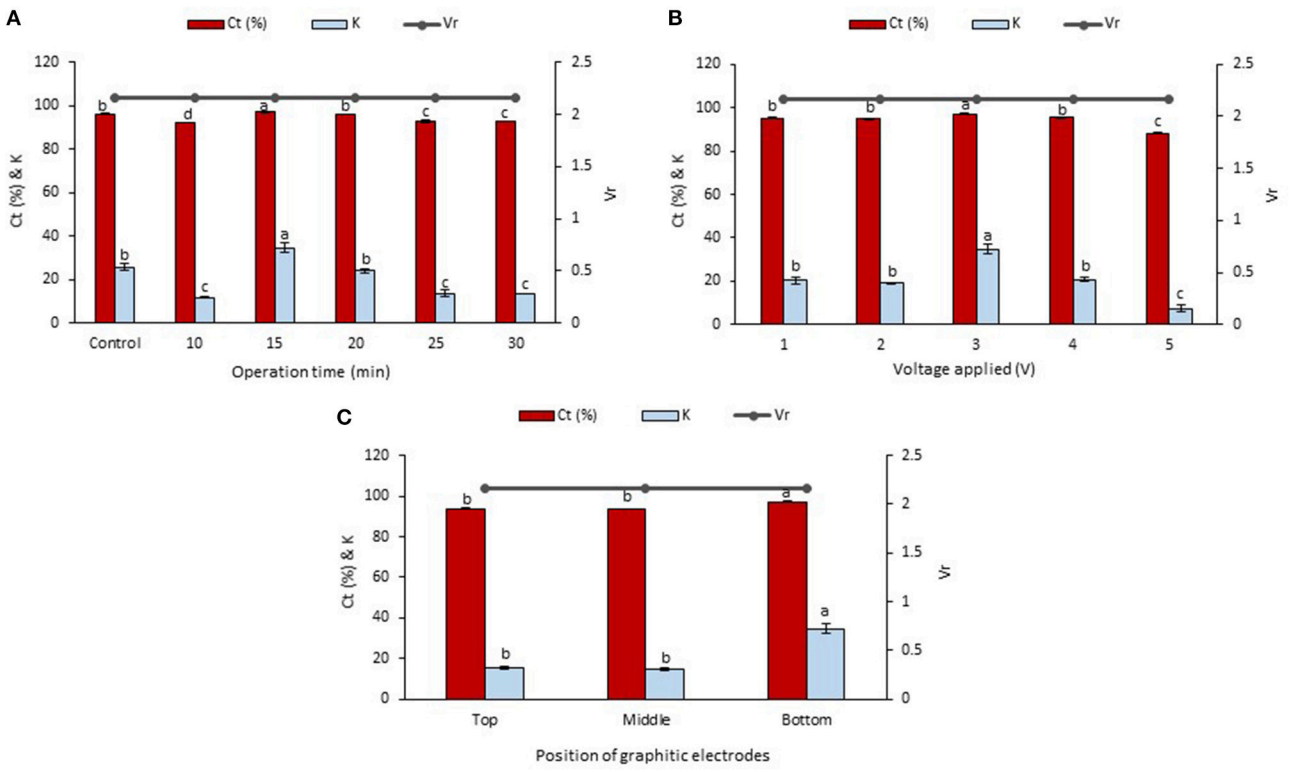


**FIGURE 4 |** Effects of various parameters in LBEPS for betacyanins extraction from flesh of red-purple pitaya; OFAT approach was applied in the optimization study: **(A)** operation time (control: LBPS), **(B)** voltage applied and **(C)** position of graphitic electrodes. Values are mean ± SD of triplicate readings. Different letter(s) represent a significant difference ($p < 0.05$) using Tukey's test within $C_t$ and K.

## Effect of the Voltage Applied in LBEPS

Effect of the voltages applied ranging from 1 to 5 V in the LBEPS for betacyanins extraction from peel and flesh of red-purple pitaya was investigated, and the results are presented in **Figures 3B**, **4B**, respectively. The betacyanins extraction using LBEPS with 3 V of voltage applied showed the significant highest values of $C_t$ and K of betacyanins from the peel (99.256 ± 0.014% and 133.433 ± 2.566, respectively) and flesh (97.189 ± 0.172% and 34.665 ± 2.253, respectively). Meanwhile, the values of $C_t$ and K of betacyanins from the peel and flesh obtained from the betacyanins extraction using LBEPS with 1, 2, and 4 V of voltage applied were noted to be no significant difference among them ($p > 0.05$). However, the betacyanins extraction using LBEPS with 5 V of voltage applied showed the significant lowest values of $C_t$ and K of betacyanins from the peel (79.737 ± 0.419% and 3.937 ± 0.101, respectively) and flesh (88.231 ± 0.162% and 7.498 ± 0.116, respectively). Additionally, with the 5 V of voltage applied, the graphitic electrodes were oxidized and graphite residue was observed in the salt-rich bottom phase, as shown in **Figure 5**. Furthermore, $V_r$ values in the LBEPS with different voltages applied for the peel and flesh showed that different voltages do not influence the biphasic separation much, due to their similar values among the others; LBEPS with peel: 1.667 and LBEPS with flesh: 2.167.

Our results inferred that LBEPS with 3 V of voltage applied achieved an optimal betacyanins extraction from the peel and flesh as shown by their significant highest values of $C_t$ and K of betacyanins. The electricity treatment supplied by the 3 V of voltage applied in the system is proved to have the highest electropermeabilization of red-purple pitaya membrane structure, in which the cell membrane structure was disrupted by short and intense electric pulses, and the increased cell membrane permeability led to the release of more betacyanins from red-purple pitaya to the extractive solvent in the system. This eventually increase the extraction efficiency of betacyanins. The betacyanins adhered to the electrodes and moved along from bottom to top phase of the system via electricity treatment. This electricity treatment is known as a non-thermal process where an external electricity is supplied to a substrate. Additionally, the effectiveness of the electricity treatment strongly depends on the electrical field strength, specific energy input, treatment duration, substance to be treated etc. (Azmir et al., 2013; Boussetta and Vorobiev, 2014; Celli and Brooks, 2017; Chemat et al., 2017; Xu et al., 2017). A study conducted by Roselló-Soto et al. (2015) reported that high voltage electrical discharges was the most effective pretreatment for the extraction of olive kernels among the other pretreatments of pulsed electric field and ultrasound, due to its highest extraction efficiency. This result was explained by the occurrence of propagation of the shock waves and explosion of cavitation bubbles during the pretreatment of olive kernel induced by the application of electrical discharges.

Moreover, in the present study, oxidation of the graphitic electrodes was observed when 5 V of voltage was applied in the LBEPS. In the same instance, this system showed the lowest betacyanins extraction from the peel and flesh. This could be explained by the fact that 10 g LBEPS cannot withstand the strong electricity treatment induced by the 5 V of voltage applied in the system. Also, the lowest betacyanins extraction might be caused by the presence of graphite residue due to oxidation of the graphitic electrodes, in which they degrade the betacyanins since betacyanins are highly sensitive pigments.

**TABLE 2 |** Color characterization of peel and flesh extract of red-purple pitaya obtained from the optimized LBEPS.

| Color parameter | Peel extract | Flesh extract |
|---|---|---|
| L* | 7.933 ± 0.306 | 11.033 ± 0.208 |
| a* | 23.633 ± 0.651 | 36.100 ± 0.529 |
| b* | 4.567 ± 0.306 | −17.167 ± 0.153 |
| C* | 24.067 ± 0.651 | 39.967 ± 0.569 |
| h° | 10.933 ± 0.666 | 334.533 ± 0.153 |

*$L^*$, $a^*$, $b^*$, $C^*$, and h° represent lightness, redness, yellowness, chroma, and hue angle, respectively. Values are mean ± SD of triplicate readings.*

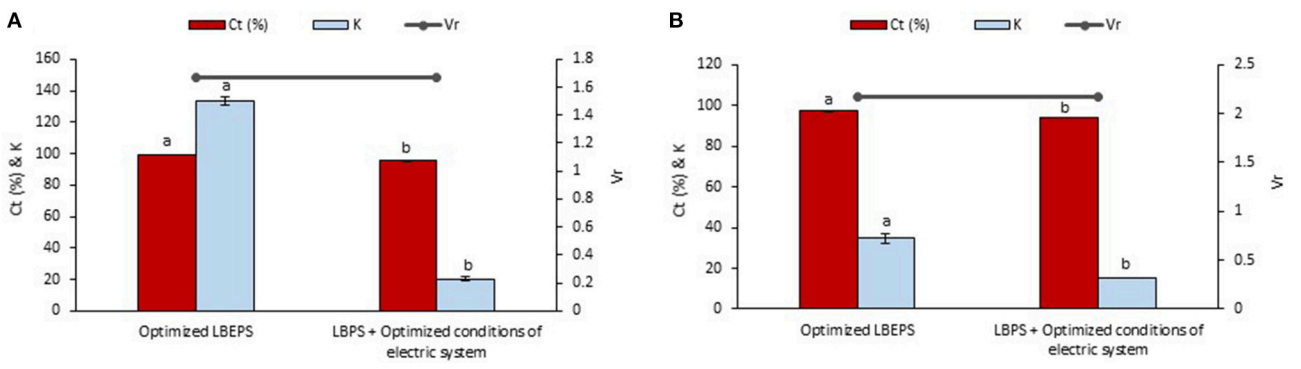


**FIGURE 6 |** Comparison study of betacyanins extraction from **(A)** peel and **(B)** flesh of red-purple pitaya using the optimized LBEPS and LBPS with the optimized conditions of electric system (as post-treatment). Values are mean ± SD of triplicate readings. Different letter(s) represent a significant difference ($p < 0.05$) using Tukey's test within $C_t$ and K.

## Effect of the Position of Graphitic Electrodes in LBEPS

Subsequently, the LBEPS with 15 min of operation time and 3 V of voltage applied for the betacyanins extraction was further assessed using different positions of graphitic electrodes in the system; the electrodes were positioned at top, middle and bottom phase in the LBEPS. Our results revealed that the electrodes located at the bottom phase in LBEPS augmented the betacyanins extraction, with the significant highest values of $C_t$ and K of betacyanins from the peel (99.256 ± 0.014% and 133.433 ± 2.566, respectively; **Figure 3C**) and flesh (97.189 ± 0.172% and 34.665 ± 2.253, respectively; **Figure 4C**). The top and middle position of the graphitic electrodes seemed to provide a slightly lower betacyanins extraction, owing to their smaller values of $C_t$ and K of betacyanins. The possible explanation could be, in the bottom position, the electrodes have the maximum electrical field influence that allows betacyanins to move along from bottom to top phase. $V_r$ values for the LBEPS in this case with the peel and flesh inferred that different positions of electrodes in the system do not have a significant impact on the biphasic separation, due to their similar values among the others; LBEPS with peel: 1.667 and LBEPS with flesh: 2.167.

## Comparison Study of Betacyanins Extraction Using Optimized LBEPS and LBPS With Optimized Conditions of Electric System as Post-treatment

Optimized conditions of electric system in the LBEPS included 15 min of operation time, 3 V of voltage applied and the electrodes located at bottom phase. The optimized LBEPS augmented the betacyanins extraction from peel and flesh of red-purple pitaya. As a result, these optimized conditions were incorporated to the LBPS as post-treatment for the betacyanins extraction, and the results obtained were compared with that of the optimized LBEPS (**Figure 6**). Our findings showed that the optimized LBEPS owned a better betacyanins extraction from the peel and flesh compared to that of using LBPS with the electric system as post-treatment ($C_t$ and K of betacyanins from the peel were 95.296 ± 0.309% and 20.323 ± 1.431, respectively, as well as from the flesh were 93.825 ± 0.012% and 15.195 ± 0.032, respectively). The reason for the results obtained could be that the LBPS with electric system as post-treatment requires longer extraction time (i.e., 35 min) that might cause oxidation of betacyanins to occur. This eventually might reduce the betacyanins extraction. On the other hand, the $V_r$ values are similar for both approaches. Therefore, an optimized LBEPS with 15 min of operation time, 3 V of voltage applied and the electrodes located at bottom phase was chosen for the betacyanins extraction from the peel and flesh of red-purple pitaya.

## Color Characterization

After the most effective extraction approach for the betacyanins extraction was determined, the color characterization of the extract was analyzed further. In this case, peel and flesh extract of red-purple pitaya (ethanol-rich top phase) used in the analysis were obtained from the optimized LBEPS. Both extracts are presented in different hues, lightness, saturations and intensities of color. They showed different degrees of lightness ($L^*$), redness ($a^*$), yellowness ($b^*$), chroma ($C^*$), and hue angle ($h^\circ$), as

**TABLE 3 |** Correlation study among the antioxidant properties, given correlation coefficient (*r*).

| | TEAC | TPC | TBC |
|---|---|---|---|
| FRAP | −0.997** | 0.853* | 0.899* |
| TEAC | – | −0.811 | −0.902* |
| TPC | – | – | 0.788 |

***Correlation is significant at $p < 0.01$ (2-tailed). *Correlation is significant at $p < 0.05$ (2-tailed).*

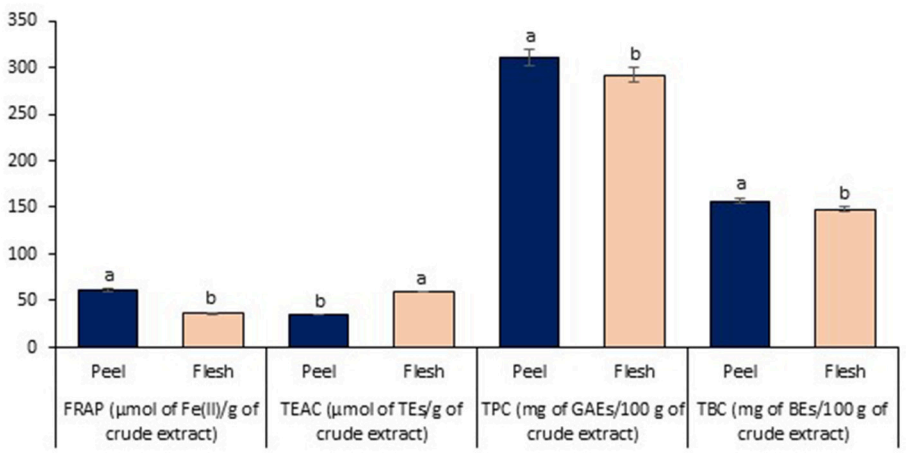


**FIGURE 7 |** Antioxidant properties assessment of peel and flesh extract of red-purple pitaya obtained from the optimized LBEPS. Values are mean ± SD of triplicate readings. Different letter(s) represent a significant difference ($p < 0.05$) using Tukey's test within FRAP, TEAC, TPC, and TBC.

presented in **Table 2**. The peel extract showed a higher degree of a* and b* as well as a smaller degree of L*, C* and h° compared to that of the flesh extract. Our results revealed that the peel and flesh extract showed different ranges of red color. The peel extract showed a red-yellowish color (positive a* and b*), whereas the flesh extract showed a red-bluish/purplish color (positive a* and negative b*). The C* and h° measure the basic tint and saturation of a color, respectively (Lancaster and Lister, 1997). Owing to their natural coloring attribute, the peel and flesh extract can be applied as natural colorants with different variations of red color.

### Antioxidant Properties Assessment

Lastly, the antioxidant properties on peel and flesh extract of red-purple pitaya (ethanol-rich top phase) were assessed in order to examine their antioxidant capability and the presence of antioxidant compound. These extracts were obtained from the optimized LBEPS. Particularly, FRAP and TEAC are used to measure the antioxidant capability, while TPC and TBC determined the quantity of antioxidant compound (Dai and Mumper, 2010). In the FRAP assessment, the peel extract (61.767 ± 1.460 μmol of Fe(II)/g of crude extract) showed a significant higher FRAP value compared to that of the flesh extract (35.916 ± 0.489 μmol of Fe(II)/g of crude extract) (standard equation: $A_{593} = 0.0006([FeSO_4{\cdot}7H_2O]) + 0.0708$ ($R^2 = 0.9984$); $A_{593}$: absorbance value at 593 nm & $[FeSO_4{\cdot}7H_2O]$: concentration of $FeSO_4{\cdot}7H_2O$). On the other hand, the peel extract (35.460 ± 0.443 μmol of TEs/g of crude extract) showed a significant lower TEAC value compared to that of the flesh extract (59.606 ± 0.857 μmol of TEs/g of crude extract) [standard equation: Percentage of scavenging (%) = 0.0966([Trolox]) + 2.8333 ($R^2 = 0.9946$)]. Other than that, in the TPC and TBC assessment, the peel extract showed the significant higher values of TPC (310.741 ± 8.486 mg of GAEs/100 g of crude extract) and TBC (156.877 ± 2.655 mg of BEs/100 g of crude extract) compared to that of the flesh extract (TPC: 292.019 ± 7.517 mg of GAEs/100 g of crude extract, TBC: 147.840 ± 3.038 mg of BEs/100 g of crude extract); standard equation for TPC: $A_{725} = 0.0036([\text{gallic acid}]) + 0.0086$ ($R^2 = 0.9995$) (**Figure 7**). Our results concluded that electricity treatment did not reduce the antioxidant properties from the red-purple pitaya, but in fact it enhanced them as the antioxidant values obtained in this study are much higher compared to the previously reported studies (Fu et al., 2011; Ramli et al., 2014). Moreover, our Pearson's correlation study conveyed that the FRAP with TEAC, TPC, and TBC were correlated among them with a significant strong positive relationship. TEAC showed a non-significant strong negative with TPC ($p > 0.05$), whereas a significant strong negative relationship between TEAC and TBC was noted. TPC and TBC demonstrated a non-significant strong positive relationship (**Table 3**).

## CONCLUSIONS

This study concludes that a satisfactory betacyanins extraction from the peel and flesh of red-purple pitaya was successfully achieved with the utilization of the optimized LBEPS. In the system, electricity treatment greatly improves extraction of biomolecules like betacyanins. In addition, the peel and flesh extract showed different variations of red color, and they are proved to demonstrate appreciable antioxidant properties. Overall, this article introduces a new, easy and effective green bioseparation technology for the biomolecules separation which could be applied in the downstream bioprocessing industries. For instance, a pilot-scale LBEPS on the biomolecules separation could be investigated, owing to its high potential to serve as an effective bioseparation technology.

## AUTHOR CONTRIBUTIONS

HL performed the experiment and data analysis as well as wrote the manuscript. Y-KC and CO revised the manuscript. CL, AJ, and PS conceived and designed the experiment.

## FUNDING

This research was financially supported by Crops For the Future (CFF) and University of Nottingham Malaysia Campus (UNMC) through the CFF-UNMC Doctoral Training Partnership (DTP) Scholarship Scheme; Fundamental Research Grant Scheme (Malaysia, FRGS/1/2015/SG05/UNIM/03/1; FP005-2013B); Ministry of Science, Technology and Innovation (Malaysia, MOSTI-02-02-12-SF0256); Prototype Research Grant Scheme (Malaysia, PRGS/2/2015/SG05/UNIM/03/1); Overseas Researcher under Fellowship of Japan Society for the Promotion of Science.

## ACKNOWLEDGMENTS

The authors gratefully acknowledge all the funding units. Additionally, the authors would like to appreciate and special thanks to Mr. Noor Hashimi Mohamad Nor (i.e., laboratory officer from Department of Electrical and Electronic Engineering, University of Nottingham Malaysia) as to provide the regulated dual DC power supply and guidance during this research.

## REFERENCES

Aberoumand, A. (2011). A review article on edible pigments properties and sources as natural biocolorants in foodstuff and food industry. *World J. Dairy Food Sci.* 6, 71–78.

Azeredo, H. M. C. (2009). Betalains: properties, sources, applications, and stability – a review. *Int. J. Food Sci. Technol.* 44, 2365–2376. doi: 10.1111/j.1365-2621.2007.01668.x

Azmir, J., Zaidul, I. S. M., Rahman, M. M., Sharif, K. M., Mohamed, A., Sahena, F., et al. (2013). Techniques for extraction of bioactive compounds from plant materials: a review. *J. Food Eng.* 117, 426–436. doi: 10.1016/j.jfoodeng.2013.01.014

Bastos, E. L., and Gonçalves, L. C. P. (2017). "Chapter 9 - Microwave-assisted extraction of betalains," in *Water Extraction of Bioactive Compounds*, eds H. D. González and M. J. G. Muñoz (Oxford, UK: Elsevier), 245–268. doi: 10.1016/B978-0-12-809380-1.00009-7

Benzie, I. F. F., and Strain, J. J. (1996). The ferric reducing ability of plasma (FRAP) as a measure of "antioxidant power": the FRAP assay. *Anal. Biochem.* 239, 70–76.

Boussetta, N., and Vorobiev, E. (2014). Extraction of valuable biocompounds assisted by high voltage electrical discharges: a review. *Comptes Rendus Chimie.* 17, 197–203. doi: 10.1016/j.crci.2013.11.011

Carocho, M., Morales, P., and Ferreira, I. C. F. R. (2015). Natural food additives: quo vadis? *Trends Food Sci. Technol.* 45, 284–295. doi: 10.1016/j.tifs.2015.06.007

Castellar, R., Obón, J. M., Alacid, M., and Fernández-López, J. A. (2003). Color properties and stability of betacyanins from *Opuntia* fruits. *J. Agric. Food Chem.* 51, 2772–2776. doi: 10.1021/jf021045h

Celli, G. B., and Brooks, M. S.-L. (2017). Impact of extraction and processing conditions on betalains and comparison of properties with anthocyanins — a current review. *Food Res. Int.* 100, 501–509. doi: 10.1016/j.foodres.2016.08.034

Chandrasekhar, J., Sonika, G., Madhusudhan, M. C., and Raghavarao, K. S. M. S. (2015). Differential partitioning of betacyanins and betaxanthins employing aqueous two phase extraction. *J. Food Eng.* 144, 156–163. doi: 10.1016/j.jfoodeng.2014.07.018

Chemat, F., Rombaut, N., Meullemiestre, A., Turk, M., Perino, S., Fabiano-Tixier, A.-S., et al. (2017). Review of green food processing techniques. Preservation, transformation, and extraction. *Innov. Food Sci. Emerg. Technol.* 41 (Suppl. C), 357–377. doi: 10.1016/j.ifset.2017.04.016

Chethana, S., Nayak, C. A., and Raghavarao, K. S. M. S. (2007). Aqueous two phase extraction for purification and concentration of betalains. *J. Food Eng.* 81, 679–687. doi: 10.1016/j.jfoodeng.2006.12.021

Chong, P. H., Yusof, Y. A., Aziz, M. G., Naim, M. N., Chin, N. L., Muhammad, S., et al. (2014). Evaluation of solvent extraction of *Amaranth* betacyanins using multivariate analysis. *Int. Food Res. J.* 21, 1569–1573.

Ciriminna, R., Fidalgo, A., Danzì, C., Timpanaro, G., Ilharco, L. M., and Pagliaro, M. (2018). Betanin: a bioeconomy insight into a valued betacyanin. *ACS Sust. Chem. Eng.* 6, 2860–2865. doi: 10.1021/acssuschemeng.7b04163

Dai, J., and Mumper, R. J. (2010). Plant phenolics: extraction, analysis and their antioxidant and anticancer properties. *Molecules* 15, 7313–7352. doi: 10.3390/molecules15107313

Dembitsky, V. M., Poovarodom, S., Leontowicz, H., Leontowicz, M., Vearasilp, S., Trakhtenberg, S., et al. (2011). The multiple nutrition properties of some exotic fruits: biological activity and active metabolites. *Food Res. Int.* 44, 1671–1701. doi: 10.1016/j.foodres.2011.03.003

Esatbeyoglu, T., Wagner, A. E., Schini-Kerth, V. B., and Rimbach, G. (2015). Betanin-A food colorant with biological activity. *Mol. Nutr. Food Res.* 59, 36–47. doi: 10.1002/mnfr.201400484

Fincan, M., DeVito, F., and Dejmek, P. (2004). Pulsed electric field treatment for solid–liquid extraction of red beetroot pigment. *J. Food Eng.* 64, 381–388. doi: 10.1016/j.jfoodeng.2003.11.006

Fu, L., Xu, B.-T., Xu, X.-R., Gan, R.-Y., Zhang, Y., Xia, E.-Q., et al. (2011). Antioxidant capacities and total phenolic contents of 62 fruits. *Food Chem.* 129, 345–350. doi: 10.1016/j.foodchem.2011.04.079

Hajimahmoodi, M., Moghaddam, G., Ranjbar, A. M., Khazani, H., Sadeghi, N., Oveisi, M. R., et al. (2013). Total phenolic, flavonoids, tannin content and antioxidant power of some Iranian pomegranate fower cultivars (*Punica granatum* L.). *Am. J. Plant Sci.* 4, 1815–1820. doi: 10.4236/ajps.2013.49223

Khan, M. I. (2016). Stabilization of betalains: a review. *Food Chem.* 197 (Part B), 1280–1285. doi: 10.1016/j.foodchem.2015.11.043

Khan, M. I., and Giridhar, P. (2015). Plant betalains: chemistry and biochemistry. *Phytochemistry* 117, 267–295. doi: 10.1016/j.phytochem.2015.06.008

Lancaster, J. E., and Lister, C. E. (1997). Influence of pigment composition on skin color in a wide range of fruit and vegetables. *J. Am. Soc. Horticul. Sci.* 122, 594–598. doi: 10.21273/JASHS.122.4.594

Laqui-Vilca, C., Aguilar-Tuesta, S., Mamani-Navarro, W., Montaño-Bustamante, J., and Condezo-Hoyos, L. (2018). Ultrasound-assisted optimal extraction and thermal stability of betalains from colored quinoa (*Chenopodium* quinoa Willd) hulls. *Ind. Crops Prod.* 111, 606–614. doi: 10.1016/j.indcrop.2017.11.034

Leong, H. Y., Ooi, C. W., Law, C. L., Julkifle, A. L., Ling, T. C., and Show, P. L. (2018a). Application of liquid biphasic flotation for betacyanins extraction from peel and flesh of *Hylocereus polyrhizus* and antioxidant activity evaluation. *Separat. Purif. Technol.* 201, 156–166. doi: 10.1016/j.seppur.2018.03.008

Leong, H. Y., Ooi, C. W., Law, C. L., Julkifle, A. L., and Show, P. L. (2018b). Betacyanins extraction from *Hylocereus polyrhizus* using alcohol/salt-based liquid biphasic partitioning system and antioxidant activity evaluation. *Sep. Sci. Technol.* 1–12. doi: 10.1080/01496395.2018.1517795

Leong, H. Y., Show, P. L., Lim, M. H., Ooi, C. W., and Ling, T. C. (2018c). Natural red pigments from plants and their health benefits: a review. *Food Rev. Int.* 34, 463–482. doi: 10.1080/87559129.2017.1326935

Moreno, D. A., García-Viguera, C., Gil, J. I., and Gil-Izquierdo, A. (2008). Betalains in the era of global agri-food science, technology and nutritional health. *Phytochem. Rev.* 7, 261–280. doi: 10.1007/s11101-007-9084-y

Ramli, N. S., Ismail, P., and Rahmat, A. (2014). Influence of conventional and ultrasonic-assisted extraction on phenolic contents, betacyanin contents, and antioxidant capacity of red dragon fruit (*Hylocereus polyrhizus*). *Scient. World J.* 2014:964731. doi: 10.1155/2014/964731

Re, R., Pellegrini, N., Proteggente, A., Pannala, A., Yang, M., and Rice-Evans, C. (1999). Antioxidant activity applying an improved ABTS radical cation decolorization assay. *Free Rad. Biol. Med.* 26, 1231–1237. doi: 10.1016/S0891-5849(98)00315-3

Roselló-Soto, E., Barba, F. J., Parniakov, O., Galanakis, C. M., Lebovka, N., Grimi, N., et al. (2015). High voltage electrical discharges, pulsed electric field and ultrasound assisted extraction of protein and phenolic compounds from olive kernel. *Food Bioproces. Technol.* 8, 885–894. doi: 10.1007/s11947-014-1456-x

Sankaran, R., Show, P. L., Lee, S. Y., Yap, Y. J., and Ling, T. C. (2018). Integration process of fermentation and liquid biphasic flotation for lipase separation from *Burkholderia cepacia*. *Bioresour. Technol.* 250, 306–316. doi: 10.1016/j.biortech.2017.11.050

Santos, R. P., Souza, L. M., Balieiro, A. L., Soares, C. M. F., Lima, Á. S., and Souza, R. L. (2018). Integrated process of extraction and purification of betanin from *Opuntia ficus-indica* using aqueous two-phase systems based on THF and sodium salts. *Sep. Sci. Technol.* 53, 734–744. doi: 10.1080/01496395.2017.1397022

Show, P. L., Ooi, C. W., Anuar, M. S., Ariff, A., Yusof, Y. A., Chen, S. K., et al. (2013). Recovery of lipase derived from *Burkholderia cenocepacia* ST8 using sustainable aqueous two-phase flotation composed of recycling hydrophilic organic solvent and inorganic salt. *Sep. Purif. Technol.* 110, 112–118. doi: 10.1016/j.seppur.2013.03.018

Singleton, V. L., Orthofer, R., and Lamuela-Raventós, R. M. (1999). "Analysis of total phenols and other oxidation substrates and antioxidants by means of Folin-Ciocalteu reagent," in *Methods in Enzymology*, ed L. Packer (San Diego, CA: Academic Press), 152–178. doi: 10.1016/S0076-6879(99)99017-1

Stintzing, F. C., and Carle, R. (2007). Betalains – emerging prospects for food scientists. *Trends Food Sci. Technol.* 18, 514–525. doi: 10.1016/j.tifs.2007.04.012

Tang, W. L., and Zhao, H. (2009). Industrial biotechnology: tools and applications. *Biotechnol. J.* 4, 1725–1739. doi: 10.1002/biot.200900127

Wang, L., and Weller, C. L. (2006). Recent advances in extraction of nutraceuticals from plants. *Trends Food Sci. Technol.* 17, 300–312. doi: 10.1016/j.tifs.2005.12.004

Xu, D.-P., Li, Y., Meng, X., Zhou, T., Zhou, Y., Zheng, J., et al. (2017). Natural antioxidants in foods and medicinal plants: Extraction, assessment and resources. *Int. J. Mol. Sci.* 18:96. doi: 10.3390/ijms18010096

Yau, Y. K., Ooi, C. W., Ng, E.-P., Lan, J. C.-W., Ling, T. C., and Show, P. L. (2015). Current applications of different type of aqueous two-phase systems. *Biores. Bioprocess.* 2:49. doi: 10.1186/s40643-015-0078-0

Zimmermann, S., Scheeder, C., Zimmermann, P. K., Bogsnes, A., Hansson, M., Staby, A., et al. (2017). High-throughput downstream process development for cell-based products using aqueous two-phase systems (ATPS) – a case study. *Biotechnol. J.* 12:1600587. doi: 10.1002/biot.201600587

**Conflict of Interest Statement:** The authors declare that the research was conducted in the absence of any commercial or financial relationships that could be construed as a potential conflict of interest.

frontiers in Chemistry

REVIEW
published: 09 April 2019
doi: 10.3389/fchem.2019.00213

# Giant Vesicles Encapsulating Aqueous Two-Phase Systems: From Phase Diagrams to Membrane Shape Transformations

*Yonggang Liu*[1]*, *Reinhard Lipowsky*[2] and *Rumiana Dimova*[2]*

[1] State Key Laboratory of Polymer Physics and Chemistry, Changchun Institute of Applied Chemistry, Chinese Academy of Sciences, Changchun, China, [2] Department of Theory and Bio-Systems, Max Planck Institute of Colloids and Interfaces, Potsdam, Germany

In this review, we summarize recent studies on giant unilamellar vesicles enclosing aqueous polymer solutions of dextran and poly(ethylene glycol) (PEG), highlighting recent results from our groups. Phase separation occurs for these polymer solutions with concentration above a critical value at room temperature. We introduce approaches used for constructing the phase diagram of such aqueous two-phase system by titration, density and gel permeation chromatography measurements of the coexisting phases. The ultralow interfacial tension of the resulting water-water interface is investigated over a broad concentration range close to the critical point. The scaling exponent of the interfacial tension further away from the critical point agrees well with mean field theory, but close to this point, the behavior disagrees with the Ising value of 1.26. The latter discrepancy arises from the molar mass fractionation of dextran between coexisting phases. Upon encapsulation of the PEG–dextran system into giant vesicles followed by osmotic deflation, the vesicle membrane becomes completely or partially wetted by the aqueous phases, which is controlled by the phase behavior of the polymer mixture and the lipid composition. Deflation leads to a reduction of the vesicle volume and generates excess area of the membrane, which can induce interesting transformations of the vesicle morphology such as vesicle budding. More dramatically, the spontaneous formation of many membrane nanotubes protruding into the interior vesicle compartment reveals a substantial asymmetry and spontaneous curvature of the membrane segments in contact with the PEG-rich phase, arising from the asymmetric adsorption of polymer molecules onto the two leaflets of the bilayers. These membrane nanotubes explore the whole PEG-rich phase for the completely wetted membrane but adhere to the liquid-liquid interface as the membrane becomes partially wetted. Quantitative estimates of the spontaneous curvature are obtained by analyzing different aspects of the tubulated vesicles, which reflect the interplay between aqueous phase separation and spontaneous curvature. The underlying mechanism for the curvature generation is provided by the weak adsorption of PEG onto the lipid bilayers, with a small binding affinity of about 1.6 $k_BT$ per PEG chain. Our study builds a bridge between nanoscopic membrane shapes and membrane-polymer interactions.

**Keywords: phase diagram, membrane shape transformation, giant vesicles, aqueous two-phase systems, dextran, poly(ethylene glycol), wetting, membrane tubes**

OPEN ACCESS

***Edited by:***
*John Paul Frampton, Dalhousie University, Canada*

***Reviewed by:***
*Pasquale Stano, University of Salento, Italy*
*Kanta Tsumoto, Mie University, Japan*

***Correspondence:**
*Yonggang Liu*
*yonggang@ciac.ac.cn*
*Rumiana Dimova*
*rumiana.dimova@mpikg.mpg.de*

***Specialty section:***
*This article was submitted to Chemical Engineering, a section of the journal Frontiers in Chemistry*

***Received:*** *26 October 2018*
***Accepted:*** *18 March 2019*
***Published:*** *09 April 2019*

***Citation:***
*Liu Y, Lipowsky R and Dimova R (2019) Giant Vesicles Encapsulating Aqueous Two-Phase Systems: From Phase Diagrams to Membrane Shape Transformations. Front. Chem. 7:213. doi: 10.3389/fchem.2019.00213*

## INTRODUCTION

Phase separation can occur when solutions of two different polymers or a polymer and a salt are mixed above a certain concentration in water. These aqueous two-phase systems (ATPSs) provide a particularly mild environment with extremely low interfacial tension on the order of 1–100 μN/m, which enable many applications of ATPS in biotechnology and bioengineering (Walter et al., 1985; Albertsson, 1986). One such system of great interest is provided by mixing aqueous solutions of dextran and polyethylene glycol (PEG). These solutions undergo phase separation above the critical concentration at a certain temperature, yielding two coexisting phases in equilibrium with each phase containing predominantly one of the polymer species and water. Phase separation in polymer solutions depends on the thermodynamic properties of the system, which is theoretically described by the Flory-Huggins theory (Flory, 1941, 1953; Huggins, 1941). When the entropy of mixing is not sufficient to compensate the enthalpy of demixing, the polymer solutions undergo phase separation.

Recently, renewed interest in PEG–dextran systems arose because of its potential biotechnological applications, as well as its suitability as a model system for mimicking the crowded environment in cells (Dimova and Lipowsky, 2012, 2017; Keating, 2012). The PEG–dextran ATPS was encapsulated into giant unilamellar vesicles (GUVs), cell-sized containers (Dimova et al., 2006; Walde et al., 2010; Dimova, 2012, 2019). The group of Keating initiated the study of aqueous phase separation in GUVs (Helfrich et al., 2002), and observed the asymmetric protein microcompartmentation in these systems which resembles the crowded environment of the cytosol (Long et al., 2005). The partitioning of biomolecules in ATPS is influenced by the affinities of these molecules being separated to the coexisting phases or the liquid-liquid interface, as well as by the physico-chemical properties of the employed ATPS itself (Zaslavski, 1995), which requires a detailed and quantitative characterization of its phase behavior. During the last decade, these hybrid soft matter systems containing both membranes and polymers are investigated experimentally (Li et al., 2008, 2011, 2012; Long et al., 2008; Kusumaatmaja et al., 2009; Andes-Koback and Keating, 2011; Liu et al., 2016) and theoretically (Lipowsky, 2013, 2014, 2018). A number of interesting phenomena, such as vesicle budding (Long et al., 2008; Li et al., 2012), wetting transitions (Li et al., 2008; Kusumaatmaja et al., 2009), division of vesicles (Andes-Koback and Keating, 2011), and formation of membrane nanotubes (Li et al., 2011; Liu et al., 2016), have been observed. All these phenomena were governed by the interplay between polymer-membrane interactions and the fluid-elastic properties of the membrane (Lipowsky, 2013, 2014, 2018). Precise experimental studies of the aqueous phase separation and the resulting aqueous phases are challenging, but are required to fully understand their role in the associated membrane transformations. This review focuses on precisely this topic, highlighting results from our groups that have been obtained over the past decade.

The text is organized as follows. We first discuss the phase diagram of the PEG–dextran system. More specifically, we introduce a density method for the measurement of the tie lines between the coexisting phases, and compare it with a method based on gel permeation chromatography (GPC). We then compare the scaling exponent of the interfacial tension to the values obtained in mean field theory and in the Ising model, and correlate the discrepancy of the Ising value in the vicinity of the critical point to the molar mass fractionation of dextran between coexisting phases. Afterwards, we focus on membrane-associated effects (such as wetting and morphological changes) in GUVs encapsulating ATPS. The observed complete-to-partial wetting transition of the giant vesicle membrane by the PEG-rich phase is discussed by introducing a hidden material parameter, the intrinsic contact angle (Kusumaatmaja et al., 2009), which characterizes the affinity of the phases to the membranes but has not been directly measured by optical microscopy. We then discuss the formation of membrane nanotubes resulting from the deflation of giant vesicles encapsulating aqueous mixture of dextran and PEG. Theoretical analysis of the GUV shapes with nanotubes protruding into the interior of the vesicles revealed the presence of a negative spontaneous curvature (Li et al., 2011). Depending on the properties of the aqueous phases and the vesicle membranes, three different tube patterns have been observed within vesicles of three distinct morphologies (Liu et al., 2016). Quantitative estimation of the spontaneous curvature is obtained by image analysis of the vesicle shapes, for membranes of different lipid compositions with distinct fluid-elastic properties. The molecular mechanism underlying the observed curvature generation is provided by the weak adsorption of PEG molecules onto the membranes, according to theoretical considerations, control experiments with PEG solution, and molecular dynamics simulations. Finally, we discuss possible future directions in the field.

## PHASE DIAGRAM OF THE PEG–DEXTRAN SYSTEMS

At a certain temperature, the phase diagram for an aqueous solution of dextran and PEG depends on their weight fractions $w_d$ and $w_p$. The diagram includes the binodal (the boundary of the two-phase coexistence region), the critical point and the tie lines, as illustrated in **Figure 1**. The phase diagram is divided by the binodal curve into a region of polymer concentrations that will form two immiscible aqueous phases (above the binodal in **Figure 1**) and one homogeneous phase (at and below the binodal in **Figure 1**). A tie line connects two points of the binodal, which represent the final compositions of the polymer components in the coexisting phases. Also located on the binodal is the critical demixing point. Above this point but close to the binodal (see **Figure 1**), the compositions and volumes of both phases are nearly identical. Different methods have been proposed to construct the phase diagram of PEG–dextran system (Hatti-Kaul, 2000). Below, we will review some of them.

### Binodal and Critical Point

The binodal determined by cloud-point titration is shown in **Figure 2A** for aqueous solutions of dextran (with weight-average

molar mass $M_w$ = 400–500 kg/mol) and PEG (with $M_w$ = 8 kg/mol) (Liu et al., 2012). The aqueous mixture of dextran and PEG undergoes phase separation when the total polymer weight fractions exceed a few percent. Titration experiments from the one-phase to the two-phase region, or the other way around, lead to the same phase boundary.

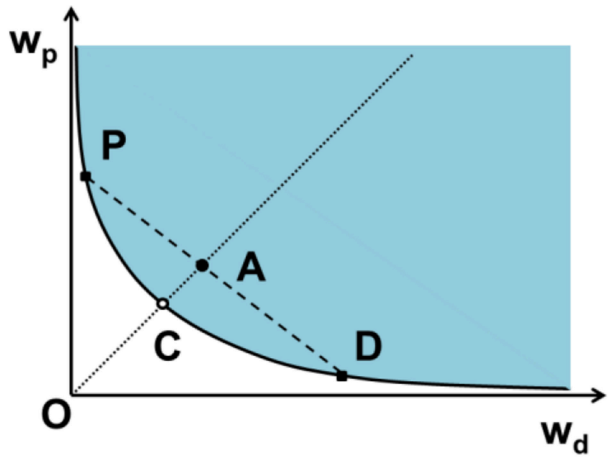


**FIGURE 1 |** Schematic phase diagram for an aqueous two-phase system, in our case dextran (d) and PEG (p), by plotting the weight fraction of PEG $w_p$ as a function of the weight fraction of dextran $w_d$. The phase diagram is divided into regions of two-phase coexistence (blue) and one homogeneous phase (white) by the binodal (solid curve). The critical point C, at which the volumes of the two coexisting phases become identical, is located infinitely close to and above the binodal. The mixture A with the same polymer ratio as the critical point, located above the binodal undergoes phase separation and forms two coexisting phases with compositions D and P in equilibrium, which are dextran-rich and PEG-rich phases, respectively. Solutions with composition lying on this tie line (dashed line) separate into coexisting phases with the same final compositions (D and P) but different volume fractions. The composition difference of the coexisting phases is characterized by the length of the tie line DP, which becomes shorter at lower polymer concentration and converges to a single point called the critical demixing point (C).

The critical point of the system, at which the volumes of the coexisting phases are equal, can be estimated by gradually approaching the binodal via titration of the PEG–dextran mixture in the two-phase region with water. In this experiment, a series of mixtures of dextran and PEG solutions are prepared at certain weight ratios $w_d/w_p$, and the volume fractions of the coexisting phases are measured by bringing the system stepwise to the binodal. Using data obtained from titration trajectories with different values of $w_d/w_p$, one can find the weight ratio $w_d/w_p$ at which the two phases have equal volumes in the vicinity of the binodal, in this case $w_d/w_p$ = 1.25 is found, as shown in **Figure 2B** (Liu et al., 2012). Carefully studying solutions with such a weight ratio close to the binodal provides an estimate of the polymer composition of the critical point, which is located at a total polymer weight fraction $w_{cr}$ = 0.0812 ± 0.0002. The critical concentration for phase separation of the studied PEG–dextran system is then given by $c_{cr} = \rho_{cr} w_{cr}$ = 0.0829 ± 0.0002 g/mL with $\rho_{cr}$ being the solution mass density at the critical point.

It should be mentioned that there is a temperature dependence for the phase diagram of the PEG–dextran system (Helfrich et al., 2002), one can therefore use either temperature or concentration as experimental control parameters for the phase state of the PEG–dextran system. Additionally, new phase diagrams should be measured when new lots of polymer are used, due to the batch-to-batch differences of the polymers in molar mass distributions, even if they are obtained from the same manufacturer (Helfrich et al., 2002).

## Tie Line Determination

To assess the polymer concentrations and build the tie lines in ATPSs, one has to separate the phases and measure some physical properties that related to the polymer concentrations.

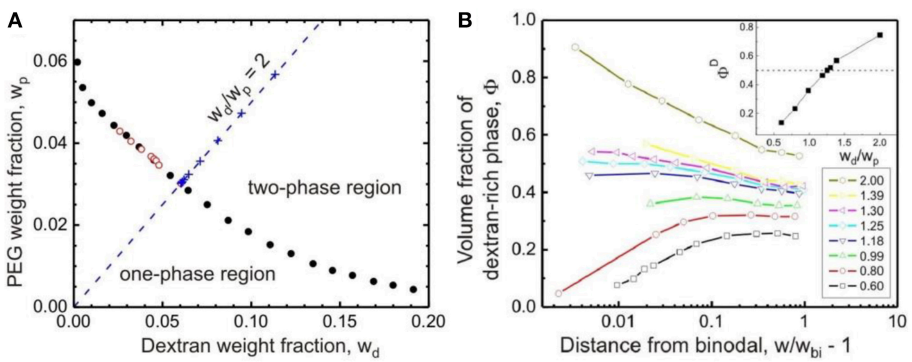


**FIGURE 2 | (A)** Binodal of the aqueous solution of dextran (molar mass between 400 and 500 kg/mol) and PEG (molar mass 8 kg/mol) at 24 ± 0.5°C obtained by titration from the one-phase to the two-phase region (solid circles) and vice versa (open circles). The "+" symbols are experimental points along the titration trajectory with $w_d/w_p$ = 2.0 (dashed line). The intersection of such a trajectory with the binodal defines the polymer weight fraction $w_{bi}$. **(B)** Volume fraction $\Phi^D$ of the dextran-rich phase as a function of the normalized distance from the binodal, $w/w_{bi}$ – 1, for polymer solutions of different weight ratios $w_d/w_p$ between dextran and PEG ranging from 0.60 to 2.00. See the lower inset with the color code. The upper inset shows the dependence of the volume fraction $\Phi^D$ on the weight ratio $w_d/w_p$ very close to the phase boundary at $w/w_{bi}$ = 1.02. For $\Phi^D$ = 0.50 (dashed line), the polymer weight ratio $w_d/w_p$ = 1.25 was found. Reprinted with permission from Liu et al. (2012). Copyright (2012) American Chemical Society.

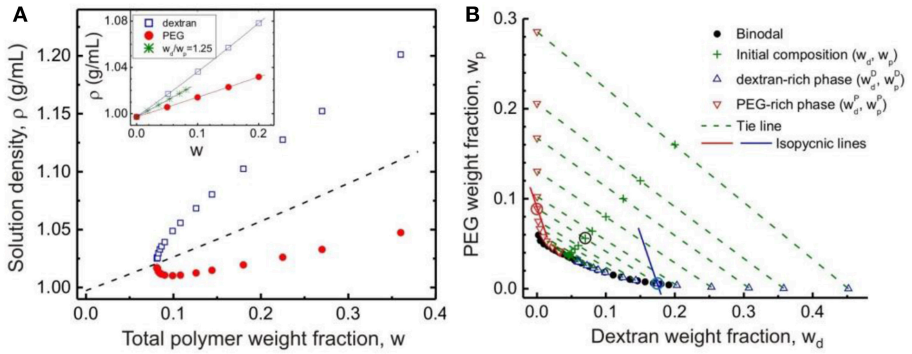


**FIGURE 3 | (A)** Densities of the coexisting dextran-rich (open squares) and PEG-rich (solid circles) phases for polymer solutions with weight ratio $w_d/w_p = 1.25$ as functions of the total initial polymer weight fraction w. The dashed line is the calculated density of the polymer solution with $w_d/w_p = 1.25$. In the inset, the densities of pure dextran and pure PEG solutions and their mixtures with $w_d/w_p = 1.25$ in the one-phase region are plotted as functions of the total polymer weight fraction $w$. The lines are fits to Equation (1) with specific volumes $v_d = 0.62586 \pm 0.00046$ mL/g and $v_p = 0.83494 \pm 0.00043$ mL/g. **(B)** Tie lines in the PEG–dextran phase diagram at 24 ± 0.5°C. The solid circles show the data for the experimentally measured binodal. The compositions of the initial solutions (with weight ratio $w_d/w_p = 1.25$) for which the phase densities after phase separation were measured are indicated by "+" symbols. The end points of the respective tie lines consist of upward-pointing triangles indicating the compositions of the dextran-rich phases and downward-pointing triangles indicating the compositions of the PEG-rich phases. The solid lines represent two examples of isopycnic lines calculated following Equations (2) and (3) for the initial solution composition indicated with an encircled "+" symbol in the graph: $(w_d, w_p) = (0.0700, 0.0560)$. The intersections of the isopycnic lines with the binodal yield the compositions of the two phases, also encircled. Reprinted with permission from Liu et al. (2012). Copyright (2012) American Chemical Society.

For the PEG–dextran system, one normally measures the optical activity and the refractive index of the solutions, because dextran is optically active but PEG is not. Then dextran concentrations in the coexisting phases are obtained from the known specific rotation of dextran, while the PEG concentrations are determined after subtracting the contribution of dextran to the solution refractive index. To make it simpler, a gravimetric method had been employed for the tie line determination of ATPS containing a PEG polymer and a salt, by forcing the end points of the tie-line on a binodal determined separately (Merchuk et al., 1998). However, for ATPS containing polymers with large dispersities, the tie line end points deviates from the binodal, and the mismatch grows with increasing polymer dispersity. It makes the gravimetric method not applicable to the PEG–dextran systems, because the generally available dextran has a broad molar mass distribution. Below we show that the tie lines of an ATPS can be accurately determined by density and gel permeation chromatography measurements of the coexisting phases.

## Density Method

This method for determining the tie lines of ATPS is based on accurate density measurements of the coexisting phases (Liu et al., 2012). Here we assume that the specific volume of the aqueous polymer solution is the sum of the contributions from all components. Then, the mass density $\rho$ of the mixture is related to the specific volume of each component via

$$\frac{1}{\rho} = \left(1 - w_d - w_p\right) v_s + w_d v_d + w_p v_p \qquad (1)$$

Here the specific volume of water, dextran and PEG at 24°C are found to be $v_s = 1.00271$ mL/g, $v_d = 0.62586$ mL/g and $v_p = 0.83494$ mL/g, respectively (see inset of **Figure 3A**).

In Liu et al. (2012), we prepared PEG–dextran solutions in the concentration range $w_{cr} < w < 0.36$ at the same weight ratio $w_d/w_p$ as for the critical point. These solutions were kept at a constant temperature of 24°C for a few days to reach equilibrium before the coexisting phases separated and their densities accurately measured by a density meter. As expected, the top PEG-rich phase always has a lower density than the bottom dextran-rich phase, and the density difference between the coexisting phases vanish at the critical point (**Figure 3A**). The normalized distance of the corresponding tie line from the critical point is taken to be the reduced concentration $\varepsilon \equiv \frac{c}{c_{cr}} - 1$, which lies in the range of $0 < \varepsilon < 3.82$.

The compositions of the dextran-rich (D) and PEG-rich (P) phases, are then determined based on their densities $\rho^D$ and $\rho^P$, respectively. By rewriting Equation (1), the PEG weight fractions of the coexisting phases, $w_p^D$ and $w_p^P$, are related to the corresponding dextran weight fractions, $w_d^D$ and $w_d^P$, via (Liu et al., 2012):

$$w_p^D = \frac{1}{v_p - v_s}\left[\frac{1}{\rho^D} - v_s - (v_d - v_s)\, w_d^D\right] \qquad (2)$$

for the dextran-rich phase, and

$$w_p^P = \frac{1}{v_p - v_s}\left[\frac{1}{\rho^P} - v_s - (v_d - v_s)\, w_d^P\right] \qquad (3)$$

for the PEG-rich phase, respectively.

Equations (2) and (3) represent straight isopycnic lines in the $w_d$-$w_p$ plane with a constant slope of $-(v_d - v_s)/(v_p - v_s)$, and the intercepts of these lines reflect the different values of the phase densities $\rho^D$ and $\rho^P$. The compositions of the coexisting dextran-rich and PEG-rich phase can be then estimated from the

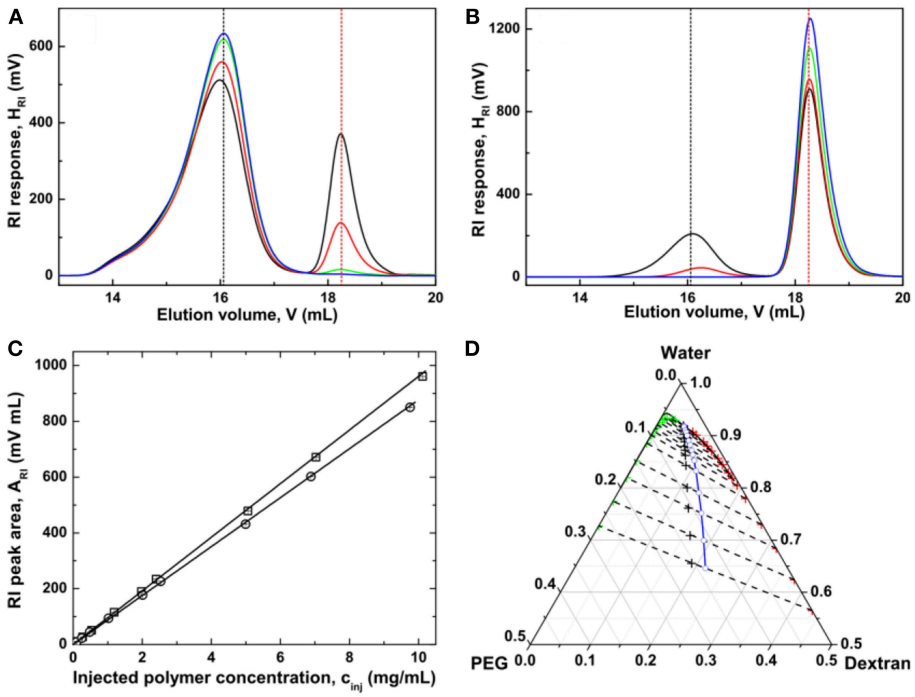


**FIGURE 4 |** GPC chromatograms of coexisting dextran-rich **(A)** and PEG-rich phases **(B)** at $\varepsilon = 0.030$ (black), 0.200 (red), 0.982 (green), and 2.087 (blue). The peak retention volumes of the native dextran and PEG are 16.06 mL (black dashed line) and 18.25 mL (red dashed line), respectively. **(C)** Dependence of the RI peak area $A_{RI}$ on polymer concentration $c_{inj}$ of the solutions injected into the size-exclusion chromatography columns for dextran (squares) and PEG (circles). **(D)** The resulting phase diagram of the PEG–dextran–water system. In the phase diagram, the cloud point curve is shown as a solid curve. The compositions of the initial solutions for which size-exclusion chromatography measurements after phase separation were performed are indicated by black crosses. The end points of the respective tie lines (dashed lines) consist of red crosses indicating the compositions of the dextran-rich phases and green crosses indicating the compositions of the PEG-rich phases. The midpoints (blue circles) of the tie lines were extrapolated to the binodal to determine the critical point. Adapted with permission from Zhao et al. (2016b). Copyright (2016) Chem. J. Chinese Universities.

intersections of these isopycnic lines with the binodal established in section Binodal and Critical Point.

The accuracy of this density-based method in constructing the tie lines is demonstrated by the close proximity of the coordinates ($w_d$, $w_p$) for the starting mixtures to the corresponding tie lines, as shown in **Figure 3B**. The tie lines determined by the density method are in excellent agreement with reported tie lines obtained with traditional methods for similar PEG–dextran systems at comparable temperatures. Below we will show that the density method can be further validated by an independent method based on quantitative GPC measurements of the coexisting phases.

## GPC Method

The density method is relatively simple to determine the tie lines of ATPS. However, it relies on the assumption that the tie line end points coincide with the predetermined binodal, which is a good approximation for ATPS with polymers of narrow dispersities. For PEG–dextran systems with two polymer species which can be completely separated by GPC, the compositions of the coexisting phases can be directly quantified by GPC with a single concentration detector (Connemann et al., 1991; Zhao et al., 2016a,b). Below we give the details of this method.

To quantify polymer concentrations within the two coexisting phases of an ATPS, the polymer solutions are typically diluted and their GPC chromatograms are recorded, with baseline separation of dextran from PEG on a differential refractive index (RI) detector (Zhao et al., 2016b). It can be seen from **Figures 4A,B** that further away from the critical point, more dextran molecules are accumulating in the dextran-rich phase, while more PEG molecules are partitioning into the PEG-rich phase. At sufficient distance from the critical point, no dextran molecules are present in the PEG-rich phase, and PEG molecules are completely absent in the dextran-rich phase. The polymer compositions in the coexisting phases can be directly obtained from their peak areas, with the pre-established concentration dependences of the RI peak areas for dextran and PEG, respectively (**Figure 4C**). It is found that the tie line end points superpose to the binodal curve, with an exception of those data for the PEG-rich phases in the vicinity of the critical point (**Figure 4D**). This discrepancy is most probably due to molar mass fractionation of dextran between the coexisting phases (see section Molar Mass Fractionation).

Interestingly, the tie lines established by the density and GPC methods agreed well with each other. The density method requires the density measurements of the phases

together with a pre-established binodal, which makes it a simple and convenient method. The GPC method requires the chromatography measurements of all phases and accurate calibration of the RI detector for both components. Although the GPC method is tedious and time-consuming, it does not depend on the binodal curve. More importantly, molar mass distribution and molar mass averages of each polymer species in the coexisting phases can be obtained by the GPC method (see section Molar Mass Fractionation). It should be noted, however, that the GPC method with RI as the concentration detector is only applicable to certain ATPSs, whose components can be separated into two peaks by the GPC columns without polymer adsorption. The coupling to a laser light scattering detector gives additional information on molar mass of the components. If the elution peaks of these two polymer components are overlapping, one must use two concentration detectors, for example a RI and an additional optical rotation detector, to quantify the compositions of the polymer mixtures (Edelman et al., 2003a,b).

## Molar Mass Fractionation

Since dextran and PEG components in the coexisting phases are completely separated from each other by the GPC columns (**Figures 4A,B**), one can also determine the molar mass distributions of each component after calibrating the system either with narrow polymer standards or by a laser light scattering detector (Zhao et al., 2016a). We first take a look at the dextran component in the coexisting phases. Inspection of the GPC chromatograms (**Figures 4A,B**) indicates that the relative intensity of the elution peak of dextran in the PEG-rich phase is much less than that in its coexisting dextran-rich phase. Additionally, the elution peak of dextran in the PEG-rich phase is shifting toward higher retention volume, indicating a lower molar mass than that in the dextran-rich phase. Further away from the critical point, the difference for the dextran elution peaks between the two coexisting phases increases. The evolution of the PEG elution peaks shows a different behavior. Although the relative intensity of PEG elution peak in the dextran-rich phase is lower than that in the PEG-rich phase, there is however, hardly any change in retention volumes for PEG components in the two coexisting phases. It indicates that PEG components in the two coexisting phases have similar molar mass, albeit less PEG is distributed into the dextran-rich phase.

Quantitative calculation of the molar mass and polymer dispersities for dextran and PEG in the coexisting phases are obtained from GPC measurements and the results are shown in **Figure 5**. For the system explored here, it is found that the weight-average molar mass $M_w$ of dextran in the dextran-rich phase is significantly larger than that in its coexisting PEG-rich phase (**Figure 5A**). As the polymer concentration increases, the $M_w$ of dextran in the dextran-rich phase approaches the value of the original dextran with $M_w$ = 380 kg/mol, while the $M_w$ of dextran in the PEG-rich phase shows a continuous decrease down to 82.2 kg/mol at $\varepsilon = 0.73$. This is because the used dextran had a broad molar mass distribution, characterized by the dispersity index $M_w/M_n$, the ratio between the weight-average molar mass $M_w$ and the number-average molar mass $M_n$, of 2.19. With more dextran of high molar mass component partitioning into the dextran-rich phase, the molar mass of dextran component in the PEG-rich phase decreases. It also leads to an $M_w$ value larger than that of the native dextran in the dextran-rich phase, agreeing with the tiny shift of the dextran peak to lower retention volume (**Figure 4A**). However, when the initial polymer concentration is sufficiently high, no dextran is found in the PEG-rich phase, leading to the same $M_w$ value of dextran in the dextran-rich phase as for native dextran. In contrast, PEG in the two coexisting phases have similar weight-average molar masses, close to the value of the original PEG with $M_w$ = 8.45 kg/mol (**Figure 5B**), and such behavior is independent of the initial polymer concentration. This is due to the narrow dispersity of the employed PEG, with $M_w/M_n = 1.11$. In ATPS with broad molar mass distributions for both polymers, molar mass fractionation of both components is observed (Edelman et al., 2003a,b).

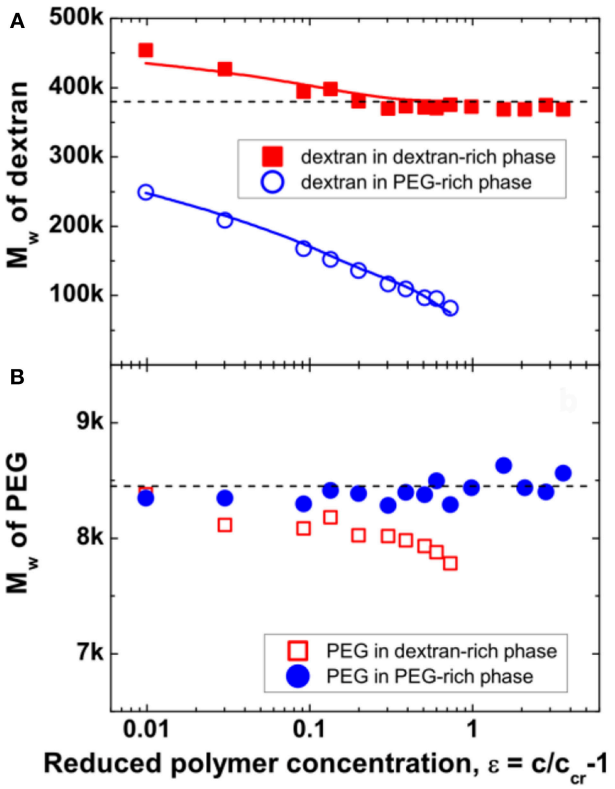


**FIGURE 5 |** Weight-average molar mass $M_w$ of dextran **(A)** and PEG **(B)** in the dextran-rich (squares) and PEG-rich (circles) phases. The dashed lines indicate the average molar mass $M_w$ = 380 kg/mol for dextran and $M_w$ = 8.45 kg/mol for PEG, respectively. The values of $M_w$ for dextran in the two phases, which were obtained from the calculated molar mass distribution of dextran, are shown as solid lines in **(A)**. Reprinted from Zhao et al. (2016a), Copyright (2016), with permission from Elsevier.

With the compositions of the coexisting phases accurately measured, we can obtain the distribution coefficient $f_x$(N) of each polymer component between the coexisting phases. According to the Flory-Huggins theory, the distribution coefficient, also called

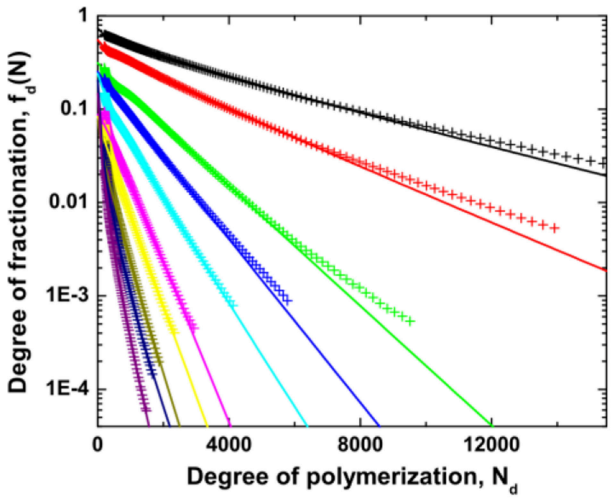


**FIGURE 6 |** Degree of fractionation $f_d(N)$ for dextran as a function of the degree of polymerization $N_d$ of dextran for different values of the reduced polymer concentration $\varepsilon \equiv \frac{c}{c_{cr}} - 1$ which is varied from 0.01 (top right) to 0.73 (bottom left). The lines are fits to the data by the empirical relation $f_d(N) = A \times exp\left(-\sigma_d N - \sigma_{d2} N^{0.5}\right)$. Reprinted from Zhao et al. (2016a), Copyright (2016), with permission from Elsevier.

the degree of fractionation, is defined as (Flory, 1953):

$$f_x(N) \equiv \frac{c_{x,poor}(N)}{c_{x,rich}(N)} = \exp(-\sigma_x N) \quad (4)$$

where $c_{x,poor}(N)$ and $c_{x,rich}(N)$ are the concentrations of component $x$ (in our case, dextran or PEG) containing $N$ monomers in the phases poor and rich in $x$ component, respectively. Theory predicted an exponential decay behavior for the degree of fractionation $f_x(N)$ as a function of chain length $N$ (Flory, 1953; Koningsveld et al., 2001), suggesting that the longer the $x$-chain, the less it distributed in the $x$-poor phase. The separation parameter $\sigma_x$ represents the free energy change per monomer during transferring a chain of length $N$ between the liquid-liquid phases.

In **Figure 6**, the degree of fractionation $f_d(N)$ for dextran is plotted vs. the chain length $N_d$ at different distance $\varepsilon$ from the critical point. An exponential dependence is observed over a certain range of chain length for all values of $\varepsilon$, although the data deviate slightly. However, there are two distinct differences of the experimental results with the mean field prediction. First, the degree of fractionation starts to deviate from the exponential dependence at a certain chain length. Second, the value extrapolated to $N_d = 0$ does not reach the expected value of 1, implying that the mean field theory is insufficient to quantitatively describe the degree of fractionation for dextran in ATPS. Such a discrepancy has been observed in previous experiments (Edelman et al., 2003a,b), as well as in computer simulations (van Heukelum et al., 2003). The data can be fitted to an empirical relation by introducing additional fitting parameters $A$ and $\sigma_{d2}$, as shown in **Figure 6**.

For the current ATPS containing dextran chains with a large dispersity and near-monodisperse PEG chains, molar mass fractionation leads to a chain length dependent redistribution of dextran chains between the coexisting phases. High molar mass dextran chains are enriched in the dextran-rich phase and depleted from the PEG-rich phase, leading to a significant decrease of the $M_w$ of dextran in the PEG-rich phase and a slight increase of that in the coexisting dextran-rich phase. This is the underlying origin for the mismatch between the binodal curve and the end points of the tie lines for the PEG-rich phase in the vicinity of the critical point. As a result, the compositions of the PEG-rich phase locate above the binodal (**Figure 3B**). It is also expected that the compositions of the corresponding dextran-rich phases lie slightly below the binodal, which is not observable in experiments. The results are in good agreement with previous studies about polymer dispersity effect on the tie lines (Kang and Sandler, 1988). Therefore, to obtain the tie line for such an ATPS system by the density method close to the critical point (Liu et al., 2012), the composition for the dextran-rich phase can be determined from the intersection of the corresponding isopycnic line with the binodal. However, the composition for the PEG-rich phase must be estimated from the intersection of its isopycnic line with a straight line passing through the composition of the initial polymer solution and that of the dextran-rich phase.

## INTERFACIAL TENSION AND SCALING LAWS

The interfacial tension between coexisting phases of ATPS is on the order of 1–100 μN/m, which can be determined by measuring the equilibrium shape of liquid-liquid interface under some external forces, such as gravity or centrifugal force, as well as by methods based on time evolution of the interface shape (Tromp, 2016). Different techniques, such as the drop volume method (Mishima et al., 1998), drop retraction analysis (Ding et al., 2002), sessile and pendant drop shape analysis (Atefi et al., 2014), capillary length analysis (Vis et al., 2015) and spinning drop method (Ryden and Albertsson, 1971; Liu et al., 2012), have been employed for the interfacial tension measurement of the water-water interfaces.

Here, we summarize some data for the interfacial tension $\Sigma_{pd}$ between the coexisting liquid-liquid phases of the PEG–dextran system obtained by a spinning drop tensiometer (Liu et al., 2012) (see **Figure 7A**). In this broad concentration range, the interfacial tension increases by 4 orders of magnitude with increasing distance from the critical point, i.e. from 0.21 μN/m at reduced polymer concentration $\varepsilon = 0.02$, to 769 μN/m at $\varepsilon = 3.82$.

Quantitative description of the phase separation of polymer solution in the vicinity of the critical point remains as an interesting problem in polymer physics. The phase separation of polymer solution is usually studied at temperature $T$ close to its critical demixing temperature $T_c$. Various physical quantities, including the susceptibility $\chi$, the correlation length $\xi$, the order parameters, and the interfacial tension $\Sigma$, have been studied in

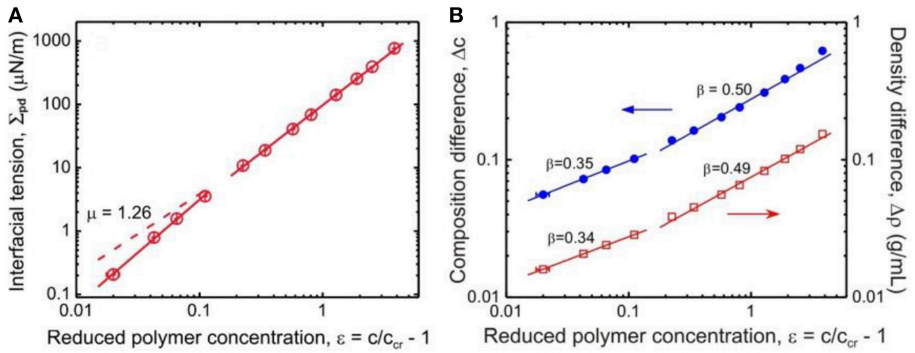


**FIGURE 7 | (A)** Interfacial tension $\Sigma_{pd}$ between coexisting dextran-rich and PEG-rich phases as functions of the reduced polymer concentration $\varepsilon = c/c_{cr} - 1$. The solid lines are fits to the data with exponent of 1.67 ± 0.10 for $0.02 < \varepsilon < 0.12$, and 1.50 ± 0.01 for $0.2 < \varepsilon < 3$. The dashed line shows the expected asymptotic behavior with $\mu = 1.26$. **(B)** Composition difference $\Delta c$ (solid circles) and density difference $\Delta\rho$ (open squares) of the coexisting phases as functions of the reduced polymer concentration $\varepsilon$. In the concentration range $0.02 < \varepsilon < 0.12$, the fits to the data give for the scaling exponent $\beta$ a value of 0.337 ± 0.018 as estimated from the density difference dependence or 0.351 ± 0.018 as estimated from the composition difference dependence, while in the range $0.2 < \varepsilon < 3$ we obtain $\beta = 0.491$ ± 0.014 from the density difference dependence or $\beta = 0.503 \pm 0.018$ from the composition difference dependence. Reprinted with permission from Liu et al. (2012). Copyright (2012) American Chemical Society.

details for different polymer solutions (Sanchez, 1989; Widom, 1993). Several theoretical models, such as the mean field theory, the Ising model, and the crossover theory, have been developed to explain the observed scaling behaviors of the these properties, depending on proximity to the critical point as characterized by the reduced temperature $\tau = |1 - T/T_c|$. A good example is provided by accurate light scattering measurements of polymer solutions close to $T_c$ (Melnichenko et al., 1997; Anisimov et al., 2002), where the scaling for the susceptibility $\chi \sim \tau^{-\gamma}$ with $\gamma$ changed from 1.24 to 1, and that for the correlation length $\xi \sim \tau^{-\nu}$ with $\nu$ decreased from 0.63 to 1/2, respectively. The crossover from the Ising model to the mean field behavior occurs at a correlation length scale on the order of the chain size of the polymers. Measurement of the coexistence curves for polymer solutions also revealed such a crossover for the composition difference $\Delta\varphi \sim \tau^{\beta}$ with the exponent $\beta$ changed from 0.326 to 1/2 (Dobashi et al., 1980). The crossover for the interfacial tension $\Sigma \sim \tau^{\mu}$ in exponent $\mu$ is theoretically predicted but its experimental verification is still lacking. Instead, scaling exponents $\mu$ ranged from 1.17 to 1.60 have been reported in the literature for a few polymer systems close to $T_c$ (Shinozaki et al., 1982; Heinrich and Wolf, 1992; Widom, 1993), where the crossover from the Ising value 1.26 to the mean field value 3/2 were not observed.

One can use a similar approach for ATPS of dextran and PEG, by scaling analysis of the interfacial tension and the order parameters vs. the reduced concentration $\varepsilon$ (Liu et al., 2012). The scaling exponent $\mu$ of the interfacial tension $\Sigma_{pd} \sim \varepsilon^{\mu}$ shows a crossover behavior depending on proximity to the critical point (**Figure 7A**). Further away from the critical point, the obtained value $\mu = 1.50 \pm 0.01$ is in excellent agreement with mean field theory. However, closer to this point, the increased value of 1.67 ± 0.10 deviates significantly from the Ising value 1.26. In contrast, as the critical point is approached, the scaling exponent $\beta$ of the order parameters, does exhibit the expected crossover from mean field value of $\beta = 1/2$ to Ising value 0.326 (see **Figure 7B**).

Such a crossover from mean field to Ising behavior is further supported by the normalized coexistence curve of the studied PEG–dextran system, which has a similar shape with the prediction from the crossover theory based on near-tricritical-point (theta point) Landau expansion renormalized by fluctuations (Anisimov et al., 2000). As shown in **Figure 8**, the reduced polymer concentration approximates the Ising limit with scaling exponent $\beta = 0.326$ in the vicinity of the critical point, where the correlation length of the concentration fluctuations is larger than the polymer molecular size (Liu et al., 2012). However, the data at the highest polymer concentration approaches the tricritical mean field limit with $\beta = 1$, indicating that the polymer molecular size is larger than the correlation length. Therefore, the crossover theory from critical Ising behavior to tricriticality of polymer solutions can also be applied to the PEG–dextran system in our study.

The discrepancy for the scaling exponent of the interfacial tension close to the critical point might arise from the molar mass fractionation of dextran. As shown in **Figure 5A**, in the vicinity of the critical point, the $M_w$ of dextran in the dextran-rich phase is larger than that of the original dextran, leading to a reduction of the interfacial tension. While further away from the critical point, the $M_w$ of dextran in the dextran-rich phase is similar to that of the original dextran and there is no influence on the interfacial tension. Therefore, the scaling exponent $\mu$ is unaffected in the mean field region, but an increased value of 1.67 is observed in the Ising limit region.

## WETTING OF MEMBRANES BY ATPS

The phase separation process and its consequences on membranes in contact with the two phases can be directly observed when the aqueous polymer solutions of dextran and

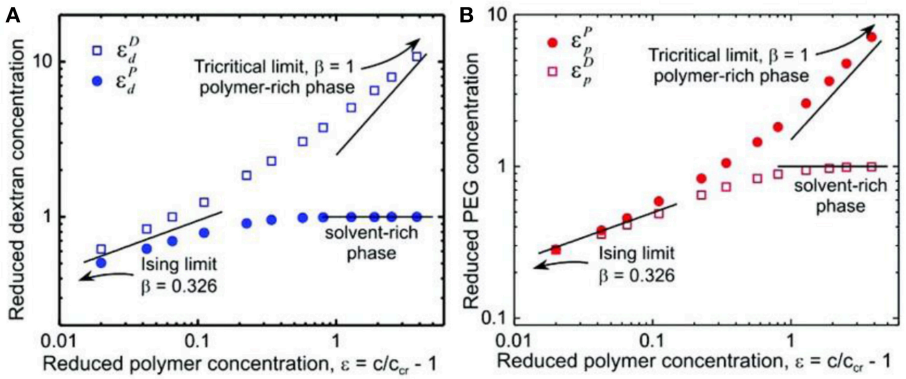


**FIGURE 8 |** Logarithmic scaling plots of phase-coexistence curves for **(A)** dextran and **(B)** PEG. The solid lines are guides to the eye with scaling exponents of 0.326 for the Ising model limit and 1 for the tricritical limit and a constant of 1 for the solvent-rich phase. Reprinted with permission from Liu et al. (2012). Copyright (2012) American Chemical Society.

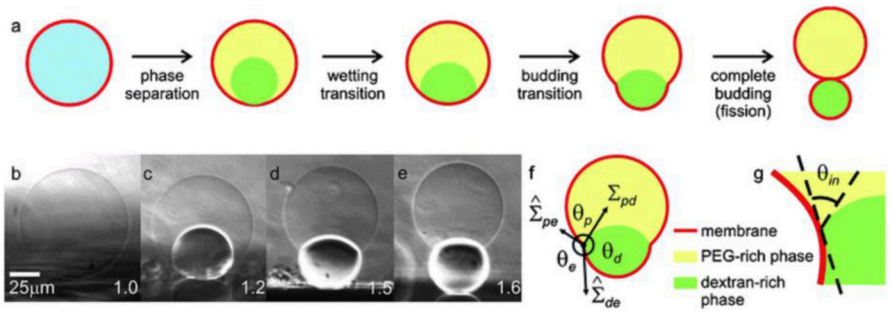


**FIGURE 9 |** Response of giant vesicles encapsulating ATPS when exposed to osmotic deflation. **(a)** Schematic illustration of the steps upon deflation: phase separation within the vesicle, wetting transition, vesicle budding, and fission of the enclosed phases into two membrane-wrapped droplets. **(b–e)** Side-view phase contrast images of a vesicle sitting on a glass substrate. The vesicle contains the PEG–dextran ATPS. After phase separation **(b,c)**, the interior solution consists of two liquid droplets consisting of PEG-rich and dextran-rich phases, respectively. Further deflation of the vesicle causes the dextran-rich droplet to bud out as shown in **(d,e)**. The numbers on the snapshots indicate the osmolarity ratio between the external medium and the initial internal polymer solution. In the sketch in **(f)**, the three effective contact angles as observed with optical microscopy are indicated, as well as the two membrane tensions and the interfacial tension $\Sigma_{pd}$. The contact line is indicated by the circled dot. The intrinsic contact angle $\theta_{in}$, which characterizes the wetting properties of the membrane by the PEG-rich phase at the nanometre scale, is sketched in **(g)**. Reproduced from Dimova and Lipowsky (2012) with permission from the Royal Society of Chemistry.

PEG in the one-phase region are encapsulated within GUVs (Li et al., 2011; Liu et al., 2016). In these studies, the polymer solutions undergo phase separation when the system is brought into two-phase region via osmotic deflation by exposing the vesicles to a hypertonic medium, i.e., vesicles deflation (note that the lipid membrane is permeable to water, but not to the polymers, which become concentrated as water permeates out). The deflation not only leads to a reduction of the vesicle volume and the formation of two immiscible aqueous phases within vesicles, but also generates excess area of the membrane. This results in a variety of interesting changes in the vesicle morphology, such as vesicle budding (Long et al., 2008; Li et al., 2012), wetting transition (Li et al., 2008; Kusumaatmaja et al., 2009), and complete budding of the vesicles (Andes-Koback and Keating, 2011) as schematically shown in **Figure 9a**. The overall vesicle shape can be observed from confocal microscopy cross sections of the vesicles, as well as from side-view phase-contrast images (**Figures 9b–e**) on a horizontally aligned microscope (Li et al., 2011; Liu et al., 2016).

Depending on the phase state of encapsulated ATPS and the interactions between the aqueous phases with the vesicle membrane, the liquid droplet may exhibit zero or non-zero contact angles corresponding, respectively, to complete or partial wetting. In the vicinity of the critical point, the membrane is completely wetted by the PEG-rich phase, while further away from this point, both phases partially wet the membranes. For GUV encapsulating PEG–dextran mixture, a complete-to-partial wetting transition had been observed for a number of lipid compositions (Li et al., 2008, 2011; Kusumaatmaja et al., 2009; Liu et al., 2016).

When the vesicle membrane becomes partially wetted by the aqueous phases, it is separated into two different segments: one is in contact with the PEG-rich phase, and the other with the dextran-rich phase. These two membrane segments and the pd

interface, i.e., the interface between the PEG-rich and dextran-rich phases, have spherical cap morphology. Then from the geometry of the vesicle, three effective contact angles $\theta_d$, $\theta_p$, and $\theta_e$ can be obtained, with $\theta_p+\theta_d+\theta_e = 2\pi$, as shown in **Figure 9f**. The force balance of the tensions (of the two membrane segments and the pd interface) at the three-phase contact line implies that the three tensions form a triangle, which leads to the relations (Kusumaatmaja et al., 2009; Li et al., 2011; Lipowsky, 2018):

$$\hat{\Sigma}_{pe} = \Sigma_{pd} \sin\theta_d / \sin\theta_e \quad (5)$$

$$\hat{\Sigma}_{de} = \Sigma_{pd} \sin\theta_p / \sin\theta_e \quad (6)$$

between these tensions and the effective contact angles. Here, $\hat{\Sigma}_{pe}$ is the tension of the pe membrane segment in contact with the PEG-rich phase, and $\hat{\Sigma}_{de}$ is the tension of the de membrane segment in contact with the dextran-rich phase; e describes the external phase outside the vesicle. The membrane tensions can then be calculated from the interfacial tension $\Sigma_{pd}$ as measured in section Interfacial Tension and Scaling Laws and the effective contact angles, which are obtained from the microscopy images.

When viewed with optical resolution, the shape of budded vesicles as in **Figures 9d,e** exhibits a kink at the three-phase contact line. However, the bending energy of the membrane kink would become infinite if it persists to smaller length scales (Kusumaatmaja et al., 2009). Therefore, the membrane in vicinity of the contact line should be smoothly curved when viewed with a super resolution microscopy (Zhao et al., 2018), which reveals the existence of an intrinsic contact angle $\theta_{in}$, as shown schematically in **Figure 9g** (Kusumaatmaja et al., 2009). If the two membrane segments have identical curvature-elastic properties, the force balance along the three phase contact line gives (Lipowsky, 2018)

$$\hat{\Sigma}_{de} - \hat{\Sigma}_{pe} = W_{de} - W_{pe} = \Sigma_{pd}\cos\theta_{in} \quad (7)$$

Here $W_{de}$ and $W_{pe}$ are adhesive strengths of the two membrane segments. Therefore, the intrinsic contact angle $\theta_{in}$ is related to three material parameters, the adhesive strengths $W_{de}$ and $W_{pe}$ and the interfacial tension of the liquid-liquid interface (Lipowsky, 2018). However, if the two membrane segments have the same elastic properties but different spontaneous curvatures, additional terms resulting from the different curvature-elastic properties emerges, and the truncated force balance relation as given by Equation (7) may lead to unreliable estimates for the intrinsic contact angle (Lipowsky, 2018).

## FORMATION OF MEMBRANE NANOTUBES IN VESICLE ENCAPSULATING ATPS

Osmotic deflation of giant vesicles enclosing PEG–dextran solutions, can lead to spectacular shape changes as evidenced by the formation of many membrane nanotubes protruding into the interior of the vesicle. Because the membrane is not pulled by an external force, the driving force for the spontaneous tubulation of vesicles is provided by a membrane tension generated from a substantial spontaneous curvature, which is much larger than the curvature of the GUV membranes. The spontaneous curvature is the preferred curvature the membrane would adopt when left at rest. It can be modulated by various factors such as leaflet compositional asymmetry, adsorption and depletion of molecular species and ions (Lipowsky, 2013; Bassereau et al., 2018). In the system considered here, the spontaneous curvature arising from the polymer-membrane interactions can be estimated using three different and independent methods of image analysis on the vesicle morphologies (Liu et al., 2016). A combination of experiment, theoretical analysis and computer simulation reveals the molecular mechanism for the membrane spontaneous curvature generated in the system of giant vesicles encapsulating ATPS.

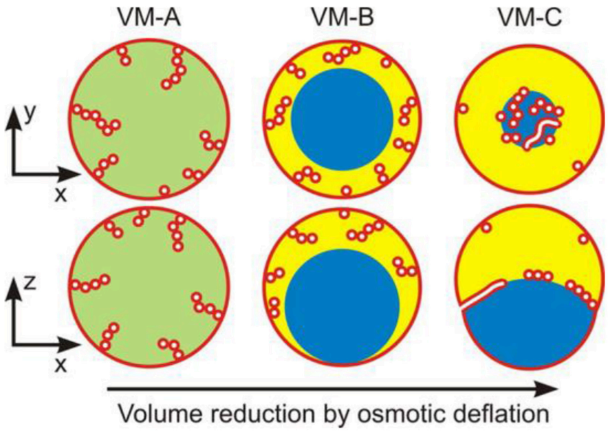


**FIGURE 10 |** Three nanotube patterns (VM-A, VM-B, and VM-C) corresponding to the distinct vesicle morphologies (VM) observed along the deflation path: Schematic views of horizontal *xy*-scans (top row) and of vertical *xz*-scans (bottom row) across the deflated vesicles. In all cases, the tubes are filled with external medium (white); the membrane is shown in red. For the VM-A morphology, the interior polymer solution is uniform (green), whereas it is phase-separated (blue and yellow) for the morphologies VM-B and VM-C, with complete and partial wetting, respectively, of the membrane by the PEG-rich aqueous phase (yellow). For the VM-B morphology, the nanotubes explore the whole PEG-rich (yellow) droplet but stay away from the dextran-rich one (blue). For the VM-C morphology, the nanotubes adhere to the interface between the two aqueous droplets forming a thin and crowded layer over this interface. It is expected that in the VM-A and VM-B morphologies, these nanotubes are necklace-like consisting of a number of small spheres connected by narrow or closed membrane necks, while in the VM-C morphology, cylindrical tubes with a uniform diameter along the nanotubes co-exist with the necklace-like ones. Reprinted with permission from Liu et al. (2016). Copyright (2016) American Chemical Society.

### Three Patterns of Flexible Nanotubes

Upon deflation of vesicles enclosing ATPS, three types of nanotube patterns have been observed, corresponding to three different vesicle shapes as schematically shown in **Figure 10** (Liu et al., 2016). These different morphologies can be observed upon osmotic deflation of the vesicles. In the example given in **Figure 10**, the membrane is composed of three lipid components: dioleoylphosphatidylcholine (DOPC), dipalmitoylphosphatidylcholine (DPPC), and cholesterol (Chol), which can exhibit different phase state depending on the exact

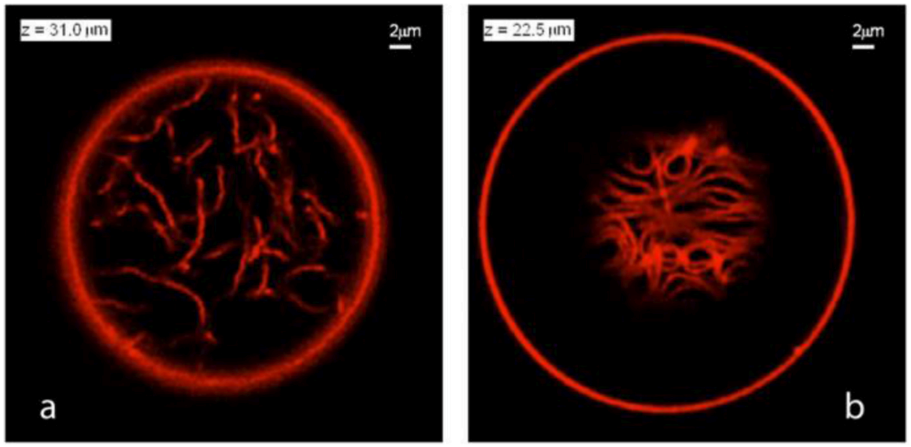


**FIGURE 11 |** Nanotube patterns within Ld-phase vesicles as observed for the VM-B and VM-C morphologies corresponding to complete and partial wetting of the membranes. **(a)** Disordered pattern corresponding to a confocal *xy*-scan of the VM-B morphology. Because the Ld membrane is completely wetted by the PEG-rich phase, the nanotubes explore the whole PEG-rich droplet but stay away from the dextran-rich phase located below the imaging plane. **(b)** A layer of densely packed tubes as visible in an *xy*-scan of the VM-C morphology. As a result of partial wetting, the nanotubes now adhere to the pd interface between the two aqueous droplets and form a thin layer in which crowding leads to short-range orientational order of the tubes. Note that the tube layer is only partially visible because the pd interface is curved into a spherical cap. Both in **(a,b)**, the diameter of the tubes is below the diffraction limit, but the tubes are theoretically predicted to have necklace-like and cylindrical shapes in panels **(a,b)**, respectively. Reprinted with permission from Liu et al. (2016). Copyright (2016) American Chemical Society.

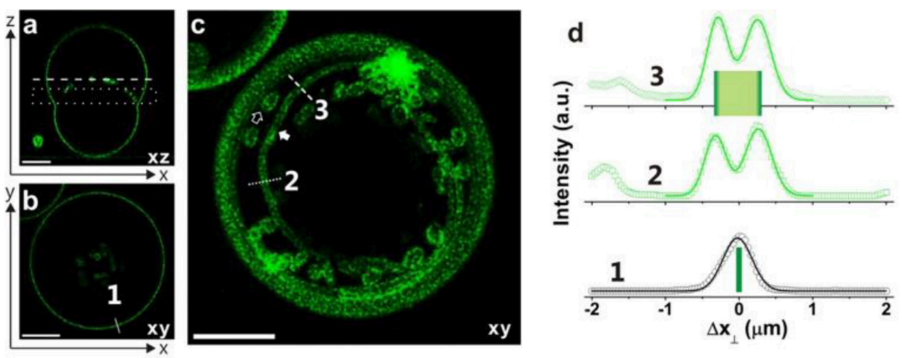


**FIGURE 12 |** Necklace-cylinder tube coexistence for giant vesicles with Lo membranes: **(a)** confocal *xz*-scan; **(b)** confocal *xy*-scan corresponding to the dashed line in panel a; **(c)** superposition of 6 confocal *xy*-scans located in the dotted rectangle in panel a. This projection image reveals the coexistence of several long cylindrical tubes and several short necklace-like tubes. All scale bars are 10 µm. **(d)** Fluorescent intensity along the solid white line 1 in panel **(b)** perpendicular to the GUV contour and along the dotted and dashed white lines 2 and 3 in panel **(c)** across a cylindrical tube. The quantity $\Delta x_\perp$ is the coordinate perpendicular to the GUV contour or membrane tube. The intensity profiles can be well-fitted by Gaussian distributions with a half-peak width of $0.35 \pm 0.05\,\mu$m. The peak-to-peak separations for the lines 2 and 3 lead to the estimated tube diameters $2R_{cy} = 0.58$ and $0.54\,\mu$m, respectively. Reprinted with permission from Liu et al. (2016). Copyright (2016) American Chemical Society.

composition. Bilayer phases such as the liquid-disordered (Ld) and liquid-ordered (Lo) phases and their coexistence can be directly observed as fluid domains in GUVs (Lipowsky and Dimova, 2003) using fluorescence microscopy (Dietrich et al., 2001). In the case of GUVs enclosing ATPS (Liu et al., 2016), we employed two different membrane compositions, corresponding to a Ld membrane with lipid composition DOPC:DPPC:Chol = 64:15:21 (mole fractions) and a Lo one with lipid composition DOPC:DPPC:Chol = 13:44:43 (see **Figures 11**, **12**), respectively. These two membranes are both in the single phase region and have different elastic property, with the bending rigidities $\kappa_{Ld} = 0.82 \times 10^{-19}$ J for the Ld membranes and $\kappa_{Lo} = 3.69 \times 10^{-19}$ J for the Lo membranes (Heinrich et al., 2010).

To obtain the observed morphologies, we prepare spherical vesicles that enclose a homogeneous solution of PEG–dextran mixture. Deflation of these vesicles is then induced by gradually exchanging the exterior solution to a hypertonic one containing fixed concentrations of the two polymer components with increasing amount of sucrose up to 15.6 mM. In this low concentration regime, the effect of sucrose on the bending rigidity and spontaneous curvature of the membranes can be neglected (Döbereiner et al., 1999; Vitkova et al., 2006; Lipowsky,

2013; Dimova, 2014). For more details of the experimental procedure, the readers are referred to the original article (Liu et al., 2016). Upon small deflation, the interior polymer solution still remains as a uniform aqueous phase with $c < c_{cr}$ (see VM-A morphology in **Figure 10**), but the area needed to enwrap the (reduced) volume of the vesicle is now in excess, which result in the formation of tubes (the excess area is stored in them). Subsequent deflation steps with $c > c_{cr}$, result in phase separation of the interior solution into two aqueous phases, a lighter PEG-rich and a heavier dextran-rich phase, both confined by the vesicles as liquid droplets. When the membrane is completely wetted by the PEG-rich droplet, the dewetted dextran-rich droplet is surrounded by the PEG-rich phase and has no contact with the membrane, which defines the VM-B morphology of the vesicles (**Figure 10**). The dextran-rich droplet sinks to the bottom of the vesicle because its density is always larger than the density of the coexisting PEG-rich phase (**Figure 3A**). Upon further deflation, both aqueous phases are in contact with the membranes, indicating a partial-wetting state of the two aqueous phases. This is defined as the VM-C morphology for the vesicles (**Figure 10**). The two membrane segments and the pd interface form non-zero contact angles (see **Figure 9f**). It is found that the complete-to-partial wetting transitions are located between different deflation steps for the Ld and Lo membranes, reflecting different wetting property of ATPS on these membranes.

Due to the different wetting properties of the aqueous phases on the membranes, different nanotube patterns formed in the VM-B and VM-C morphologies are observed by the confocal microscope (see **Figure 11**). For the complete wetting morphology VM-B, these nanotubes explore the interior of the whole PEG-rich droplet, and undergo strong thermally excited undulations. The length of the individual nanotubes can be estimated from stack of three-dimensional scans of the vesicles, which is on the order of 20 μm for Ld vesicles. For the partial wetting morphology VM-C, these nanotubes adhere to the pd interface between the two liquid droplets, where one can immediately see the long tube segments in a single scan. The local adhesion of the nanotubes to the liquid-liquid interface is a reflection of the complete-to-partial wetting transition.

These nanotubes can be either necklace-like consisting of a number of small spheres connected by narrow or closed membrane necks or cylindrical with a uniform diameter along the nanotube (**Figure 10**). Theoretical investigation of the nucleation and growth of the tubes indicated that these membrane nanotubes prefer necklace-like shape at short length but cylindrical one above a critical length, which can be understood by minimization of the membrane bending energy (Liu et al., 2016). The necklace-cylinder transformation occurs at the critical tube length of about three times of the mother vesicle radius, and the tubes can reshape themselves via a series of intermediate unduloids (Liu et al., 2016). For the partial wetting morphology VM-C, due to additional contribution from adhesion free energy of the tubes at the pd interface, the critical length for necklace-cylinder transformation depends on the material parameters and can become as low as a few micrometers. Therefore, the shape of the Ld tubes in the VM-A and VM-B morphologies are predicted to be necklace-like, but a co-existence of necklace-like and cylindrical shape is expected for Ld tubes in the VM-C morphology. In contrast, the tubes of the stiffer Lo membranes are so thick that their shapes can be directly observed from the confocal images. Necklace-like shape tubes are observed for all three morphologies of the Lo vesicles. Surprisingly, the confocal images in **Figure 12** revealed the co-existence of several long cylindrical tubes and a few short necklace-like tubes at the pd interface. The length of these cylindrical tubes is above the critical length for the necklace–cylinder transformation.

## Spontaneous Curvatures of Vesicle Enclosing ATPS

Several approaches for deducing the membrane spontaneous curvature have been developed in Li et al. (2011), Lipowsky (2013, 2014), Liu et al. (2016), Bhatia et al. (2018), and Dasgupta et al. (2018), some of which have been reviewed in section Measuring the Membrane Spontaneous Curvature of Bassereau et al. (2018). Stable membrane nanotubes were first observed for vesicles encapsulating ATPS in Li et al. (2011), and the theoretical analysis of the corresponding GUV shapes revealed the presence of a negative spontaneous curvature of about −1/(240 nm). We then developed three different and independent methods to determine this curvature based on image analysis of tubulated vesicles made of both Ld and Lo membranes (Liu et al., 2016). As shown in **Figure 13**, all these methods led to consistent values of the spontaneous curvatures for both Ld and Lo vesicles of three different morphologies.

The first method is based on direct measurement of the tube thickness by confocal microscopy. For the Lo membranes, the tubes have diameters well above the optical resolution, which made it possible to measure the tube size directly from the confocal scans. Short necklace-like tubes are observed for

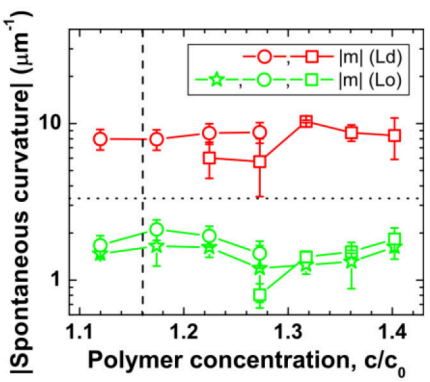


**FIGURE 13 |** Variation of deduced spontaneous curvature of Ld (red) and Lo (green) membranes with polymer concentration modulated by osmotic deflation of the vesicles. The vertical dashed lines correspond to the critical concentration $c_{cr}$. The data were obtained by direct shape analysis of the nanotubes (green stars), area partitioning analysis as given by Equation (8) (open circles), and force balance analysis described by Equation (9) (open squares). The horizontal dotted line corresponds to the optical resolution limit of 1/(300 nm). Reprinted with permission from Liu et al. (2016). Copyright (2016) American Chemical Society.

all Lo vesicles in the VM-A and VM-B morphologies, which leads to the estimate of the spontaneous curvature via $m = -1/<R_{ss}>$. The relative standard deviation of the radius $R_{ss}$ for the quasi-spherical beads is about 20%. The direct shape analysis is also applicable for Lo tubes in the VM-C morphology where the cylindrical tubes co-exist with the necklace-like ones. For the vesicles shown in **Figure 12**, measurement of the average diameter $<2R_{cy}>$ of the cylindrical tubes leads to the spontaneous curvature $m = -1/<2R_{cy}> = -1.82\ \mu m^{-1}$, with an accuracy of about ±13%. While measurement of the average bead radius $<R_{ss}>$ of the necklace-like tubes gives the estimation of $m = -1/<R_{ss}> = -1.56\ \mu m^{-1}$, having an uncertainty of about ±19%. Interestingly, nearly identical $m$-values for the cylindrical and necklace-like tubes formed from the same vesicle are obtained, indicating the uniformity of the membrane spontaneous curvature. Thus, the spontaneous curvatures of Lo membranes are determined by the direct shape analysis for all vesicle morphologies, and the results are shown in **Figure 13** as green stars. This method is, however, not applicable for Ld tubes, because they are so thin that their shape is not resolvable by the confocal microscope.

The second method is based on the membrane area partitioning between nanotubes and the mother vesicle. The shapes of the nanotubes for Ld vesicles cannot be resolved by confocal microscope because the tube diameter is below the optical resolution. But we can calculate the spontaneous curvature via two measurable geometric quantities: the area $A$ and length $L$ of all tubes. It is based on the fact that the excess area generated by deflation is stored as nanotubes. Upon deflation, the vesicle apparent area $A_{app}$ is less than the initial vesicle area $A_0$, both areas can be obtained from the vesicle shape and their difference ($A_0 - A_{app}$) is the missing area stored as tubes. While the length $L$ can be measured from 3D scans of the vesicle by confocal microscope. Then the spontaneous curvature of the membrane can be estimated via (Liu et al., 2016):

$$m = -(2 - \Lambda)\,\pi L/A \tag{8}$$

Here $\Lambda$ is the fraction of the total tube length in cylindrical shape, and the rest part is necklace-like.

For short necklace-like tubes observed for all Lo vesicles in the VM-A and VM-B morphologies, $\Lambda = 0$ is obtained. For Lo tubes in the VM-C morphology with a co-existence of the cylindrical and necklace-like tubes, non-zero $\Lambda$-value is observed. However, for the Ld tubes with thickness below the optical resolution, the fraction $\Lambda$ cannot be estimated from the confocal images. These flexible Ld tubes in the VM-A and VM-B morphologies are predicted to be necklace-like, which leads to $\Lambda = 0$. For Ld tubes in the VM-C morphology, a co-existence of the cylindrical and necklace-like tubes is expected, but one cannot estimate the fraction $\Lambda$. In this case, we have to take all possible $\Lambda$-values into account. The spontaneous curvatures for the Ld membranes are then estimated using Equation (8) with $\Lambda = 0$ for VM-A and VM-B morphologies and $0 \leq \Lambda \leq 1$ for VM-C morphology. The $m$-values obtained by area partitioning analysis for both Lo and Ld membranes are shown in **Figure 13** as green and red circles, respectively. The accuracy of this method is ±15%, resulting mainly from the uncertainty of the measured tube length $L$. It should be noted that when the tubes are too crowded at the pd interface for the highest polymer concentrations of VM-C morphology, it becomes rather difficult to estimate the total tube length and then this method is not applicable.

For the VM-C morphologies, where two membrane segments and the pd interface form non-zero contact angles due to partial wetting of the aqueous phases, the membrane spontaneous curvature can be estimated via a third method based on force balance of the tensions at the three-phase contact line. Since the tubes are always protruded into the PEG-rich phase and adhere to the liquid-liquid interface for VM-C morphology, one can estimate the spontaneous curvature via (Lipowsky, 2013, 2014; Liu et al., 2016):

$$m = -\left(\frac{\Sigma_{pd}}{2\kappa}\frac{\sin\theta_d}{\sin\theta_e}\right)^{1/2} \tag{9}$$

Here $\kappa$ is the bending rigidity of membrane. One can calculate the $m$-values for both Lo and Ld membranes, with the separately measured interfacial tension $\Sigma_{pd}$, the effective contact angles $\theta_d$ and $\theta_e$, and the bending rigidities $\kappa_{Lo}$ and $\kappa_{Ld}$ (Heinrich et al., 2010). The obtained results are shown in **Figure 13** as green and red squares, respectively. It is obvious that all three modes of image analysis led to consistent values for the spontaneous curvatures of these membranes.

It should be noted that the spontaneous curvatures of these two membranes were found to be almost constant, with $m_{Ld} \cong -8\ \mu m^{-1}$ and $m_{Lo} \cong -1.7\ \mu m^{-1}$ over the range of studied polymer concentrations. Their spontaneous curvature ratio of $m_{Ld}/m_{Lo} \cong 4.7$ is nearly identical to their bending rigidity ratio of $\kappa_{Lo}/\kappa_{Ld} \cong 4.5$. The observed inverse proportionality between the spontaneous curvature and the bending rigidity is in accord with the generation of these curvatures by adsorption, as shown in next section.

## Molecular Mechanism of Curvature Generation in Vesicles Enclosing ATPS

Because the formation of nanotubes in the GUVs was observed only in the presence of polymers, the spontaneous curvature of the vesicle membranes should be generated by the interactions between membrane and the encapsulated polymers. Depending on the effectively attractive or repulsive force with the membranes, polymer molecules can form either adsorption or depletion layers on the membrane, and result in bulging of the lipid bilayer toward the solution with higher concentration of polymer adsorption or lower concentration of polymer depletion.

In all three vesicle morphologies shown in **Figure 10**, the concentration of PEG in the interior solution is always larger than that in the exterior solution. However, the concentration of dextran in the interior solution is larger for VM-A morphology but smaller for VM-B and VM-C morphologies than the exterior dextran concentration. At the same time, all deflation steps led to the formation of tubes protruding into the interior of vesicles with a negative spontaneous curvature. Therefore, the observation is consistent with the theoretical prediction (Breidenich et al., 2005), only if the spontaneous curvature is generated by adsorption of PEG onto the membrane. This

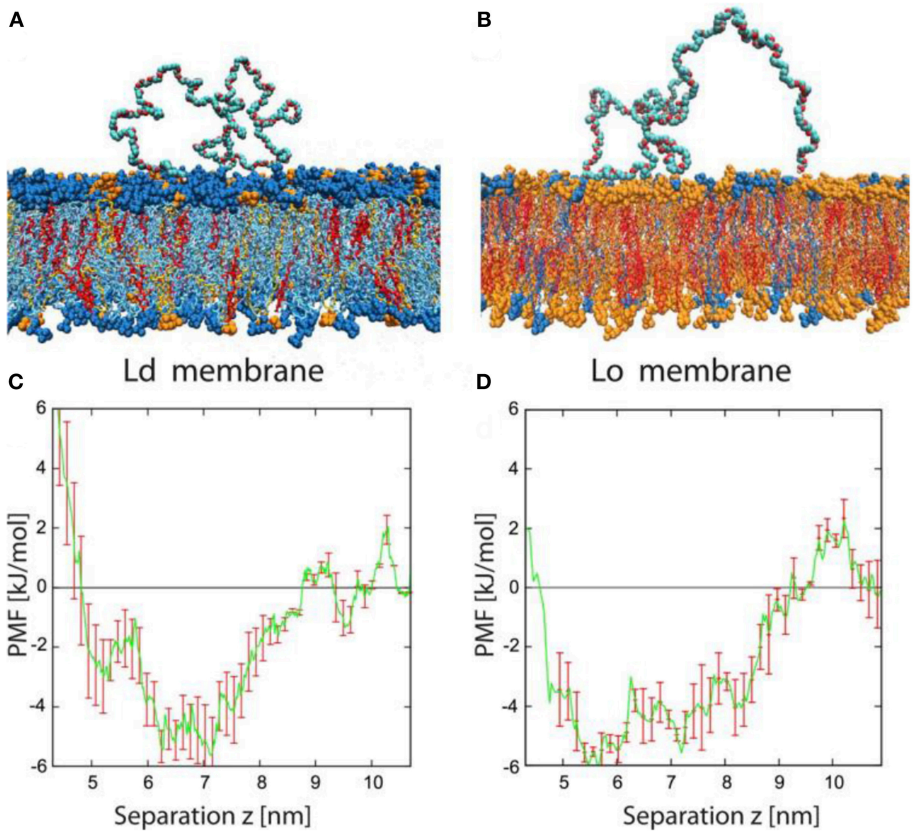


**FIGURE 14 |** Typical conformation and potential of mean force for adsorbed PEG molecules. **(A,B)** Simulation snapshots of PEG molecule adsorbed onto Ld and Lo bilayer. The color code for the lipids is blue for DOPC, orange for DPPC, and red for cholesterol. The PEG molecules consist of 180 monomers corresponding to the average molecular weight used in the experiments. Each lipid membrane is immersed in about 27,000 water molecules (not shown). **(C,D)** Potential of mean force (PMF) for Ld and Lo membranes as a function of the separation $z$ between the polymer's center-of-mass and the bilayer midplane. The potential wells are relatively broad, with a width of about 4 nm, because the polymer end groups can adsorb even for relatively large $z$-values. The binding free energy of a single PEG chain is about 4 kJ/mol or 1.6 $k_BT$ for both types of membranes. Reprinted with permission from Liu et al. (2016). Copyright (2016) American Chemical Society.

conclusion was supported by control experiments with both Ld and Lo vesicles enclosing pure PEG solution without dextran. Deflation of these vesicles led to nanotubes protruding into the interior of the vesicles with higher PEG concentration.

To further elucidate conformations of the PEG chains adsorbed on the membranes and the role of PEG-membrane interactions on the curvature generation of the membranes, we performed atomistic molecular dynamics simulations on the same hybrid lipid-polymer systems as in the experiments (Liu et al., 2016). Typical conformations of the PEG molecules adsorbed onto the Ld and Lo membranes are shown in **Figures 14A,B**. It indicated that PEG chains are only weakly bound to the membranes, with long loops dangled between some short adsorption segments. It is often observed that the PEG chain binds to the membrane by hydrogen bonds formed between the two terminal OH groups and the head groups of the lipid. Less frequently, a few contacts form between the PEG backbones and the membranes. The affinity of the PEG molecules to the membranes is further quantified by the potentials of mean force, as shown in **Figures 14C,D**. It indicated that the studied PEG chains have the same binding affinity to the Ld and Lo membranes, with a relatively small binding energy of about 4 kJ/mol or 1.6 $k_BT$ per PEG molecule. It is consistent with the experimental results where the spontaneous curvature ratio $m_{Ld}/m_{Lo}$ is equal to the bending rigidity ratio $\kappa_{Lo}/\kappa_{Ld}$.

## CONCLUSIONS

In summary, we discussed the model system of GUVs encapsulating ATPS emphasizing aspects of both polymer physics and membrane biophysics, highlighting recent results from our groups.

We illustrated how the phase diagram for ATPS of dextran and PEG can be constructed by cloud titration and presented methods based on density and GPC measurements of the coexisting phases. The ultralow interfacial tension between the coexisting phases was studied over a broad polymer concentration range above the critical point. It was found that the scaling exponent of the interfacial tension with the reduced polymer concentration gives a value of 1.67 in vicinity of the critical point, which disagrees with the expected value 1.26 for the

Ising model. The latter discrepancy arises from the molar mass fractionation of dextran during phase separation.

When encapsulating these ATPS into giant vesicles, the membranes may be completely or partially wetted by the two aqueous phases, depending on the lipid and polymer composition. A complete-to-partial wetting transition of ATPS is observed via osmotic deflation of the vesicle volume. The associated volume reduction generates excess area of the membrane, which folds into many membrane nanotubes protruding into the interior vesicle compartment revealing a substantial asymmetry and negative spontaneous curvature of the membranes. Quantitative estimates of the spontaneous curvature have been obtained in Liu et al. (2016) by three different and independent methods of image analysis. The spontaneous curvature is generated by the weak PEG adsorption onto the lipid membranes, with a binding affinity of about 1.6 $k_BT$ per PEG molecule for either liquid-ordered or liquid-disordered membranes, based on molecular dynamics simulation.

Membrane nanotubes are also observed in the living cells, for example in the Golgi apparatus and the smooth endoplasmic reticulum. However, the underlying mechanism for the tube formation in cells remains to be elucidated. The cellular membranes are often exposed to asymmetric aqueous environments with a large amount of proteins, which plays central role in the tubulation process. The model system of GUV encapsulating ATPS provides a controllable platform for understanding the remodeling of membranes in the living cells. It would be interesting to include proteins in the GUV/ATPS system to mimic the cellular behavior more closely.

## AUTHOR CONTRIBUTIONS

All authors listed have made a substantial, direct and intellectual contribution to the work, and approved it for publication.

## FUNDING

This work was funded by the Partner Group Program of the Max Planck Society and the Chinese Academy of Sciences, and the National Natural Science Foundation of China (21774125).

## REFERENCES

Albertsson, P. Å. (1986). *Partition of Cell Particles and Macromolecules: Separation and Purification of Biomolecules, Cell Organelles, Membranes, and Cells in Aqueous Polymer Two-Phase Systems and Their Use in Biochemical Analysis and Biotechnology*. New York, NY: Wiley.

Andes-Koback, M., and Keating, C. D. (2011). Complete budding and asymmetric division of primitive model cells to produce daughter vesicles with different interior and membrane compositions. *J. Am. Chem. Soc.* 133, 9545–9555. doi: 10.1021/ja202406v

Anisimov, M. A., Agayan, V. A., and Gorodetskii, E. E. (2000). Scaling and crossover to tricriticality in polymer solutions. *JETP Lett.* 72, 578–582. doi: 10.1134/1.1348485

Anisimov, M. A., Kostko, A. F., and Sengers, J. V. (2002). Competition of mesoscales and crossover to tricriticality in polymer solutions. *Phys. Rev. E* 65, 051805. doi: 10.1103/PhysRevE.65.051805

Atefi, E., Mann, J. A., and Tavana, H. (2014). Ultralow interfacial tensions of aqueous two-phase systems measured using drop shape. *Langmuir* 30, 9691–9699. doi: 10.1021/la500930x

Bassereau, P., Jin, R., Baumgart, T., Deserno, M., Dimova, R., Frolov, V. A., et al (2018). The 2018 biomembrane curvature and remodeling roadmap. *J. Phys. D Appl. Phys.* 51, 343001. doi: 10.1088/1361-6463/aacb98

Bhatia, T., Agudo-Canalejo, J., Dimova, R., and Lipowsky, R. (2018). Membrane nanotubes increase the robustness of giant vesicles. *ACS Nano* 12, 4478–4485. doi: 10.1021/acsnano.8b00640

Breidenich, M., Netz, R., and Lipowsky, R. (2005). The influence of non-anchored polymers on the curvature of vesicles. *Mol. Phys.* 103, 3169–3183. doi: 10.1080/00268970500270484

Connemann, M., Gaube, J., Leffrang, U., Muller, S., and Pfennig, A. (1991). Phase equilibria in the system poly(ethylene glycol) + dextran + water. *J. Chem. Eng. Data* 36, 446–448. doi: 10.1021/je00004a029

Dasgupta, R., Miettinen, M., Fricke, N., Lipowsky, R., and Dimova, R. (2018). The glycolipid GM1 reshapes asymmetric biomembranes and giant vesicles by curvature generation. *Proc. Natl. Acad. Sci. U.S.A.* 115, 5756–5761. doi: 10.1073/pnas.1722320115

Dietrich, C., Bagatolli, L. A., Volovyk, Z. N., Thompson, N. L., Levi, M., Jacobson, K., et al. (2001). Lipid rafts reconstituted in model membranes. *Biophys. J.* 80, 1417–1428. doi: 10.1016/S0006-3495(01)76114-0

Dimova, R. (2012). "Giant vesicles: a biomimetic tool for membrane characterization," in *Advances in Planar Lipid Bilayers and Liposomes*, ed A. Iglic (Amsterdam: Academic Press), 1–50.

Dimova, R. (2014). Recent developments in the field of bending rigidity measurements on membranes. *Adv. Coll. Interf. Sci.* 208, 225–234. doi: 10.1016/j.cis.2014.03.003

Dimova, R. (2019). Giant vesicles and their use in assays for assessing membrane phase state, curvature, mechanics and electrical properties. *Annu. Rev. Biophys.* 48:1. doi: 10.1146/annurev-biophys-052118-115342

Dimova, R., Aranda, S., Bezlyepkina, N., Nikolov, V., Riske, K. A., and Lipowsky, R. (2006). A practical guide to giant vesicles. Probing the membrane nanoregime via optical microscopy. *J. Phys. Condens. Matter* 18, S1151–S1176. doi: 10.1088/0953-8984/18/28/S04

Dimova, R., and Lipowsky, R. (2012). Lipid membranes in contact with aqueous phases of polymer solutions. *Soft Matter* 8, 6409–6415. doi: 10.1039/c2sm25261a

Dimova, R., and Lipowsky, R. (2017). Giant vesicles exposed to aqueous two-phase systems: membrane wetting, budding processes, and spontaneous tubulation. *Adv. Mater. Interfaces* 4, 1600451. doi: 10.1002/admi.201600451

Ding, P., Wolf, B., Frith, W. J., Clark, A. H., Norton, I. T., and Pacek, A. W. (2002). Interfacial tension in phase-separated gelation/dextran aqueous mixtures. *J. Colloid Interface Sci.* 253, 367–376. doi: 10.1006/jcis.2002.8572

Dobashi, T., Nakata, M., and Kaneko, M. (1980). Coexistence curve of polystyrene in methylcyclohexane. 2. Comparison of coexistence curve observed and calculated from classical free-energy. *J. Chem. Phys.* 72, 6692–6697. doi: 10.1063/1.439128

Döbereiner, H. G., Selchow, O., and Lipowsky, R. (1999). Spontaneous curvature of fluid vesicles induced by trans-bilayer sugar asymmetry. *Eur. Biophys. J.* 28, 174–178. doi: 10.1007/s002490050197

Edelman, M. W., Tromp, R. H., and van der Linden, E. (2003a). Phase-separation-induced fractionation in molar mass in aqueous mixtures of gelatin and dextran. *Phys. Rev. E* 67, 021404. doi: 10.1103/PhysRevE.67.021404

Edelman, M. W., van der Linden, E., and Tromp, R. H. (2003b). Phase separation of aqueous mixtures of poly(ethylene oxide) and dextran. *Macromolecules* 36, 7783–7790. doi: 10.1021/ma0341622

Flory, P. J. (1941). Thermodynamics of high polymer solutions. *J. Chem. Phys.* 9, 660–661. doi: 10.1063/1.1750971

Flory, P. J. (1953). *Principles of Polymer Chemistry*. Ithaca: Cornell University Press.

Hatti-Kaul, R. (2000). *Methods in Biotechnology, Vol. 11, Aqueous Two-Phase Systems: Methods and Protocols*. Totowa: Humana Press.

Heinrich, M., Tian, A., Esposito, C., and Baumgart, T. (2010). Dynamic sorting of lipids and proteins in membrane tubes with a moving phase boundary. *Proc. Natl. Acad. Sci. U.S.A.* 107, 7208–7213. doi: 10.1073/pnas.0913997107

Heinrich, M., and Wolf, B. A. (1992). Interfacial tension between solutions of polystyrenes: establishment of a useful master curve. *Polymer* 33, 1926–1931. doi: 10.1016/0032-3861(92)90494-H

Helfrich, M. R., Mangeney-Slavin, L. K., Long, M. S., Djoko, K. Y., and Keating, C. D. (2002). Aqueous phase separation in giant vesicles. *J. Am. Chem. Soc.* 124, 13374–13375. doi: 10.1021/ja028157+

Huggins, M. L. (1941). Solutions of long chain compounds. *J. Chem. Phys.* 9, 440. doi: 10.1063/1.1750930

Kang, C. H., and Sandler, S. I. (1988). Effects of polydispersivity on the phase behavior of the aqueous two-phase polymer systems. *Macromolecules* 21, 3088–3095. doi: 10.1021/ma00188a029

Keating, C. D. (2012). Aqueous phase separation as a possible route to compartmentalization of biological molecules. *Acc. Chem. Res.* 45, 2114–2124. doi: 10.1021/ar200294y

Koningsveld, R., Stockmayer, W. H., and Nies, E. (2001). *Polymer Phase Diagrams*. New York, NY: Oxford University Press.

Kusumaatmaja, H., Li, Y., Dimova, R., and Lipowsky, R. (2009). Intrinsic contact angle of aqueous phases at membranes and vesicles. *Phys. Rev. Lett.* 103, 238103. doi: 10.1103/PhysRevLett.103.238103

Li, Y., Kusumaatmaja, H., Lipowsky, R., and Dimova, R. (2012). Wetting-induced budding of vesicles in contact with several aqueous phases. *J. Phys. Chem. B* 116, 1819–1823. doi: 10.1021/jp211850t

Li, Y., Lipowsky, R., and Dimova, R. (2008). Transition from complete to partial wetting within membrane compartments. *J. Am. Chem. Soc.* 130, 12252–12253. doi: 10.1021/ja8048496

Li, Y., Lipowsky, R., and Dimova, R. (2011). Membrane nanotubes induced by aqueous phase separation and stabilized by spontaneous curvature. *Proc. Natl. Acad. Sci. U.S.A.* 108, 4731–4736. doi: 10.1073/pnas.1015892108

Lipowsky, R. (2013). Spontaneous tubulation of membranes and vesicles reveals membrane tension generated by spontaneous curvature. *Faraday Discuss.* 161, 305–331. doi: 10.1039/c2fd20105d

Lipowsky, R. (2014). Remodeling of membrane compartments: some consequences of membrane fluidity. *Biol. Chem.* 395, 253–274. doi: 10.1515/hsz-2013-0244

Lipowsky, R. (2018). Response of membranes and vesicles to capillary forces arising from aqueous two-phase systems and water-in-water droplets. *J. Phys. Chem. B* 122, 3572–3586. doi: 10.1021/acs.jpcb.7b10783

Lipowsky, R., and Dimova, R. (2003). Domains in membranes and vesicles. *J. Phys. Condens. Matter* 15, S31–S45. doi: 10.1088/0953-8984/15/1/304

Liu, Y., Agudo-Canalejo, J., Grafmüller, A., Dimova, R., and Lipowsky, R. (2016). Patterns of flexible nanotubes formed by liquid-ordered and liquid-disordered membranes. *ACS Nano* 10, 463–474. doi: 10.1021/acsnano.5b05377

Liu, Y., Lipowsky, R., and Dimova, R. (2012). Concentration dependence of the interfacial tension for aqueous two-phase polymer solutions of dextran and polyethylene glycol. *Langmuir* 28, 3831–3839. doi: 10.1021/la204757z

Long, M. S., Cans, A. S., and Keating, C. D. (2008). Budding and asymmetric protein microcompartmentation in giant vesicles containing two aqueous phases. *J. Am. Chem. Soc.* 130, 756–762. doi: 10.1021/ja077439c

Long, M. S., Jones, C. D., Helfrich, M. R., Mangeney-Slavin, L. K., and Keating, C. D. (2005). Dynamic microcompartmentation in synthetic cells. *Proc. Natl. Acad. Sci. U.S.A.* 102, 5920–5925. doi: 10.1073/pnas.0409333102

Melnichenko, Y. B., Anisimov, M. A., Povodyrev, A. A., Wignall, G. D., Sengers, J. V., and van Hook, W. A. (1997). Sharp crossover of the susceptibility in polymer solutions near the critical demixing point. *Phys. Rev. Lett.* 79, 5266–5269. doi: 10.1103/PhysRevLett.79.5266

Merchuk, J. C., Andrews, B. A., and Asenjo, J. A. (1998). Aqueous two-phase systems for protein separation studies on phase inversion. *J. Chromatogr. B* 711, 285–293. doi: 10.1016/S0378-4347(97)00594-X

Mishima, K., Matsuyama, K., Ezawa, M., Taruta, Y., Takarabe, S., and Nagatani, M. (1998). Interfacial tension of aqueous two-phase systems containing poly(ethylene glycol) and dipotassium hydrogenphosphate. *J. Chromatogr. B* 711, 313–318. doi: 10.1016/S0378-4347(97)00660-9

Ryden, J., and Albertsson, P. A. (1971). Interfacial tension of dextran-polyethylene glycol-water two-phase systems. *J. Colloid Interface Sci.* 37, 219–222. doi: 10.1016/0021-9797(71)90283-9

Sanchez, I. C. (1989). Critical amplitude scaling laws for polymer solutions. *J. Phys. Chem.* 93, 6983–6991. doi: 10.1021/j100356a021

Shinozaki, K., Vantan, T., Saito, Y., and Nose, T. (1982). Interfacial tension of demixed polymer solutions near the critical temperature: polystyrene + methylcyclohexane. *Polymer* 23, 728–734. doi: 10.1016/0032-3861(82)90059-3

Tromp, R. H. (2016). "Water-water interphases," in *Soft Matter at Aqueous Interfaces. Lecture Notes in Physics*, eds P. Lang, Y. Liu (Cham: Springer), 159–186.

van Heukelum, A., Barkema, G. T., Edelman, M. W., van der Linden, E., de Hoog, E. H. A., and Tromp, R. H. (2003). Fractionation in a phase-separated polydisperse polymer mixtures. *Macromolecules* 36, 6662–6667. doi: 10.1021/ma025736q

Vis, M., Peters, V. F. D., Blokhuis, E. M., Lekkerkerker, H. N. W., Erne, B. H., and Tromp, R. H. (2015). Effects of electric charge on the interfacial tension between coexisting aqueous mixtures of polyelectrolyte and neutral polymer. *Macromolecules* 48, 7335–7345. doi: 10.1021/acs.macromol.5b01675

Vitkova, V., Genova, J., Mitov, M. D., and Bivas, I. (2006). Sugars in the aqueous phase change the mechanical properties of lipid mono- and bilayers. *Mol. Cryst. Liq. Cryst.* 449, 95–106. doi: 10.1080/15421400600582515

Walde, P., Cosentino, K., Engel, H., and Stano, P. (2010). Giant vesicles: preparations and applications. *ChemBioChem* 11, 848–865. doi: 10.1002/cbic.201000010

Walter, H., Brooks, D. E., and Fisher, D. (1985). *Partitioning in Aqueous Two-phase Systems: Theory, Methods, Uses, and Applications to Biotechnology*. Orlando: Academic Press.

Widom, B. (1993). Phase separation in polymer solutions. *Phys. A* 194, 532–541. doi: 10.1016/0378-4371(93)90383-F

Zaslavski, B. Y. (1995). *Aqueous Two-Phase Partitioning: Physical Chemistry and Bioanalytical Applications*. New York, NY: Marcel Dekker.

Zhao, Z., Li, Q., Ji, X., Dimova, R., Lipowsky, R., and Liu, Y. (2016a). Molar mass fractionation in aqueous two-phase polymer solutions of dextran and poly(ethylene glycol). *J. Chromatogr. A* 1452, 107–115. doi: 10.1016/j.chroma.2016.04.075

Zhao, Z., Li, Q., Xue, Y., Ji, X., Bo, S., and Liu, Y. (2016b). Composition and molecular weight determination of aqueous two-phase system by quantitative size exclusion chromatography, *Chem. J. Chin. Univ.* 37, 167–173. doi: 10.7503/cjcu20150567

Zhao, Z., Roy, D., Steinkühler, J., Robinson, T., Knorr, R., Lipowsky, R., et al. (2018). Super resolution imaging of highly curved membrane structures in giant unilamellar vesicles encapsulating polymer solutions. *Biophys. J.* 114, 100a−101a. doi: 10.1016/j.bpj.2017.11.591

**Conflict of Interest Statement:** The authors declare that the research was conducted in the absence of any commercial or financial relationships that could be construed as a potential conflict of interest.

The reviewer PS declared a past co-authorship with one of the authors RD to the handling editor.

frontiers in Chemistry

METHODS
published: 22 May 2019
doi: 10.3389/fchem.2019.00311

# Stigmatic Microscopy Enables Low-Cost, 3D, Microscale Particle Imaging Velocimetry in Rehydrating Aqueous Two-Phase Systems

*Cameron Yamanishi*[1,2†], *C. Ryan Oliver*[2,3†], *Taisuke Kojima*[1] *and Shuichi Takayama*[1,2,4*]

[1] The Wallace H Coulter Department of Biomedical Engineering, Georgia Institute of Technology and Emory School of Medicine, Atlanta, GA, United States, [2] Department of Biomedical Engineering, University of Michigan, Ann Arbor, MI, United States, [3] Department of Internal Medicine, University of Michigan, Ann Arbor, MI, United States, [4] The Parker H Petit Institute for Bioengineering and Bioscience, Georgia Institute of Technology, Atlanta, GA, United States

This paper describes the construction of a novel stigmatic microscope and image analysis algorithm to simultaneously analyze convective mixing both inside and outside of rehydrating μL-scale aqueous two-phase system (ATPS) droplets. Stigmatic microscopy is inexpensive and advantageous because it modifies the point-spread function of fluorescent particles to enable measurement of their 3D positions from single 2D images, without needing to take slices. In one application of the technique, the convection patterns captured clarify how different ATPS formulations succeed or fail to exclude cells for patterning. Particle flow traces reveal speed and directionality of circulation, indicating temporary eddies at the outer edge of the rehydrating droplet. In another application, the speed of circulation during rehydration was analyzed for different ATPS formulations and the results used to develop a new fast ELISA procedure. While this paper focuses on ATPS rehydration, the microscope and algorithm should be applicable to a broad range of microfluidic flows where microscale 3D convection is important.

**Keywords: ATPS, rehydration, convection, ELISA, particle imaging velocimetry, stigmatic microscope, micropatterning**

OPEN ACCESS

***Edited by:***
*Brendan M. Leung,*
*Dalhousie University, Canada*

***Reviewed by:***
*Antti Ilmari Koponen,*
*VTT Technical Research Centre of Finland Ltd, Finland*
*Takahiko Ban,*
*Osaka University, Japan*

***Correspondence:**
*Shuichi Takayama*
*takayama@gatech.edu*

*†These authors have contributed equally to this work*

***Specialty section:***
*This article was submitted to Chemical Engineering, a section of the journal Frontiers in Chemistry*

***Received:*** *24 August 2018*
***Accepted:*** *18 April 2019*
***Published:*** *22 May 2019*

***Citation:***
*Yamanishi C, Oliver CR, Kojima T and Takayama S (2019) Stigmatic Microscopy Enables Low-Cost, 3D, Microscale Particle Imaging Velocimetry in Rehydrating Aqueous Two-Phase Systems. Front. Chem. 7:311. doi: 10.3389/fchem.2019.00311*

## INTRODUCTION

Aqueous two-phase systems (ATPS) can form when immiscible polymers are mixed in water. In these systems, many cells and biomolecules partition preferentially and predictably into one phase or the other (Per-Ake, 1960). These characteristics enable separation and compartmentalization of biomolecules (Hatti-Kaul, 2001; Rito-Palomares, 2004; Iqbal et al., 2016). ATPS-assisted techniques have harnessed these characteristics to address several emerging applications such as reagent delivery to cells (Tavana et al., 2009), bacterial patterning (Yaguchi et al., 2010) and sensing (Byun et al., 2013), and selective immuno-staining of cells (Frampton et al., 2015). They have been designed using dehydrated reagents, which initiate the assay upon rehydration (Frampton et al., 2014; Eiden et al., 2016). The rehydration process of ATPS droplets may dictate reagent mixing and influence the overall assay performance (Bathany et al., 2013; Lee et al., 2016). However, the dynamic behavior of the convection within rehydrating ATPS micro-droplets has been difficult to measure (Ban et al., 2016; Bansal et al., 2017). Due to this, many ATPS-assisted applications remain in the nascent development phase, lacking consensus design principles.

The ability to measure internal convective flow would prove important in the process of forming these principles, thereby enabling many applications to mature. Flow tracking approaches have been explored for other applications such as particle image velocimetry (PIV), optical coherence tomography (OCT), and confocal microscopy. PIV has been utilized to deduce the trajectory of a 2d flow by tracking beads within the flow as they are scanned using a light sheet (Lai et al., 2018). Two-camera PIV further enables 3D tracking, though it is somewhat limited by the necessary multiple viewing angles. At higher resolution, μPIV has been integrated into microscopy systems, but it requires an additional prism system to enable 3D tracking (Hagsater, 2008). OCT measures the back scattering of coherent light to produce high resolution 3D images (Fujimoto et al., 2000; Lee et al., 2016). Confocal microscopy can produce high resolution 3D images, but the z-scanning method requires long image acquisition times (Moschakis et al., 2006). Spinning disk confocal has somewhat reduced that time. These techniques have all produced remarkable advances in many fields, however it would be attractive to collect 3D information about flow dynamics from a single image on a simple, low-cost laboratory setup.

To address this need we have developed a microscopy technique called stigmatic microscopy which separates the sagittal and tangential focal planes. This is achieved by introducing an astigmatism into the microscopy system. This concept was first proposed by Huang et al. who utilized it to improve reconstruction in super-resolution microscopy (Huang et al., 2008). We proposed that the optical concept could be adapted at a lower magnification and combined with three-dimensional flow tracking software to study and optimize the flow dynamics in ATPS rehydrating droplets for ATPS-based applications. Here we present the design and validation of the stigmatic microscope, then describe our insights into the flow dynamics of rehydrating ATPS droplets and finally apply this technique to illustrate flow dynamics in a cell exclusion assay (Tavana et al., 2011) and a fast ELISA system that we have previously demonstrated for multiplex readouts (Eiden et al., 2016).

# MATERIALS AND METHODS

## Modeling Stigmatic Microscope Parameters

As introduced before, it would be attractive to measure the convective mixing inside of a rehydrating droplet in real time. This would enable the indirect measurement of the forces in the droplet that drive convective rehydration. These forces cannot currently be measured. Here we introduce stigmatic microscopy, a microscopy technique in which astigmatic aberrations in the imaging system are used to determine the vertical position of an object relative to the focal plane (**Figure 1A**). When combined with bead tracking in the x and y directions we can track a bead in three-dimensions as it is carried by flow inside a droplet.

Astigmatism occurs when an oblique bundle of rays impinges a lens that does not have a symmetrical front (Seward, 2010). The resulting image appears foreshortened in the plane of incidence (tangential plane) and elongated in the sagittal plane. The difference between the image points in the tangential and sagittal planes is the astigmatic difference or the aberration called astigmatism. If the astigmatic difference is large, then the image of a bead will appear elongated in the sagittal plane above the focal plane and elongated in the tangential plane below the focal plane. Here we demonstrate that by designing an infinity corrected microscope with a prescribed astigmatism, we can derive a relationship between the position of the bead in the z direction relative to the x-y focal plane and the image of the bead.

Most modern microscopes are designed using an infinity corrected design (Seward, 2010). This term implies that the objective projects the bundle of rays it has imaged as parallel rays. In an ideal system, these would travel to infinity if not for the tube lens, which focuses these rays onto an eye piece or camera (CCD, CMOS or other). To convert an infinity corrected design into a stigmatic microscope, a toroidal lens is inserted between the objective and the tube lens (**Figure 1A**). Because a toroidal lens has different focal lengths in the sagittal and tangential directions it will introduce an astigmatism into the final image.

As shown in **Figure S1A** the paraxial layout establishes the focal lengths and overall size of the microscope. The lens system is composed of two lens groups, the objective (Nikon 4X CFI Achromat, NA 0.1) and tube lens (Thorlabs, LJ1516RM), with a stop in between them and an entrance pupil (20 mm) controlled by the objective. There is also a doublet relay lens (Thorlabs, AC254-050-A) to alter the magnification of the image onto the camera. Here $f_1$ is the focal length of the objective, $f_2$ is the distance between the tube lens and the relay lens, $f_3$ is the distance between the relay lens and the camera, and $d$ is the distance between the objective and the tube lens. They are arranged such that the objective is one focal length (50 mm) away from the substrate and the camera is 86.7 mm away from the tube lens. Without the relay lens this distance would be one tube lens focal length (154 mm). To introduce astigmatism, a half round toroidal lens was inserted into the system 3 mm in front of the tube lens and the system was re-focused using the RMS centroid spot size (49.7 mm). These elements were used as the basis of our idealized model of the optical system.

The paraxial model of the microscope was developed in the optical design software ZEMAX (Geary, 2002). It is important to note that some prescriptions of optical components used in experiments are proprietarily held by Nikon and data on them is unavailable, so the model presented here is for an idealized infinity corrected microscope. As an example of the contribution to astigmatism by the toroidal lens, **Figure 1B** shows the shape of a bead above and below the focal plane when a 1,000 mm toroidal lens is used. The strength of the toroidal lens must be carefully selected to produce a sufficient astigmatism without excessively disrupting image quality, as expressed by the modulation transfer function (**Figure S1C**). We demonstrate how the strength of the toroidal lens can be mapped to the distance between the best focus for the sagittal and tangential directions (**Figures S1D,E**). This data is necessary to calibrate the microbead z-position from the image (**Figure 1C**).

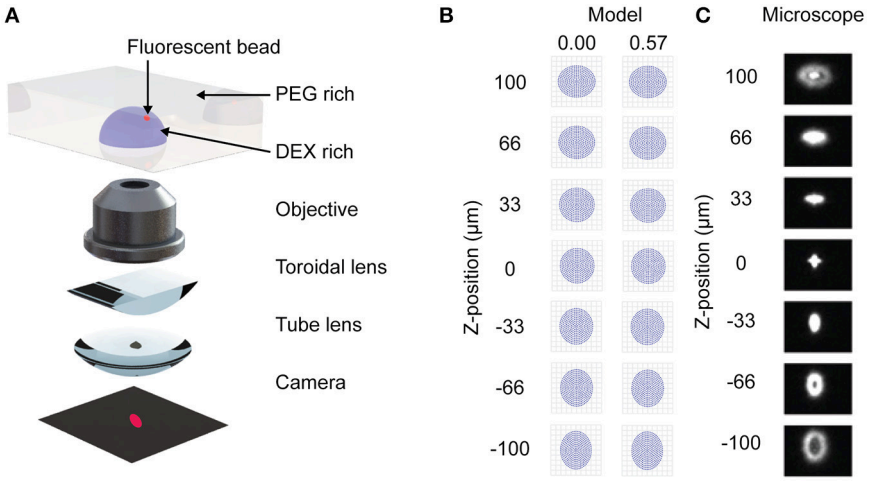


**FIGURE 1 |** Stigmatic microscopy design and model. **(A)** Diagram showing microscope components. Adapted from Huang et al. (2008). Reprinted with permission from AAAS. **(B)** ZEMAX model of stigmatic control under microscope design for two fields (0.00, 0.57). **(C)** Confirmation of stigmatic imaging on a 3 μm bead when the bead is between −100 and 100 μm above and below the focal plane of the microscope.

## Constructing Stigmatic Microscope

For our test microscope we adapted an inverted Nikon TS100 microscope by inserting off the shelf components from Thorlabs (TTL, a 200 mm tube lens and LJ1703RM, a 1,000 mm toroidal lens) as guided by the model. The focal length of the tube lens was chosen to match the Nikon 200 mm focal lengths specified by the company. The microscope was constructed by unthreading the Nikon tube lens and replacing it with the Thorlabs toroidal and tube lenses, respectively. The toroidal lens was placed 3 mm in front of the tube lens. Note that the rotational alignment of the toroidal lens with the camera is critical for subsequent analysis.

## Calibrating Microbead z Position

To calibrate the microbead z position from a captured image we measured the astigmatic aberration using an algorithm in Python and the library OpenCV (**Figure 2A**) (Bradski and Kaehler, 2008). A single 3 μm yellow-green fluorescent bead was placed in a 96-well plastic microplate inside a droplet and allowed to settle to the bottom of the well (**Figure 2B**). Images were taken at 5.5 μm intervals from −200 μm below the bead to 200 μm above the bead, then fed into the software algorithm.

The z-calibration loop collected particle height and width for each image, then appended the particle dimensions to an array labeled by z-stack position, as follows. For each image, a threshold was used to generate a binary image. From the binary image, a bounding ellipse was fit to the bead dimensions to find the center of the bead using the built-in functions in OpenCV (Fornaciari and Prati, 2012). The particle was found using blob detection and a region of interest (ROI) was used to extract just the particle from the image, as depicted in **Figure 2B**. A line histogram was applied along the x and y axes of the image to project the 2D point spread function of the bead. A smoothing spline was fit to calculate the full width at half maximum (FWHM) of the data. The line histogram data was filtered to only include lines two sigma from the mean to filter noise. The distance between the roots of the spline provided the width and height of the bead. This algorithm enables simultaneous detection of multiple beads at multiple z heights from the same image, but overlapping beads can interfere with each other.

This same technique was applied after imaging at known intervals above and below the focal plane to produce a scatter plot of the width and height of the bead at different z positions. The result of fitting a spline to this data is the calibrated relationship of the PSF of the bead to its position relative to the focal plane of the objective. The z position of an unknown bead can then be calculated using a least-squares fit on the calibrated relationship, which attempts to minimize the error between both the width and height of the bead to the calibrated model. Note that the least-squares fit on the spline function is somewhat sensitive to initial z estimate, so we pre-filtered the z estimate by fitted ellipse area and by width to height ratio. Finally, we plot the measured z-position of several beads to the known z-position of those beads that were back calculated, as shown in **Figure 2C**.

## Preparation of DEX–PEG Aqueous Two-Phase Systems

Two aqueous two-phase systems were selected, based on prior experience in ATPS micropatterning. Our group has previous published work on the multiplex ELISA and cell exclusion assay using PEG (MW 35,000, Sigma) and DEX (MW 500,000, Sigma) (Tavana et al., 2011; Frampton et al., 2014). Flows in a PEG and Ficoll (MW 400,000, Sigma) system were also examined. We generated phase diagrams for both systems using a conventional dilution method (Kojima and Takayama, 2013). Briefly, we prepared concentrated polymer solutions in PBS (20% w/w polymer) and mixed the biphasic solutions in a range of different volume ratios. The resulting cloudy mixtures (two-phase) were diluted by a PBS solution until the binodal point where the mixtures turned transparent (one-phase). A univariate spline was

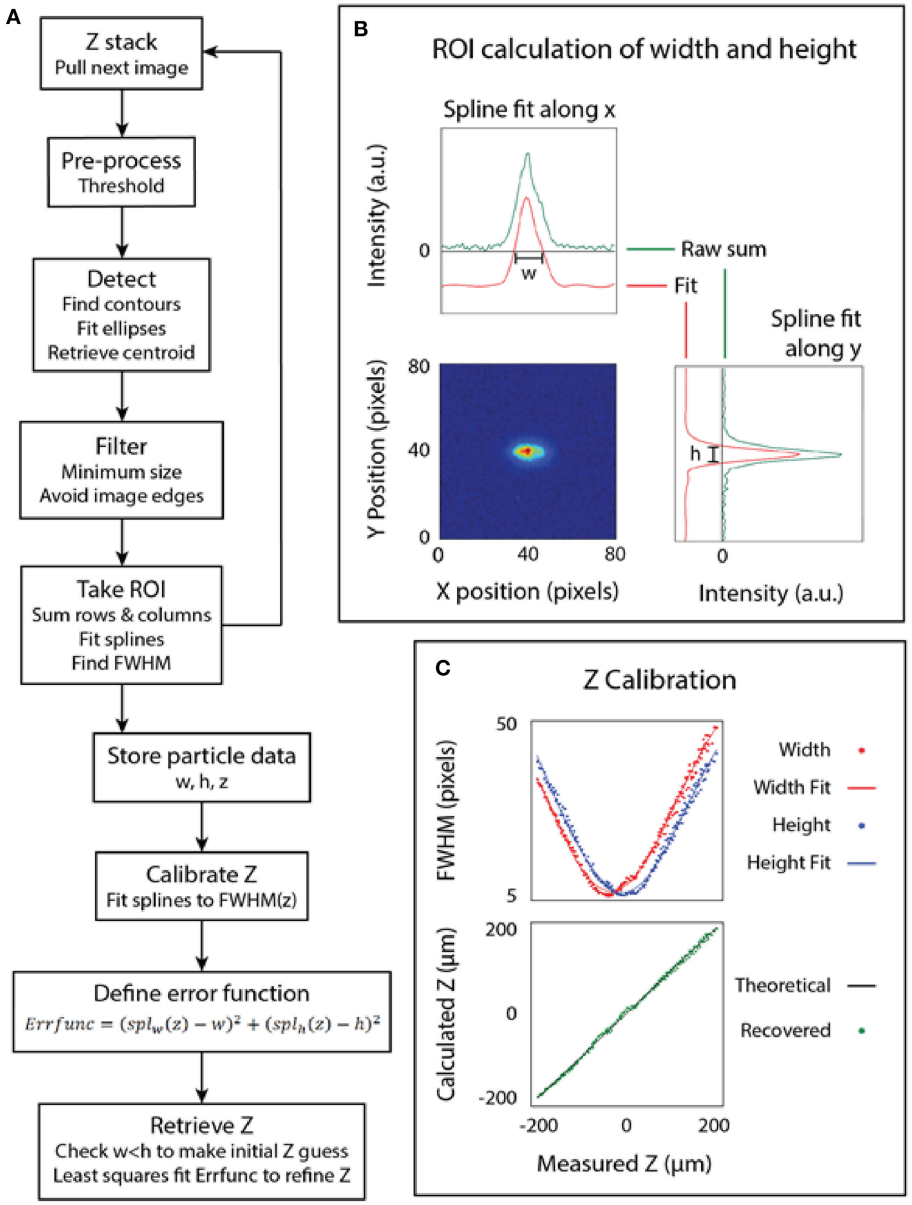


**FIGURE 2 |** Calibration of the microscope. **(A)** The algorithm used to calibrate the microscope. **(B)** The point spread function (measured and fit) of a bead. **(C)** The bead dimensions plotted against the focus position (z) and the final calibrated relationship.

fit to the resulting set of points to indicate the binodal curve (Kojima and Takayama, 2013). Separate solutions above the tie-line were prepared to measure the resulting top phase/bottom phase volume ratio. Using the conservation of mass, the volume ratio can be calculated from the ratio of distances between the bulk concentration and either intersection of the tie-line with the binodal curve. Tie-lines were fit to the phase diagram using a custom Python script. A least-squares fit was used to find the slope of the tie-line that matched the volume ratio calculated by the relative tie-line lengths to the measured volume ratio. The intersection of the tie-line with the binodal curve was found by least-squares fitting between the binodal spline and the tie-line with a fitted slope that passed through the bulk concentration point. Note that the univariate spline does not accurately describe the binodal curve at near-zero values of the independent variable, so an inverse spline was also found and used for the opposite end of the binodal curve, i.e., y(x) for low values of y and x(y) for low values of x. Phase diagrams are included in **Figure S2**.

We measured convection in rehydrating ATPS that mimics the situation seen in the multiplex immunoassay format (Frampton et al., 2014; Eiden et al., 2016) and cell exclusion patterning (Tavana et al., 2011). Solutions of the DEX phase in DI-water were spotted in 1 µL droplets in a clear, flat-bottom 96-well microplate with 3 µm yellow-green fluorescent

polystyrene beads (polysciences), diluted to ∼10–20 particles per μL. The plates were dried in a vacuum desiccator overnight prior to rehydration. DEX microdroplets were rehydrated on the stigmatic microscope with indicated concentrations of PEG in PBS and imaged over indicated times. For flow exclusion studies, beads were diluted to 10–20 particles per μL in the PEG-rich phase to track flow outside of the rehydrating droplet.

## Flow Tracking

Time course images were collected using Nikon NIS Elements and saved as 16-bit .nd2 files. These files were converted to 8-bit .tiff images, conserving the low intensity region of the data using a FIJI macro. We wrote analysis in Python to calculate 3D bead positions and track their movement (**Figure 3**).

The image thresholding and bead position calculation followed the same algorithm as in the calibration protocol. For each period t, several bead positions were calculated and indexed. Each existing bead was then compared to beads in frame t+1 and linked to the nearest neighbor by x, y, z distance in microns, checking against a maximum travel distance threshold. If a match was found, that bead pair was removed from subsequent matching to prevent flow traces from artificially merging. The remaining beads from period t were similarly matched to the remaining beads in frame t+1. Any beads that were not matched were held for five time frames before terminating that bead path. The resulting flow trace matrix contained x, y, z positions, time points, and bead identity indices. Traces containing fewer than five hundred time points were eliminated as noise.

For flow exclusion studies, the field of view was aligned to contain the outer edge of the droplet. To view the flow at the droplet interface, a 400 px (600 μm) slice was taken by filtering the trace data in the y-dimension. The traces were then projected to the x-z plane. Flow traces were color-coded by time to visualize the direction of flow.

Flow traces were imported to MATLAB and smoothed using a Loess filter in x, y, and z. Once smoothed, the time derivative of 3D distance traveled could be calculated numerically to find particle speed. For the 15-min traces, the root-mean-square of the speed was calculated for each particle to find a general metric for mixing efficiency. To distinguish between the fast mixing eddy regions and the larger central flow, flow traces were plotted in a 3D interactive diagram using open-source plotly functions, color-coded by time, and examined for annotation. To determine droplet rehydration height, traces were examined in the interactive plots, as well as using x-z projections.

## Cell Exclusion

Cell exclusion assays were performed by rehydrating 1 μL DEX drops in which the PEG phase also contained MDA-MB-231 cells (ATCC) to observe if the DEX spotting would exclude the cells from adhering to the spotted region. Three conditions were studied, including a 2.5% PEG-6.4% DEX (w/w) ATPS system, a 2.5% (w/w) PEG only system, and MEM-only system. The DEX was prepared first at 6.4% (w/w) in DMEM F12 (Invitrogen) labeled with FITC-DEX (0.1% w/w, Sigma). Each solution was filtered (0.22 μm PVDF syringe filter) in a sterile environment after the reagents had been prepared and dissolved. The 2.5%

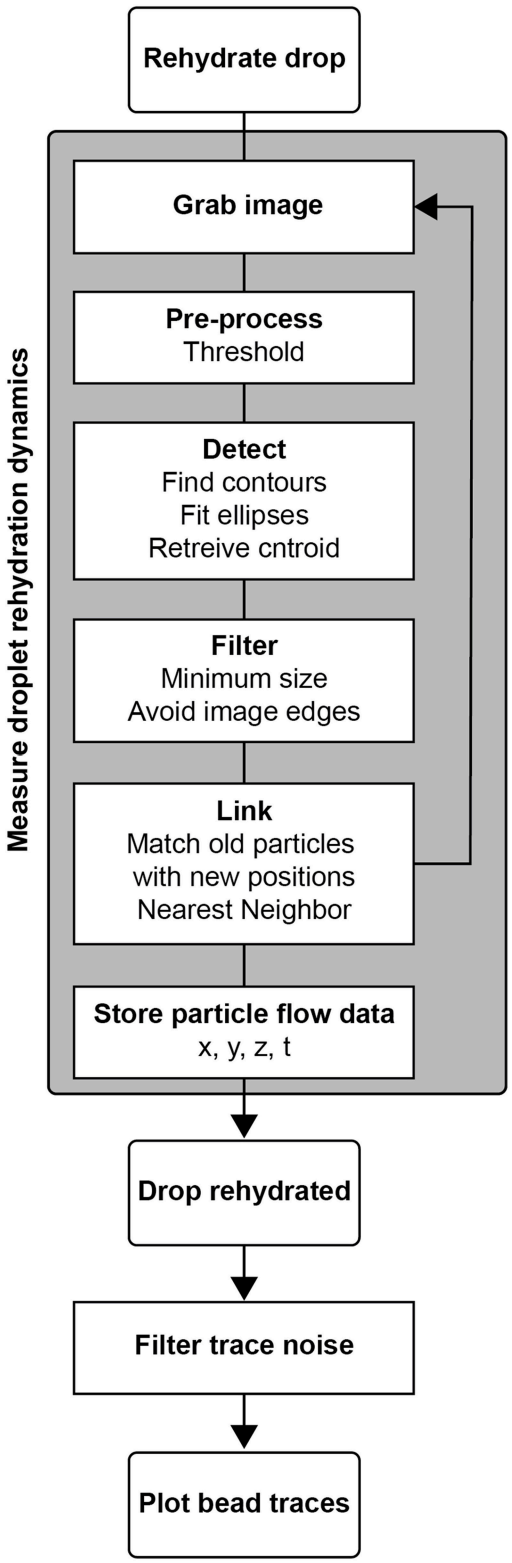


**FIGURE 3 |** Algorithm for measuring droplet rehydration dynamics in stigmatic microscopy. The process for measurement involved rehydrating the drop under microscopic imaging, during which the particles were tracked, and their X, Y, and Z positions were reported.

PEG-6.4% DEX system was pre-equilibrated by centrifugation at 25°C, 3,000 rpm for 15 min, and the top phase was extracted for cell exclusion experiments. The resulting cell suspension solutions are indicated in **Figure 5A**.

The DEX solution was spotted in 1 μL drops into clear, flat-bottom 96-well tissue culture microplates using an Integra Biosciences Viaflo 96-well pipetting robot (pipet function, speed 8 with a Z height of 11.2 for the receiving plate) and were dried overnight in the incubator to maintain sterility. The top phase of the 2.5% PEG-6.4% DEX solution or the 2.5% PEG only or MEM-only solutions were prepared in DMEM F12 as described above. Cells were resuspended in these solutions at a concentration of 400,000 cells/mL, then added to the dried DEX spot plate to rehydrate the DEX. The cells were stained with NucBlue Live (Thermofisher) according to the manufacturers protocol. The plates were incubated for 2 h at 37°C to allow cell settling, then imaged.

## ATPS ELISA

The current work adapts the protocol from our group's previous publication (Eiden et al., 2016) using a human IL-8 DuoSet kit (R&D Systems). ELISAs were performed in custom 96-well injection molded plates with 1.7 mm diameter microbasins (9 per well) (Xcentric Mold and Engineering). Plates were washed with ethanol and distilled water, then dried overnight in a desiccator. Capture antibody solutions at the manufacturer recommended concentration in PBS (4 μg/mL) were applied in 1 μL spots to the microbasins. The plates were sealed and incubated for 90 min to allow adsorption. Free capture antibody was then washed 3x using 200 μL wash buffer (0.05% Tween 20 in PBS), followed by addition of 100 μL of 5% sucrose (Sigma) in PBS for 1 h to block unused surfaces. The sucrose was emptied, and the plates were dried in a vacuum desiccator for 40 min. Once dry, 5% BSA in PBS was spotted 1 μL per microbasin on top of the IL-8 capture antibody spots to further block reaction surfaces. The BSA was dried in the vacuum desiccator for 40 min. Detection antibody was mixed in solutions of 5% (w/w) dextran MW 500,000 in water (Sigma). These detection antibody solutions were then spotted 1 μL per microbasin and dried in a vacuum desiccator overnight.

To run the assay, IL-8 standards from the kit were diluted in an assay buffer consisting of 5% (w/w) or 10% (w/w) PEG MW 35,000 (Sigma), 0.05% Tween 20 (Sigma), and 0.5% BSA (Sigma) in PBS (Gibco). An 8-point standard curve was generated with 2-fold dilutions from 2,000 pg/mL in quadruplicate. To avoid biasing the plate by sample addition order in the fast ELISA, samples were loaded onto a feeder plate in a randomized plate layout. The samples were then simultaneously transferred from the feeder plate to the assay plate using the Viaflo 96-well robotic pipet. The assay was initiated upon addition of the PEG-sample solutions, which immediately began to rehydrate the dried DEX and antibody reagents. Samples and standards were incubated in the dark at room temperature for 15 min. The plates were washed 6x with wash buffer to clear out the viscous ATPS components. Streptavidin-HRP conjugate (R&D Systems) was added at the manufacturer's recommended concentration and incubated for 20 min. Plates were washed 3x, then filled with SuperSignal ELISA Femto Maximum Sensitivity Substrate (ThermoFisher) and the plates were imaged using a BioRad ChemiDoc MP+ chemiluminescent blot reader.

ELISA plate images were analyzed using a custom ImageJ plugin to outline microbasin regions and calculate chemiluminescent intensity. The standard curve was plotted using the ggplot2 library in CRAN-R. ANOVA was used to test effects of row, column, ATPS condition, and IL-8 concentration in a randomized plate design with a confidence interval of 95%. Following ANOVA, a *post hoc* Tukey test was performed with a 95% confidence interval. A linear model was used to fit the data and remove effects from row and column location within the plate to plot the standard curve.

## RESULTS AND DISCUSSION

### Stigmatic Microscope Validation

Z-stacks from an individual fluorescent bead indicated that the stigmatic microscope transformed the point spread function (PSF) as expected (**Figure 2B**; **Figure S1B**). **Figure 1B** shows sample images taken along a stack of z positions, where the spread of light follows the shape predicted in the spot diagram. The 3 μm bead diameter corresponds to 2 pixels in image-space, making it a reasonable approximation for a PSF. Smaller beads were also examined, but the tradeoff between fluorescent intensity and size led to the selection of the 3 μm bead. The 3 μm beads are expected to respond to gravitational force for sedimentation (Laidlaw I. M. A. R. C. S., 2005) and other forces for convection (Binks and Horozov, 2006). Generally, smaller beads will be less sensitive to gravitational effects and therefore better for flow tracking. However, small beads contain less dye and have low fluorescent intensity, requiring longer exposure times to capture the shape of the PSF. Exposure can be further tuned to sacrifice depth of field for imaging frequency. For applications examining shallower flows, smaller beads may still be appropriate. In this work, a 500 ms exposure provided sufficient detail about the shape of the PSF to detect z-position within at least the calibrated 400 μm range. Faster flows requiring shorter exposure can be detected by decreasing the exposure time and sacrificing z-range or by introducing a photo-multiplier tube into the system.

After performing the calibration outlined in **Figures 2A,B** on 3 different beads, the images were fed back into the z-retrieval algorithm to recover z-position. **Figure 2C** indicates accurate recovery of the z-position.

### Rehydration Dynamics of Rehydrating ATPS Droplets

Three primary types of flow dynamics emerged during the rehydration process (**Figure 4A**). The first was the volcano current, in which direction of flow is up the center of the droplet. The second is the inverse volcano, in which the current flows down the center of the droplet. We also observed transient micro eddies in high mixing regions where particles would rapidly rotate near the bottom, outer edge of a droplet.

Inverse volcano currents were observed in PEG-Ficoll ATPS drops while both volcano and inverse volcano currents were

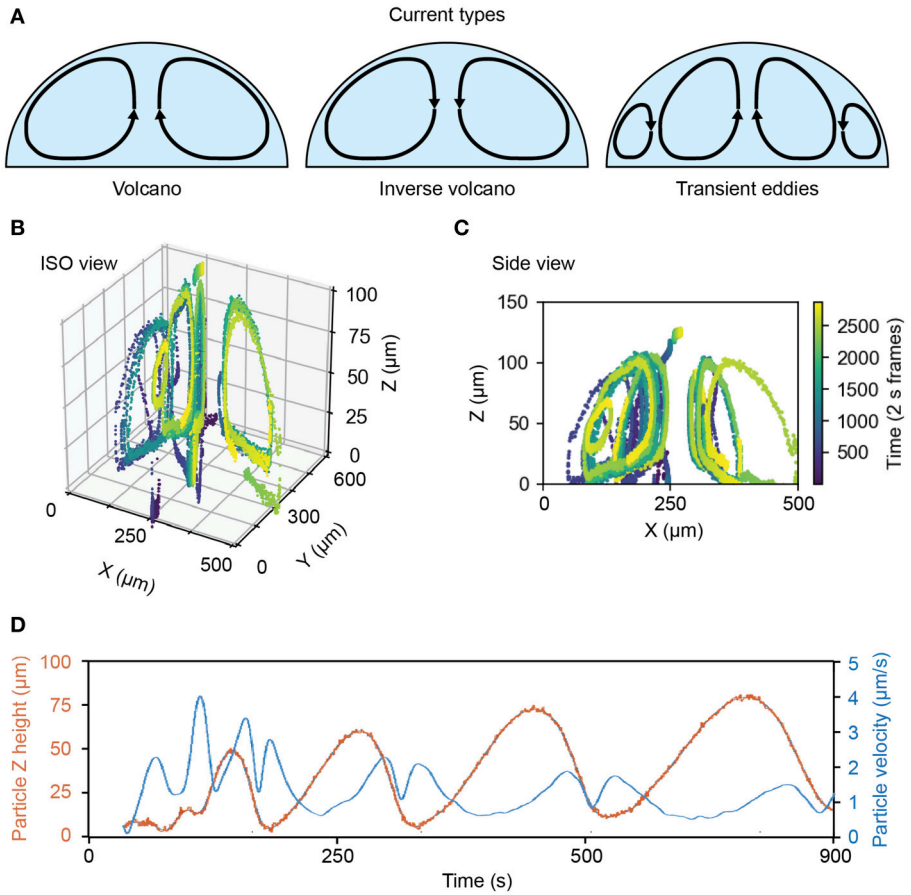


**FIGURE 4 |** Flow dynamics and rates of rehydrating ATPS droplets. **(A)** Examples of observed flows inside of rehydrating ATPS droplets. **(B)** 3D plot showing the flow dynamics of an exemplary rehydrating Ficoll-rich droplet. **(C)** 2D slice of the center of the same Ficoll drop over several flow cycles. **(D)** Dynamics and rate of rehydration as measured for a drop showing particle positions over time (red) and particle velocity over time (blue) in the drop.

observed in PEG-DEX ATPS drops, depending on specific ATPS composition. Interestingly, the micro eddies were only present in the DEX ATPS drops. **Figures 4B,C** show an example of a PEG-Ficoll inverse volcano. **Figure 4B** shows the ISO view of particles being tracked in the droplet over 50 min. **Figure 4C** shows the side view of the same droplet in which individual beads show a uniform current around the drop. This is just an example of the measurements that are observed using the stigmatic microscope system.

For many applications, knowing the velocity of the current and the cycling rate of the fluid in the drop may be useful for optimizing conditions. **Figure 4D** shows an example of the flow dynamics of a bead in the fluid. The z position of the bead in this example increases in both amplitude and period with time. Moreover, the velocity of the bead shows a double peak pattern after reaching the peak of the drop. The maximum z-position the particle reaches increases with time in this case from 50 to 75 μm, and it is inversely proportional to the maximum velocity per flow cycle, as the droplet becomes more well-mixed and loses some of the chemical potential gradient that may be driving flow.

## Cell Exclusion

The correlation between flow behavior and rehydrated ATPS cell exclusion patterning was examined. Previously reported experiments indicated a change in cell exclusion efficiency depending on the composition of the ATPS. In this assay, cells in solution sediment and attach to the growth plate in a pattern excluded by a dried 1 μL 6.4% DEX spot. To further examine this behavior, we tested three continuous phase conditions, all with a dried 1 μL DEX spot in each well (**Figure 5A**): "Top phase"–the extracted top phase from the 2.5% PEG-6.4% DEX system, "2.5% PEG"–a sub-critical ATPS, made of 2.5% PEG, and "MEM only"–cell culture media alone. These conditions are marked by red Xs on phase diagrams in **Figure 5A**. Note that the sub-critical ATPS contains a small overall concentration of DEX from the dried 1 μL DEX spot. However, that overall concentration of DEX (0.064%) does not bring the total system above the binodal curve. In contrast, the "Top phase" condition yields a higher concentration of PEG, as it has already phase separated from the initial composition, indicated by following the blue line from the gray dot to the red X in **Figure 5A**. This higher

PEG concentration brings the overall system above the binodal curve, producing equilibrium phase separation. For imaging, the field of view was shifted to include the edge of the droplet to see flow behavior at that region of interest during rehydration, as indicated in **Figure 5B**. In **Figure 5B**, the time of each detected bead position is encoded by color.

Visual examination of the flow both inside and outside of the droplet added new explanation to the success of cell exclusion patterning. In the two-phase condition (labeled "Top phase" in **Figure 5**), flow tracking within and around the rehydrating droplet indicates a volcano-pattern circulation within the droplet, and a downward/outward flow in the surrounding media (**Figure 5B**, left). This generates a small stagnant zone at the center of the droplet, which corresponds to the typical location of cells that evade exclusion and attach near the center of the droplet (Tavana et al., 2011). This experiment indicates that convective flow is present and may help drive cell seeding away from the droplet, in addition to the previously hypothesized interfacial exclusion (Tavana et al., 2011).

In sub-critical ATPS (**Figure 5B**, "2.5% PEG"), initial flow is similar to the "Top phase" condition, but at long times the "2.5% PEG" condition resembles the "MEM only" condition, after the ATPS dissipates and becomes homogenous. There is a transient flow exclusion for ∼1 h, while the DEX-rich phase is at a temporary, locally high concentration. However, the bulk phase and DEX-rich phase will ultimately become homogeneous, as the total composition of the system is below the binodal curve. Over time, the DEX may be diffusing across the droplet interface into the bulk phase while the droplet phase is also diluted by infiltrating osmosis, reducing the local concentration of DEX below the binodal curve. Time-lapse imaging of FITC-DEX droplets indicate that the distinct droplet phase disappears within 2 h (**Figure 5C**). Temporal analysis of the convective flow paths shows that after ∼1 h, beads settle through the area previously obstructed by the temporary phase boundary. In the absence of PEG, flow consists only of settling straight downward (**Figure 5B**, right).

The efficacy of cell exclusion correlates with the flow profiles (**Figure 5C**). Representative brightfield and fluorescence images indicate near total cell exclusion in the two-phase condition, but no noticeable exclusion in the sub-critical ATPS or the media-only control. The lack of cell exclusion in the sub-critical ATPS result indicates either that convection alone was insufficient to direct cell patterning, or that cell settling continued to occur beyond the 1 h of transient exclusion flow.

The difference between the pre-equilibrated two-phase condition and the sub-critical ATPS emphasizes the need for clarity in ATPS research when communicating ATPS concentrations, particularly near the critical point. Some papers describe the overall concentration (mid-tie-line, as in this experiment), while others describe the resulting phases used along the binodal curve.

## ATPS ELISA

The impact of ATPS composition on ELISA performance could arise from a variety of factors. These include partition behavior, volume ratio, convective mixing, and viscous limitations on diffusion. The partition coefficient and volume ratio determine the concentrating effect from ATPS (Mashayekhi et al., 2012). Partition coefficients and volume ratios further from unity cause higher concentrations of reagents into one phase, in this case the DEX phase. Techniques already exist to determine partition coefficients, volume ratios, and viscosity, but internal convective mixing has been difficult to measure.

The stigmatic microscope presented here can add missing information regarding convective mixing and transient volume ratio in non-equilibrium ATPS. We examine two ATPS conditions, with low or high PEG concentrations (5 or 10% w/w, respectively) to rehydrate a dried 1 μL droplet of 5% DEX, for overall ATPS consisting of 5% PEG and 0.05% DEX or 10% PEG and 0.05% DEX. We will refer to these conditions as 5% PEG-5% DEX and 10% PEG-5% DEX, respectively. Recent work suggests that convection in non-equilibrium ATPS is driven by a chemical potential gradient (Ban et al., 2016). The chemical potential gradient is higher for the higher concentration PEG, which lies on a longer tie-line. However, the resulting concentrations of PEG and DEX in the top and bottom phases are also higher, leading to higher viscosity and associated drag on convective flow.

We quantified spontaneous convective mixing in rehydrating ATPSs. As depicted in **Figure 4D**, flow traces were smoothed in x-, y-, and z- dimensions as functions of time for numerical differentiation to find the speed over time. Speed was then quantified using the root-mean-square (RMS) to summarize each flow trace into a single measurement. The flow traces were visually examined to annotate each trace as a short eddy or a larger, center flow. The RMS speeds were analyzed between conditions using ANOVA, followed by a *post hoc* Tukey test at a 95% confidence interval. The center flow was significantly faster for the 5% PEG-5% DEX compared to the 10% PEG-5% DEX, while the difference between eddies did not meet the 95% confidence interval (**Figure 6A**). We suggest that the additional drag effects from viscosity in the 10% PEG-5% DEX condition seem to outweigh its higher chemical potential gradient driving forces.

Overall droplet height was roughly identical for the 5% PEG and 10% PEG conditions (**Figure S3**). The indistinguishable droplet heights do indicate that potential differences in volume ratio between ATPS conditions are not present. Therefore, differences in ELISA signal may be attributed primarily to differences in convective mixing.

The extensive mixing effect seen in the 5% PEG condition correlated with higher signal intensity in the standard curve of a rehydrated ATPS ELISA for human IL-8. ANOVA with *post hoc* Tukey test indicated that the 5% PEG-5% DEX condition gave higher intensity than 10% PEG-5% DEX at a 95% confidence interval. The row-column corrected standard curve is shown in **Figure 6B**. We suggest that this result occurs because greater internal convection provides more binding opportunities between the detection antibodies confined within the DEX droplet and the IL-8 sample in the bulk PEG-rich phase. The convection also allows additional binding opportunities for the IL-8 sample to the capture antibody on the microplate surface.

Furthermore, we have shown an ELISA with only a 15 min incubation, 16x faster than our previously reported protocol

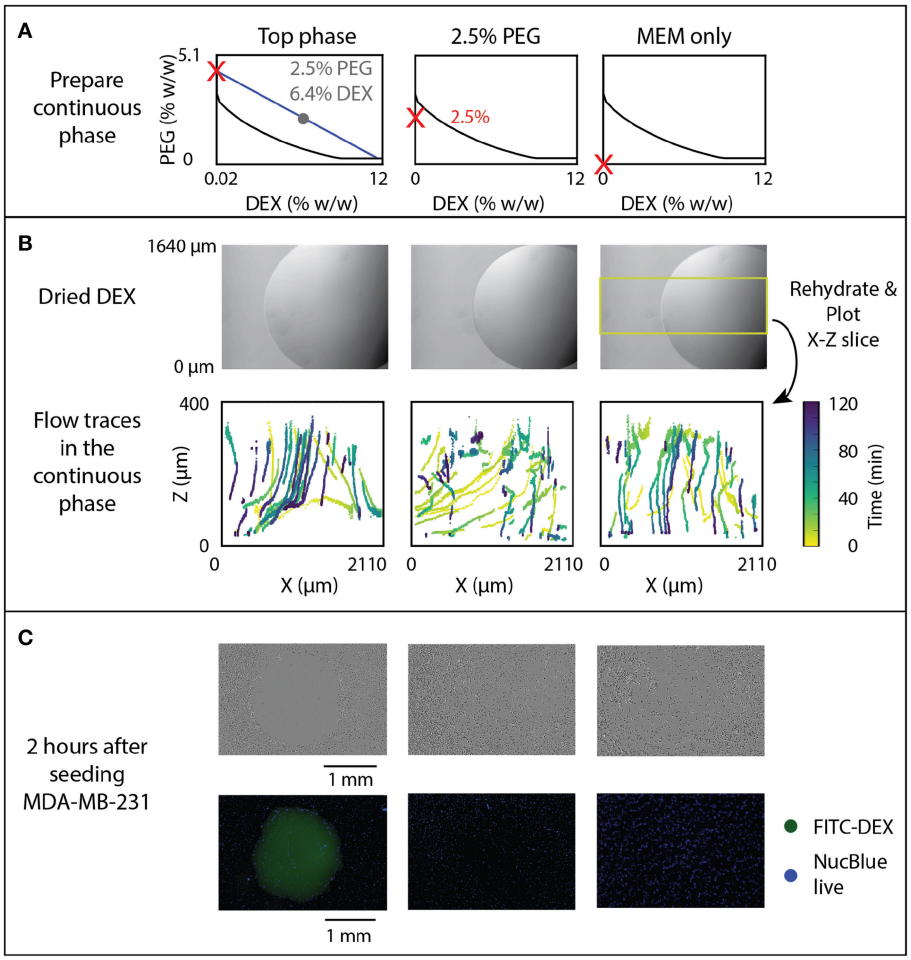


**FIGURE 5 |** Effect of rehydration dynamics on cell exclusion. **(A)** ATPS solutions indicated by red Xs were used to rehydrate DEX droplets, shown prior to rehydration in panel **(B)**. **(B)** Flow traces of beads in the continuous phase, with color-coded time, were measured and 3D sections indicated by the yellow box were projected to the X-Z plane. **(C)** Cell exclusion was imaged 2 h after seeding MDA-MB-231 cancer cells using phase contrast (top) and fluorescent imaging with FITC-labeled DEX and NucBlue Live Stain (bottom).

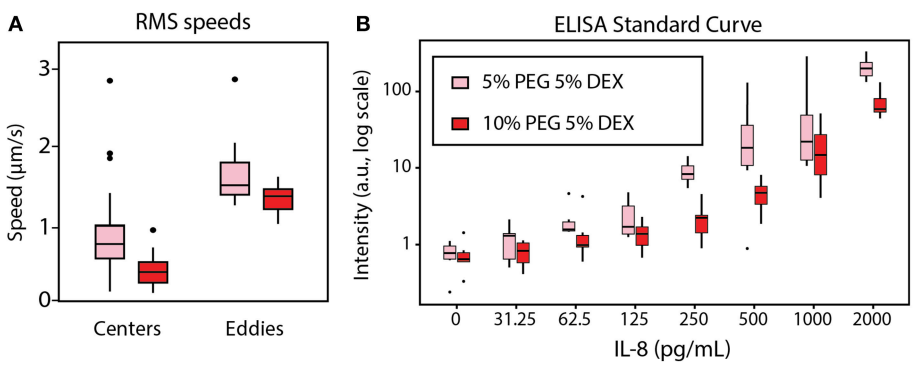


**FIGURE 6 |** Effect of rehydration dynamics on ELISA performance between 5% PEG−5% DEX (pink) and 10% PEG−5% DEX (red). **(A)** Individual speed traces were summarized using their root-mean-square (RMS) values, then plotted in boxplots. Each eddy was significantly different from each center with a 95% confidence interval. The difference between center RMS speed was also significant at a 95% confidence interval. **(B)** The standard curve for the row-column-corrected IL-8 ELISA was determined. The difference in signal intensity between 5% PEG-5% DEX and 10% PEG-5% DEX was statistically significant at 95% confidence interval by ANOVA with a *post hoc* Tukey test.

(Eiden et al., 2016). This study demonstrates the ability to measure convective mixing using stigmatic microscopy, which will be critical for further analysis and optimization of this short incubation ELISA. These studies will include analysis of other ATPSs and their impact on signal intensity and variation.

## CONCLUSION

The design of the microscope is both simple and flexible, enabling it to be integrated into most off the shelf microscope systems without a deep knowledge of optics. The principle is that a weak cylindrical or toroidal lens (1,000 mm or greater) will introduce enough astigmatism to enable stigmatic microscopy but will not interfere significantly with the imaging performance of the system. This provides complementary advantages over other methods (PIV, OCT, Confocal) in that the temporal detail is only limited by the exposure time of a single image. With our particular microscope system, this worked for 500 ms exposures, but shorter exposures should be possible with a photo-multiplier tube or more sensitive camera. Moreover, because no scanning of a laser or light sheet is necessary, the rate of capture may ultimately be much faster.

The results shown for both ELISA and cell exclusion demonstrate that insights into the performance of ATPS driven assays can be captured using stigmatic microscopy. In ELISA, we found that viscous effects outweigh driving forces, while cell exclusion was found to be controlled by choosing either a critical or sub-critical ATPS condition. Moreover, we demonstrated immunoassay incubation times 16x faster than those previously demonstrated by our group.

Future work will further explore the application of stigmatic microscopy to multiplexed ELISA and will enable the derivation of complete flow fields of the droplet over time. We also believe additional work will enable accurate detection of the droplet shape and morphological changes as required by new applications.

In conclusion, we present a stigmatic microscope designed to enable facile measurement of convective mixing both inside and outside of ATPS droplets. The specific observations as well as general methodology should aid in the development of design principles for various ATPS applications. The ability to conveniently image 3D flows in the μm-mm regime is also envisioned to be useful in understanding the forces and dynamics that drive a number of microfluidic and droplet-based systems beyond ATPS systems.

## AUTHOR CONTRIBUTIONS

CY, CO, TK, and ST: conceptualization. CY and CO: methodology. CO and CY: software. CY: validation. CO and CY: formal analysis. CY, CO, and TK: investigation. ST: resources. CY: data curation. CY, CO, TK, and ST: writing–original draft. CY, CO, TK, and ST: writing–review and editing. CO and CY: visualization. ST: supervision.

## ACKNOWLEDGMENTS

We thank Prof. Shu Jia for advice on Z calibration to the PSF shape. We thank Prof. Harvey Qu for his suggestion to use row-column design to remove plate layout effects. We thank the NIH: HL136141 (CY), T32CA009676 (CO), and AI116482 (CO) and the NSF: CBET 0939511 (CY) for funding.

## SUPPLEMENTARY MATERIAL

The Supplementary Material for this article can be found online at: https://www.frontiersin.org/articles/10.3389/fchem.2019.00311/full#supplementary-material

## REFERENCES

Ban, T., Fukuyama, T., Makino, S., Nawa, E., and Nagatsu, Y. (2016). Self-propelled vesicles induced by the mixing of two polymeric aqueous solutions through a vesicle membrane far from equilibrium. *Langmuir* 32, 2574–2581. doi: 10.1021/acs.langmuir.6b00105

Bansal, L., Chakraborty, S., and Basu, S. (2017). Confinement-induced alterations in the evaporation dynamics of sessile droplets. *Soft Matter*. 13, 969–977. doi: 10.1039/C6SM02429g

Bathany, C., Park, J., Cho, Y. K., and Takayama, S. (2013). Dehydrated aqueous two-phase system micro-domains retain their shape upon rehydration to allow patterned reagent delivery to cells. *J. Mater. Chem. B.* 1, 6020–6026. doi: 10.1039/c3tb21004a

Binks, B. P., and Horozov, T. S. (2006). *Colloidal Particles at Liquid Interfaces: An Introduction*. New York, NY: Cambridge University Press. doi: 10.1017/CBO9780511536670.002

Bradski, G., and Kaehler, A. (2008). "Chapter 8: Learning openCV," in *Computer Vision with the OpenCV Library, 1st Edn*, ed M. Loukides (Cambridge: O'Reilly Media Inc).

Byun, C. K., Hwang, H., Choi, W. S., Yaguchi, T., Park, J., Kim, D., et al. (2013). Productive chemical interaction between a bacterial microcolony couple is enhanced by periodic relocation. *J. Am. Chem. Soc.* 135, 2242–2247. doi: 10.1021/ja3094923

Eiden, L., Yamanishi, C., Takayama, S., and Dishinger, J. F. (2016). Aqueous two-phase system rehydration of antibody-polymer microarrays enables convenient compartmentalized multiplex immunoassays. *Anal. Chem.* 88, 11328–11334. doi: 10.1021/acs.analchem.6b02960

Fornaciari, M., and Prati, A. (2012). *Very Fast Ellipse Detection for Embedded Vision Applications*. Distrib Smart Cameras (ICDSC). Available online at: http://ieeexplore.ieee.org/xpls/abs_all.jsp?arnumber=6470150

Frampton, J. P., Tsuei, M., White, J. B., Abraham, A. T., and Takayama, S. (2015). Aqueous two-phase system-mediated antibody micropatterning enables multiplexed immunostaining of cell monolayers and tissues. *Biotechnol. J.* 10, 121–125. doi: 10.1002/biot.201400271

Frampton, J. P., White, J. B., Simon, A. B., Tsuei, M., Paczesny, S., and Takayama, S. (2014). Aqueous two-phase system patterning of detection antibody solutions for cross-reaction-free multiplex ELISA. *Sci. Rep.* 4, 14–16. doi: 10.1038/srep04878

Fujimoto, J. G., Pitris, C., Boppart, S. A., and Brezinski, M. E. (2000). Optical coherence tomography: an emerging technology for biomedical imaging and optical biopsy. *Neoplasia* 2, 9–25. doi: 10.1038/sj.neo.7900071

Geary, J. (2002). *Introduction to Lens Design : With Practical ZEMAX Examples*. Richmond, VA: Willmann-Bell.

Hagsater, M. (2008). *Development of Micro-PIV Techniques for Applications in Microfluidic Systems Sven Melker Hagsater*. Technical University of Denmark. Available online at: http://orbit.dtu.dk/files/4942065/melker_hags%C3%A4ter.pdf

Hatti-Kaul, R. (2001). Aqueous two-phase systems. *Mol. Biotechnol.* 19, 269–277. doi: 10.1385/MB:19:3:269

Huang, B., Wang, W., Bates, M., and Zhuang, X. (2008). Three-dimensional super-resolution reconstruction microscopy. *Science* 319, 810–814. doi: 10.1126/science.1153529

Iqbal, M., Tao, Y., Xie, S., Zhu, Y., Chen, D., Wang, X., et al. (2016). Aqueous two-phase system (ATPS): an overview and advances in its applications. *Biol. Proced.* 18, 1–18. doi: 10.1186/s12575-016-0048-8

Kojima, T., and Takayama, S. (2013). Microscale determination of aqueous two phase system binodals by droplet dehydration in oil. *Anal. Chem.* 85, 5213–5218. doi: 10.1021/ac400628b

Lai, H. C., Chew, T. F., and Razak, N. A. (2018). Evaluation of particle image velocimetry measurement using multi-wavelength illumination. *IOP Conf Ser Mater Sci Eng.* 370:1. doi: 10.1088/1757-899X/370/1/012044

Laidlaw I. M. A. R. C. S. (2005). "Introduction to differential sedimentation," in *Ultracentrifugation: Techniques and Methods*, eds D. J. Scott, S. E. Harding, and A. J. Rowe (Analytical Cambridge: The Royal Society of Chemistry). p. 270–290.

Lee, J., Bathany, C., Ahn, Y., Takayama, S., and Jung, W. (2016). Volumetric monitoring of aqueous two phase system droplets using time-lapse optical coherence tomography. *Laser Phys. Lett.* 13:2. doi: 10.1088/1612-2011/13/2/025606

Mashayekhi, F., Le, A. M., Nafisi, P. M., Wu, B. M., and Kamei, D. T. (2012). Enhancing the lateral-flow immunoassay for detection of proteins using an aqueous two-phase micellar system. *Anal. Bioanal. Chem.* 404, 2057–2066. doi: 10.1007/s00216-012-6278-y

Moschakis, T., Murray, B. S., and Dickinson, E. (2006). Particle tracking using confocal microscopy to probe the microrheology in a phase-separating emulsion containing nonadsorbing polysaccharide. *Langmuir* 22, 4710–4719. doi: 10.1021/la0533258

Per-Ake, A. (1960). *Partition of Cell Particles and Macromolecules*. 2nd Ed. New York, NY: John Wiley & Sons.

Rito-Palomares, M. (2004). Practical application of aqueous two-phase partition to process development for the recovery of biological products. *J. Chromatogr. B Anal. Technol. Biomed. Life Sci.* 807, 3–11. doi: 10.1016/j.jchromb.2004.01.008

Seward, G. H. (2010). *Optical Design of Microscopes*. Bellingham, WA: SPIE. Available online at: http://ebooks.spiedigitallibrary.org/book.aspx?

Tavana, H., Jovic, A., Mosadegh, B., Lee, Q. Y., Liu, X., Luker, K. E., et al. (2009). Nanolitre liquid patterning in aqueous environments for spatially defined reagent delivery to mammalian cells. *Nat. Mater.* 8, 736–741. doi: 10.1038/nmat2515

Tavana, H., Kaylan, K., Bersano-Begey, T., Luker, K. E., Luker, G. D., and Takayama, S. (2011). Rehydration of polymeric, aqueous, biphasic system facilitates high throughput cell exclusion patterning for cell migration studies. *Adv. Funct. Mater.* 21, 2920–2926. doi: 10.1002/adfm.201002559

Yaguchi, T., Lee, S., Choi, W. S., Kim, D., Kim, T., Mitchell, R. J., et al. (2010). Micropatterning bacterial suspensions using aqueous two phase systems. *Analyst* 135, 2848–2852. doi: 10.1039/c0an00464b

**Conflict of Interest Statement:** The authors declare that the research was conducted in the absence of any commercial or financial relationships that could be construed as a potential conflict of interest.

The handling editor declared a past collaboration with one of the authors ST.

frontiers in Chemistry

ORIGINAL RESEARCH
published: 18 June 2019
doi: 10.3389/fchem.2019.00441

# Confinement of Suspension-Cultured Cells in Polyethylene Glycol/Polyethylene Oxide-Albumin Aqueous Two-Phase Systems

*Alyne G. Teixeira[1], Alex Kleinman[2], Rishima Agarwal[1], Nicky W. Tam[1], Jun Wang[3,4] and John P. Frampton[1]**

[1] School of Biomedical Engineering, Dalhousie University, Halifax, NS, Canada, [2] Pomona College, Claremont, CA, United States, [3] Department of Microbiology and Immunology, Dalhousie University, Halifax, NS, Canada, [4] Canadian Center for Vaccinology, IWK Health Centre, Halifax, NS, Canada

OPEN ACCESS

**Edited by:**
*Jean-Michel Lavoie, Université de Sherbrooke, Canada*

**Reviewed by:**
*Maizirwan Mel, International Islamic University Malaysia, Malaysia*
*Boris Yurii Zaslavsky, Cleveland Diagnostics, United States*
*Scott Tsai, Ryerson University, Canada*

***Correspondence:**
*John P. Frampton*
*john.frampton@dal.ca*

**Specialty section:**
*This article was submitted to Chemical and Process Engineering, a section of the journal Frontiers in Chemistry*

**Received:** *10 October 2018*
**Accepted:** *28 May 2019*
**Published:** *18 June 2019*

**Citation:**
*Teixeira AG, Kleinman A, Agarwal R, Tam NW, Wang J and Frampton JP (2019) Confinement of Suspension-Cultured Cells in Polyethylene Glycol/Polyethylene Oxide-Albumin Aqueous Two-Phase Systems. Front. Chem. 7:441. doi: 10.3389/fchem.2019.00441*

Aqueous two-phase systems (ATPSs) have numerous applications in separation science, and more recently, in bioassays enabled by the solution micropatterning of cells. The most frequently used ATPS in these applications is the polyethylene glycol (PEG)-dextran (Dex) system, as the polymers that form this ATPS have been extensively characterized in terms of their physicochemical properties. However, in addition to this well-known system, there exist many other ATPSs with properties that may be exploited to improve upon the PEG-dextran system for specific applications. One of these underexplored systems is the ATPS formed from PEG/polyethylene oxide (PEO) and albumin. In this article, we characterize the phase separation of PEG (35 kDa) and polyethylene oxide (PEO) (200, 900, and 4,000 kDa) with bovine serum albumin (BSA). We describe the microscopic emulsion behavior of these systems in the presence of NaCl and compounds ($NaHCO_3$, $NaH_2PO_4$, and HEPES) commonly used in buffer solutions and cell culture media. We further demonstrate that PEG- and PEO-albumin systems can be used in place of the PEG-dextran system for confinement of suspension-cultured cells (Jurkat T cells and RPMI-8226 B cells). Cell viability and morphology are examined for various polymer formulations relative to the commonly used PEG 35 kDa-Dex 500 kDa system and polymer-free cell culture medium. In addition, we examine cell activation for various phase-separating medium components by measuring IL-2 and IL-6 secretion. We demonstrate that we can confine immune cells and cytokines in the PEG-BSA system, and that this system can be employed to screen immune responses by enzyme-linked immunospot (ELISpot) assay. This new system represents a promising ATPS formulation for applications where low levels of baseline cell activation are required, for instance, when culturing immune cells.

**Keywords: aqueous two-phase systems, cell partitioning, polyethylene glycol, polyethylene oxide, bovine serum albumin, immune cells, ELISpot**

## INTRODUCTION

Aqueous two-phase systems (ATPSs) form when two incompatible polymers, a polymer and a salt, or a polymer and a surfactant exceed threshold concentrations in a common aqueous solvent (Albertsson, 1971; Akbulut et al., 2012). Each system can be characterized by a phase diagram that displays the concentrations at which the solutes phase-separate. A curved line called the binodal separates two areas: compositions represented by points above the binodal that give rise to phase separation and compositions represented by points below the binodal that mix to form a single phase (Albertsson, 1971; Teixeira et al., 2018). Phase separation can be influenced by physiochemical properties such as the polymer molecular weight (MW) and concentration, temperature, pH, and ionic concentration (Diamond and Hsu, 1992; Kaul, 2000; Cabral, 2007). For instance, higher MW polymers require lower concentrations for phase separation (Albertsson, 1971). In addition, the binodal curve delineating sub-critical concentrations from supercritical concentrations becomes more asymmetrical with increasing difference in MW between the two polymers (Albertsson, 1971). The system properties also influence the distribution of cells and biomolecules between the two phases.

ATPSs provide a mild non-toxic and non-denaturing environment for the partitioning of cells and biomolecules with applications ranging from isolation and recovery of antibodies (Muendges et al., 2015; Ferreira et al., 2016), proteins (da Silva et al., 2015; de Albuquerque Wanderley et al., 2017), virus-like particles (Jacinto et al., 2015; Ladd Effio et al., 2015), antibiotics (Pereira et al., 2012; Marques et al., 2013), (Johansson et al., 2012; Wiendahl et al., 2012), cells (Cabral, 2007; Zimmermann et al., 2016), extracellular vesicles (Shin et al., 2015), and hormones (He et al., 2005; Li et al., 2015) to solution micropatterning of cancer cells, hepatocytes and keratinocytes (Frampton et al., 2013; Agarwal et al., 2017). The most extensively used ATPS for these applications is the polyethylene glycol (PEG)-dextran (Dex) system. The cost-effectiveness and lack of acute cytotoxicity of the PEG-Dex system allows the precise positioning of cells by dispensing single-microliter or sub-microliter droplets of a cell-laden Dex solution within a PEG solution. The interfacial tension formed between the two polymer solutions confines the cells in the Dex droplets, where they can then adhere to the culture substrate. For adherent cells, the polymer solutions are removed once the cells attach to the substrate. However, confinement of suspension-cultured cells in an ATPS poses a challenge, as the polymers must remain in place for longer periods of time to maintain cell confinement. For culture periods longer than 24 h, cytotoxicity and cellular activation can vary by polymer type and concentration.

Here, we present an under-explored system for confinement of suspension-cultured cells that utilizes a PEG/polyethylene oxide (PEO) and bovine serum albumin (BSA) ATPS. Our objectives were to characterize phase separation of this novel system, evaluate the effects of PEG, PEO, and BSA on immune cell cytotoxicity and activation, and to demonstrate the utility of the PEG-BSA system for confinement of immune cells and reagents to reduce assay costs associated with the gold-standard enzyme linked immunospot (ELISpot) assay for measuring cytokine secretion from suspension-cultured cells. PEG and PEO have the same chemical structure. Industry conventions refer to low MW ethylene glycol polymers (less than ∼35,000 Da) as PEG, while ethylene glycol polymers greater than ∼35,000 Da are referred to as PEO (Wang et al., 2000). PEG and PEO are applied extensively in the food, cosmetic, and pharmaceutical industries. PEG and PEO are also widely used as biomaterials to alter surface properties to repel proteins (Lee et al., 1995), and have been applied for biomedical applications such as coating of medical devices and nanoparticles (Aqil et al., 2008). As a major amphiphilic plasma protein, albumin has been used as an essential nutrient for cell culture. Albumin has also been widely used in cell culture due to its role as an antioxidant and carrier of important biomolecules (Francis, 2010). ATPSs have been used for the extraction of BSA from biological fluids (Pei et al., 2009; Lu et al., 2010). However, to the best of our knowledge, this article is the first to use BSA as an ATPS-forming polymer. We demonstrate that PEG- and PEO-albumin systems are promising ATPS formulations for confinement of suspension-cultured cells such as T cells and B cells that require low levels of baseline cell activation. This ATPS-mediated technique enables T cell and B cell culture over the course of 72 h with minimal activation, as monitored by IL-2 and IL-6 secretion.

## MATERIALS AND METHODS

### PEG- and PEO-BSA Binodals

Unless otherwise noted, all polymer solutions are reported as percent weight solutions. Stock solutions of 30% BSA (Sigma-Aldrich), 20% PEG 35 kDa (Sigma-Aldrich), 10% PEO 200 kDa, 3% PEO 900 kDa, and 2.0% PEO 4,000 kDa (Dow Chemical) were dissolved in Dulbecco's Modified Eagle's Medium (DMEM; VWR). PEO solutions were centrifuged to sediment and remove silica particles introduced by the manufacturer. Concentrated stock solutions of BSA, PEG, and PEO were introduced to 96-well plates and mixed to form super-critical emulsions. Each super-critical concentration was then titrated with polymer-free culture medium until phase separation was no longer observed using methods similar to those reported previously for binodal determination in 96-well plates (Ruthven et al., 2017). The final BSA, PEG, and PEO concentrations were determined according to

$$C_i(V_i) = C_f(V_f),$$

where $C_i$ refers to the initial concentration,$V_i$ refers to the initial volume, $C_f$ refers to the final concentration and $V_f$ refers to the final volume. A Nikon Eclipse Ti microscope equipped with a 10x objective lens was used to observe microscopic emulsion characteristics.

### Microdroplet Characterization

Equilibrated ATPSs composed of 15% BSA and either 7% PEG 35 kDa, 4% PEO 200 kDa, 1.5% PEO 900 kDa, or 1.5% PEO 4,000 kDa were used to characterize the stability of dispensed

microdroplets. PEG- and PEO-BSA systems were centrifuged at 3,000 rcf to separate the phases for collection. Once collected, the top and bottom phases were centrifuged again at 3,000 rcf to allow removal of traces of the other phase transferred during collection. For each system, a 1 μL droplet of BSA-rich bottom phase was added to 500 μL of the PEG- or PEO- rich top phase. After 20 min (to allow droplet stabilization), a Nikon Eclipse Ti microscope equipped with a 2x objective lens was used to observe the droplets.

## Effects of Salt on Phase Separation

Solutions of 15% BSA and 1.5% PEO 900 kDa were prepared in distilled, de-ionized water containing the following salts: sodium bicarbonate (Fisher Scientific), HEPES (Sigma-Aldrich), sodium phosphate monobasic (Sigma-Aldrich) and sodium chloride (Fisher Scientific). Salts were tested at the following concentrations: 2, 4, 6, and 8 g/L. Microscopic emulsion characteristics in the presence of each salt were observed using a 10x objective lens on a Nikon Eclipse Ti microscope to determine the effects that individual medium components had on phase separation without extensively characterizing binodal curves for each system.

## Jurkat T Cell Culture

Jurkat T cells, clone E6-1 (ATCC: TIB-152), were cultured in a humidified incubator at 37°C under 5% $CO_2$ in RPMI 1640 medium (VWR) supplemented with 10% fetal bovine serum (FBS) and 1% antibiotics. Medium was replaced every 2–3 days and cell density was maintained below $1 \times 10^6$ cells/mL for cell propagation. Three types of plates were examined for suspension cell confinement in the PEG-BSA system: flat-bottom, round-bottom and V-bottom. Jurkat T cells were confined in the BSA phase (bottom). The BSA-phase was labeled with FITC-conjugated Dex and the cells were labeled with CellTracker Red™ CMTPX (Life Technologies) to aid in visualization. Cells cultured in the PEG-BSA system were observed using a 4x objective lens on a Nikon Eclipse Ti microscope.

## RPMI-8226 B Cell Culture

RPMI-8226 B cells (ATCC: CCL-155), were cultured in a humidified incubator at 37°C under 5% $CO_2$ in RPMI 1640 medium (VWR) supplemented with 10% fetal bovine serum (FBS) and 1% antibiotics. Medium was replaced every 2–3 days and cell density was maintained below $1 \times 10^6$ cells/mL for cell propagation.

## Cell Viability Assessment

Cells were seeded in 96-well culture plates at a density of $5 \times 10^3$ cells per well. The cells were then incubated for 72 h in 100 μL of either the individual filter-sterilized polymer solutions or BSA at concentrations exceeding those required for phase-separation. The following polymer/BSA concentrations in RPMI 1640 medium supplemented with 10% FBS and 1% antibiotics were examined: 7% PEG 35 kDa, 2% PEO 200 kDa, 0.5% PEO 900 kDa, 0.1% PEO 4,000 kDa, 7% Dex 500 kDa (T500; Pharmacosmos), and 10% BSA. Several lots of BSA were examined including BSA (Sigma-Aldrich cat # A7906), Albumax™ I (Gibco cat # 11020-021), HyClone (GE Life Sciences cat # SH30574.02) and Cellect™ Bovine Albumin Low IgG (MP Biomedicals cat # 180576). Cells were cultured in these solutions in a humidified incubator at 37°C under 5% $CO_2$ for 72 h prior to viability assessment.

Cell viability in the presence of individual polymers was assessed by live/dead staining with Calcein-AM (C-AM, Biotium) and Propidium Iodide (PI, Sigma-Aldrich). C-AM can enter live cells, where it is hydrolyzed in the cytoplasm to calcein, producing a fluorescent signal at 530 nm upon excitation with blue light (Weston and Parish, 1990). PI can only enter dead cells, where it subsequently binds to nucleic acids, primarily in the nucleus (Suzuki et al., 1997). Thus, C-AM was used to identify live cells (shown in green), whereas PI was used to identify dead cells (shown in red). A C-AM/PI stock solution (25 μM C-AM/25 μM PI) was prepared in RPMI 1640 medium. A volume of 12 μL of the stock solution was added to each well to achieve a final concentration of 3 μM for each dye. Cells were incubated in the presence of the dyes at 37°C under 5% $CO_2$ for 20 min. The cells were observed by epifluorescence microscopy using a Nikon Eclipse Ti Microscope. Images were processed using ImageJ to subtract background and adjust brightness.

## Jurkat T Cell Activation

Jurkat T cells were seeded at $5 \times 10^5$ cells/well in 24-well plates. The cells were stimulated with phorbol-12-myristate-13-acetate (PMA) and 300 ng/mL ionomycin. To determine the best PMA concentration to stimulate the cells as a positive control for cell activation, the following PMA concentrations were tested in culture medium: 25, 50, 100, and 200 ng/mL. Supernatants from PMA/ionomycin-stimulated cells were collected at three time points: 6-, 12- and 24-h post-stimulation. To assess Jurkat T cell activation in the presence of polymers/BSA, cells were seeded in 24-well culture plates at a density of $5 \times 10^5$ cells/well in the following polymer and BSA solutions in RPMI 1640 medium supplemented with 10% FBS and 1% antibiotics: 7% PEG 35 kDa, 7% Dex 500 kDa, 10% BSA Sigma, 10% BSA Albumax, and 10% BSA HyClone. After 6, 12, and 24 h, supernatants were collected to measure IL-2 secretion.

## RPMI-8226 B Cell Activation

RPMI-8226 B cells were seeded at $5 \times 10^5$ cells/well in 24-well plates. The cells were stimulated with lipopolysaccharide (LPS) from *Salmonella enterica serotype minnesota* (Sigma-Aldrich). To determine the best LPS concentration to stimulate the cells as a positive control for cell activation, the following LPS concentrations were tested in culture medium: 50, 100, and 200 ng/mL. Supernatants from LPS-stimulated cells were collected at two time points: 24- and 48-h post-stimulation. To assess RPMI-8226 B cell activation in the presence of polymers/BSA, cells were seeded in 24-well culture plates at a density of $5 \times 10^5$ per well in the following polymer and BSA solutions in RPMI 1640 medium supplemented with 10% FBS and 1% antibiotics: 7% PEG 35 kDa, 7% Dex 500 kDa, and 10% BSA Albumax. After 24 h, supernatants were collected to measure IL-6 secretion.

## Measurement of IL-2 and IL-6 Secretion

Concentrations of IL-2 and IL-6 in the supernatants were determined by enzyme-linked immunosorbent assay (ELISA) according to the manufacturer's instructions (R&D Systems cat # S2050 and cat # DY206) using antibody concentrations recommended by the manufacturer. Briefly, 96-well microplates were coated overnight with capture antibodies diluted in phosphate buffered saline (PBS). The next day, the plates were washed three times in PBS containing 0.2% Tween 20 (PBST) and blocked for 1 h with 1% BSA in PBS. After blocking, the plates were washed three times in PBST and incubated with the samples and recombinant protein standards for 2 h. Next, the plates were washed three times in PBST and incubated for 2 h with detection antibodies. The plates were then washed three times in PBST and incubated with streptavidin-conjugated horseradish peroxidase (HRP) for 20 min. Finally, the plates were washed three times in PBST and incubated with SuperSignal ELISA Pico Chemiluminescent Substrate (Thermo Fisher Scientific) for 10 min. All incubation and wash steps were performed at room temperature. Luminescence was measured using a FilterMax F5 microplate reader. Unknown values were determined by extrapolation from a four-parameter logistic standard curve.

## Confinement of Cells in the PEG-BSA System for ELISpot Assay

To demonstrate the utility of the PEG-BSA (Albumax) system, an optimized formulation was used to confine immune cells and reduce reagent consumption in the ELISpot assay. Briefly, 96-well ELISpot plates (Millipore Sigma) were coated with a working solution of 10 μg/mL IL-6 capture antibody from R&D Systems cat # DY206 diluted in PBS. The plates were stored at 4°C overnight. The next day, the plates were washed with sterile water and blocked for 1 h with complete RPMI medium for 2 h. After blocking, the medium was removed, and RPMI-8226 B cells were added to each well at various cell seeding densities. To stimulate the RPMI-8226 B cells, a final concentration of 100 ng/mL of LPS was added to the 10% BSA solution. Next, a 20 μL volume of the mixture was placed in each well of the ELISpot 96-well plate and covered with 80 μL of 7% PEG solution. A conventional ELISpot assay without cell confinement in the PEG-BSA system was performed in parallel as described above, with cells and LPS mixed in RPMI medium and 100 μL of the mixture added to each well. Following 24 h of culture for both the ATPS-based assay and the conventual assay, the plates were washed with PBS containing 0.01% Tween 20 and incubated with the IL-6 detection antibody (0.1 μg/mL antibody from R&D Systems cat # DY206) at 37°C for 2 h. The plates were then washed with PBS containing 0.01% Tween 20 and incubated with streptavidin-alkaline phosphatase (Biotium) (1:1000 dilution in sterile PBS) for 45 min. Finally, the plates were washed with PBS containing 0.01% Tween 20, followed by three washes with PBS, and incubated with 100 μL of BCIP/NBT substrate (Sigma-Aldrich) per well for 5–10 min. Spot development was stopped by extensive washing under running tap water. Plates were left to dry overnight in the dark. IL-6 producing cell spots were counted with an ImmunoSpot S6 (Cellular Technology Limited).

## Measurement of IL-6 Confinement

IL-6 confinement was examined for two ATPS formulations: 7% PEG 35 kDa-10% BSA (Albumax) and 5% PEG 35 kDa-6.4% Dex 500 kDa. Both systems were formed in complete RPMI 1640 medium. A total of 500 pg/mL of recombinant IL-6 was added to the bottom phase of each system (i.e., in either BSA or Dex). A 50 μL volume of each bottom phase solution was added to a 200 μL microtube and covered with a 150 μL layer of either 7% PEG for the PEG-BSA system or 5% PEG for the PEG-Dex system. Both systems were left to achieve thermodynamic equilibrium at room temperature, and the phases were collected separately at three time points: 2, 24, and 48 h. Three replicates were used for each system. Concentrations of recombinant IL-6 in the respective phases of the PEG-BSA and PEG-Dex systems were measured by ELISA according to the manufacturer's instructions (R&D Systems cat # DY206) using the same ELISA procedure described above.

## Statistical Analysis

Kruskal-Wallis one-way analysis of variance (ANOVA) and Tukey multiple comparison tests were conducted to compare the effects of phase-separating solutions on cell viability over 72 h. Kruskal-Wallis ANOVA and Tukey multiple comparison tests were performed to compare the effects of PMA and LPS concentrations on cell activation. Kruskal-Wallis ANOVA and Dunn's multiple comparison tests were performed to compare the effects of phase-separating solutions on IL-2 and IL-6 secretion by Jurkat T cells and RPMI-8226 B cells, respectively, over 24 h. One-way ANOVA and Tukey multiple comparison tests were conducted to compare IL-6 confinement ratios over time, and the number of IL-6 secreting cell spots as a function of cell density. Data are represented as mean values + standard deviations. Statistical significance was defined as $^{*}p < 0.05$.

# RESULTS

ATPSs readily formed from mixtures of PEG and PEO with BSA (**Figure 1**). As expected, increasing the PEG/PEO MW and concentration favored phase separation with BSA. Thus, PEG 35 kDa and PEO 200 kDa required higher concentrations to achieve phase separation with BSA as compared to PEO 900 kDa and PEO 4,000 kDa. Binodal data were fit according to

$$y = a \exp\left(bx^{0.5} - cx^{3}\right),$$

where y and x are the polymer concentrations (in weight percentage), and a, b and c represent fitting parameters (Merchuk et al., 1998). Fitting parameters are displayed for each binodal in **Figure 1**. Consistent with previous observations, as the polymer MW increased (thus increasing the MW difference between PEG/PEO and BSA), the binodal curves became increasingly asymmetric. **Figures 1A,D,G,J** also show two coordinates (points 1 and 2) that represent the total compositions of both phases. **Figures 1B,E,H,K** display the corresponding macroscopic and microscopic images after equilibration of the phases. In **Figure 1A**, point 1 corresponds to a system comprised of 7% PEG and 15% BSA, and point 2 corresponds to a system comprised

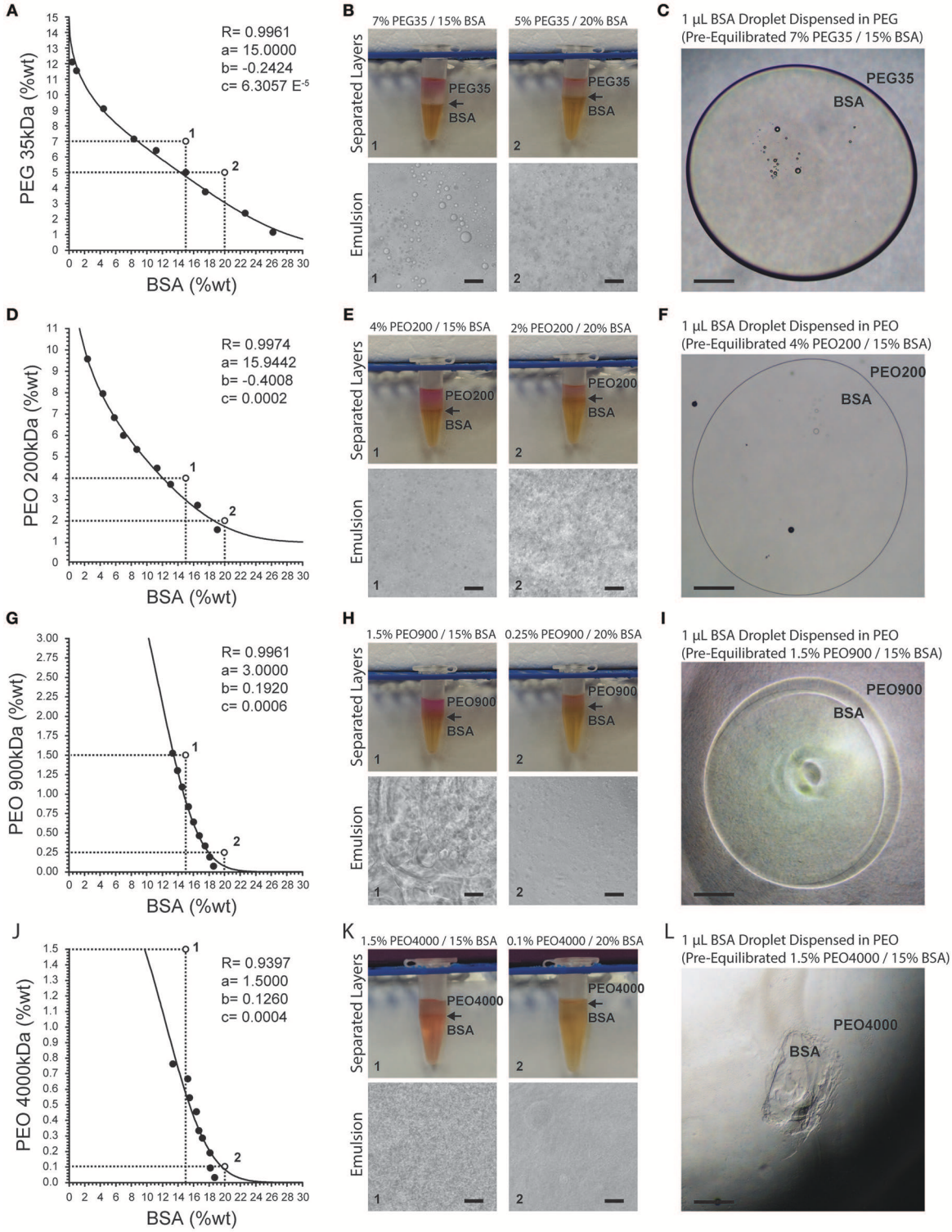


**FIGURE 1 |** Binodal curves for PEG- and PEO-BSA systems. **(A)** PEG 35 kDa-BSA, **(D)** PEO 200 kDA-BSA, **(G)** PEO 900 kDa-BSA and **(J)** PEO 4000 kDa-BSA. R is the correlation coefficient. Fitting parameters are denoted by a, b, and c. Points 1 and 2 correspond to formulations shown in images to the right. **(B**,**E**,**H**,**K)** show macroscopic and microscopic images of PEG, PEO, and BSA at different concentrations indicated by numbered points on the binodal graphs. Arrows indicate the location of the interface between the phases. **(C**,**F**,**I**,**L)** show microscopic images of pre-equilibrated BSA droplets dispensed in pre-equilibrated PEG and PEO solutions. Scale bars in **(B**,**E**,**H**,**K)** are 50 µm. Scale bars in **(C**,**F**,**I**,**L)** are 500 µm.

of 5% PEG and 20% BSA. Comparing the systems formed from points 1 and 2, one can appreciate that the relative volume of the bottom phase is greater for point 2, as would be predicted from estimation of the tie lines. Although systems on the same tie line have different total polymer concentration and different volume ratios after mixing, they should have the same final polymer concentrations in the top and bottom phases (Kaul, 2000).

Microscopically, one can observe formation of droplet structures for supercritical concentrations of solutes, similar to oil-in-water emulsions. In an ATPS-emulsion, the phase with the greatest volume fraction forms the continuous phase. For instance, in the system composed of 5% PEG and 20% BSA (**Figure 1B**), the continuous phase is BSA with PEG droplets dispersed within it. Although the interfacial tension of these ATPSs is orders of magnitude lower than oil-in-water systems, the formation of droplets indicates the presence of considerable interfacial tension between the two aqueous phases (Esquena, 2016).

Increasing the molecular weight and concentration of PEG/PEO increased the viscosities of the systems, resulting in longer settling times. The relatively high viscosities of the PEO 200 kDa, PEO 900 kDa, and PEO 4,000 kDa systems resulted

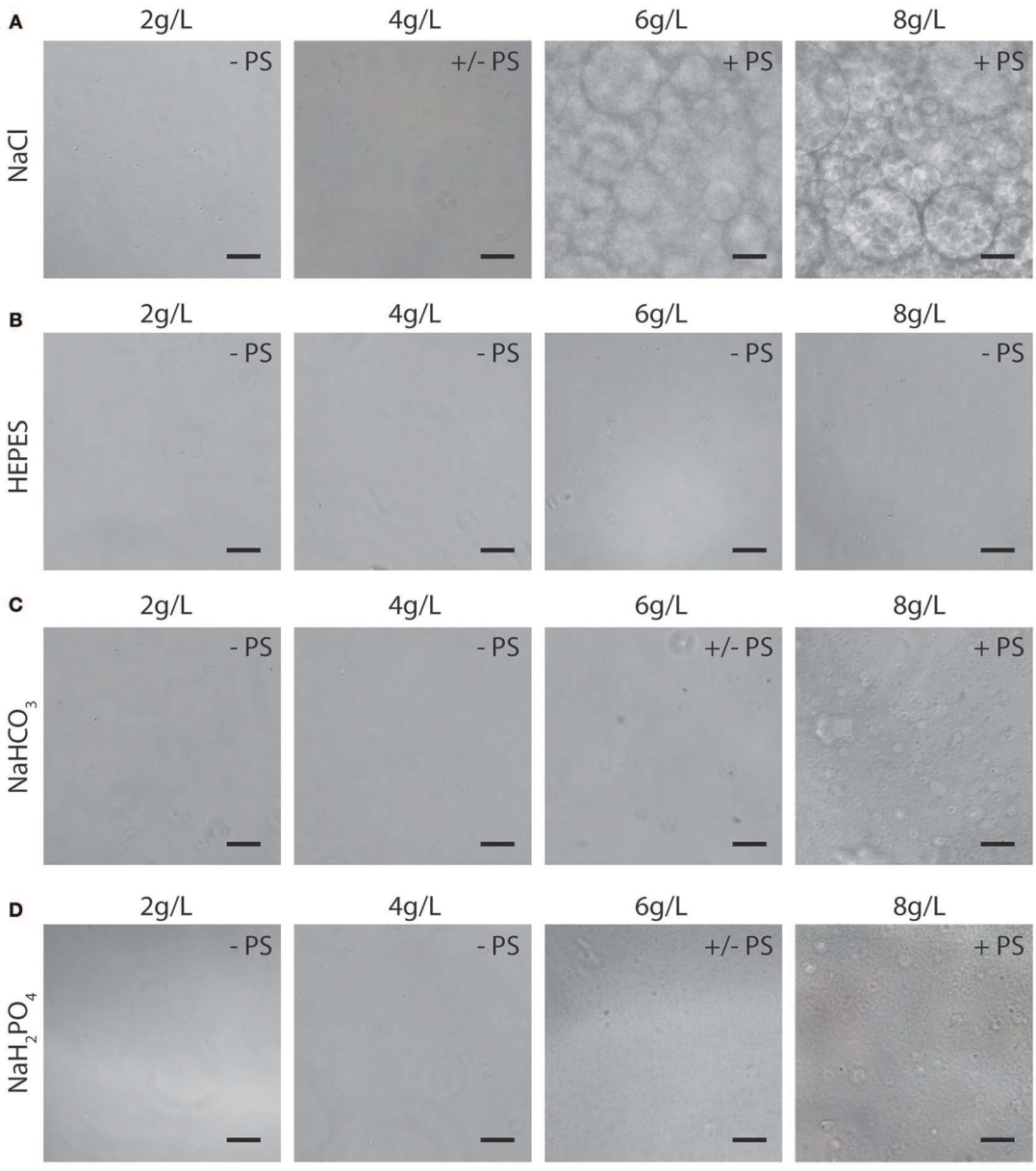


**FIGURE 2 |** Representative images (10X) of microdroplet emulsions in PEO 900 kDa-BSA systems with addition of NaCl **(A)**, HEPES **(B)**, $NaHCO_3$ **(C)**, $NAH_2PO_4$ **(D)**. PS: no phase separation; +/– PS: near critical system/slight phase separation; + PS: super-critical system with apparent phase separation. Scale bars are 50 μm.

in highly deformed microdroplets present in the emulsions (**Figures 1E,H,K**). The interfacial tension between the phases coupled with their viscosity can enable confinement of cells as well as select biomolecules by way of biomolecular partitioning. However, solutions of PEO 900 kDa above 1.5% and PEO 4,000 kDa above 0.7% are too viscous to experimentally analyze phase separation with BSA and display handling properties that preclude downstream applications. High viscosities of these polymer solutions make pipetting difficult, leading to inaccurate dispensed volumes. This is evident in the images of dispensed droplets of BSA-rich bottom phase into the top PEG-rich phase in **Figures 1C,F,I,L**. Systems composed of PEG 35 kDa, PEO 200 kDa, and PEO 900 kDa offer workable viscosities that allow dispensing of BSA microdroplets into a continuous phase of PEG/PEO.

In terms of ATPS thermodynamics, the free energy of mixing must be positive for phase separation to occur, which means that the enthalpy of mixing must dominate over the entropy of mixing (Frith, 2010). The addition of certain salts to an ATPS is thought to decrease the entropic penalty, thereby promoting de-mixing of the system at lower polymer concentrations (Frith, 2010; Johansson et al., 2011). We reasoned that salts and buffering compounds present in various cell culture medium formulations would therefore influence phase separation of PEG/PEO-BSA ATPSs. The influence of salts such as NaCl and buffering compounds such as HEPES, $NaHCO_3$ and $NaH_2PO_4$ on phase separation was therefore examined for a single ATPS formulation without extensive characterization of binodal phase diagrams (**Figure 2**). As shown in **Figure 2A**, increasing NaCl concentration promoted ATPS formation. Concentrations of NaCl in cell culture medium range from 4.5 to 7.6 g/L. Therefore, the NaCl concentration of a typical cell culture medium formulation is sufficient to promote phase separation of PEG/PEO and BSA. In contrast, HEPES, a buffering compound present in Iscove's Modified Dulbecco's Media (IMDM) at ∼6 g/L did not promote ATPS formation (**Figure 2B**). Sodium bicarbonate and sodium phosphate monobasic (also present in various medium formulations at concentrations ranging from ∼1.2 to 3.7 g/L, and ∼0.100 to 0.580 g/L, respectively) had modest effects on ATPS formation as shown in **Figures 2C,D**. The type of salt added to the system also influenced the shape and size of the microdroplets. Microdroplet emulsions formed in systems containing NaCl displayed droplets that were more well-defined and rounder than droplets formed in systems containing sodium bicarbonate and sodium phosphate monobasic, indicating that addition of NaCl influences the interfacial tension by strongly favoring de-mixing of the polymers.

Having characterized the phase separation of this novel system, we next sought to determine the effects that PEG/PEO and BSA had on cell viability and function. We evaluated the viability of Jurkat T cells in individual phase-separating solutions present in the PEG/PEO-BSA and PEG-Dex systems to assess the suitability of these polymers for long term cell culture. As shown in **Figures 3A,B**, culturing Jurkat T cells for 72 h in 7% PEG, resulted in ∼70% cell viability, as compared to >89% viability when the cells were cultured in the three types of PEO tested. Among the PEOs, 0.1% PEO 4,000 kDa had the least impact on cell viability with ∼98% cell viability. Therefore, polymer concentration has a considerable effect on cell viability over time. Addition of either technical grade BSA from Sigma or HyClone BSA to the medium resulted in <40% cell viability. However, addition of cell culture grade Albumax BSA to the medium resulted in 98% cell viability. Addition of low IgG BSA to the medium resulted in ∼90% cell viability. Cells cultured in Dex were ∼97% viable. We also evaluated the viability of RPMI-8226 B cells in a selection of individual phase-separating solutions to confirm the results obtained for T cells using an additional suspension-cultured immune cell line (**Figures 3C,D**). Culturing RPMI B cells for 72 h in 7% PEG 35kDa resulted in ∼76% cell viability. The 7% Dex solution had a similar impact on B cell viability with ∼73% cell viability. Cells cultured in the technical grade BSA (Sigma) were ∼44% viable, which was significantly different compared to control (∼80% cell viability). Since the impact of Sigma BSA on RPMI-8226 B cell viability was slightly lower in comparison with Jurkat T cells, we presumed that the cell culture grade Albumax BSA would not affect B cell viability. These results suggest that both PEG-BSA and PEG-Dex systems are suitable for culture of T cells and B over 72 h.

All polymer solutions examined tended to cause T cell aggregation, as shown in **Figure 3B**. Aggregation was most evident in the PEO, BSA, and Dex conditions. This effect can result from either excessive cell growth or immune cell activation. Therefore, we decided to investigate the effects of the phase-separating solutions on cell activation by measuring IL-2 secretion from Jurkat T cells and IL-6 secretion from RPMI-8226 B cells as these are the main cytokines secreted by these cells upon activation. As a positive control for T cell activation, Jurkat T cells were treated with PMA and ionomycin (**Figure 4A**). To find the optimal PMA concentration to activate the cells, we performed a dose-response experiment with PMA concentrations ranging from 25 to 200 ng/mL. There were no significant differences between the four different PMA concentrations tested over the first 6 h. After 12 h of exposure, 50 ng/mL PMA resulted in the highest level of IL-2 secretion out of any of the concentrations tested (∼390 pg/mL IL-2), reaching a peak of ∼470 pg/mL IL-2 after 24 h. As shown in **Figure 4B**, the polymers themselves do not stimulate IL-2 secretion over 24 h. Activation of Jurkat T cells by PMA/ionomycin treatment in polymer/BSA-containing medium was also confirmed. Thus, although Albumax, HyClone, and Dex cause cell aggregation, they do not stimulate IL-2 secretion and are therefore unlikely to have significant effects on cell activation.

To confirm that the polymer solutions did not stimulate RPMI-8626 B cells, we measured IL-6 secretion. As a positive control for B cell activation, RPMI-8226 B cells were treated with LPS (**Figure 4C**). To find the optimal LPS concentration to activate the cells, we performed a dose-response experiment with LPS concentrations ranging from 50 to 200 ng/mL. There were no significant differences between the four different LPS concentrations tested over the first 24 h. After 48 h of exposure, however, 200 ng/mL LPS resulted in the highest level of IL-6 secretion out of any of the concentrations tested (∼175 pg/mL IL-6) and was significantly different from the control (∼9.5 pg/mL IL-6). As shown in **Figure 4D**, the polymers themselves

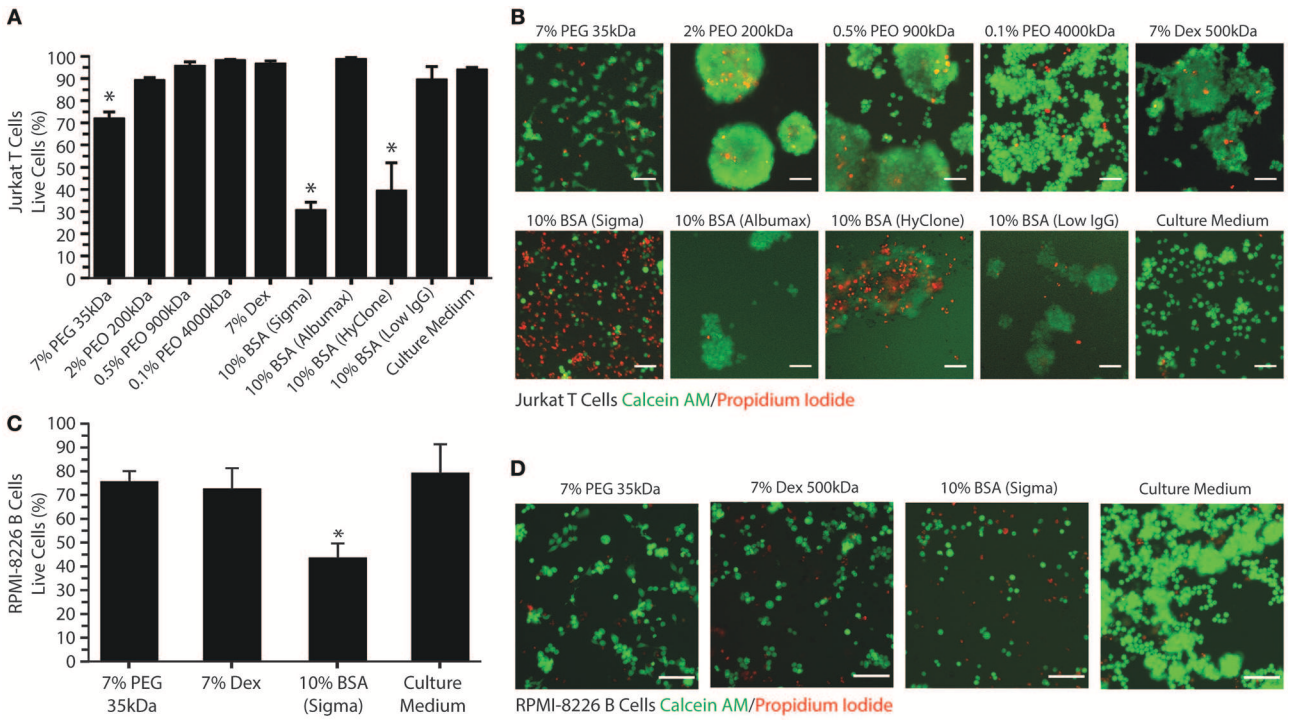


**FIGURE 3 |** Jurkat T cell and RPMI-8226 B cell viability in ATPS-polymer solutions. **(A)** Percentage of viable Jurkat T cells present for various polymer/BSA medium additives after 72 h. **(B)** Representative images (10X) of live Jurkat T cells (in green, stained with C-AM) and dead cells (in red, stained with PI) for various polymer/BSA medium additives after 72 h. **(C)** Percentage of viable RPMI-8226 B cells present for various polymer/BSA medium additives after 72 h. **(D)** Representative images (10X) of live RPMI-8226 B cells (in green) and dead cells (in red) for various polymer/BSA medium additives after 72 h. Scale bars are 50 μm. Significant reductions in cell viability relative to the control are indicated by *.

do not stimulate IL-6 secretion. Thus, Albumax, PEG, and Dex solutions do not stimulate IL-6 secretion and are therefore unlikely to have significant effects on cell activation, although additional cytokines should be examined in the future to confirm this observation.

Due to the mild environment provided by ATPSs, many applications have been developed in cell biology, e.g., for cell purification and more recently for micropatterning of cells for tissue engineering and high-throughput drug screening (Tavana and Takayama, 2011; Atefi et al., 2014; Agarwal et al., 2017). These techniques mainly use the well-known PEG-Dex system to specifically confine cells to one of the phases or to the interface between the phases (Tavana et al., 2011; Frampton et al., 2015). Previous work has focused on applications using adherent cells where the polymers are applied acutely to confine the cells and are subsequently washed away once the cells attach or assemble into aggregates. For applications involving suspension-cultured cells such as immune cells, however, the phase-separating solutions must remain in place to confine the cells over longer periods of time. **Figure 5A** shows a schematic diagram comparing ATPS-based immune cell culture with the conventional cell culture. The PEG-BSA system can potentially be applied for confining immune cells to reduce cell and reagent consumption in screening assays (e.g., adjuvants and antigens for vaccine development). For ATPS-based cell culture, immune cells and reagents are mixed in a BSA solution and covered with a PEG solution. Over 24 h of stimulation, immune cells produce cytokines, which remain confined in the bottom phase. For conventional cell culture, immune cells, and reagents such as adjuvants are mixed in culture medium only. Over 24 h of stimulation, immune cells secrete cytokines that diffuse throughout the culture medium.

To begin optimizing this system, we compared the confinement of immune cells in 96-well plates with three distinct well bottom shapes: flat-bottom, round-bottom, and V-bottom. In addition, we added different volume ratios of PEG:BSA (10:190, 20:180, 50:150, 60:140) (**Figure 5B**). Both variables (plate type and ATPS volume ratio) were evaluated in terms of cell confinement and ability to perform microscopic imaging. To better visualize the ATPS phases and the cells, the BSA phase was labeled with FITC-Dex and the Jurkat T cells were stained with CellTracker Red™ CMTPX. As shown in **Figure 5B**, both PEG and BSA phases can be easily visualized in each well type. In terms of cell confinement, the V-bottom well was most effective at localizing cells to a central well region, as shown in **Figure 5C**, with the effect of the ATPS mainly to prevent cell disruption during medium changes and supernatant collection. All four volume ratios enabled confinement and imaging of cells.

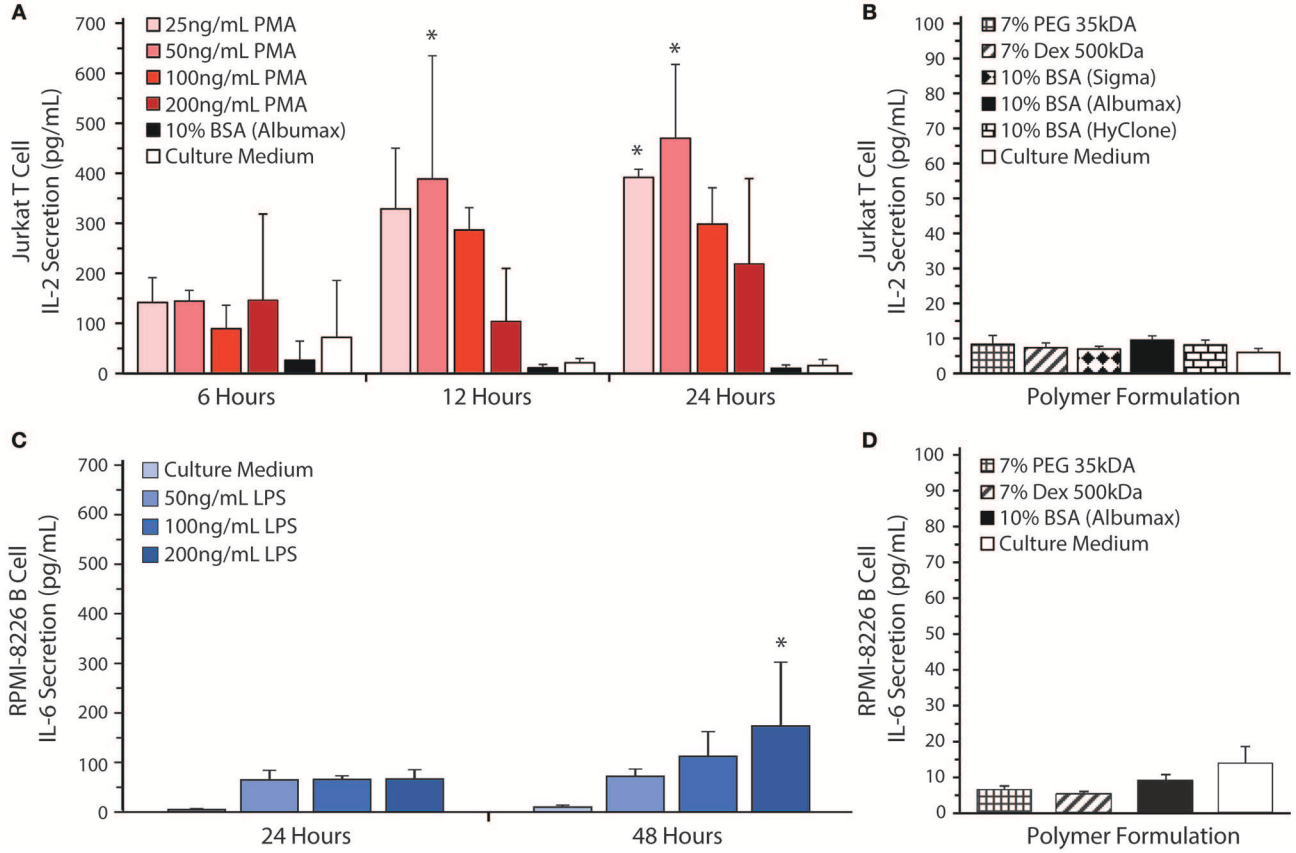


**FIGURE 4 |** Cytokine secretion by Jurkat T cells and RPMI-8226 B cells. **(A)** IL-2 levels were measured by ELISA in culture supernatants from Jurkat T cells at 6, 12, and 24 h after stimulation with 25, 50, 100, or 200 ng/mL of PMA in RPMI 1640 medium as a positive control for cell stimulation. All the stimulation conditions also received 300 ng/mL of ionomycin. The IL-2 secretion by Jurkat T-cells was also measured when the cells were cultured in 10% BSA (Albumax) without stimulation. RPMI 1640 medium was used as a negative control. Significant differences in cell activation relative to the control are indicated by *. **(B)** Jurkat T cells were cultured in 10% BSA (Albumax, Sigma, or HyClone) 7 % Dex, and 7% PEG. RPMI 1640 medium was used as a control. **(C)** IL-6 levels were measured by ELISA in culture supernatants from RPMI-8226 B cells at 24 and 48 h after stimulation with 50, 100, or 200 ng/mL of LPS in RPMI 1640 medium as a positive control for cell stimulation. RPMI 1640 medium without LPS was used as a negative control. Significant differences in cell activation relative to the control are indicated by *. **(D)** RPMI-8226 B cells were cultured in 10% BSA (Albumax) 7% Dex and 7% PEG 35 kDa. Both Jurkat T cell and RPMI-8226 B cell stimulation in various medium additives remained near baseline with no significant differences noted between polymer conditions and the culture medium control.

Thus, the 10:190 volume ratio is the most advantageous volume ratio for minimizing cell and reagent consumption.

In order to evaluate the potential of the PEG-BSA system for screening vaccine adjuvants *in vitro*, we conducted an ATPS-based ELISpot using the PEG-BSA system. **Figure 6A** shows a schematic diagram comparing the ATPS-based ELISpot with the conventional ELISpot assay. Both procedures follow the same protocol, except that the ATPS-based ELISpot confines cells and cytokines in the bottom BSA phase. **Figure 6B** compares ELISpot results obtained from the PEG-BSA system with those obtained from the PEG-Dex system and the conventional assay system. The PEG-BSA system produced spots that were qualitatively similar to those produced using the conventional assay protocol. Artifacts were more frequently observed for the PEG-Dex and conventional assay than in the PEG-BSA assay, as indicated by arrows pointing to line artifacts from cell movement, ring artifacts along the well edges and regions of the well devoid of spots. When the ELISpot assay was conducted using the PEG-Dex system to confine the cells, the overall signals and quality of the spots were appreciably diminished compared to the PEG-BSA and conventional assay formats.

We also examined IL-6 confinement in the 7% PEG-10% BSA and 5% PEG-6.4% Dex systems by adding 150 μL of the top phase (7% PEG or 5% PEG) on top of 50 μL of the bottom phase (10% BSA or 6.4% Dex), with the bottom phase spiked with recombinant IL-6 (500 pg/mL). After thermodynamic equilibration at room temperature, we collected each phase separately for analysis, measured the IL-6 concentration in each phase and plotted the ratio of IL-6 concentration between the top phase and bottom phase. As shown in **Figure 6C**, IL-6 was more strongly confined in the BSA phase of the PEG-BSA system than in the Dex phase of the PEG-Dex system, suggesting that the PEG-BSA system is superior to the PEG-Dex phase system for confining cytokines in the ELISpot assay and in other

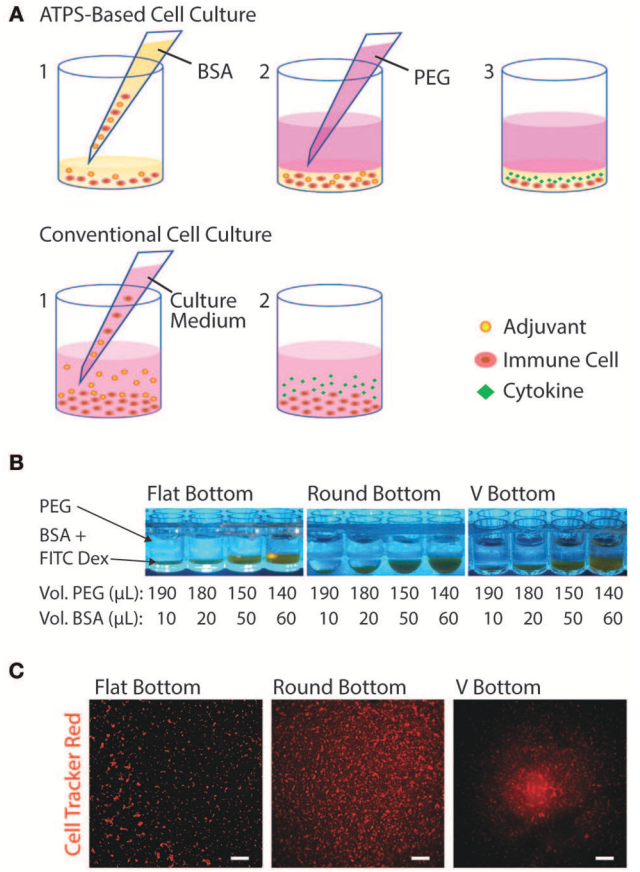


**FIGURE 5 |** Schematic diagram of the PEG-BSA system for compartmentalized immune cell culture. **(A)** Experiment setup using ATPS: (1) Immune cells are suspended in the BSA solution containing reagents (e.g., adjuvants), and 20 μL of the mixture is added to each well of a 96-well plate. (2) An 80 μL volume of the PEG solution is added to the well to cover the BSA-bottom phase, confining cells and reagents in the BSA solution. (3) Over 24 h of adjuvant stimulation, immune cells produce cytokines, which remain confined in the bottom phase. Conventional experiment setup: (1) Immune cells and reagents are mixed in culture medium and added to each well. (2) Over 24 h of stimulation, immune cells secrete cytokines that diffuse throughout the culture medium. **(B)** PEG-BSA systems in three 96-well plate geometries: flat-bottom, round bottom, and V bottom. The BSA-phase (bottom) is labeled with FITC-Dex. **(C)** Representative images (4X) of Jurkat T cells cultured in the PEG-BSA system in flat-bottom, round-bottom, and V-bottom 96-well plates. The cells were stained with CellTracker Red$^{TM}$ CMTPX. Scale bars are 100 μm.

immunoassays used for screening cell responses. This may also partially explain why the quality of the spots in the ELISpot assay were better for the PEG-BSA system as compared to the PEG-Dex system.

Finally, **Figures 6D,E** compares images of ATPS-based ELISpot using the PEG-BSA system and conventional ELISpot as a function of cell seeding density. Compared to the conventional technique, ATPS-based ELISpot presented less background noise and a lower frequency of spot development. As shown in **Figure 6F**, the number of spots developed using the ATPS-based ELISpot is smaller in comparison with the conventional assay across different cell densities. However, there is a significant difference in spot number between ATPS-based ELISpot and conventional ELISpot assay for each cell density. Interestingly, using the ATPS-based assay there is a significant difference between each cell density, whereas with the conventional method, there is no significant difference between $10 \times 10^3$ and $5 \times 10^3$ cells per well, suggesting that the ATPS technique may improve assay sensitivity when measuring low numbers of cytokine secreting cells.

## DISCUSSION

Microscale technologies are frequently used to investigate cell-material interactions (Anderson et al., 2005; Khetani and Bhatia, 2008), engineer and control cell shape and function (Singhvi et al., 1994), and evaluate cell responses (Chen et al., 2005) in a high-throughput manner. These technologies offer tight control of the cellular microenvironment, significantly reduce the consumption of cells and reagents required to perform experiments, and in some cases, improve reaction efficiencies (Chung et al., 2007). Many of these platforms rely on microfluidics to manipulate the small volumes of fluid used for cell culture and analysis. Microfluidic array platforms have been developed for high-throughput cytotoxicity screening, where three types of mammalian cell lines were screened against low and high concentrations of five toxins (digitonin, saponin, $CoCl_2$, $NiCl_2$, and acrolein) (Wang et al., 2007). Another example is the sophisticated system developed by Choi and Cunningham, which integrates a 96-well microplate with microfluidic networks and biosensors to measure the binding of IgG molecules (20 μL IgG solution consumed) to immobilized protein A (30 μL protein A solution consumed) (Choi and Cunningham, 2007). Although both systems are able to analyze cell viability and biomolecular interactions in a multiplex format while minimizing reagent consumption, the specialized technical expertise and equipment required to operate systems such as these limits their utility in life science laboratories.

In contrast to Dex, BSA is ionic and amphiphilic, which may intensify BSA interactions with cells and biomolecules. Our findings suggest that the PEG-BSA system has potential utility in confining immune cells in the bottom phase without significantly affecting cellular viability and activation. In addition, the BSA phase promotes superior IL-6 confinement over time compared to the Dex phase which may be advantageous for detection by various immunoassays such as ELISpot. In terms of practical application, our ATPS-based multiplex screening does not rely on expensive and complex equipment and can be easily adapted to any laboratory familiar with commonly-available liquid handing tools such as handheld micropipettes. The approach presented here can micropattern immune cells in an ATPS, while retaining high cell viability and minimizing cell activation as measured by IL-2 and IL-6 secretion.

There is considerable interest in polymers that are naturally immunostimulatory. Short cationic amphiphilic peptides are produced by several different cell types and can modulate the

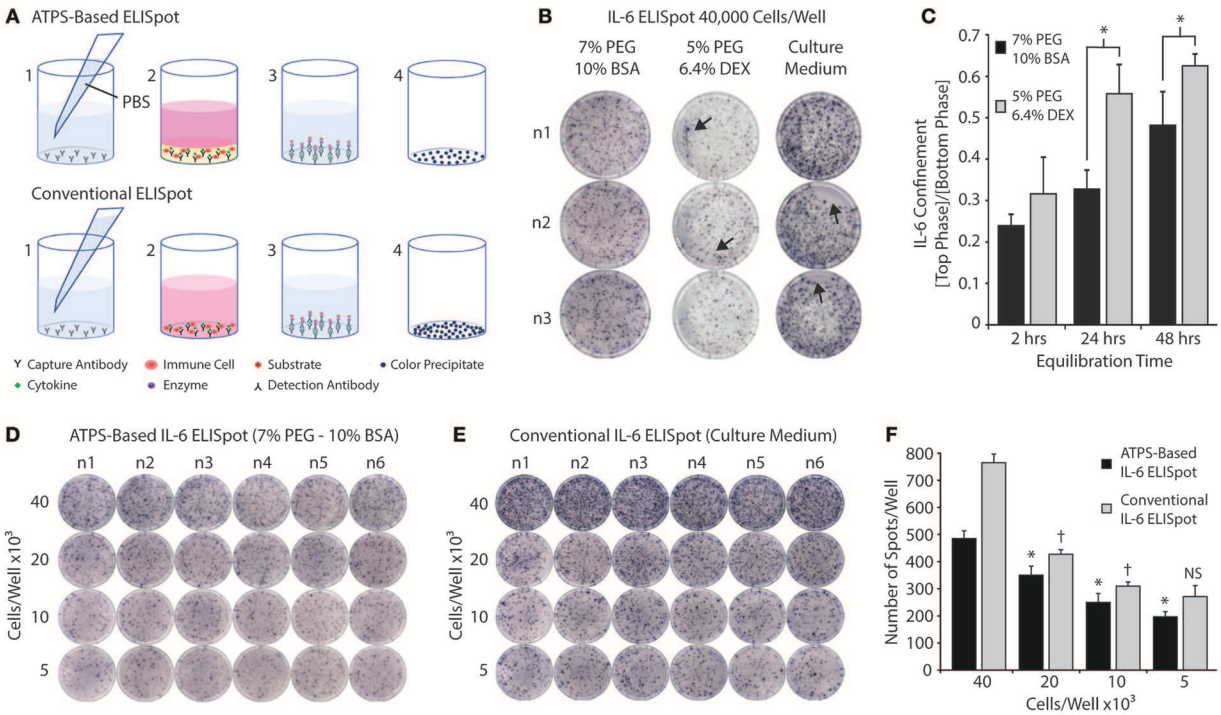


**FIGURE 6 |** Screening immune cells in the PEG-BSA system by ELISpot. **(A)** ATPS-Based ELISpot: (1) Capture antibodies are diluted in PBS and added to each well. After overnight incubation, the capture antibodies are washed away and replaced with immune cells and adjuvants mixed in the BSA-phase. Over 24 h of stimulation, cytokines are produced by the immune cells and become confined in the BSA-phase where they bind to the capture antibodies. (3) The PEG-BSA system is washed away and it is replaced with detection antibodies mixed in PBS, followed by streptavidin-alkaline phosphatase and substrate solutions. (4) Each colored spot detected on the membrane at the bottom of each well corresponds to a cytokine-secreting cell. Conventional ELISpot: (1) Capture antibodies are mixed in PBS and added to each well of an ELISpot plate. After overnight incubation, the capture antibodies are washed away and replaced with immune cells suspended in culture medium containing adjuvants. Over 24 h of stimulation, the cytokines produced by immune cells bind to capture antibodies. (3) The culture medium is washed away and it is replaced with detection antibodies mixed in PBS, followed by enzyme and substrate solutions. (4) Each colored spot detected on the membrane at the bottom of each well corresponds to a cytokine-secreting cell. **(B)** Representative ELISpot results for RPMI-8226 B cells stimulated with LPS and incubated in 7% PEG-10% BSA, 5% PEG-6.4% Dex, and culture medium for 24 h. Artifacts are indicated by arrows pointing to line artifacts from cell movement, ring artifacts along the well edges, and regions of the well devoid of spots. **(C)** IL-6 confinement in the bulk phases of two ATPS formulations over time: 10%BSA-7%PEG and 6.4%Dex-5%PEG. $^*p < 0.05$ (ANOVA with Tukey *post-hoc* test). **(D)** Representative ELISpot results for RPMI-8226 B cells stimulated with LPS and incubated for 24 h in the 7% PEG-10% BSA system. **(E)** Representative ELISpot results for RPMI-8226 B cells stimulated with LPS and incubated for 24 h in culture medium (conventional method). **(F)** The spots formed within wells using both methods were counted and plotted as a function of cell density. The * denotes significant differences from the next highest cell density for the ATPS-based method. The †denotes significant differences from the next highest cell density for the conventional method. NS denotes no significant difference from the next highest cell density.

innate immune response, which makes them useful as adjuvants (Hancock et al., 2016). Polysaccharides also stimulate immune responses and have been used as adjuvants. For example, inulin-based adjuvants have been shown to activate both humoral and cellular immune responses (Petrovsky, 2006; Kumar et al., 2016). Chitosan is another polysaccharide that elicits a cellular immune response (Moran et al., 2018). We anticipate that our system may be used to confine various biomolecules and immunostimulatory polymers and particles within the BSA phase via biomolecular partitioning for future applications in screening novel immunotherapies and adjuvant formulations. In this future work, it will be important to consider the handling properties of the ATPS-forming solutions and to more completely characterize the phenotype of cells used in experiments by assessing other types of immune cells and secreted cytokines. This cell characterization work will be particularly important in light of the cell aggregation phenomenon we observed for Jurkat T cells, since cell-cell interactions are functionally important for T cell signaling, as they are for other immune cells (Sabatos et al., 2008). However, our data for IL-2 secretion suggest that aggregation of Jurkat T cells cultured in ATPSs does not necessarily correlate with cell activation.

Although most ATPSs used in cell culture applications have been used to biopattern adherent cells (Tavana et al., 2009; Frampton et al., 2013), ATPS techniques have also been developed to form non-adherent cell aggregates. By exploiting the interfacial forces between PEG and Dex, Frampton et al. developed a simple method to confine cells and promote their assembly into tissue constructs (Frampton et al., 2015). Initially, cells were suspended in the PEG phase, which was layered on top of the Dex phase. The cells were then allowed to settle by gravity to the PEG-Dex interface. Once at the interface,

cell-cell connections were formed, leading to the self-assembly of constructs over several hours. ATPS techniques have also enabled generation of tumor spheroids by confining cells within a nanoliter-volume droplet of Dex immersed in a PEG phase (Atefi et al., 2014; Han et al., 2015). However, to the best of our knowledge, an ATPS has not been used to confine suspension-cultured cells such as immune cells. Confining suspension-cultured cells in an ATPS can be more challenging than adherent cells because the polymers must remain in place to continue to confine the cells.

A novel application for the PEG-BSA system is in confinement of immune cell and reagents such as adjuvants and antigens used in vaccine formulation development. ELISpot is a technique widely used for screening vaccine candidates by measuring cellular immune responses to a specific stimulus (Chambers et al., 2010). The ATPS-based ELISpot was used to demonstrate the application of the PEG-BSA system to confine immune cells to facilitate vaccine adjuvant screening *in vitro*. When conducting ELISpot using BSA as the bottom phase, the BSA solution reduced spot development by blocking non-specific binding and consequently improving the sensitivity of the assay. One can notice a significant difference between each cell density using the PEG-BSA system to confine cells and cytokines. However, with the conventional method, there is no significant difference between the lowest cell densities ($10 \times 10^3$ and $5 \times 10^3$ cells/well), which means that the ATPS-based ELISpot has potential to improve the sensitivity of this assay. Addressing how additional adjuvants and cytokines other than IL-6 partition between the PEG and BSA phase will be of paramount importance in determining the broad utility of this approach.

Finally, the ATPS-based approach described here opens up possibilities for applications beyond the culture of immune cell lines for screening applications. For example, mixtures of adherent and non-adherent cell types can potentially be co-cultured in this platform to investigate cell interactions and better understand the complexity of immune cell signaling in various tissues. Furthermore, the PEG-BSA system has potential to be applied to separate and purify biomolecules according to their affinity for each phase. The PEG/PEO-BSA system may also find applications in the encapsulation of drugs and biomolecules. Thus, characterization of this novel ATPS and preliminary evaluation of the cytotoxicity and cellular responses to the phase-forming solutes may be valuable for exploration of a variety of future biomedical applications.

## CONCLUSION

We characterized a new ATPS and demonstrated that immune cells and cytokines can be confined in a PEG-BSA system without compromising cell viability and activation. We showed that this new system can be employed to improve the sensitivity of a conventional ELISpot assay by reducing background noise and detecting differences between small numbers of cytokine secreting cells. We anticipate that this new system will enable more robust and cost-effective multiplex screening of adjuvants and other compounds known to stimulate immune cells.

## AUTHOR CONTRIBUTIONS

AT performed or assisted with all experiments and wrote the paper. AK performed the phase-separation characterization and helped write the paper. RA helped analyze data and edited the paper. NT helped analyze data and edited the paper. JW contributed to the initial concept of this work and assisted with experimental planning. JF oversaw all experiments and edited the paper.

## FUNDING

This work was supported by Canada Research Chairs Program, Canada Foundation for Innovation (Project# 33533), and the Natural Sciences and Engineering Research Council of Canada (NSERC–RGPIN-2016-02498).

## ACKNOWLEDGMENTS

AT acknowledges a scholarship from the Nova Scotia Provincial Government (NSGS Doctoral Scholarship). NT acknowledges scholarships from the Dalhousie University Faculty of Medicine (Graduate Studentship Award) and Beatrice Hunter Cancer Research Institute (Telus Ride for Dad and Prostate Cancer Fight Foundation).

## REFERENCES

Agarwal, R., Ko, K. R., Gratzer, P. F., and Frampton, J. P. (2017). Biopatterning of keratinocytes in aqueous two-phase systems as a potential tool for skin tissue engineering. *MRS Adv.* 2, 2443–2449. doi: 10.1557/adv.2017.357

Akbulut, O., Mace, C. R., Martinez, R. V., Kumar, A. A., Nie, Z., Patton, M. R., et al. (2012). Separation of nanoparticles in aqueous multiphase systems through centrifugation. *Nano Lett.* 12, 4060–4064. doi: 10.1021/nl301452x

Albertsson, P.-Å. (1971). *Partition of Cell Particles and Macromolecules; Distribution and Fractionation of Cells, Mitochondria, Chloroplasts, Viruses, Proteins, Nucleic Acids, and Antigen-Antibody Complexes in Aqueous Polymer Two-Phase Systems*. New York, NY: Wiley-Interscience.

Anderson, D. G., Putnam, D., Lavik, E. B., Mahmood, T. A., and Langer, R. (2005). Biomaterial microarrays: rapid, microscale screening of polymer-cell interaction. *Biomaterials* 26, 4892–4897. doi: 10.1016/j.biomaterials.2004.11.052

Aqil, A., Vasseur, S., Duguet, E., Passirani, C., Benoît, J. P., Roch, A., et al. (2008). PEO coated magnetic nanoparticles for biomedical application. *Eur. Polym. J.* 44, 3191–3199. doi: 10.1016/j.eurpolymj.2008.07.011

Atefi, E., Lemmo, S., Fyffe, D., Luker, G. D., and Tavana, H. (2014). High throughput, polymeric aqueous two-phase printing of tumor spheroids. *Adv. Funct. Mater.* 24, 6509–6515. doi: 10.1002/adfm.201401302

Cabral, J. M. S. (2007). Cell partitioning in aqueous two-phase polymer systems. *Adv. Biochem. Eng. Biotechnol.* 106, 151–171. doi: 10.1007/10_2006_045

Chambers, I. R., Cone, T. R., Oswald-Richter, K., and Drake, W. P. (2010). Enzyme-linked immunospot assay (ELISPOT): Quantification of Th-1 cellular immune responses against microbial antigens. *J. Vis. Exp.* doi: 10.3791/2221

Chen, D. S., Soen, Y., Stuge, T. B., Lee, P. P., Weber, J. S., Brown, P. O., et al. (2005). Marked differences in human melanoma antigen-specific T cell

responsiveness after vaccination using a functional microarray. *PLoS Med.* 2:e265. doi: 10.1371/journal.pmed.0020265

Choi, C. J., and Cunningham, B. T. (2007). A 96-well microplate incorporating a replica molded microfluidic network integrated with photonic crystal biosensors for high throughput kinetic biomolecular interaction analysis. *Lab. Chip* 7, 550–556. doi: 10.1039/b618584c

Chung, B. G., Kang, L., and Khademhosseini, A. (2007). Micro- and nanoscale technologies for tissue engineering and drug discovery applications. *Expert Opin. Drug Discov.* 2, 1653–1668. doi: 10.1517/17460441.2.12.1653

da Silva, N. R., Ferreira, L. A., Madeira, P. P., Teixeira, J. A. C., Uversky, V. N., and Zaslavsky, B. Y. (2015). Analysis of partitioning of organic compounds and proteins in aqueous polyethylene glycol-sodium sulfate aqueous two-phase systems in terms of solute-solvent interactions. *J. Chromatogr. A* 1415, 1–10. doi: 10.1016/j.chroma.2015.08.053

de Albuquerque Wanderley, M. C., Neto, J. M. W. D., Albuquerque, W. W. C., de Araújo Viana Marques, D., de Albuquerque Lima, C., da Cruz Silvério, S. I., et al. (2017). Purification and characterization of a collagenase from Penicillium sp. UCP 1286 by polyethylene glycol-phosphate aqueous two-phase system. *Protein Expr. Purif.* 133, 8–14. doi: 10.1016/j.pep.2017.02.010

Diamond, A. D., and Hsu, J. T. (1992). "Aqueous two-phase systems for biomolecule separation BT - Bioseparation," in *Aqueous two-phase systems for biomolecule separation*, ed G. T. Tsao (Berlin: Springer), 89–135.

Esquena, J. (2016). Water-in-water (W/W) emulsions. *Curr. Opin. Colloid Interface Sci.* 25, 109–119. doi: 10.1016/j.cocis.2016.09.010

Ferreira, A. M., Faustino, V. F., Mondal, D., Coutinho, J. A., and Freire, M. G. (2016). Improving the extraction and purification of immunoglobulin G by the use of ionic liquids as adjuvants in aqueous biphasic systems. *J. Biotechnol.* 236, 166–175. doi: 10.1016/j.jbiotec.2016.08.015

Frampton, J. P., Leung, B. M., Bingham, E. L., Lesher-Perez, S. C., Wang, J. D., Sarhan, H. T., et al. (2015). Rapid self-assembly of macroscale tissue constructs at biphasic aqueous interfaces. *Adv. Funct. Mater.* 25, 1694–1699. doi: 10.1002/adfm.201403825

Frampton, J. P., White, J. B., Abraham, A. T., and Takayama, S. (2013). Cell co-culture patterning using aqueous two-phase systems. *J. Vis. Exp.* 73:50304. doi: 10.3791/50304

Francis, G. L. (2010). Albumin and mammalian cell culture: implications for biotechnology applications. *Cytotechnology* 62, 1–16. doi: 10.1007/s10616-010-9263-3

Frith, W. J. (2010). Mixed biopolymer aqueous solutions - phase behaviour and rheology. *Adv. Colloid Interface Sci.* 161, 48–60. doi: 10.1016/j.cis.2009.08.001

Han, C., Takayama, S., and Park, J. (2015). Formation and manipulation of cell spheroids using a density adjusted PEG/DEX aqueous two phase system. *Sci. Rep.* 5:11891. doi: 10.1038/srep11891

Hancock, R. E. W., Haney, E. F., and Gill, E. E. (2016). The immunology of host defence peptides: beyond antimicrobial activity. *Nat. Rev. Immunol.* 16, 321–334. doi: 10.1038/nri.2016.29

He, C., Li, S., Liu, H., Li, K., and Liu, F. (2005). Extraction of testosterone and epitestosterone in human urine using aqueous two-phase systems of ionic liquid and salt. *J. Chromatogr. A* 1082, 143–149. doi: 10.1016/j.chroma.2005.05.065

Jacinto, M. J., Soares, R. R. G., Azevedo, A. M., Chu, V., Tover, A., Conde, J. P., et al. (2015). Optimization and miniaturization of aqueous two phase systems for the purification of recombinant human immunodeficiency virus-like particles from a CHO cell supernatant. *Sep. Purif. Technol.* 154, 27–35. doi: 10.1016/j.seppur.2015.09.006

Johansson, H.-O., Feitosa, E., and Junior, A. P. (2011). Phase diagrams of the aqueous two-phase systems of poly(ethylene glycol)/sodium polyacrylate/salts. *Polymers* 3, 587–601. doi: 10.3390/polym3010587

Johansson, H.-O., Matos, T., Luz, J. S., Feitosa, E., Oliveira, C. C., Pessoa, A., et al. (2012). Plasmid DNA partitioning and separation using poly(ethylene glycol)/poly(acrylate)/salt aqueous two-phase systems. *J. Chromatogr. A* 1233, 30–35. doi: 10.1016/j.chroma.2012.02.028

Kaul, A. (2000). "The phase diagram," in *Aqueous Two-Phase Systems: Methods and Protocols, Vol. 11, Methods in Biotechnology*, ed R. Hatti-Kaul (Totowa, N.J: Humana Press), 11–21.

Khetani, S. R., and Bhatia, S. N. (2008). Microscale culture of human liver cells for drug development. *Nat. Biotechnol.* 26, 120–126. doi: 10.1038/nbt1361

Kumar, S., Kesharwani, S. S., Kuppast, B., Rajput, M., Ali Bakkari, M., and Tummala, H. (2016). Discovery of inulin acetate as a novel immune-active polymer and vaccine adjuvant: synthesis, material characterization, and biological evaluation as a toll-like receptor-4 agonist. *J. Mater. Chem. B* 4, 7950–7960. doi: 10.1039/C6TB02181F

Ladd Effio, C., Wenger, L., Ötes, O., Oelmeier, S. A., Kneusel, R., and Hubbuch, J. (2015). Downstream processing of virus-like particles: single-stage and multi-stage aqueous two-phase extraction. *J. Chromatogr. A* 1383, 35–46. doi: 10.1016/j.chroma.2015.01.007

Lee, J. H., Lee, H. B., and Andrade, J. D. (1995). Blood compatibility of polyethylene oxide surfaces. *Prog. Polym. Sci.* 20, 1043–1079. doi: 10.1016/0079-6700(95)00011-4

Li, N., Yang, X., Nian, L., Wang, Z., Lei, L., Wang, K., et al. (2015). Determination of steroid hormones in milk using aqueous two-phase extraction coupled to liquid chromatography. *Anal. Methods* 7, 2514–2522. doi: 10.1039/C4AY03036B

Lu, Y. M., Yang, Y. Z., Zhao, X. D., and Xia, C. B. (2010). Bovine serum albumin partitioning in polyethylene glycol (PEG)/potassium citrate aqueous two-phase systems. *Food Bioprod. Process.* 88, 40–46. doi: 10.1016/j.fbp.2009.12.002

Marques, C. F. C., Mourão, T., Neves, C. M. S. S., Lima, Á. S., Boal-Palheiros, I., Coutinho, J. A. P., et al. (2013). Aqueous biphasic systems composed of ionic liquids and sodium carbonate as enhanced routes for the extraction of tetracycline. *Biotechnol. Prog.* 29, 645–654. doi: 10.1002/btpr.1708

Merchuk, J. C., Andrews, B. A., and Asenjo, J. A. (1998). Aqueous two-phase systems for protein separation: studies on phase inversion. *J. Chromatogr. B Biomed. Sci. Appl.* 711, 285–293 doi: 10.1016/S0378-4347(97)00594-X

Moran, H. B. T., Turley, J. L., Andersson, M., and Lavelle, E. C. (2018). Immunomodulatory properties of chitosan polymers. *Biomaterials* 184, 1–9. doi: 10.1016/j.biomaterials.2018.08.054

Muendges, J., Zalesko, A., Górak, A., and Zeiner, T. (2015). Multistage aqueous two-phase extraction of a monoclonal antibody from cell supernatant. *Biotechnol. Prog.* 31, 925–936. doi: 10.1002/btpr.2088

Pei, Y., Wang, J., Wu, K., Xuan, X., and Lu, X. (2009). Ionic liquid-based aqueous two-phase extraction of selected proteins. *Sep. Purif. Technol.* 64, 288–295. doi: 10.1016/j.seppur.2008.10.010

Pereira, J. F. B., Santos, V. C., Johansson, H.-O., Teixeira, J. A. C., and Pessoa, A. (2012). A stable liquid–liquid extraction system for clavulanic acid using polymer-based aqueous two-phase systems. *Sep. Purif. Technol.* 98, 441–450. doi: 10.1016/j.seppur.2012.08.008

Petrovsky, N. (2006). Novel human polysaccharide adjuvants with dual Th1 and Th2 potentiating activity. *Vaccine* 24 (Suppl. 2):S2-26-9. doi: 10.1016/j.vaccine.2005.01.107

Ruthven, M., Ko, K. R., Agarwal, R., and Frampton, J. P. (2017). Microscopic evaluation of aqueous two-phase system emulsion characteristics enables rapid determination of critical polymer concentrations for solution micropatterning. *Analyst* 142, 1938–1945. doi: 10.1039/C7AN00255F

Sabatos, C. A., Doh, J., Chakravarti, S., Friedman, R. S., Pandurangi, P. G., Tooley, A. J., et al. (2008). A synaptic basis for paracrine Interleukin-2 signaling during homotypic T cell interaction. *Immunity* 29, 238–248. doi: 10.1016/j.immuni.2008.05.017

Shin, H., Han, C., Labuz, J. M., Kim, J., Kim, J., Cho, S., et al. (2015). High-yield isolation of extracellular vesicles using aqueous two-phase system. *Sci. Rep.* 5:13103. doi: 10.1038/srep13103

Singhvi, R., Kumar, A., Lopez, G. P., Stephanopoulos, G. N., Wang, D. I., Whitesides, G. M., et al. (1994). Engineering cell shape and function. *Science* 264, 696–698. doi: 10.1126/science.8171320

Suzuki, T., Fujikura, K., Higashiyama, T., and Takata, K. (1997). DNA staining for fluorescence and laser confocal microscopy. *J. Histochem. Cytochem.* 45, 49–53. doi: 10.1177/002215549704500107

Tavana, H., Jovic, A., Mosadegh, B., Lee, Q. Y., Liu, X., Luker, K. E., et al. (2009). Nanoliter liquid patterning in aqueous environments for spatially-defined reagent delivery to mammalian cells. *Nat. Mater.* 8, 736–741. doi: 10.1038/nmat2515

Tavana, H., Kaylan, K., Bersano-Begey, T., Luker, K. E., Luker, G. D., and Takayama, S. (2011). Rehydration of polymeric, aqueous, biphasic system facilitates high throughput cell exclusion patterning for cell migration studies. *Adv. Funct. Mater.* 21, 2920–2926. doi: 10.1002/adfm.201002559

Tavana, H., and Takayama, S. (2011). Aqueous biphasic microprinting approach to tissue engineering. *Biomicrofluidics* 5:13404. doi: 10.1063/1.3516658

Teixeira, A. G., Agarwal, R., Ko, K. R., Grant-Burt, J., Leung, B. M., and Frampton, J. P. (2018). Emerging biotechnology applications of aqueous two-phase systems. *Adv. Healthc. Mater.* 7:1701036. doi: 10.1002/adhm.201701036

Wang, P., Tan, K. L., and Kang, E. T. (2000). Surface modification of poly(tetrafluoroethylene) films via grafting of poly(ethylene glycol) for reduction in protein adsorption. *J. Biomater. Sci. Polym. Ed.* 11, 169–186. doi: 10.1163/156856200743634

Wang, Z., Kim, M. C., Marquez, M., and Thorsen, T. (2007). High-density microfluidic arrays for cell cytotoxicity analysis. *Lab. Chip* 7, 740–745. doi: 10.1039/b618734j

Weston, S. A., and Parish, C. R. (1990). New fluorescent dyes for lymphocyte migration studies. Analysis by flow cytometry and fluorescence microscopy. *J. Immunol. Methods* 133, 87–97. doi: 10.1016/0022-1759(90)90322-M

Wiendahl, M., Oelmeier, S. A., Dismer, F., and Hubbuch, J. (2012). High-throughput screening-based selection and scale-up of aqueous two-phase systems for pDNA purification. *J. Sep. Sci.* 35, 3197–3207. doi: 10.1002/jssc.201200310

Zimmermann, S., Gretzinger, S., Schwab, M.-L., Scheeder, C., Zimmermann, P. K., Oelmeier, S. A., et al. (2016). High-throughput downstream process development for cell-based products using aqueous two-phase systems. *J. Chromatogr. A* 1464, 1–11. doi: 10.1016/j.chroma.2016.08.025

**Conflict of Interest Statement:** The authors declare that the research was conducted in the absence of any commercial or financial relationships that could be construed as a potential conflict of interest.

frontiers in Chemistry

CORRECTION
published: 04 October 2019
doi: 10.3389/fchem.2019.00670

# Corrigendum: Confinement of Suspension-Cultured Cells in Polyethylene Glycol/Polyethylene Oxide-Albumin Aqueous Two-Phase Systems

*Alyne G. Teixeira[1], Alex Kleinman[2], Rishima Agarwal[1], Nicky W. Tam[1], Jun Wang[3,4] and John P. Frampton[1]**

[1] School of Biomedical Engineering, Dalhousie University, Halifax, NS, Canada, [2] Pomona College, Claremont, CA, United States, [3] Department of Microbiology and Immunology, Dalhousie University, Halifax, NS, Canada, [4] Canadian Center for Vaccinology, IWK Health Centre, Halifax, NS, Canada

OPEN ACCESS

**Approved by:**
Frontiers Editorial Office, Frontiers Media SA, Switzerland

***Correspondence:**
John P. Frampton
john.frampton@dal.ca

**Specialty section:**
This article was submitted to Chemical and Process Engineering, a section of the journal Frontiers in Chemistry

**Received:** 23 August 2019
**Accepted:** 20 September 2019
**Published:** 04 October 2019

**Citation:**
Teixeira AG, Kleinman A, Agarwal R, Tam NW, Wang J and Frampton JP (2019) Corrigendum: Confinement of Suspension-Cultured Cells in Polyethylene Glycol/Polyethylene Oxide-Albumin Aqueous Two-Phase Systems. Front. Chem. 7:670. doi: 10.3389/fchem.2019.00670

**Keywords: aqueous two-phase systems, cell partitioning, polyethylene glycol, polyethylene oxide, bovine serum albumin, immune cells, ELISpot**

## A Corrigendum on

**Confinement of Suspension-Cultured Cells in Polyethylene Glycol/Polyethylene Oxide-Albumin Aqueous Two-Phase Systems**

*by Teixeira, A. G., Kleinman, A., Agarwal, R., Tam, N. W., Wang, J., and Frampton, J. P. (2019). Front. Chem. 7:441. doi: 10.3389/fchem.2019.00441*

**Jun Wang** was not included as an author in the published article. The corrected Author Contributions Statement appears below:

"AT performed or assisted with all experiments and wrote the paper. AK performed the phase-separation characterization and helped write the paper. RA helped analyze data and edited the paper. NT helped analyze data and edited the paper. JW contributed to the initial concept of this work and assisted with experimental planning. JF oversaw all experiments and edited the paper."

The authors apologize for this error and state that this does not change the scientific conclusions of the article in any way. The original article has been updated.

# Advantages of publishing in Frontiers

**OPEN ACCESS**
Articles are free to read for greatest visibility and readership

**FAST PUBLICATION**
Around 90 days from submission to decision

**HIGH QUALITY PEER-REVIEW**
Rigorous, collaborative, and constructive peer-review

**TRANSPARENT PEER-REVIEW**
Editors and reviewers acknowledged by name on published articles

**Frontiers**
Avenue du Tribunal-Fédéral 34
1005 Lausanne | Switzerland

**Visit us:** www.frontiersin.org
**Contact us:** info@frontiersin.org | +41 21 510 17 00

**REPRODUCIBILITY OF RESEARCH**
Support open data and methods to enhance research reproducibility

**DIGITAL PUBLISHING**
Articles designed for optimal readership across devices

**FOLLOW US**
@frontiersin

**IMPACT METRICS**
Advanced article metrics track visibility across digital media

**EXTENSIVE PROMOTION**
Marketing and promotion of impactful research

**LOOP RESEARCH NETWORK**
Our network increases your article's readership